SHAHROKHI, Firouz, 1938-
NUMERICAL TECHNIQUE FOR CALCULATION OF RADIANT ENERGY FLUX TO TARGETS FROM FLAMES.

The University of Oklahoma, Ph.D., 1966
Engineering, mechanical

THE UNIVERSITY OF OKLAHOMA

GRADUATE COLLEGE

NUMERICAL TECHNIQUE FOR CALCULATION OF RADIANT ENERGY FLUX TO TARGETS FROM FLAMES

A DISSERTATION

SUBMITTED TO THE GRADUATE FACULTY

in partial fulfillment of the requirements for the

degree of

DOCTOR OF PHILOSOPHY

BY

FIROUZ SHAHROKHI

Norman, Oklahoma

1965

NUMERICAL TECHNIQUE FOR CALCULATION OF RADIANT ENERGY FLUX TO TARGETS FROM FLAMES

Tom J. Love

Raymond V. Kasey

Edward F. Blick

Arthur Bernhart

Omer A. [illegible]

DISSERTATION COMMITTEE

ABSTRACT

This is a study to predict total flux at a given surface from a flame which has a specified shape and dimension. The solution to the transport equation for an absorbing and emitting media has been calculated based on a thermodynamic equilibrium and non-equilibrium flame. In the thermodynamic equilibrium case, it is assumed that the circumstances are such that at each point in the flame a local temperature T is defined and the volume emission coefficient at that point is given in terms of volume absorption coefficient by the Kirchhoff's Law. The flame's monochromatic intensity of volume emission in a thermodynamic equilibrium is assumed to be the product of monochromatic volume extinction coefficient and the black body intensity. In the non-equilibrium case, a measured monochromatic intensity of volume emission of a given flame is used as well as the measured monochromatic volume extinction coefficient.

Geometrical relations are derived for sheet, cylindrical and conical flames applicable to both thermodynamic equilibrium and non-equilibrium case. The monochromatic flux of a methanol and an acetone flame with a specified shape and dimension to a given target has been calculated and plotted based on these geometrical relations and the

two methods indicated above. The Gauss numerical integration method is used to calculate total radiative flux from the monochromatic flux plots. Some experimental measurements of total radiative flux have been made and compared to the predicted values.

ACKNOWLEDGEMENT

The author wishes to express his deep appreciation to Dr. T.J. Love, Jr. for his guidance and cooperation throughout the progress of this study. The other members of the Doctoral Committee who gave their time and advice also have the author's appreciation and thanks, especially Dr. Omer Pipkin.

The author extends his thanks to the staff of the Osage Computer Center. Mr. Paul Johnson's aid in the development of the computer program is sincerely appreciated.

Many individuals have made significant contributions to the completion of this study. Most particularly is Mr. James Hood for his active participation and assistance in the experimental phase of the study.

The author extends thanks to Mrs. Robert Brown for providing valuable help in preparing this manuscript along with the staff of the Oklahoma University Research Institute; particularly Mr. George Droescher, the draftsman and Mr. Harold Brummer, the reproduction supervisor.

Support for this research was provided by Chemical Research and Development Laboratories, Edgewood Arsenal, through Contract DA-18-035-AMC-116(A).

Finally, I wish to thank my family for their limitless patience and understanding during the undertaking and completion of this study; especially my wife, Kay, who edited and prepared this manuscript; and to my parents, who made it all possible.

TABLE OF CONTENTS

LIST OF TABLES

LIST OF ILLUSTRATIONS

Figure | Page

Figure		Page

Figure | Page

Figure | Page

Figure		Page

Figure		Page

Figure Page

NUMERICAL TECHNIQUE FOR CALCULATION OF RADIANT ENERGY FLUX TO TARGETS FROM FLAMES

CHAPTER I

INTRODUCTION

Spectroscopic methods of gas-radiative property measurements are potentially useful engineering tools. Success in exploiting these methods depends upon understanding fundamental flame processes, as well as upon good instrument design. One of such properties is the gas temperature, which has received considerable attention. R.H. Tourin (59) discusses the existence of temperature gradient in many hot gases, due to a special type of non-equilibrium. Spectroscopic and optical mapping techniques have been developed for application of several monochromatic methods of gas temperature measurements (57). The idea of determining the temperature of hot gases from the optical radiation they emit and absorb is at least as old as the century. An optical method of flame pyrometry using the visible range was presented by F. Kurlbaum (29) in 1902. Infrared pyrometry was used by W.W. Coblentz (18) and H. Schmidt (47) in 1905 and 1909, respectively. These methods were based on purely thermodynamic considerations. Following the application of the quantum theory of atomic and molecular spectra, more complex spectroscopic methods of gas temperature measurement were developed. In recent years, some of these methods have reached a high degree of sophistication in the hands of a number of investigators such as H.P. Broida (12) and H.C. Hottel, G.C. Williams and W.P. Jansen (27).

The effect of a general spectrometer response function (slit function) on the measured transmission and emission of gases was investigated by H.J. Babrov (6,7). It is shown that, although both the measured absorption and emission of hot gases as distorted by the slit function, the temperature determined by the infrared monochromatic radiation method is independent of the slit function. It is also shown that the conditions for the invariance of the integrated transmission are much milder than those previously assumed.

Instrumentation has been developed for measurement of infrared emission and absorption spectra of gases heated under a controlled condition in a few laboratories in recent years. The Warner and Swasey Company has been engaged in measuring infrared spectral emissivities of hot gases. Their apparatus now in use consists of a specially made quartz gas cell heated by a tube furnace, and an optical system which illuminates the entrance slit of a monochromator with radiation from the gas sample or the globar source. Spectra are measured with a modified Perkin-Elmer Infrared Spectrometer. In the work done by the Warner and Swasey Company and reported G.J. Penzias and R.H. Tourin (42), emissivities have been determined from infrared absorption spectra of gas samples heated under controlled conditions. For a gas in thermal equilibrium, spectral emissivity and spectral absorptivity are equal at every wave length (Kirchhoff's Law). Emissivities can, therefore, be read directly from the measured absorption spectrum. This method of measuring emissivities is reported by G.J. Penzias and R.H. Tourin (42) to be usually more accurate and convenient than the alternative procedure of comparing gas emission to black body emissions. It is desired to extrapolate from these laboratory measurements, to predict spectral emissivities of hot gases in various cases of practical interest. The simplest extrapolation formula is Beer's Law, which applies to spectral regions of finite width, if the observed spectrum is continuous over the experimental spectral slit width.

Although much work has been done on radiative properties of hot gases, radiation heat transfer from a flame with specified geometry to a given target has been neglected. T. Sato and R. Matsumoto (45) discuss a theoretical analysis of the radiation from a luminous flame under the assumptions of uniform temperature and particle distribution, and the fundamental mechanism of luminous flame radiation. S. Yokohori (65) has formulated, theoretically, the equations for calculation of the emissivity of the gas, using the dimensions, distributions and amount of particles within the combustion chamber.

Radiative transfer theory is the quantitative study, on a phenomenological level, of the transfer of radiant energy through media that absorbs, scatters and emits radiant energy.

In this study, the Eulerian point of view is adopted and the variation in the energy of a stationary field is considered from point to point, taking into account all photons present in the neighborhood of a given point.

The total radiation flux at a given surface from a flame with specified shape and dimensions is to be predicted. The basis of the calculation of spectral radiance of both thermodynamic equilibrium and non-equilibrium for steady state flames is outlined. The possible source of discrepancies in the input parameters and the approximations involved in calculation are discussed. The results will display the frequency-dependent radiance of the various species.

In the discussion of Chapter II, the background for the calculations leading to monochromatic flux and total flux are outlined qualitatively. These are geometric and radiative calculations with a discussion of the numerical method used. In addition, the use of the tables and graphs will be discussed. An important function of the discussion is to emphasize the facets of theory and the input parameters. The material presented here is divided into eight chapters. In Chapter II, a discussion is given about the monochromatic properties of a flame. This involves derivation of equations leading to the calculation of total flux based on thermodynamic equilibrium and measured monochromatic volume absorption and emission coefficients. Chapter III is devoted primarily to the geometry of sheet, cylindrical and conical flames, their origin and a few remarks about them. Chapter IV will involve the numerical method used to evaluate total radiation flux of a given flame. A closed form integration for a special case of a flame in thermodynamic equilibrium is discussed in Chapter V. The discussion on calculated total radiation flux based on the two methods mentioned and experimental values are given in Chapters VI and VII.

CHAPTER II

THEORETICAL BASIS

In any quantitative description of the radiation from a gas, one may choose to deal with the gaseous absorption coefficient, the gaseous emissivity, or the actual intensity in unit of energy per unit of surface area emitted at some boundary of the gas. Discussion will cover all three descriptions, so one may use the one most suited to his needs.

When one speaks of absorption coefficient of gases and vapors, one usually means by this the attenuation of a monochromatic light beam when it passes through a known amount of the absorber.

Quantitatively this is expressed by Lambert's Law

$$I_{\nu} = I_{o,\nu} \exp(-\varkappa_{\nu} x) \qquad (2\text{-}1)$$

Where $I_{o,\nu}$ is the intensity in the incident beam, I_{ν} is the intensity in the beam after it traverses x units of the gas and $\varkappa$ is the linear absorption coefficient of the gas. In so far as this equation is concerned, it may be applied at a particular radiant frequency (monochromatic), as a mean over a band of frequencies, or as a mean over the entire spectrum. The value of $\varkappa$ must be considered for each of the types of radiation absorbing processes, and, if there are several for the frequency or frequency region of interest, they must be summed.

Equation 2-1 describes empirically the observed attenuation of radiation and is valid in all instances when the absorption coefficient of the individual atoms or molecules do not overlap, i.e., when the pressure is sufficiently low. The absorption coefficient can be obtained as a function of wave length by measuring the quantities in the above equation. In order to understand the observed plots of absorption coefficients versus wave length, one must take recourse to the data, on the molecule in question, which have been supplied by the spectroscopist in terms of his analysis of the molecular energy level. Absorption coefficients in a certain region of the spectrum can be associated with the dissociation of the molecule in another region with photoionization of the molecule; and finally, perhaps, with a region of dissociative ionization. It is not infrequent that one finds superimposed over all three regions many discrete absorption bands, some converging to dissociation limits, others to various ionization limits and still other bands requiring more complex interpretations.

For most purposes, gas temperature is of interest as a measure of the kinetic energy of the gas (9). Radiation, however, results from internal motions of gas molecules, atoms and ions, and not directly from their translational motion. A particular type of radiation will be useful as a gas thermometer only if that radiation is in equilibrium with the gas kinetic energy. This question of thermal equilibrium has received much attention.

Temperature is defined in terms of states of thermal equilibrium. Departures from thermal equilibrium have the practical effect of introducing an intrinsic uncertainty into the measurement of temperature. If the departure from thermal equilibrium is sufficiently extreme, the temperature concept is no longer useful. Departures from thermal equilibrium in gases are associated most often with the internal degrees of freedom of gas particles, rather than their kinetic energy. As long as the distribution of particle velocities is Maxwellian, the gas has a meaningful temperature. The possible lack of equilibrium with respect to an internal degree of freedom need not concern one, provided that degree of freedom is not selected as the gas thermometer, and provided that no significant fraction of total energy of the gas is locked up in that degree of freedom.

A thermodynamic system is said to be in equilibrium if its state variables do not change when it is left isolated from outside influences for an indefinite period of time. A system whose equilibrium has been disturbed will come to equilibrium again if left undisturbed for some time. Giving enough time for the system to return to equilibrium condition is called the relaxation phenomena. This trend is seen in the simplest form of representation, such as for a quantity z of a system,

$$\frac{dz}{dt} = -\frac{1}{\tau}(z - \bar{z}) \qquad (2\text{-}2)$$

where $\bar{z}$ is the final or equilibrium value of z, t is the time and τ is the relaxation time. Upon integration of Equation 2-2, one obtains

$$z = \bar{z} + (z_o - \bar{z})e^{-t/\tau} \qquad (2\text{-}3)$$

where z_o is the initial value of z. The influence of the initial value disappears exponentially. Examples of such a trend are found in the chemical reaction rate and the transition between states in gases. Since the transfer of energy in a gas can only occur through collisions and since the number of collisions a molecule suffers per second is proportional to pressure (for a given temperature), it is convenient to write

$$\tau = Z\tau_c \qquad (2\text{-}4)$$

where Z is the number of collisions necessary to bring about equilibirum, and τ_c is the time between collisions.

$\tau_c \approx 2 \times 10^{-10}$ from translational to rotational degrees of freedom, $Z \approx 2$ to 6 at standard conditions. For vibrations Z and τ vary more widely. The radiative lifetime associated with molecular vibrational transitions giving rise to infrared emission from a hot gas is of the order $> 10^{-3}$

seconds, while the time required to reach equilibrium between the kinetic and vibrational degrees of freedom is only of the order 10^{-6} seconds. If equilibrium exists, a meaningful temperature exists and can be measured, provided time associated with measurement is relatively long compared to the time required to reach equilibrium between the kinetic and internal degrees of freedom following a disturbance from that equilibrium. A quantitative discussion of equilibrium in flames was given by Benedict and Phyler some years ago (10).

If the intensities in the direction $\vec{x}$ at the ends of the cylindrical element are $I_\nu(x)$ and $I_\nu(x + dx)$, then, the corresponding energies are, respectively

$$I_\nu(x)dAd\omega\, d\nu dt \quad \text{and} \quad I_\nu(x + dx)dAd\omega\, d\nu dt$$

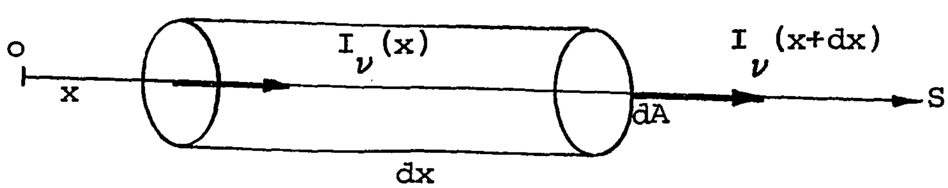

The energy at $(x + dx)$ must be the sum of the Lagrangian residue of the $I_\nu(x)$ and the energy 'emitted' by the element in the direction $\vec{x}$, i.e.

$$\{I_\nu(x+dx)dAd\omega d\nu\, dt\} = \{I_\nu(x)-\rho\varkappa_\nu I_\nu(x)dx\}dAd\omega\, dtd\nu + j_\nu(x)dmd\omega\, dt \tag{2-5}$$

where

$$dm = \rho dAdx$$

Upon the simplification of Equation 2-5, one obtains the equation of transfer for an absorbing and emitting media:

$$\frac{dI_\nu(x)}{dx} = -\rho\varkappa_\nu I_\nu(x) + \rho j_\nu \tag{2-6}$$

$$\beta_\nu = \rho\varkappa_\nu \quad \text{and} \quad J_\nu = \rho j_\nu \tag{2-7}$$

I_ν = monochromatic intensity along optical axis

J_ν = monochromatic emission energy (intensity of volume emission)

$\varkappa_\nu$ = absorption coefficient

β_ν = volume extinction coefficient

Equation 2-6 may be rewritten:

$$\frac{dI_\nu(x)}{dx} = -\beta_\nu I_\nu(x) + J_\nu \tag{2-8}$$

The solution to such a differential equation is:

$$I_\nu(x) = Ae^{-\beta_\nu x} + \frac{J_\nu}{\beta_\nu} \tag{2-9}$$

One of the boundary conditions is that there is no incident intensity on a flame. Thus,

$$\text{at } x = 0, \qquad I_\nu(0) = 0$$

and

$$I_\nu(0) = 0 = A_1 + \frac{J_\nu}{\beta_\nu}$$

$$A = \frac{-J_\nu}{\beta_\nu} \tag{2-10}$$

Upon substituting these results into Equation 2-9, one obtains

$$I_\nu(x) = \frac{J_\nu}{\beta_\nu}(1 - e^{-\beta_\nu x}) \qquad (2\text{-}11)$$

Equation 2-11 will be handled by two different methods. Method I involves the measurement of both emitted and transmitted radiation from controlled laboratory flames of different fuels. The analysis of the monochromatic measurements involves calculation of β_ν, the volume extinction coefficient, and J_ν, the intensity of the volume emission of the flame. These values (β_ν and J_ν) are assumed to be constant over the optical path. In Method II, it is assumed that thermal equilibrium exists where the expression

$$J_\nu = \rho\varkappa_\nu I_{bb,\nu}(T) = \beta_\nu I_{bb,\nu}(T) \qquad (2\text{-}12)$$

applies, with $I_{bb,\nu}(T)$ being the monochromatic black body intensity at temperature T. The emission of a black body is given by Planck's radiation law:

$$I_{bb,\nu}(T) = \frac{C_1\lambda^{-5}}{\exp(\frac{C_2}{\lambda T})-1} \qquad (2\text{-}13)$$

$C_1 = 1.191 \times 10^{-3}$ erg micron^2 sec^{-1}

$C_2 = 14387$ micron deg K^{o}

λ = wave length micron

The purpose of this work is not to actually obtain flame spectrum data, but to construct a tool by which these data may be used for determining theoretical monochromatic flux; and, consequently, the total flux. With this in mind, the spectrum data used in the above two methods are taken from different investigators. The sources of such data will be given as they are introduced.

Method I

As in other branches of spectroscopy, the greatest emphasis has been placed on the measurement of spectral frequencies, because these frequencies are directly related to quantized energy levels of the flame molecules. Interest in quantitative measurement of the magnitude of emission and absorption at a given frequency has developed only in recent years. To calculate J_ν and β_ν, one starts with Equation 2-9:

$$I_\nu(x) = Ae^{-\beta_\nu x} + \frac{J_\nu}{\beta_\nu} \qquad (2\text{-}14)$$

Using the flame as a source, the following boundary conditions apply to Equation 2-9:

$$\text{at } x = 0, \qquad I_\nu(0) = 0$$

$$x = a, \qquad I_\nu(a) = I_\nu(\text{flame})$$

Therefore,

$$I_\nu(\text{flame}) = \frac{J_\nu}{\beta_\nu}(1 - e^{-\beta_\nu a}) \qquad (2\text{-}15)$$

The quantity I_ν(globar) represents the relative intensity of radiation from the globar in the absence of burning fuel. Therefore, the boundary condition is:

$$\text{at } x = 0, \qquad I_\nu(0) = I_\nu(\text{globar})$$

and

$$A = I_\nu(\text{globar}) - \frac{J_\nu}{\beta_\nu} \qquad (2\text{-}16)$$

The absorption spectrum is obtained by passing a globar beam through the flame. Upon substituting Equation 2-16 into 2-9 with the following boundary condition:

$$\text{at } x = a, \qquad I_\nu(a) = I_\nu(\text{globar + flame})$$

one obtains

$$\begin{aligned} I_\nu(\text{globar + flame}) &= \left[I_\nu(\text{globar}) - \frac{J_\nu}{\beta_\nu}\right]e^{-\beta_\nu a} + \frac{J_\nu}{\beta_\nu} \\ &= \frac{J_\nu}{\beta_\nu}(1 - e^{-\beta_\nu a}) + I_\nu(\text{globar})e^{-\beta_\nu a} \\ &= I_\nu(\text{flame}) + I_\nu(\text{globar})e^{-\beta_\nu a} \end{aligned} \qquad (2\text{-}17)$$

Upon simplifying Equation 2-17, it reduces to:

$$e^{-\beta_\nu a} = \frac{I_\nu(\text{globar + flame}) - I_\nu(\text{flame})}{I_\nu(\text{globar})} \qquad (2\text{-}18)$$

The output of the spectrometer is displayed as a deflection on a recorder, which in turn can be calibrated and translated into the energy emitted by the source of the radiation. Equation 2-18 can be rewritten as a function of the recorder pen deflection; i.e.,

$$e^{-\beta_\nu a} = \frac{DGF - DF}{DG} \qquad (2\text{-}19)$$

where

DGF = flame + globar pen deflection

DF = flame pen deflection

DG = globar pen deflection

Utilizing Beer's Law and the definition of ϵ_ν the relationship between emittance and the monochromatic volume extinction coefficient is:

$$\epsilon_\nu = 1 - e^{-\beta_\nu a} \qquad (2\text{-}20)$$

ϵ_ν = monochromatic effective emittance

Therefore,

$$\epsilon_\nu = \frac{DG + DF - DGF}{DG} \tag{2-21}$$

These pen deflections and the technique used for this measurement, as well as several characteristics of spectrometer calibration, have been discussed fully in reference (26). Such pen deflections are presented in Tables I and II for methanol and acetone, respectively (see Appendix A). For the data of reference (26), the optical depth is a = 0.8cm, and the resulting relationship between the monochromatic volume extinction coefficient and emittance given in this specific data is:

$$\beta_\nu = - \frac{1}{a} \ln(1 - \epsilon_\nu) \tag{2-22}$$

where a = 0.8cm.

Equations 2-21 and 2-22 have been calculated for 108 wave lengths and recorded in Tables III and IV for methanol and acetone, respectively (see Appendix A).

The conversion factors of flame pen deflection to energy in watts are:

$E_\nu = 4.342 \times 10^{-6} \times DF$ from 1700 to 1795 drum reading

$E_\nu = 1.027 \times 10^{-6} \times DF$ from 1800 to 1900 drum reading

where

E_ν = emitted energy from the flame as the source

The monochromatic emitted intensity of the flame is obtained from:

$$I_\nu(\text{ flame}) = \frac{E_\nu}{A\Omega\Delta\lambda} \tag{2-23}$$

where

A = observed area

Ω = solid angle

$\Delta\lambda$ = increment in wave length

The values of A, Ω and $\Delta\lambda$ are also given in Tables I and II. The spectral intensity of the flame is calculated from Equation 2-23; therefore, J_ν from Equation 2-15 is:

$$J_\nu = \beta_\nu I_\nu(\text{flame}) \left[1 - e^{-\beta_\nu a}\right]^{-1} \tag{2-24}$$

where a = 0.8cm.

The monochromatic intensity of the volume emission is calculated and recorded in Tables III and IV for methanol and acetone, respectively (see Appendix A).

Method II

In this method, the transport Equation 2-8

$$\frac{dI_\nu(x)}{dx} = -\beta_\nu I_\nu(x) + J_\nu \tag{2-25}$$

is solved by assuming that local thermodynamic equilibrium is maintained, or, equivalently, that Kirchhoff's Law holds. Kirchhoff's Law is arrived at by consideration of radiant energy interchange when a small body is placed in an isothermal enclosure and allowed to attain equilibrium. In order to avoid violation of the second law of thermodynamics, it is found that spectral absorptance must be equal to the spectral emittance. Under these conditions, the gaseous emissivity may be written as:

$$\alpha_{\nu} = \epsilon_{\nu} = 1 - e^{-\beta_{\nu} x} \tag{2-26}$$

where

$$\alpha_{\nu} = \text{spectral absorptance}$$

In local thermodynamic equilibrium, it is assumed that the circumstances are such that one can define at each point in the atmosphere a local temperature T such that the volume emission coefficient at that point is given in terms of the volume absorption coefficient by Kirchhoff's Law; i.e., at each point there is the relation

$$J_{\nu} = \beta_{\nu} I_{bb,\nu}(T) \tag{2-27}$$

where $I_{bb,\nu}(T)$ is the monochromatic black body intensity at temperature (T), defined by Equation 2-13. From Equations

2-8 and 2-27.

$$\frac{dI_{\nu}(x)}{dx} = \beta_{\nu}\{I_{bb,\nu}(T) - I_{\nu}(x)\} \tag{2-28}$$

Differential Equation 2-28 is an explicit function of optical depth x, but there is a temperature distribution along the center line of the flow and outward; therefore, the temperature is also an explicit function of optical depth.

$$T = T(x) \tag{2-29}$$

From the above logic, the black body intensity is an implicit function of optical depth and Equation 2-28 becomes

$$\frac{dI_{\nu}(x)}{dx} = \beta_{\nu}\ \{I_{bb,\nu}(x) - I_{\nu}(x)\} \tag{2-30}$$

In general, the volume absorption coefficient β_{ν} depends on the state of the gas, which may be specified by total pressure P(x), temperature $T_g(x)$ and mole fraction of the gas S(x). For the feneral case, Equation 2-30 yields

$$I_{\nu} = I_{\nu}(0)\exp(-\int_0^x \beta_{\nu}\ dx') + \int_0^x \beta_{\nu} I_{bb,\nu}(x')\exp(-\int_{x'}^x \beta_{\nu} dx'')dx \tag{2-31}$$

The first term on the right side of Equation 2-31 indicates the portion of incident intensity $I_{\nu}(0)$ transmitted from o to x, and the second term gives the intensity originating in all elements of length dx' and transmitted from x' to x. The exact expression for β_ν can be derived, in principle, from molecular constants by use of quantum mechanics. The complexity of the calculation has so far made this approach largely impractical for other than diatomic molecules; but, it is possible to measure this quantity, β_ν fluctuates greatly as ν sweeps the line structure of the band. Furthermore, it is assumed that there is no temperature trace throughout the flame, only constant temperature everywhere. In other words, the volume emission is constant within the solid angle (this assumption was also made in Method I). With constant volume emission, the solution to Equation 2-30 is:

$$I_\nu(a) = I_{bb,\nu}(T)(1 - e^{-\beta_\nu a}) \qquad (2\text{-}32)$$

The monochromatic black body intensity has been presented in Appendix A, in two different forms. Figures 9, 10 and 11 are black body intensity versus wave lengths at different temperatures. The temperature and wave length ranges for these figures are:

Temperature: 1000 K^o to 1700 K^o

Wave length: 1 micron to 15 microns

These figures are presented in order to illustrate that, although the spectral emittance may be quite high at certain wave lengths, the emitted intensity can, in the same cases, be negligible because the black body intensity is one or two orders of magnitude lower at that particular wave length and temperature. In these discussions, it is convenient to discuss monochromatic radiation in terms of characteristic wave lengths of the radiation. The wave length characterization is often important when discussing the interaction of radiation and matter. This is of special interest when the concern is with surface roughnesses or particular matter with physical dimensions of the same order of magnitude as the wave length of the radiation. In order to evaluate Equation 2-32, the monochromatic data for volume absorption coefficient and the burning temperature of the fuel are needed. Such data for infrared spectra of hydrocarbon flames are available in references (41) and (44). The range of frequency in these reports are 1 - 15μ. In the data reported, infrared emission and absorption of flames were measured under controlled conditions for the purpose of obtaining definitive measurements of the flame's infrared radiance. This measurement program required a means of producing flames for study and a means for measurement of flame spectra. An experimental combustion system and an infrared flame spectrometer were used to satisfy these requirements. The equipment used, measured the globar spectrum, an absorption spectrum and an emission spectrum. The quantity $I_{\nu o}$ represents the relative intensity of radiation from the globar in the absence of burning fuel. The absorption spectrum $I_{\nu 1}$ is obtained by passing a globar beam through the flame. Emission spectrum $I_{\nu g}$ was obtained by using the flame as a source. Therefore, $I_{\nu o}$, $I_{\nu 1}$ and $I_{\nu g}$ represent the relative intensities, or just the pen deflection at a given wave length, of the globar spectrum, the absorption spectrum and emission spectrum, respectively. With these measurements taken under exactly the same conditions, the spectral emittance of the flame is then given by the expression:

$$\epsilon_\nu = \frac{I_{\nu 1} - I_{\nu g}}{I_{\nu o}} \tag{2-33}$$

These measurements are done similarly to those in reference (26) in Method I. A more detailed discussion of the experimental technique of obtaining this monochromatic emissivity can be found in references (41) and (44). Infrared spectra of hexane-oxygen, methanol-oxygen and kerosene-oxygen flames in the 1 - 15μ region were measured at several mixture ratios and at several different distances from the nozzle. Three mixture ratios were used for each fuel: stoichiometric, lean and rich. The leanness or richness of the mixture ratio was the extreme commensurate with flame stability and clean burning. The mixture ratio is defined as the mass of oxygen consumed per unit time to the mass of fuel consumed per unit time. Observations of the flame were made: downstream from the flame, at the flame tip and near the base of the flame. In all measurements the geometrical path length through the flame was 12.7cm. The principal results are described in references (41) and (44). As might be expected, spectral emissivity of the lean and stoichiometric flames is higher than that of the rich flame, for the latter is somewhat cooler. Emissivities at the base of the flame are higher than those at the tip of the flame. The temperature at the flame base is higher than that at the flame tip, so that the populations of excited vibrational energy levels involved in the transitions near 4.9μ are relatively higher. The variations in spectral emissivity for different mixture ratios were very small and in some cases almost negligible for a given fuel (41, 44). The temperatures were taken at different locations in the flames with chromel-alumel thermocouples. The temperature used to calculate black body intensity in Equations 2-13 and 2-32 is the average flame temperature. The volume extinction coefficient used in this method is taken from spectral emissivity data reported in references (41) and (44) and Equation 2-13.

$$\beta_\nu = -\frac{1}{a}\ln(1 - \epsilon_\nu) \qquad (2\text{-}34)$$

where a = 12.7cm.

These data are reported in Appendix A.

CHAPTER III

GEOMETRICAL EQUATIONS TO CALCULATE MONOCHROMATIC FLUX

Intensities given by Equations 2-11 and 2-32 for Methods I and II, respectively, are defined to be radiant energy leaving a differential element of area of an imaginary plane within the time interval t and t + dt and having a direction of propagation contained in differential solid angle $\Delta\omega$ whose central direction is normal to the imaginary plane. Therefore, the monochromatic flux q_ν would be

$$q_\nu = \int^{\omega} I_\nu d\omega \approx I_\nu \Delta\omega = \frac{I_\nu A}{r^2} \cos\theta$$

or

$$q_\nu = I_\nu \Omega \cos\theta \tag{3-1}$$

where

Ω = solid angle

θ = angle between normal to the surface and the central directions of the solid angle

The analytical study of q_ν is concerned with applying the β_ν and J_ν data of a fuel to larger flames with various geometries. Here the study is concerned with the division of the flame into n zones. Thus, Equation 3-1 represents the monochromatic flux from one zone. The expression for the monochromatic flux incident on a surface from the m zones will be in the following form:

$$q_\nu = \frac{J_\nu}{\beta_\nu} \sum_{m=1}^{M} (1 - e^{-\beta_\nu a_m}) \, \Omega_m \cos \theta_m \tag{3-2}$$

In this analysis the flame is divided into N x M zones. Hence, the total monochromatic flux from a flame, with any size or shape, to a given target is:

$$q_\nu = \frac{J_\nu}{\beta_\nu} \sum_{m=1}^{M} \sum_{n=1}^{N} (1 - e^{-\beta_\nu a_{m,n}}) \, \Omega_{m,n} \cos \theta_{m,n} \tag{3-3}$$

and

$$q_\nu = I_{bb,\nu}(T) \sum_{m=1}^{M} \sum_{n=1}^{N} (1 - e^{-\beta_\nu a_{m,n}}) \, \Omega_{m,n} \cos \theta_{m,n} \tag{3-4}$$

for Methods I and II, respectively.

I_ν = monochromatic intensity along optical axis with emissivity being constant within the solid angle

β_ν = volume extinction coefficient

J_ν = intensity of volume emission

$I_{bb,\nu}(T)$ = black body intensity at temperature T

$a_{m,n}$ = average optical depth of (m,n)th zone

$\Omega_{m,n}$ = solid angle subtended by the (m,n)th zone

$\theta_{m,n}$ = angle between normal to the surface and the central direction of the solid angle

The theoretical analysis is based on the following assumptions:

1. All necessary dimensions of the flame are known in order to identify the given geometry. The distance of the target from the base of flame is known. The target and base of the flame are co-planar.

2. β_ν and J_ν are assumed constant throughout the flame, and are assumed to be known.

The flame geometries considered are:

1. Sheet of flame
2. Tilted sheet of flame
3. Conical flame
4. Cylindrical flame

Sheet of Flame

The dimensions of a sheet of flame H, B, C and the distance D to the target are known as illustrated in Figures 1 and 2. The center of the coordiante system is situated at the mid-point of the flame base plane. The target is on xz plane and the x axis passes through its center.

The flame is divided in N segments in the vertical direction and M segments in the horizontal direction.

$$\frac{B}{N} = B_n, \qquad \text{where } B_1 = B_2 = \ldots B_n = \ldots B_N$$

$$\frac{H}{M} = H_m, \qquad \text{where } H_1 = H_2 = \ldots H_m = \ldots H_M$$

$\Phi_{m,n}$ is the angle between the central direction of the solid angle and the target surface. This angle is constant throughout each row, therefore, i.e.,

$$\Phi_{m,n} = \Phi_m \qquad (3\text{-}5)$$

According to this definition

$$\theta_{m,n} = \theta_m = \frac{\pi}{2} - \Phi_m \qquad (3\text{-}6)$$

The sweep angle for each row, $\mathcal{L}_{m,n}$, is the angle between central direction of the solid angles of different columns in a given row. From the flame geometry, it is observed that

$$K = \frac{N}{2} \qquad (3\text{-}7)$$

$$\tan \Phi = \frac{(m - \frac{1}{2}) \quad H_m}{D + \frac{C}{2}} \qquad (3\text{-}8)$$

$$\tan \mathcal{L}_{m,k} = \frac{\frac{B}{2} - (k - \frac{1}{2}) \; B_n}{\sqrt{(D + \frac{C}{2})^2 + [(m - \frac{1}{2}) \; H_m]^2}} \qquad (3\text{-}9)$$

$A_{m,k}$ = projected area of each segment perpendicular to central direction of solid angle

$$A_{m,k} = H_m B_k \sin\left(\frac{\pi}{2} - \mathcal{L}_{m,k}\right) \sin\left(\frac{\pi}{2} - \Phi_m\right) \qquad (3\text{-}10)$$

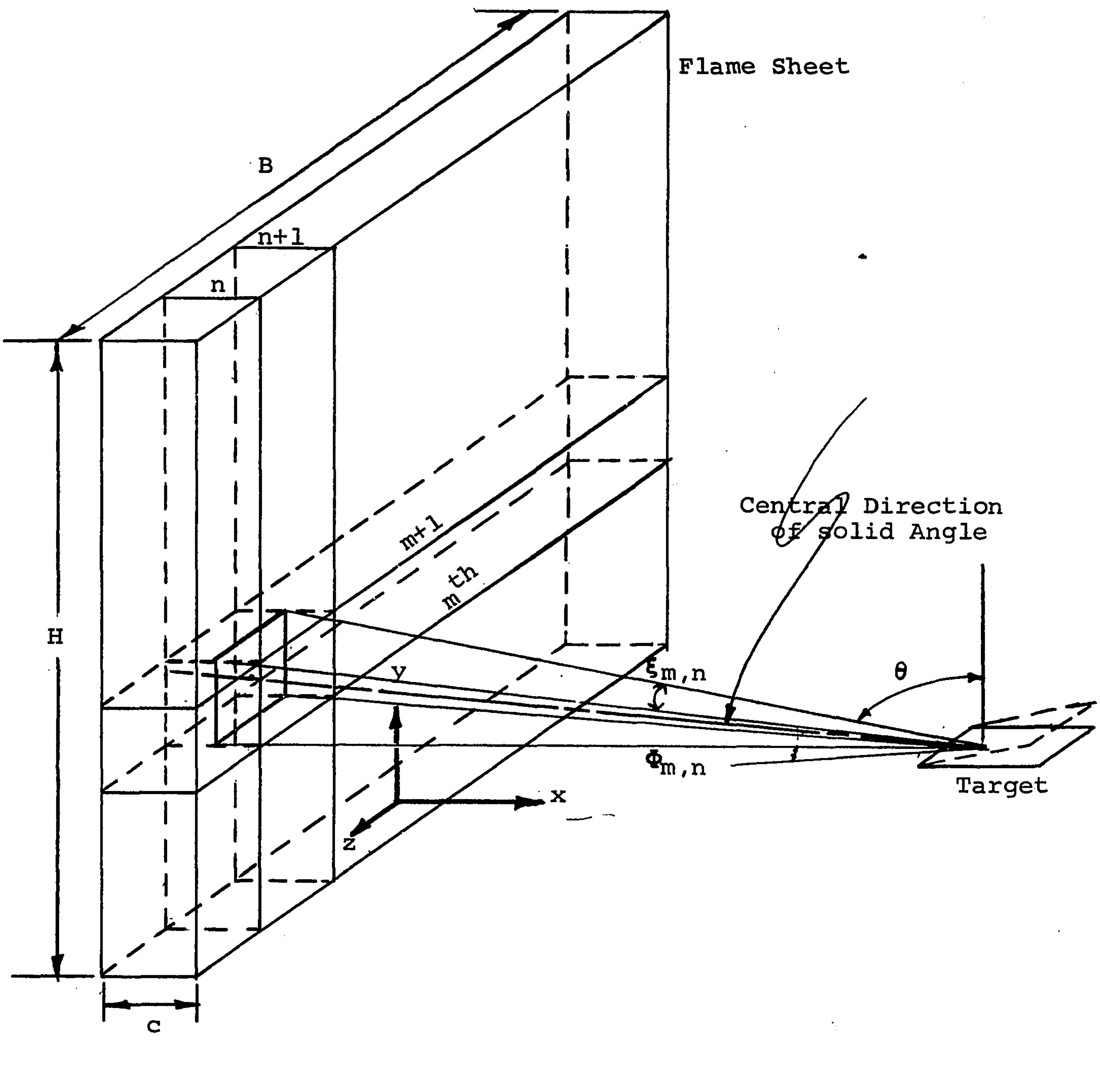

Figure 1. Geometry for Sheet Flame and Target

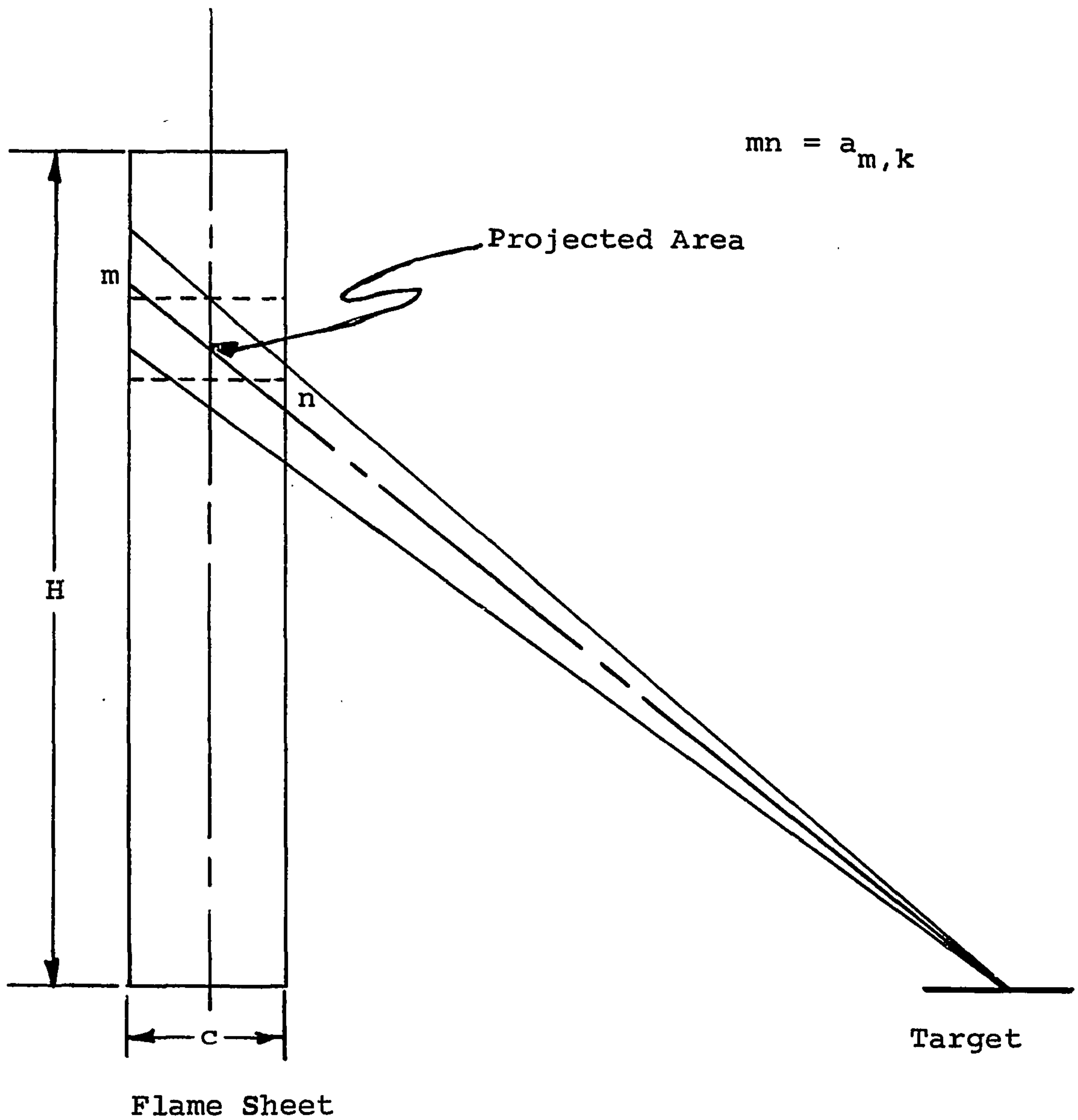

Figure 2. Sheet Flame Side View

$$\text{Solid angle} = \frac{\text{Projected area}}{(\text{distance})^2}$$

$$\Omega_{m,k} = \frac{H_m B_k \sin(\frac{\pi}{2} - \mathcal{L}_{m,k}) \sin(\frac{\pi}{2} - \Phi_m)}{\left[(D + \frac{C}{2})\right]^2 + \left[(m - \frac{1}{2}) H_m\right]^2 + \left[\frac{B}{2} - (k - \frac{1}{2}) B_k\right]^2}$$

(3-11)

$$\text{Optical depth } a_{m,k} = \frac{C}{\cos \Phi_m - \cos \mathcal{L}_{m,k}}$$

(3-12)

With these results, one can calculate the monochromatic flux with the expression

$$q_\nu = \frac{2J_\nu}{\beta_\nu} \sum_{m=1}^{M} \sum_{k=1}^{K} (1 - e^{-\beta_\nu a_{m,k}}) \Omega_{m,k} \cos(\theta_m)$$

(3-13)

Tilted Sheet of Flame

The more general case of the sheet flame is the flame in the tilted state. Tilt may occur in two directions as is shown in Figure 3. The angles of tilt of the flame in both directions, as well as its height, are assumed known. The flame is divided into cells as was done in the preceding case by planes parallel to the base and a side (see Figure 3).

The projected area of each section perpendicular to the central direction of solid angle is

$$A_{m,k} = H_m \cdot B_k \sin \alpha \sin(\beta + \Phi_m) \sin(\frac{\pi}{2} - \mathcal{L}_{m,k})$$

(3-14)

where

$$\sin \Phi_m = \frac{(m - \frac{1}{2})\, H_m \,\sin \beta}{\sqrt{(D + \frac{C}{2})^2 + \left[(m - \frac{1}{2})H_m\right]^2 - \left[2(D + \frac{C}{2})(m - \frac{1}{2})H_m\right] \cos\beta}} \tag{3-15}$$

$$\tan \mathcal{L}_{m,k} = \frac{\frac{B}{2} - (k - \frac{1}{2})\, B_k}{\sqrt{(D + \frac{C}{2})^2 + \left[(m - \frac{1}{2})H_m\right]^2 - \left[2(D + \frac{C}{2})(m - \frac{1}{2})H_m\right]\cos\beta}} \tag{3-16}$$

The area considered is the mid-section area of the optical depth. Solid angle $\Omega_{m,k}$ is:

$$\Omega_{m,k} = \frac{H_m\, B_k \sin \alpha \sin (\beta + \Phi_m) \sin (\frac{\pi}{2} - \mathcal{L}_{m,k})}{\left[(D + \frac{C}{2})\right]^2 + \left[(m - \frac{1}{2})\, H_m\right]^2 - 2(D + \frac{C}{2})(m - \frac{1}{2})H_m \cos \beta + \left[\frac{B}{2} - (k - \frac{1}{2})B_k\right]^2} \tag{3-17}$$

Optical depth $a_{m,k}$ is:

$$a_{m,k} = \frac{C \sin \beta}{\cos \mathcal{L}_{m,k} \sin (\pi - \beta - \Phi_m)} \tag{3-18}$$

$$\theta_m = \frac{\pi}{2} - \Phi_m \tag{3-19}$$

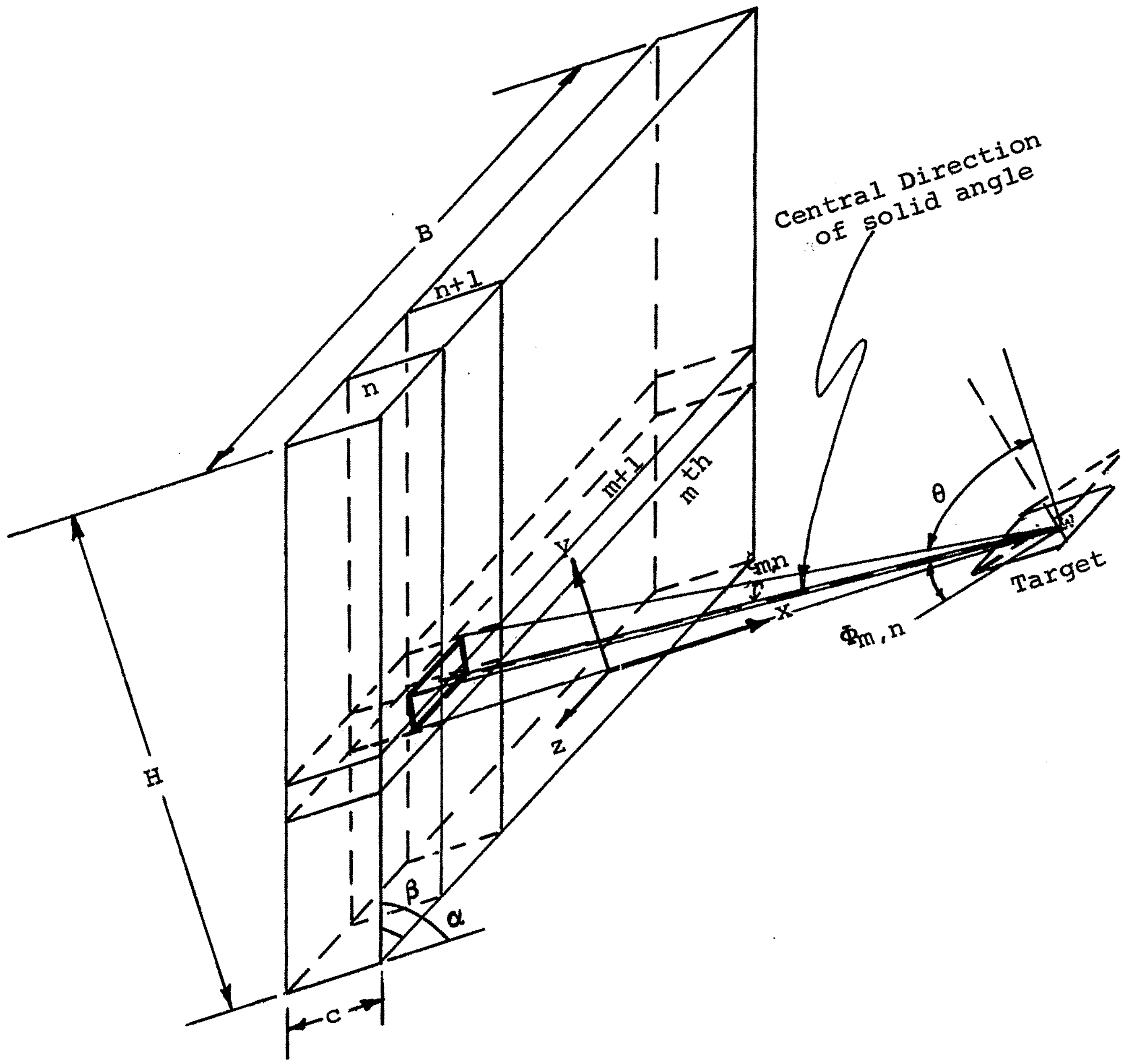

Figure 3. Geometry for Tilted Sheet Flame

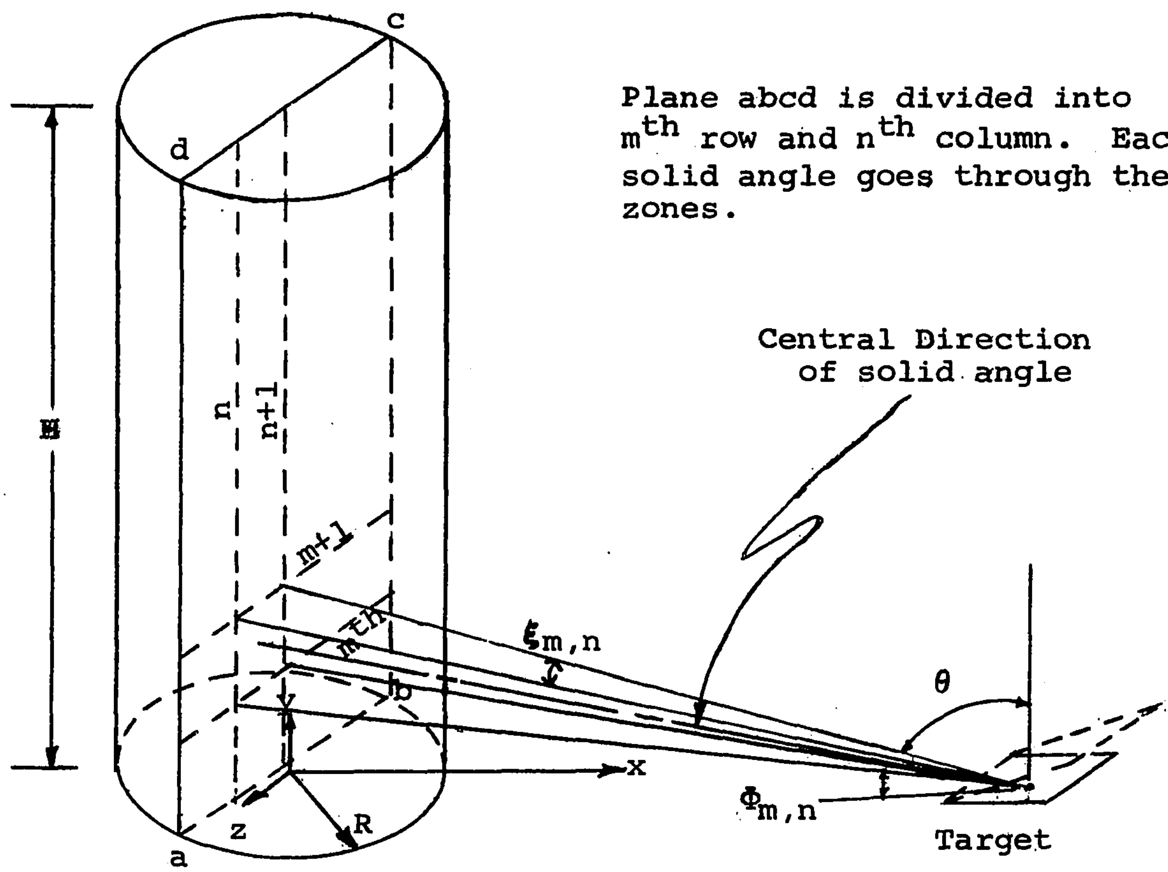

Figure 4. Geometry for Cylindrical Flame

$$q_\nu = \frac{2J_\nu}{\beta_\nu} \sum_{m=1}^{M} \sum_{k=1}^{K} (1 - e^{-\beta_\nu a_{m,k}}) \, \Omega_{m,k} \cos \theta_m \tag{3-20}$$

Cylindrical Flame

In this case, the flame sub-division is made by horizontal and vertical planes: the M horizontal planes and N vertical planes (see Figure 4). Thus,

$$K = \frac{N}{2}$$
$$H_m = \frac{H}{M}$$
$$R_k = \frac{R}{K} \tag{3-21}$$

The projected area of the mid-section of the optical depth perpendicular to the central direction of the solid angle is:

$$A_{m,k} = R_k \cdot H_m \sin \left(\frac{\pi}{2} - \mathcal{L}_{m,k}\right) \sin \Phi_m \tag{3-22}$$

where

$$\tan \mathcal{L}_{m,k} = \frac{(k - \frac{1}{2}) R_k}{\sqrt{(D + R)^2 + \left[(m - \frac{1}{2}) H_m\right]^2}} \tag{3-23}$$

$$\tan \Phi_m = \frac{D + R}{(m - \frac{1}{2}) H_m} \tag{3-24}$$

Solid angle $\Omega_{m,k}$ is:

$$\Omega_{m,k} = \frac{R_k H_m \sin\left(\frac{\pi}{2} - \mathcal{L}_{m,k}\right) \sin \Phi_m}{\left[(D + R)\right]^2 + \left[(m - \frac{1}{2})H_m\right]^2 + \left[R - (k - \frac{1}{2})R\right]^2} \tag{3-25}$$

$$a_{m,k} = \frac{R}{\sin \mathcal{L}_{m,k} \sin \Phi_m} \left[\sin (\pi - \mathcal{L}_{m,k} - \gamma_{m,k}) - \sin (\pi - \mathcal{L}_{m,k} - \beta_{m,k})\right] \tag{3-26}$$

where

$$\sin \beta_{m,k} = \frac{D \sin \mathcal{L}_{m,k}}{R} \tag{3-27}$$

$$\sin \gamma_{m,k} = \frac{(R + D) \sin \mathcal{L}_{m,k}}{R} \tag{3-28}$$

$$\theta_m = \frac{\pi}{2} - \Phi_m \tag{3-29}$$

Therefore

$$q_\nu = \frac{2J_\nu}{\beta_\nu} \sum_{m=1}^{M} \sum_{k=1}^{K} (1 - e^{-\beta_\nu a_{m,k}}) \Omega_{m,k} \cos \theta_m \tag{3-30}$$

<u>Conical Flame</u>

In this section, the flame is assumed to take the shape of a cone. The target is at a distance D away from the edge of the cone base. The flame height H and cone angle α are known. The flame cone is divided by M horizontal planes parallel to the base plane and N planes which divide the cone angle into equal divisions (see Figure 5). From the flame geometry

$$\sin \Phi_m = \frac{D + R}{\sqrt{(D + R)^2 + \left[(m - \frac{1}{2})H_m\right]^2}} \tag{3-31}$$

$$\theta_m = \Phi_m$$

The projected area of each zone perpendicular to the central direction of solid angle is:

$$A_{m,k} = \frac{1}{2}\left\{\frac{(H - mH_m)\tan\frac{\alpha}{2}}{K} + \frac{\left\{H - (m + 1)\, H_{m+1}\right]\tan\frac{\alpha}{2}}{K}\right\} H_m \sin\left(\frac{\pi}{2} - \mathcal{L}_{m,k}\right)\sin\Phi_m \tag{3-32}$$

where

$$\tan \mathcal{L}_{m,k} = \frac{(k - \frac{1}{2})\, H - (m - \frac{1}{2})\, H_m \tan\frac{\alpha}{2}}{K\sqrt{(D + R)^2 + \left[(m - \frac{1}{2})\, H_m\right]^2}} \tag{3-33}$$

and $K = \frac{N}{2}$.

Solid angle $\Omega_{m,k}$ is:

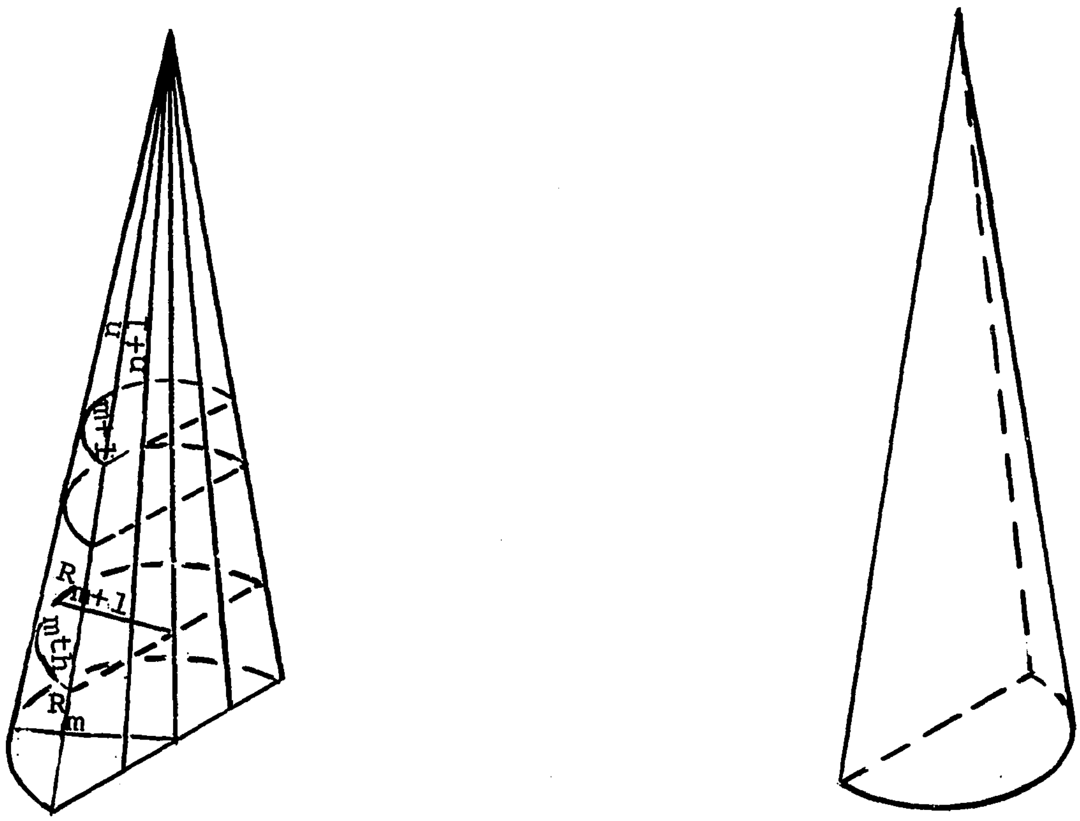

Figure 5. Geometry for Conical Flame
(Target position and angles involved
are as shown in Figure 4.)

$$\Omega_{m,k} = \frac{A_{m,k}}{(D + R)^2 + \left[(m - \frac{1}{2})H_m\right]^2 + \left\{\left[H - (m - \frac{1}{2})H_m\right] \tan\frac{\alpha}{2}\left[1 - \frac{1}{K}(k - \frac{1}{2})\right]\right\}} \qquad (3\text{-}34)$$

Optical depth $a_{m,k}$ is:

$$a_{m,k} = \left[\frac{R \sin(\pi - \gamma_{m,k} - \mathcal{L}_{m,k}) \sin(\frac{\pi - \alpha}{2})}{\sin \mathcal{L}_{m,k} \sin(\frac{\alpha}{2} + \Phi_m)}\right] - \left[\frac{R \sin(\gamma_{m,k} - \mathcal{L}_{m,k}) \sin(\frac{\pi + \alpha}{2})}{\sin \mathcal{L}_{m,k} \sin(\Phi_m - \frac{\alpha}{2})}\right] \qquad (3\text{-}35)$$

With the aid of the above equations, one can calculate monochromatic heat flux

$$q_\nu = \frac{2J_\nu}{\beta_\nu} \sum_{m=1}^{M} \sum_{k=1}^{K} (1 - e^{-\beta_\nu a_{m,k}})\, \Omega_{m,k} \cos\theta_m \qquad (3\text{-}36)$$

The foregoing geometrical relations have been used to calculate the monochromatic flux by both Methods I and II. These calculations were performed for different flame geometries and different fuels. The flames were sub-divided using N = 6 and M = 6. The number of sub-divisions was limited by computer storage.

CHAPTER IV

NUMERICAL INTEGRATION TO OBTAIN TOTAL FLUX

In the theoretical derivation, the equations of flux are given as that portion of the radiation characterized by frequencies in the interval ν and $\nu + d\nu$. It can be readily seen that the mathematical relationship that exists between the monochromatic flux and the total radiation flux is as follow:

$$q' = \int_0^\infty q_\nu \, d\nu \tag{4-1}$$

The monochromatic flux for Methods I and II are:

$$q_\nu = \frac{2J_\nu}{\beta_\nu} \sum_{m=1}^{M} \sum_{k=1}^{K} (1 - e^{-\beta_\nu a_{m,k}}) \, \Omega_{m,k} \cos \theta_m \tag{4-2}$$

and

$$q_\nu = 2I_{bb,\nu} \sum_{m=1}^{M} \sum_{k=1}^{K} (1 - e^{-\beta_\nu a_{m,k}}) \, \Omega_{m,k} \cos \theta_m \tag{4-3}$$

respectively. In Equations 4-2 and 4-3, β_ν and J_ν can not be expressed analytically. To get the total radiation flux, one must integrate the monochromatic flux q_ν numerically. The numerical integration method used to evaluate the total radiation flux q is presented here.

If the definite integral

$$\int_a^b f(x)dx \tag{4-4}$$

is to be computed from a given number of values f(x), just where should these values be taken in order to give a result of greatest possible accuracy? In other words, how shall the interval (a,b) be sub-divided so as to give the best possible results?

It turns out that the points of sub-division should not be equidistant, but they are symmetrically placed with respect to the midpoint of the interval of integration. This result is shown to be true in the development which follows.

Let

$$I = \int_a^b ydx \tag{4-5}$$

denote the integral to be computed, where

$$y = f(x) \tag{4-6}$$

On changing the variable by substitution of

$$x = \frac{(b - a)}{2} u + \frac{a + b}{2} \tag{4-7}$$

the limits of integration become

$$b = \left(\frac{b-a}{2}\right)u + \frac{a+b}{2}$$

$$\left(\frac{b-a}{2}\right) = \left(\frac{b-a}{2}\right)u, \qquad u = 1 \tag{4-8}$$

$$a = \left(\frac{b-a}{2}\right)u + \frac{b+a}{2}$$

$$-\left(\frac{b-a}{2}\right) = \left(\frac{b-a}{2}\right)u, \qquad u = -1 \tag{4-9}$$

Then the new value of y is:

$$y = f(x) = f\left[\left(\frac{b-a}{2}\right)u + \frac{a+b}{2}\right] = \Theta(u), \text{ say.} \tag{4-10}$$

Then since

$$dx = \left(\frac{b-a}{2}\right)du \tag{4-11}$$

the integral becomes

$$I = \frac{b-a}{2}\int_{-1}^{1} \Theta(u)\,du \tag{4-12}$$

Gauss's formula is (1):

$$I = \int_{-1}^{1} \Theta(u)\,du = R_1\Theta(u_1) + R_2\Theta(u_2) + \cdots + R_n\Theta(u_n) \tag{4-13}$$

where u_1, u_2, --- u_n are the points of sub-division of the interval u = 1 to u = +1. The corresponding values of x are, therefore,

$$x_1 = \left(\frac{b - a}{2}\right)u_1 + \frac{a + b}{2} \tag{4-14}$$

$$x_2 = \left(\frac{b - a}{2}\right)u_2 + \frac{a + b}{2} \tag{4-15}$$

etc.

$$I = \int_a^b f(x)dx = \left(\frac{b - a}{2}\right) \sum_{i=1}^{n} R_i \Theta(u_i) \tag{4-16}$$

A detailed derivation of Gauss's formula is not given, but it will be shown how the values of u_1, u_2, ---, u_n and R_1, R_2, ---, R_n are found and applied. Let us assume that $\Theta(u)$ can be expanded in a convergent power series in the interval

$$u = -1 \text{ to } u = 1$$

Hence, one writes

$$\Theta(u) = \sum_{i=0}^{n} a_i u^i \tag{4-17}$$

One also assumes that the integral can be expressed as a linear function of the ordinates of the form given in reference (1). Integrating Equation 4-16 between the limits -1 and 1 yields

$$I = \int_{-1}^{1} \Theta(u)du = \int_{-1}^{1} (a_o + a_1 u + a_2 u^2 + --- + a_n u^n + ---)du$$

$$= 2a_o + \frac{2}{3} a_2 + \frac{2}{5} a_4 + \frac{2}{7} a_6 + ---$$

$$= 2 \sum_{i=0}^{n} \frac{a_{2i}}{2i + 1} \qquad (4\text{-}18)$$

From Equation 4-13, one also obtains

$$\Theta(u_1) = \sum_{i=0}^{m} a_i \; u_1^i$$

$$\Theta(u_2) = \sum_{i=0}^{m} a_i \; u_2^i$$

----- ---------

----- ---------

$$\Theta(u_n) = \sum_{i=0}^{m} a_i u_n^i \qquad (4\text{-}19)$$

Upon substituting these values of $\Theta(u_1)$, $\Theta(u_2)$, ---, $\Theta(u_n)$ into Equation 4-17, the integral becomes

$$I = \sum_{j=1}^{n} \sum_{i=0}^{m} R_j \; a_i \; u_j^i \qquad (4\text{-}20)$$

or rearranging

$$I = \sum_{i=0}^{n} \sum_{j=1}^{m} a_i R_j u_j^i \qquad (4\text{-}21)$$

Now if the integral I in Equation 4-21 is to be identically the same as the I in Equation 4-18 for all values of a_o, a_1, etc; that is, if Equation 4-21 is to be identical with Equation 4-18 regardless of the form of function $\Theta(u)$, then the corresponding coefficients a_o, a_1, a_2, etc., in Equations 4-21 and 4-18 must be equal. Thus, it is observed that

$$\sum_{j=1}^{n} R_j = 2 \qquad (4\text{-}22)$$

$$\sum_{j=1}^{n} R_j u_j = 0 \qquad (4\text{-}23)$$

$$\sum_{j=1}^{n} R_j u_j^2 = \frac{2}{3} \qquad (4\text{-}24)$$

and in general

$$\sum_{i=0}^{m} \sum_{j=1}^{n} R_j u_j^i = \frac{2}{i + 1} \text{ for even values of } i \qquad (4\text{-}25)$$

$$= 0 \qquad \text{for odd values of } i \qquad (4\text{-}26)$$

By taking 2n of these equations and solving them simultaneously, it would be theoretically possible to find

2n quantities u_1, u_2, ---, u_n and R_1, R_2, ---, R_n; however, the labor of solving these equations by the ordinary methods of algebra would be quite prohibitive even for small values of n. Fortunately, a formula from mathematics makes such labor unnecessary.

It can be shown without difficulty that if $\Theta(u)$ is a polynomial of degree not higher than 2n - 1, then u_1, u_2, ---, u_n are the zeros of the Legendre polynomial $P_n(u)$, or the roots of $P_n(u) = 0$. These roots are conveniently found from the equation

$$\frac{d^n}{du^n} [u^2 - 1]^n = 0 \tag{4-27}$$

where n denotes the total number of values of the function to be realized.

The n roots u_1, u_2, ---, u_n of this nth degree equation are all real. On substituting the u values into Equation 4-25, one finds the corresponding values of R. This is illustrated for the case n = 3.

The equation to be solved is:

$$\frac{d^3}{du^3} (u^2 - 1)^3 = 0$$

$$\frac{d^3}{du^3} (u^6 - 3u^4 + 3u^2 - 1) = 0 \tag{4-28}$$

Performing the differentiation and simplifying, one obtains

$$u(5u^2 - 3) = 0 \tag{4-29}$$

$$u = 0 \quad \text{and} \quad u = \pm\sqrt{\frac{3}{5}} \tag{4-30}$$

Hence,

$$u_1 = -\sqrt{\frac{3}{5}} \qquad u_2 = 0 \qquad u_3 = \sqrt{\frac{3}{5}} \tag{4-31}$$

Then from the first three Equations 4-22, 4-23 and 4-24, it is found that

$$R_1 + R_2 + R_3 = 2 \tag{4-32}$$

$$-\sqrt{\frac{3}{5}}\, R_1 + \sqrt{\frac{3}{5}}\, R_3 = 0 \tag{4-33}$$

$$\frac{3}{5} R_1 + \frac{3}{5} R_2 = \frac{2}{3} \tag{4-34}$$

Therefore,

$$R_1 = R_3 = \frac{5}{9} \tag{4-35}$$

$$R_2 = \frac{8}{9} \tag{4-36}$$

It is to be noted that u's are symmetrically placed with respect to the midpoint of the interval of integration and that the R's are the same for each symmetric pair of u's.

To integrate the monochromatic flux curves in Appendix B, the numerical integration method was used with n = 40. To do this, a clear plastic template was made with forty divisions on it. This quadrative template was placed on each curve, then the values of functions at each u were read. These values were multiplied by corresponding weight factors and summed. Figures in Appendix C show the total predicted flux for a given geometry and fuel plotted versus the distance of the target from the flame. Such total flux values have been tabulated for both Methods I and II.

CHAPTER V

CLOSED FORM INTEGRATION

The temperature distribution in Chapters II, III and IV must be known, or it might be assumed as one average temperature as was done in Method II. This temperature distribution for the Butane-Air flame is given by K. Wohl and F. Welty (63) to be linear along the center of the flow line and outward. If such a linear distribution exists, temperature at any point is given by:

$$T_{m,k} = \frac{(k - \frac{1}{2})}{k} T_c - \left(\frac{T_h - T_o}{M}\right)(m - \frac{1}{2}) + T_o$$

$$+ \left(\frac{T_h - T_o}{M}\right)(m - \frac{1}{2}) + T_o \qquad (5\text{-}1)$$

where

T_c = measured temperature at k = K

T_h = measured temperature at m = M

T_o = measured temperature at m = 1

Since the flame is divided into small sections, it is reasonable to assume that within each section there is thermodynamic equilibrium and the temperature is given by the above equation. Thus, the monochromatic flux will be as it was in Method II with only slight modification.

$$q_\nu = 2C_1 \lambda^{-5} \sum_{m=1}^{M} \sum_{k=1}^{K} \frac{1 - e^{-\beta_\nu a_{m,k}}}{\exp(\frac{C_2}{\lambda T_{m,k}}) - 1} \Omega_{m,k} \cos \theta_m \tag{5-2}$$

The monochromatic absorption coefficient β_ν, is dependent upon the wave length of the radiation; and a convenient mathematical form for this dependence, valid over a limited wave length range, is:

$$\beta_\nu = \frac{P}{\lambda^\alpha} \tag{5-3}$$

Hottel (27) determined the value of α as 0.95 and 1.39 for the infrared and visible region, respectively. Schack (46) determined the value $P = 5.7 \times 10^5$ for the visible region. In order to simplify the mathematical manipulation, the value of α is taken as 1.0 in order to calculate the total flux.

$$q = \int_0^\infty q_\nu d\nu \tag{5-4}$$

therefore,

$$q = 2C_1 \sum_{m=1}^{M} \sum_{k=1}^{K} \int_0^\infty \left[\frac{\lambda^{-5}}{\exp\left(\frac{C_2}{\lambda T_{m,k}}\right) - 1} \left(1 - e^{-\frac{a_{m,k} P}{\lambda}}\right) \right] \left[\Omega_{m,k} \cos \theta_{m,k} \right] d\lambda \tag{5-5}$$

change of variable

$$\xi_{m,k} = \frac{C_2}{\lambda T_{m,k}} \tag{5-6}$$

$$X_{m,k} = \frac{P a_{m,k} T_{m,k}}{C_2} \tag{5-7}$$

Substituting Equations 5-6 and 5-7 into Equation 5-5

$$q = \frac{2C_1}{C_2^4} \sum_{m=1}^{M} \sum_{k=1}^{K} \left[T_{m,k}^4 \, \Omega_{m,k} \cos \theta_{m,k} \right] \left[\int_0^\infty \frac{\xi_{m,k}^3}{\left(e^{\xi_{m,k}} - 1\right)} \left(1 - e^{-X_{m,k} \xi_{m,k}}\right) d\xi \right] \tag{5-8}$$

Simplifying, one obtains

$$q = \frac{2C_1}{C_2^4} \sum_{m=1}^{M} \sum_{k=1}^{K} [T^4_{m,k}\ \Omega_{m,k} \cos \theta_{m,k}]$$

$$\left[\int_o^\infty \frac{\xi^3_{m,k}}{e^{\xi_{m,k}} - 1}\, d\xi \ - \int_o^\infty \frac{\xi_{m,k} e^{-X_{m,k}\, \xi_{m,k}}}{e^{\xi_{m,k}} - 1}\, d\xi\right] \tag{5-9}$$

From mathematics (1), one has the following integral in a general form

$$\int_o^\infty \frac{t^n}{e^t - 1}\, dt = n!\ \ \zeta(n + 1) \tag{5-10}$$

where

$$\int_o^\infty \frac{t^n}{e^t - 1}\, dt \quad \text{is the Debye Function} \tag{5-11}$$

and

$$\zeta(n + 1) \quad \text{is the Reimann Zeta Function} \tag{5-12}$$

for $n = 3$ (1).

$$\zeta(3 + 1) = \frac{\pi^4}{90} \tag{5-13}$$

Therefore, the first integral term in Equation 5-9 is:

$$\int_o^\infty \frac{\xi^3_{m,k}}{e^{\xi_{m,k}} - 1}\, d\xi = \frac{\pi^4}{15} \tag{5-14}$$

Also, one has the following integral in general form from mathematics:

$$\int_0^\infty \frac{\xi^n}{e^\xi - 1} e^{-X\xi} \, d\xi = \frac{d^{n+1}}{dX^{n+1}} \Gamma^{(X+1)}$$

$$= \Psi^{(n)} (X + 1) \qquad (5\text{-}15)$$

Therefore, the second integral term in Equation 5-9 is:

$$\int_0^\infty \frac{\xi^3_{m,k} \, e^{-X_{m,k} \, \xi_{m,k}}}{e^{\xi_{m,k}} - 1} \, d\xi = \Psi^{(3)} (X_{m,k} + 1) \qquad (5\text{-}16)$$

Substituting the integral equations into Equation 5-9

$$q = \frac{2C_1}{C_2} \sum_{m=1}^{M} \sum_{k=1}^{K} \left[T^4_{m,k} \, \Omega_{m,k} \cos \theta_{m,k} \right]$$

$$\left[\frac{\pi^4}{15} - \Psi^{(3)} (X_{m,k} + 1) \right] \qquad (5\text{-}17)$$

where $\Psi^{(3)} (X_{m,k} + 1)$ is the fourth derivative of the Gamma function with argument $(X_{m,k} + 1)$ which can be found either from the Gamma function tables or by substitution of the expression into Equation 5-17 so that its value can be calculated automatically within the computer program. In general,

$$\Psi^{(n)}(1 + z) = (-1)^{n+1} \left\{ n!\,\zeta(n + 1) + \sum_{p=2}^{\infty} \left[(-1)^{p-1}\right] \left[\frac{(n + p - 1)!}{(p - 1)!}\,\zeta(n + p) z^{p-1}\right]\right\} \tag{5-18}$$

where

$$\zeta(n) = \sum_{M=1}^{\infty} M^{-n} \tag{5-19}$$

therefore,

$$\Psi^{(3)}(1 + X_{m,k}) = \frac{\pi}{15} + \sum_{p=2}^{\infty} \left\{\left[(-1)^{p-1}\,\frac{(2 + p)!}{(p - 1)!}\right] \sum_{M=1}^{\infty} \left[M^{(3+p)}\, X_{m,k}^{p-1}\right]\right\} \tag{5-20}$$

The monochromatic flux will be

$$q = \frac{2C_1}{C_2^4} \sum_{m=1}^{M} \sum_{k=1}^{K} T_{m,k}^4\, \Omega_{m,k} \cos\theta_{m,k} \sum_{p=2}^{\infty} (-1)^p \frac{(2 + p)!}{(p - 1)!} \sum_{M=1}^{\infty} M^{(3+p)}\, X_{m,k}^{(p-1)} \tag{5-21}$$

As was mentioned before, the above equation is valid only in a limited range were monochromatic absorption coefficient is present as in Equation 5-3.

CHAPTER VI

EXPERIMENTAL FLUX MEASUREMENTS

A number of total flux measurements were made to test the validity of the predicted methods described in the preceding chapters. The experimental studies were carried out with free-burning acetone and methanol diffusion flames. The total radiation flux measurements were taken with a Hy-Cal, Constantan foil type, Pyrheliometer and recorded on a Speedomax G recorder. The radiometer output was amplified with a Hewlett-Packard 413 A DC Null voltmeter. A potentiometer was used prior to each measurement to calibrate the recorder. The apparatus used for the total flux measurements is shown in Figure 6.

The total radiation flux measurements were made from sheet and cylindrical flames. The flame shapes were obtained by burning the fuel in a channel and a circular pool, respectively. Measurements were made of the laboratory flame dimensions on the flames from which the experimental total radiation data were obtained. These dimensions were used in the flame geometry equations to calculate theoretical total radiation fluxes corresponding to the flames from which the radiation measurements were made. The target location used was described by the distance from the radiometer face to the base of the flame. Ten different distances were employed. Several of these recorded radiometer outputs are given in Appendix C. The output fluctuations are the results of flame instability and the high sensitivity of the recorder. The average value of total radiation flux was taken from these figures.

The Pyrheliometer has been calibrated against the black body source, which has a $\pm$ three (3) percent accuracy and $\pm$ one and one-half ($1\frac{1}{2}$) percent repeatability. The total flux reproducibility was within $\pm$ five (5) percent.

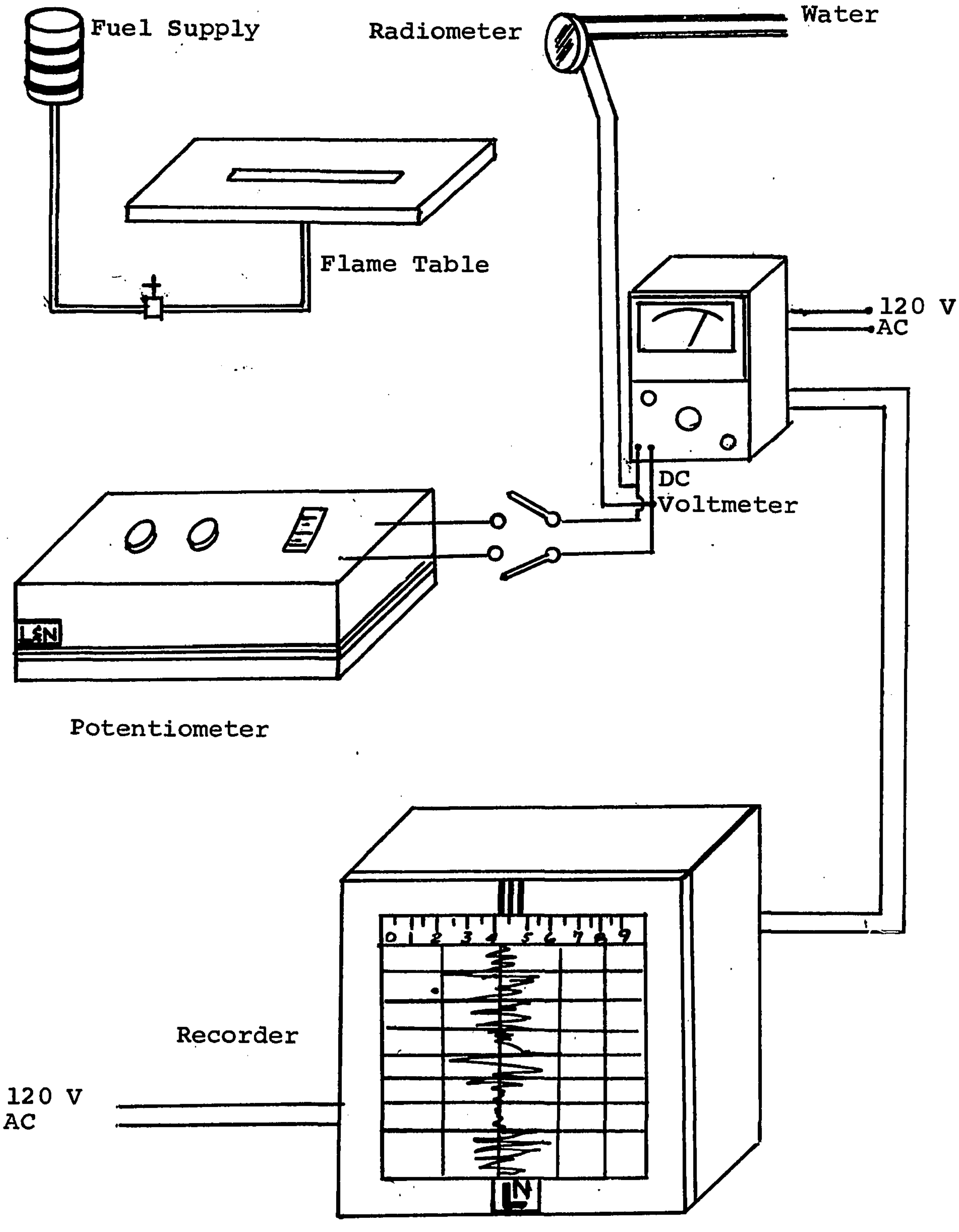

Figure 6. Instrumentation

CHAPTER VII

DISCUSSION OF RESULTS

The geometrical relations for sheet and cylindrical flames were applied in Methods I and II for the monochromatic flux calculations. Conical flames were not tested because this geometry could not be produced in the laboratory. Some difficulties in obtaining reproducible total flux measurements were encountered when the radiometer was close to the flame. However, it was possible to obtain consistency and reproducibility when the flame was sufficiently removed from the radiometer to avoid interaction effects. Total flux measurements to targets at various positions and angles of tilt were made using sheet and cylindrical shaped flames, from acetone and methanol fires. Since the laboratory flames were relatively small, the output fluctuations of the recorder became larger as the radiometer was moved closer to the flame due to interference with the natural air circulation for combustion.

The calculated total radiant energy fluxes from flames to targets were obtained by Methods I and II previously described. In each method, the total flux was obtained from the calculated monochromatic fluxes by the Gauss quadrative method. Calculated monochromatic fluxes from methanol and acetone flames for several flame-target orientations are shown in Appendix B. These calculated results were obtained on the University of Oklahoma OSAGE Computer. This machine is a relatively large high speed, digital computer designed for application to scientific data processing. The language used was OSAGE ALGOL --- a problem oriented language with a minimum of details concerning the way the machine accomplishes the computation. The programs used for the monochromatic flux calculation are presented in Appendix B.

The spectroscopic radiation properties of the flames for methanol and acetone were available up to 5 microns; above this wave length the monochromatic flux is negligible. The calculated and measured total flux results for selected flame-target geometries are shown in Appendix C for acetone and methanol flames. Method II yields a consistently higher total flux than Method I. This result is to be expected since in Method II the black body intensity $I_{bb,\nu}(T)$ corresponding to thermodynamics equilibrium, is always greater than the non-equilibrium quantity J_{ν}/β_{ν}.

It is observed in Appendix C that in all cases the experimental total fluxes are less than those calculated by Method I at larger dimensionless separation distances, but, as the separation distance is decreased, the Method I flux line is crossed and the experimental flux becomes the larger quantity. This behavior is explained by the interaction between the flame and radiometer at low S/D values.

The close agreement between the experimental measurements and those calculated by Method I suggests that the calculation technique should be suitable for engineering applications.

CHAPTER VIII

CONCLUSION

In this investigation, two facts have been established:

1. Theoretical total flux calculations based on monochromatic volume absorption and emission coefficients are in closer agreement with experimental values than are those based on the assumption of thermodynamic equilibrium.
2. The geometrical method of dividing the flame into small parts and assuming the monochromatic fluxes of all the parts to determine the flame monochromatic flux, from which the total flux to a target is found by the Gauss quadrature method, appears to be a suitable technique for engineering applications.

This work has contributed, as a final result, two computer programs, one for each method of total flux calculation. The programs permit calculation of monochromatic flux if the following information has been furnished:

1. Characteristic data of the flame:

    a. Method I. I_ν(flame), I_ν(globar), I_ν(flame + globar) and pen deflection calibration.

    b. Method II. I_ν(flame), I_ν(globar), I_ν(flame + globar) and flame average temperature.

2. Dimensions of the flame, target location and the name of the geometry.

The calculated total flux has been compared with the actual flux measured from laboratory flames of small dimensions. Verification of the calculation method for larger flames is yet to be shown.

NOMENCLATURE

A = constant

a = finite optical path length, cm

$A_{m,k}$ = projected area, cm^2

B = width of sheet flame, cm

C_1 = dimensional constant in the Planck Equation, 1.191×10^{-3}, $\frac{\text{erg micron}^2}{\text{sec}}$

C_2 = dimensional constant in the Planck Equation, 14387 micron deg K°

D = thickness of sheet flame, cm

DG = globar pen deflection

DGF = flame + globar pen deflection

DF = flame pen deflection

E = $\frac{\text{energy}}{\text{time}}$, watts

H = height, cm

I_ν = monochromatic intensity of radiation, $\frac{\text{watts}}{\text{cm}^2 - \text{cm} - \text{steradian}}$

$I_{\nu o}$ = monochromatic incident intensity of radiation, $\frac{\text{watts}}{\text{cm}^2 - \text{cm} - \text{steradian}}$

$I_{\nu g}$ = monochromatic emitted intensity of radiation, $\frac{\text{watts}}{\text{cm}^2 - \text{cm} - \text{steradian}}$

$I_{bb,\nu}$ = monochromatic black body intensity of radiation, $\frac{\text{watts}}{\text{cm}^2 - \text{cm} - \text{steradian}}$

J_ν = monochromatic volume emission coefficient, $\frac{\text{watts}}{\text{cm}^3 - \text{cm} - \text{steradian}}$

q_ν = monochromatic flux, $\frac{\text{watts}}{\text{cm}^2 - \text{cm}}$

m = mass, lb

P = defined by Equation 5-3

t = time, sec

T = temperature, deg K°

R = radius, cm

x = arbitrary optical path length, cm

X = defined by Equation 5-7

z = arbitrary quantity of a system

$\bar{z}$ = equilibrium value of z

Z = number of collisions necessary to bring about equilibrium

α_ν = monochromatic absorptance

α = angle of tilt

β_ν = monochromatic volume extinction coefficient, cm^{-1}

β = angle of tilt

ϵ_ν = monochromatic emissivity, dimensionless ratio of the energy emitted from the flame to the energy emitted from a black body at the same temperature

λ = wave length, micron

ρ = mass density, $\frac{lb}{ft^3}$

κ_ν = monochromatic absorption coefficient, cm^{-1}

τ = relaxation time, sec

τ_c = time between collisions, sec

Ω = solid angle, steradian

θ = angle between normal to the surface and the central direction of solid angle

$\mathcal{S}$ = sweep angle

Φ = angle between central direction for the solid angle and target surface

$\Theta(u)$ = function defined by Equation 4-13

ξ = function defined by Equation 5-6

ζ = Reimann Zeta Function

Γ = Gamma Function

Ψ = operator defined by Equation 5-15

ν = frequency of radiation, sec^{-1}

SUBSCRIPTS

ν = monochromatic

bb = black body

m,k = subdivision indices

BIBLIOGRAPHY

1. Abramowitz, M. and Stegun, I.A. "Handbook of Mathematical Functions with Formulas, Graphs and Mathematical Tables," National Bureau of Standards Applied Mathematics Series 55.

2. Agnew, J.T., Agnew, W.G. and Wark, K. Comparison of Emission Spectra of Low Temperature Combustion Reactions Produced in an Engine and in a Flat-Flame Burner, Sixth Symposium on Combustion and Flame (International), New York: Reinhold Publishing Corporation, 1957.

3. Agnew, W.G., Agnew, J.T. and Wark, K., Jr. Infrared Emission from Cool Flames, Stablilized Cool Flames, Engine Cool Flame Reactions, Gas Temperature Deduced from Infrared Emission, Fifth Symposium on Combustion and Flame (International), New York: Reinhold Publishing Corporation, 1957.

4. Ambrose, Eggleston and Yaill. "The Use of Models for the Investigation of Fire Spread," AD 416-537, January 1, 1964.

5. Ausloos, P. and Van Tiggelen, A. Quantitative Spectrographic Investigation of Flames, Fourth Symposium on Combustion and Flame (International), Baltimore, Maryland: The Williams and Wilkins Company, 1953.

6. Babrov, Harold J. "Experimental and Theoretical Infrared Spectral Absorptance of HC_1 at Various Temperatures," Journal of the Optical Society of America, Vol. 53, No. 8, August, 1963.

7. Babrov, Harold J. "Instrumental Effects in Infrared Gas Spectra and Spectroscopic Temperature Measurements," Journal of the Optical Society of America, Vol. 51, No. 2, February, 1961.

8. Babrov, Harold J. and Tourin, R.H. "Methods for Predicting Infrared Radiance of Flames by Extrapolation from Laboratory Measurements," Journal of Quanti-

tative Spectroscopic Heat Transfer, Vol. 3, Great Britain: Pergamon Press, Ltd., 1963.

9. Bell, E.E., Burnside, P.B. and Dickey, F.P. "Spectral Radiance of Some Flames and Their Temperature Determination," Journal of the Optical Society of America, Vol. 50, No. 12, December, 1960.

10. Benedict, W.S. and Phyler, E.K. "High-Resolution Spectra of Hydrocarbon Flames in the Infrared," National Bureau of Standards Circular, No. 523, 1954.

11. Bevans, J.T. "Radiant Heat Transfer Analysis of a Furnace or Other Combustion Enclosure," ASME Journal of Heat Transfer, Vol. 83, Series C, No. 2, May, 1961.

12. Broida, H.P. "Temperature, Its Measurement and Control in Science and Industry," Experimental Temperature Measurements in Flames and Hot Gases, Vol. II, New York: Reinhold Publishing Corporation, 1955.

13. Campbell, Heinen and Schalit. "A Theoretical Study of Some Properties of Laminar Steady State Flames As a Function of Properties of Their Chemical Components," AD 432-553, May 15, 1964.

14. Cashion, J.K. and Polanyi, J.C. "Infrared Chemiluminescence I," Proceedings of the Royal Society of London, Vol. 258, 1960.

15. Cassel, H.M., Das Gupta, A.K. and Guraswamy, S. Factors Affecting Flame Propagation Through Dust Clouds, Third Symposium on Combustion and Flame (International), Baltimore, Maryland: The Williams and Wilkins Company, 1949.

16. Chandrasekhar, S. Radiative Transfer, Dover: 1961.

17. Child, E.T. and Wohl, K. Spectrophotometric Studies of Laminar Flames, Seventh Symposium on Combustion and Flame (International), London: Butterworths Scientific Publications, 1959.

18. Coblentz, W.W. "Investigations of Infrared Spectra, Part I," Carnegie Institution of Washington, 1905.

19. Cole, D.J. and Minkoff, G.J. "Experimental Techniques for the Study of Flat Flames by Infrared Spectroscopy," Combustion and Flame, Vol. I, No. 2, London: Butterworths Scientific Publications, June, 1957.

20. Daly, E.F. and Sutherland, G.B.B.M. The Emission Spectrum of Carbon Dioxide at 4.3μ, Third Symposium on Combustion and Flame (International), Baltimore, Maryland: The Williams and Wilkins Company, 1949.

21. Davidson and Russell. "Project Hot Shot Particle Thermal Radiation," AD 418-974, February 15, 1964.

22. Eulner, R., Mertens, J. and Potter, R.L. "Thermal Radiation from Flourine-Ammonia Flames," Combustion and Flame, Vol. V, No. 1, London: Butterworths Scientific Publications, March, 1961.

23. Ferriso, C.C. The Emission of Hot CO_2 and H_2O in Small Rocket-Exit Exhaust Gases, Eighth Symposium on Combustion and Flame (International), Baltimore, Maryland: The Williams and Wilkins Company, 1962.

24. Freeman, M.P. and Katz, S. "Determination of the Radial Distribution of Brightness in a Cylindrical Luminous Medium with Self-Absorption," Journal of the Optical Society of America, Vol. 50, 1960.

25. Garvin, D. and Broida, H.P. Atomic Reactions Involving N Atoms, H Atoms and Ozone, Ninth Symposium on Combustion and Flame, New York: Academic Press, 1963.

26. Hood, J.D. Spectroscopic Study of Hydrocarbon Flames, Ph.D. Thesis, University of Oklahoma (unpublished).

27. Hottel, H.C., Williams, G.C. and Jensen, W.P. "Optical Methods of Measuring Plasma Jet Temperatures," Aeronautical Systems Division, Air Force Systems Command, Wright-Patterson Air Force Base, Ohio, 1961.

28. Hozlett, Eberhart and Davis. "Effect of High Thermal Radiation Flux on Several Metal Alloys," AD 434-448, June 1, 1964.

29. Kurlbaum, F. "Line Reversal Method for Temperature Measurement," Physikalishce Zeitscrift, Vol. 3, 1902.

30. Kushida, R. and Wohl, K. Spectrophotometric Studies of Laminar Flames II. The Flame Front, Seventh Symposium on Combustion and Flame (International), London: Butterworths Scientific Publications, 1959.

31. Lapp, M., Gray, L.D. and Penner, S.S. "Equilibirum

Emissivity Calculations for CO_2," International Developments in Heat Transfer, Part IC, ASME, 1961 (Papers presented at the 1961 International Heat Transfer Conference).

32. Leah, A. Smeeton and Watson, H. "Radiation from Explosion Flames of Carbon Monoxide," Combustion and Flame, Vol. III, No. 2, London: Butterworths Scientific Publications, June, 1959.

33. Lewis, B. and Von Elbe, G. Combustion, Flames and Explosions, New York: Academic Press, 1951.

34. Linan. "On the Structure of Laminar Diffusion Flames," AD 432-822, May 15, 1964.

35. Love, Tom J., Jr. An Investigation of Radiant Heat Transfer in Absorbing, Emitting and Scattering Media, Norman, Oklahoma: University of Oklahoma Research Institute, 1963 (Contract AF33 (657) - (8859 (ARL63-3).

36. Love, T.J., Jr. (Radiative Heat Transfer text to be published in 1966 by Charles E. Merrill Books, Inc., Columbus, Ohio).

37. Millikan, R.C. "Infrared Analysis for Acetylene in Flame Gases at 1820K," Combustion and Flame, Vol. V, No. 4, London: Butterworths Scientific Publications, December, 1961.

38. Millikan, R.C. "Optical Properties of Soot," Journal of the Optical Society of America, Vol. 51, 1961.

39. Mock, W.K. Radiative Transfer in Dust Flames, Sixth Symposium on Combustion and Flame (International), New York: Reinhold Publishing Corporation, 1957.

40. Mujama, Hajime. "Spectroscopic Studies of OH Radicals in Gaseous Detonations," Combustion and Flame, Vol. V, No. 4, London: Butterworths Scientific Publications, December, 1962.

41. Penzias, G.J., Gillman, S., Liang, E.T. and Tourin, R.H. An Atlas of Infrared Spectra of Flames, Part Two, Hydrocarbon-Oxygen Flames 4-15μ, Ammonia-Oxygen 1-15μ and Flames Burning at Reduced Pressures," AFCRL-848(II), Geophysics Research Directorate, Hanscom Field, Bedford, Massachusetts, 1961.

42. Penzias, G.J. and Tourin, R.H. "Methods for Infrared Analysis of Rocket Flames in Situ," Combustion

and Flame, Vol. VI, No. 3, London: Butterworths Scientific Publications, September, 1962.

43. Rhodes, M.S. "An Examination of Two Dimensional Heat Transfer Configuration Factors with Absorbing Medium," International Developments in Heat Transfer, Part IV, ASME, 1961 (Papers presented at the 1961 International Heat Transfer Conference).

44. Ryan, L.R., Penzias, G.J. and Tourin, R.H. "An Atlas of Infrared Spectra of Flames Part I. Infrared Spectra of Hydrocarbon Flames in the 1-5μ Region," AFCRL-848, Geophysics Research Directorate, Hanscom Field, Bedford, Massachusetts, 1961.

45. Sato, T. and Matsumoto, R. "Radiant Heat Transfer from Luminous Flame," International Developments in Heat Transfer, Part IV, ASME, 1961 (Papers presented at the 1961 International Heat Transfer Conference).

46. Schack, A. "Strahlung von Leuchtenden Flammen" Zeitschcrift Fur Technische Physick, Hahrg 6, Nr. 10, 1925.

47. Schmidt, H. "The Radiation Law of the Bunsen Flame," Annalen der Physick, Vol. 29, 1909.

48. Silverman, Shirleigh. The Determination of Flame Temperatures by Infrared Radiation, Third Symposium on Combustion and Flame, Baltimore, Maryland: The Williams and Wilkins Company, 1949.

49. Spokes, G.N. Emission and Absorption Spectra of Flat Flames, Seventh Symposium on Combustion and Flame, London: Butterworths Scientific Publications, 1959.

50. Tarifa. "Combustion of Solid Propellants and Flames Structures," AD 416-548, January 1, 1964.

51. Thring, W.W., Foster, P.J., McGrath, I.A. and Ashton, J.S. "Prediction of the Emissivity of Hydrocarbon Flames," International Developments in Heat Transfer, Part IV, ASME, 1961 (Papers presented at the 1961 International Heat Transfer Conference).

52. Thomas and Penner. "On Radiative Transfer Calculation from Non-Isothermal Gases," AD 427-623, April 1, 1964.

53. Tourin, R.H. "Spectroscopic Studies of Temperature

Gradients in Flames," Combustion and Flame, Vol. II, No. 4, London: Butterworths Scientific Publications, December, 1958.

54. Tourin, R.H. "Recent Developments in Gas Pyrometry by Spectroscopic Methods," ASME Publication, New York: paper number 63-WA-252, September, 1963.

55. Tourin, R.H. "Infrared Spectra of Thermally Excited Gases," National Bureau of Standards Circular, No. 523, Energy Transfer in Hot Gases, 1954.

56. Tourin, R.H. "Some Spectral Emissivities of Water Vapor in the 2.7μ Region," Journal of the Optical Society of America, Vol. 51, No. 11, November, 1961.

57. Tourin, R.H. "Infrared Spectral Emissivities of CO_2 in the 2.7 Micron Region," Infrared Physics, Vol. 1, Great Britain: Pergamon Press, Ltd., 1961.

58. Tourin, R.H. "Monochromatic Radiation Pyrometry of Hot Gases, Plasmas and Detonations," Temperature, Its Measurement and Control in Science and Industry, Vol. 3, Part 2, New York: Reinhold Publishing Corporation, 1962.

59. Tourin, R.H. "Measurements of Infrared Spectral Emissivities of Hot Carbon Dioxide in the 4.3μ Region," Journal of the Optical Society of America, Vol. 51, No. 2, February, 1961.

60. Tourin, R.H., Babrov, Harold J. and Penzias, G.J. "Infrared Radiation of Flames," AD 431-123, May 1, 1964.

61. Tourin, R.H. "Determination of Hot Gas Temperature Profiles from Infrared Emission and Absorption Spectra," Journal of the Optical Society of America, Vol. 53, 1963.

62. Tourin, R.H. and Babrov, Harold J. "Note on Absorption Coefficients of Hot CO_2 at 4.40μ," Journal of Chemical Physics, Vol. 37, No. 3, August 1, 1962.

63. Wohl, K. and Welty, F. Spectrophotometric Traverses through Flame Fronts, Fifth Symposium on Combustion and Flame (International), New York: Reinhold Publishing Corporation, 1955.

64. Yagi, S. and Sino, H. Radiation from Soot Particles in Luminous Flames, Eighth Symposium on Combustion and Flame (International), Baltimore, Maryland: The

Williams and Wilkins Company, 1962.

65. Yokobori, Susumu. "Study on the Emissivity of a Gas Which Contains Particles," International Developments in Heat Transfer, Part IV, ASME, 1961, (Papers presented at the 1961 International Heat Transfer Conference).

APPENDIX A

MONOCHROMATIC RADIATION PROPERTIES OF AN ACETONE AND A METHANOL FLAME.

TABLE I

MONOCHROMATIC RADIATION PROPERTIES OF A METHANOL FLAME BASED ON THERMODYNAMIC EQUILIBRIUM (41,44)

Wave Length microns λ	Absorptivity α_ν	Absorption Coefficient cm^{-1} β_ν
1.299999	.020000	.159076D-02
1.350000	.050000	.403884D-02
1.399999	.030000	.239836D-02
1.450000	.024999	.199352D-02
1.500000	.020000	.159076D-02
1.550000	.020000	.159076D-02
1.600000	.010000	.791365D-03
1.650000	.010000	.791365D-03
1.700000	.010000	.791365D-03
1.750000	.020000	.159076D-02
1.799999	.050000	.403884D-02
1.850000	.100000	.829610D-02
1.899999	.050000	.403884D-02
1.950000	.060000	.487207D-02
2.000000	.040000	.321433D-02
2.050000	.020000	.159076D-02
2.100000	.020000	.159076D-02
2.150000	.010000	.791365D-03
2.200000	.010000	.791365D-03
2.250000	.010000	.791365D-03
2.299999	.010000	.791365D-03
2.350000	.010000	.791365D-03
2.399999	.030000	.239836D-02
2.450000	.050000	.403884D-02
2.500000	.150000	.127967D-01
2.550000	.250000	.226521D-01
2.600000	.225000	.200702D-01

TABLE I--Continued

λ	α_ν	β_ν
2.650000	.100000	.829610D-02
2.700000	.450000	.470737D-01
2.750000	.400000	.402224D-01
2.799999	.350000	.339199D-01
2.850000	.320000	.303671D-01
2.899999	.274999	.253215D-01
2.950000	.200000	.175703D-01
3.000000	.150000	.127967D-01
3.050000	.100000	.829610D-02
3.100000	.080000	.656548D-02
3.150000	.050000	.403884D-02
3.200000	.040000	.321433D-02
3.250000	.030000	.239836D-02
3.299999	.030000	.239836D-02
3.350000	.030000	.239836D-02
3.399999	.030000	.239836D-02
3.450000	.030000	.239836D-02
3.500000	.030000	.239836D-02
3.550000	.030000	.239836D-02
3.600000	.030000	.239836D-02
3.650000	.030000	.239836D-02
3.700000	.030000	.239836D-02
3.750000	.050000	.403884D-02
3.799999	.060000	.487207D-02
3.850000	.070000	.571422D-02
3.899999	.090000	.742603D-02
3.950000	.100000	.829610D-02
4.000000	.100000	.829610D-02
4.050000	.120000	.100656D-01
4.100000	.140000	.118758D-01
4.150000	.150000	.127967D-01
4.200000	.950000	.235884D-00

TABLE I--Continued

λ	α_ν	β_ν
4.250000	.980000	.308033D-00
4.299999	.990000	.362611D-00
4.350000	.990000	.362611D-00
4.399999	.990000	.362611D-00
4.450000	.980000	.308033D-00
4.500000	.950000	.235884D-00
4.550000	.830000	.139524D-00
4.600000	.600000	.721488D-01
4.650000	.500000	.545785D-01
4.700000	.440000	.456549D-01
4.750000	.400000	.402224D-01
4.799999	.424999	.435736D-01
4.850000	.400000	.402224D-01
4.899999	.450000	.470737D-01
5.000000	.200000	.175703D-01
5.200000	.250000	.226521D-01
5.399999	.330000	.315336D-01
5.600000	.430000	.442613D-01
5.799999	.470000	.499904D-01
6.000000	.400000	.402224D-01
6.200000	.300000	.280846D-01
6.399999	.250000	.226521D-01
6.600000	.700000	.948010D-01
6.799999	.600000	.721488D-01
7.000000	.500000	.545785D-01
7.200000	.500000	.545785D-01
7.399999	.450000	.470737D-01
7.600000	.500000	.545785D-01
7.799999	.480000	.514902D-01
8.000000	.370000	.363807D-01
8.200000	.350000	.339199D-01

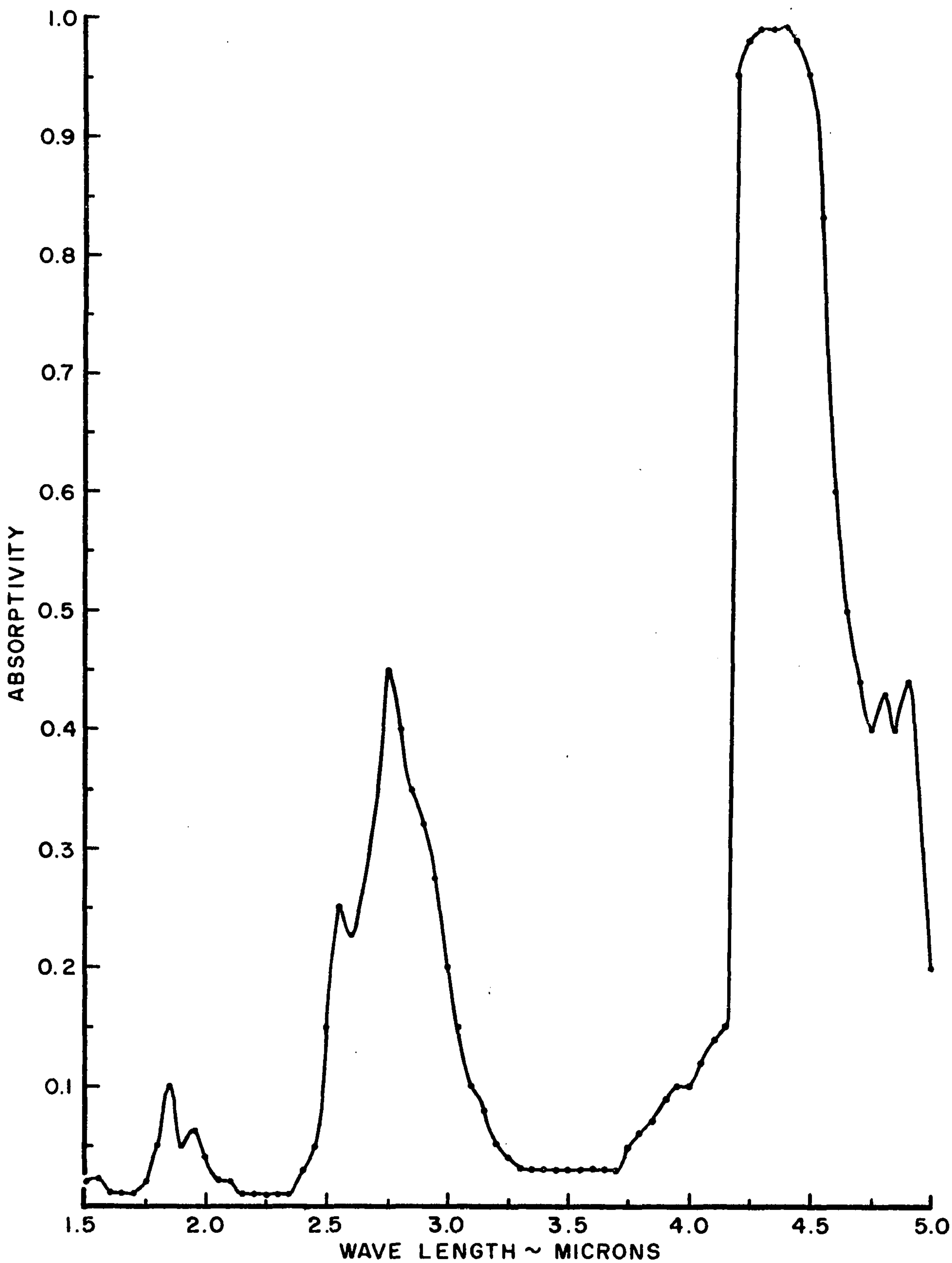

Figure 7. Spectral Absorptivity of Methanol Flame
Optical Path Length--12.7 cm
Reference: The Warner & Swasy Co. (41, 44)

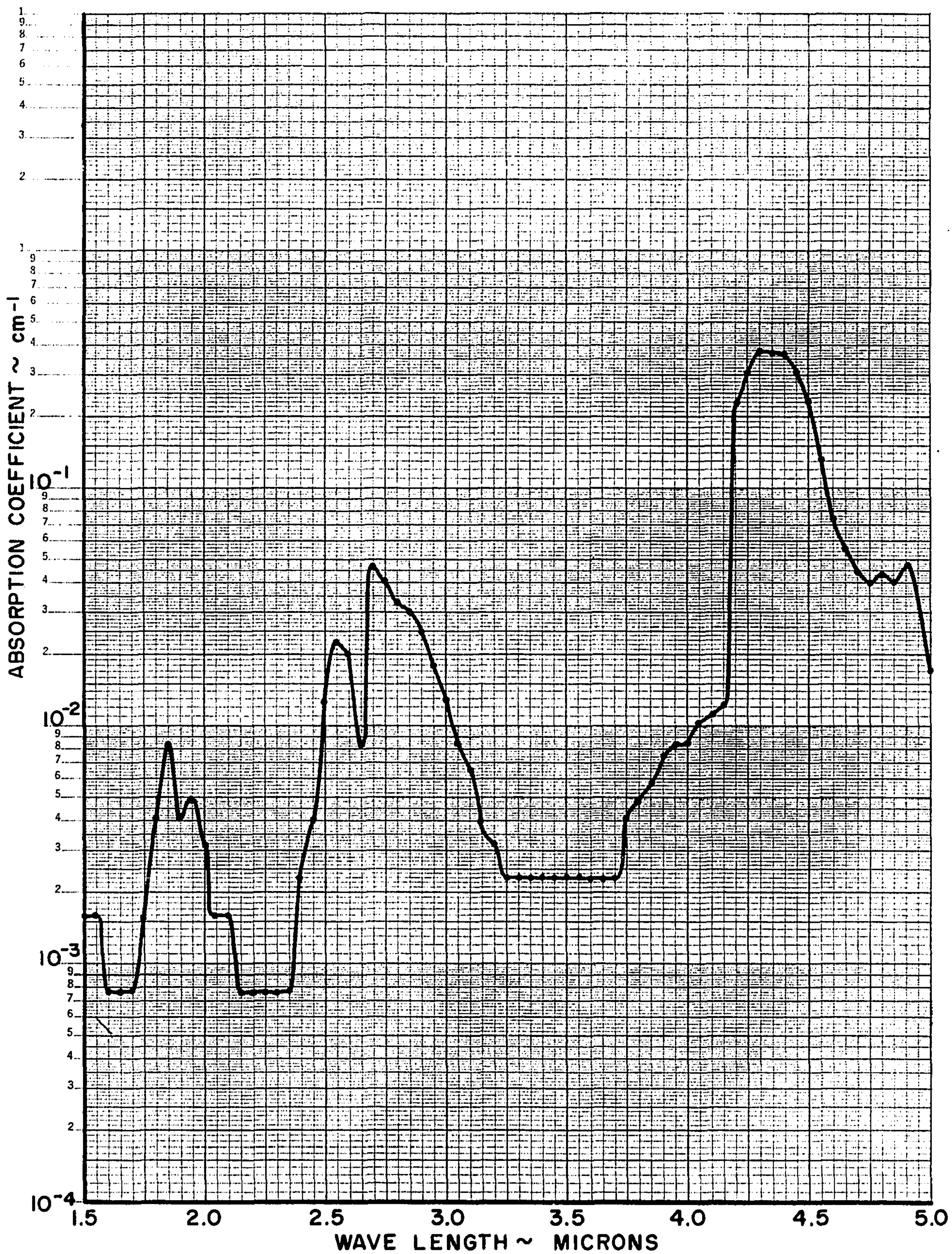

Figure 8. Spectral Absorption Coefficient of Methanol Flame

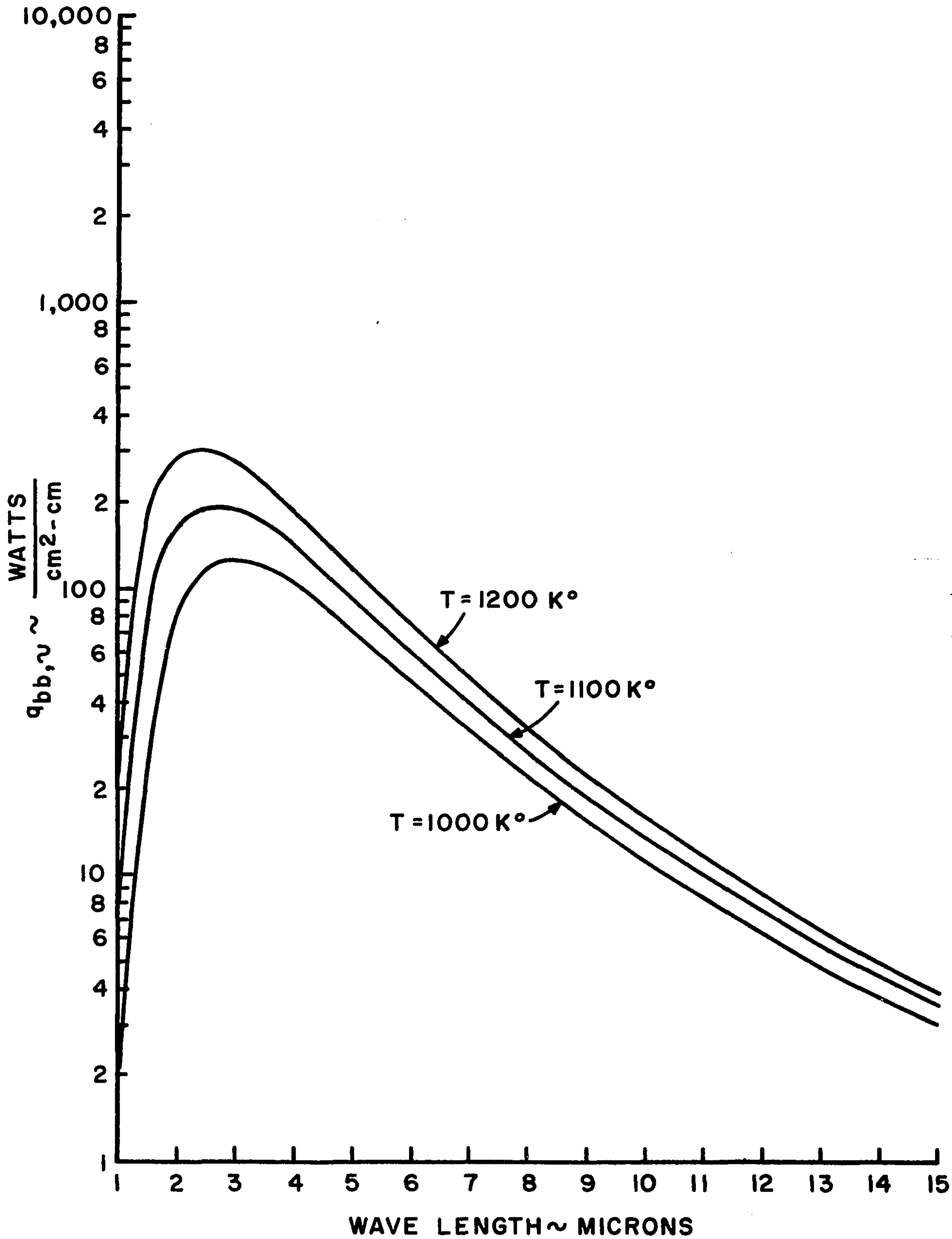

Figure 9 . Monochromatic Black Body Flux

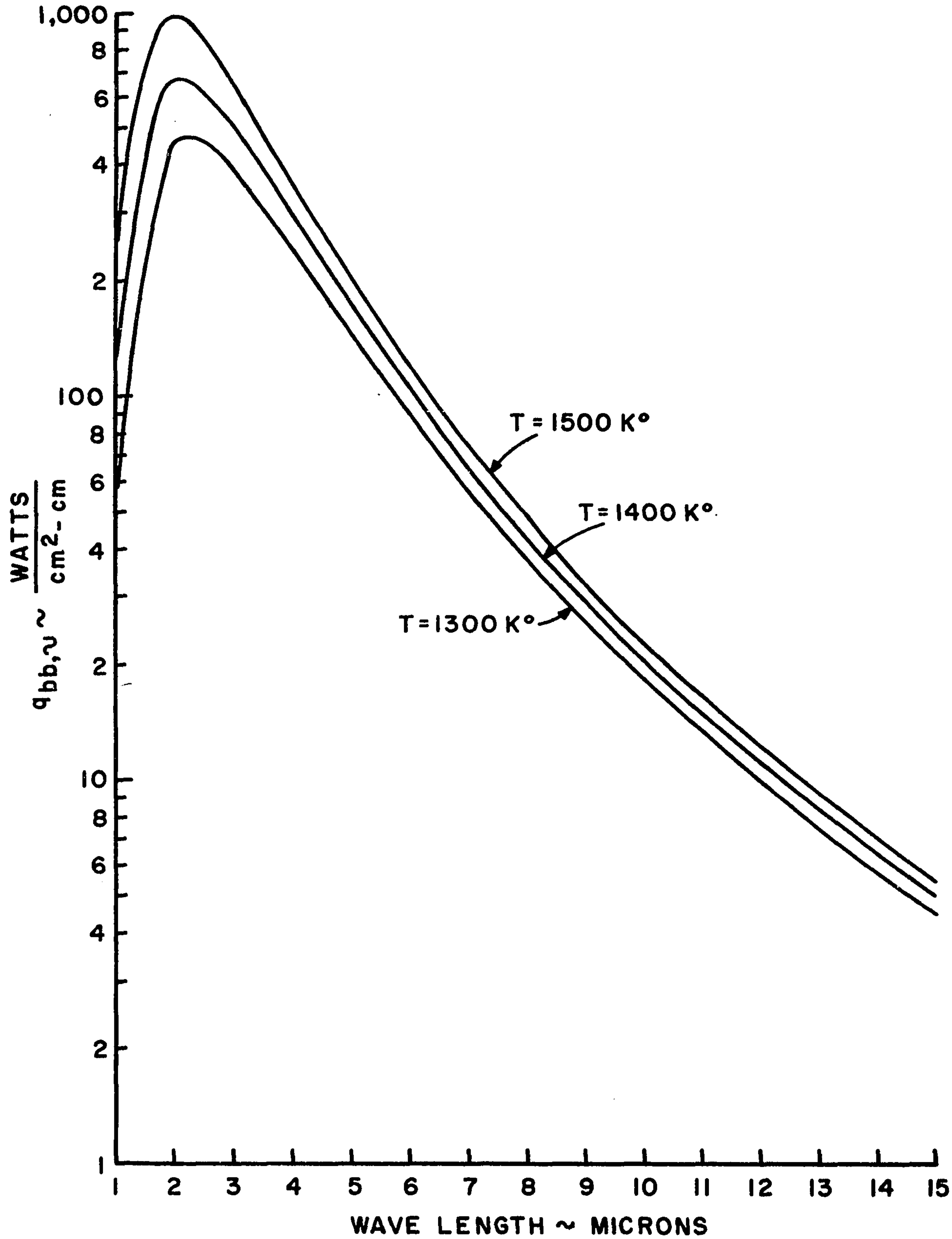

Figure 10. Monochromatic Black Body Flux

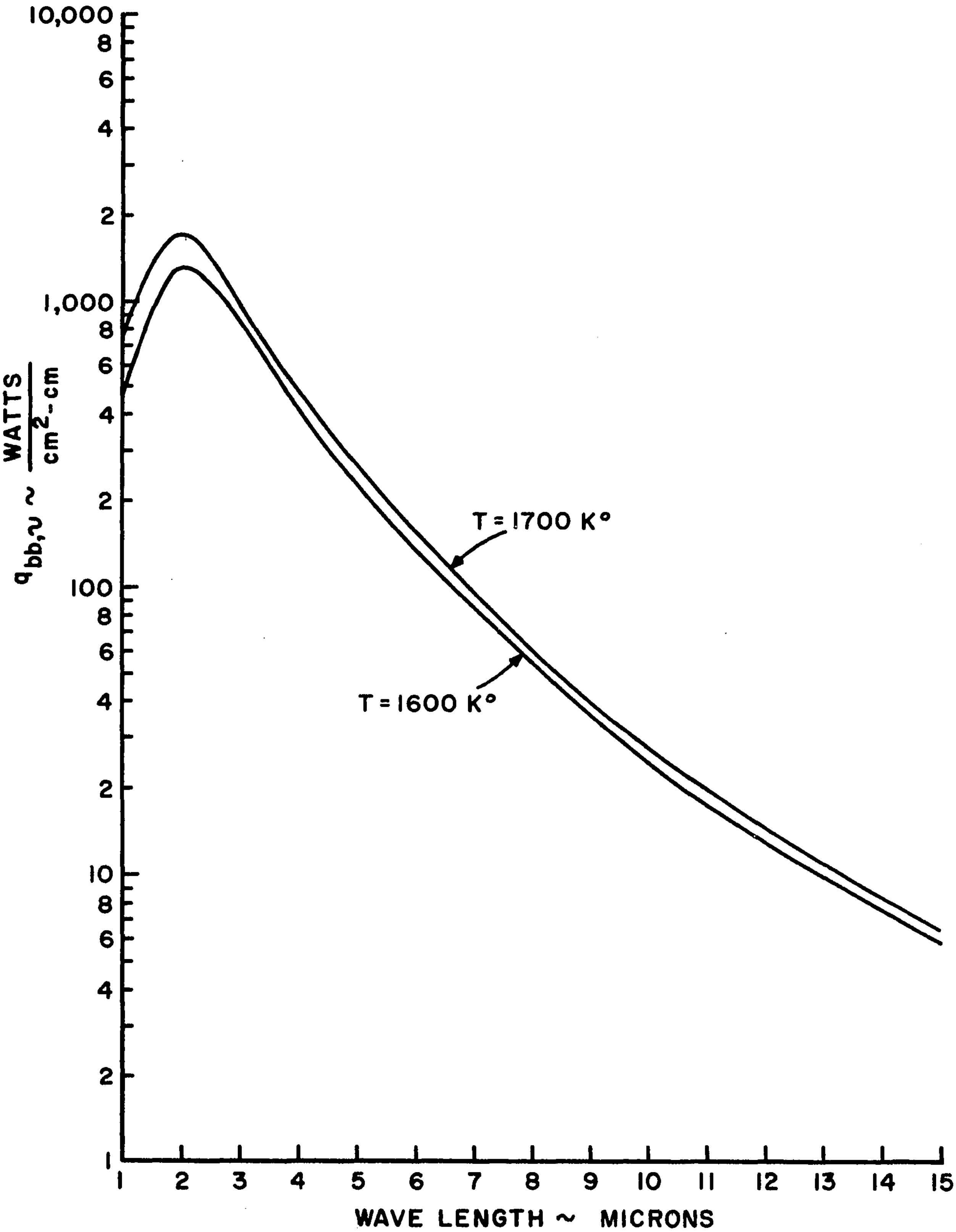

Figure 11. Monochromatic Black Body Flux

TABLE II

SPECTROSCOPIC RADIATION PROPERTIES OF A METHANOL FLAME (26)

Wave Length λ	Emitted Intensity $\frac{\text{watts}}{\text{cm}^2\text{-cm-steradian}}$ I_ν	cm^2-cm-steradian $(a\Omega\Delta\lambda) \times 10^{-9}$	Emitted Energy watts $E_\nu \times 10^{-9}$	Flame Pen Deflection DF	Globar + Flame Pen Deflection DGF	Globar Pen Deflection DG
5.22	58.087	1.176	68.31	0.010	0.120	0.115
5.07	57.020	1.198	68.31	0.010	0.140	0.134
4.99	67.578	1.213	81.972	0.012	0.147	0.138
4.91	78.069	1.225	95.634	0.014	0.154	0.142
4.83	104.922	1.237	129.789	0.019	0.160	0.147
4.75	125.690	1.250	157.113	0.023	0.175	0.152
4.73	125.190	1.255	157.113	0.023	0.179	0.156
4.71	162.772	1.259	204.930	0.030	0.184	0.154
4.69	211.101	1.262	266.409	0.039	0.190	0.155
4.67	237.788	1.264	300.564	0.044	0.200	0.156
4.65	302.369	1.264	382.536	0.056	0.208	0.158
4.64	376.809	1.269	478.170	0.070	0.220	0.158
4.62	434.993	1.272	553.311	0.081	0.236	0.160
4.60	525.462	1.274	669.438	0.098	0.255	0.160
4.58	641.911	1.277	819.720	0.120	0.275	0.160
4.57	747.725	1.279	956.340	0.140	0.300	0.161
4.55	957.617	1.284	1229.580	0.180	0.330	0.161
4.54	1072.988	1.286	1379.862	0.202	0.365	0.163
4.52	1269.899	1.291	1639.440	0.240	0.410	0.170
4.50	1536.183	1.294	1987.821	0.291	0.450	0.162

TABLE II--Continued

λ	I_ν	$(a\Omega\Delta\lambda) \times 10^{-9}$	$E_\nu \times 10^{-9}$	DF	DGF	DG
4.48	1787.945	1.299	2322.540	0.340	0.495	0.162
4.46	2037.224	1.301	2650.428	0.388	0.535	0.162
4.44	2144.495	1.306	2800.710	0.410	0.565	0.161
4.43	2369.193	1.309	3101.274	0.454	0.579	0.161
4.41	2475.000	1.311	3244.725	0.475	0.591	0.161
4.39	2580.084	1.313	3388.176	0.496	0.592	0.158
4.37	2491.550	1.316	3278.880	0.480	0.581	0.153
4.35	2192.347	1.318	2889.513	0.423	0.465	0.140
4.33	1548.980	1.323	2049.300	0.300	0.325	0.120
4.32	927.285	1.326	1229.580	0.180	0.185	0.090
4.30	461.901	1.331	614.790	0.090	0.091	0.059
4.28	178.956	1.336	239.085	0.035	0.036	0.037
4.26	81.686	1.338	109.296	0.016	0.017	0.032
4.24	81.564	1.340	109.296	0.016	0.016	0.032
4.22	81.261	1.345	109.296	0.016	0.019	0.036
4.20	121.440	1.350	163.944	0.024	0.035	0.056
4.18	302.927	1.353	409.860	0.060	0.090	0.109
4.16	423.472	1.355	573.804	0.084	0.185	0.160
4.14	301.811	1.358	409.860	0.060	0.222	0.180
4.13	100.456	1.360	136.620	0.020	0.205	0.185
4.11	20.047	1.363	27.324	0.004	0.195	0.191
4.02	19.800	1.380	27.324	0.004	0.195	0.191
3.82	19.229	1.421	27.324	0.004	0.201	0.198
3.63	18.728	1.459	27.324	0.004	0.204	0.203
3.54	32.506	1.471	47.817	0.007	0.202	0.202
3.43	15.204	1.488	22.624	0.014	0.780	0.766
3.39	20.538	1.495	30.704	0.019	0.733	0.754
3.35	21.547	1.500	32.320	0.020	0.773	0.753
3.31	22.549	1.505	33.936	0.021	0.764	0.743
3.27	25.736	1.507	38.784	0.024	0.763	0.755

TABLE II-- Continued

λ	I_ν	$(a\Omega\Delta\lambda) \times 10^{-9}$	$E_\nu \times 10^{-9}$	DF	DGF	DF
3.22	32.063	1.512	48.480	0.030	0.755	0.741
3.17	43.676	1.517	66.256	0.041	0.756	0.737
3.12	61.582	1.522	93.728	0.058	0.769	0.730
3.08	81.594	1.525	124.432	0.077	0.760	0.710
3.04	111.120	1.527	169.680	0.105	0.772	0.691
2.99	168.047	1.529	256.944	0.159	0.813	0.678
2.97	201.868	1.529	308.656	0.191	0.834	0.670
2.95	232.518	1.529	355.520	0.220	0.860	0.659
2.92	275.154	1.527	420.160	0.260	0.890	0.651
2.90	328.068	1.527	500.960	0.310	0.911	0.639
2.88	376.184	1.525	573.680	0.355	0.950	0.625
2.86	422.809	1.525	644.784	0.399	0.963	0.610
2.84	425.766	1.522	648.016	0.401	0.948	0.590
2.82	414.087	1.522	630.240	0.390	0.900	0.561
2.80	382.234	1.522	581.760	0.360	0.820	0.525
2.78	338.084	1.520	513.888	0.318	0.735	0.480
2.76	287.620	1.517	436.320	0.270	0.575	0.430
2.74	270.576	1.517	410.464	0.254	0.520	0.380
2.72	302.933	1.515	458.944	0.284	0.540	0.352
2.69	323.841	1.512	489.648	0.303	0.545	0.350
2.67	299.656	1.510	452.480	0.280	0.480	0.330
2.65	228.710	1.505	344.208	0.213	0.405	0.310
2.63	152.981	1.500	229.472	0.142	0.386	0.324
2.61	108.094	1.495	161.600	0.100	0.380	0.340
2.59	96.526	1.490	143.824	0.089	0.351	0.325
2.57	104.469	1.485	155.136	0.096	0.334	0.309
2.54	143.231	1.478	211.696	0.131	0.445	0.335
2.52	197.878	1.470	290.880	0.180	0.565	0.400
2.50	253.533	1.466	371.680	0.230	0.660	0.450
2.49	269.886	1.461	394.304	0.244	0.699	0.478
2.47	244.680	1.453	355.520	0.220	0.666	0.482

TABLE II--Continued

λ	I_{ν}	$(a\Omega\Delta\lambda) \times 10^{-9}$	$E_{\nu} \times 10^{-9}$	DF	DGF	DG
2.45	173.223	1.446	250.480	0.155	0.595	0.476
2.43	112.535	1.436	161.600	0.100	0.530	0.465
2.41	56.662	1.426	80.800	0.050	0.480	0.455
2.38	33.073	1.417	46.864	0.029	0.455	0.444
2.37	20.674	1.407	29.088	0.018	0.433	0.429
2.32	10.448	1.392	14.544	0.009	0.401	0.405
2.28	8.227	1.375	11.312	0.007	0.370	0.374
2.24	8.348	1.355	11.312	0.007	0.341	0.348
2.21	8.467	1.336	11.312	0.007	0.314	0.321
2.18	11.052	1.316	14.544	0.009	0.291	0.292
2.14	14.963	1.296	19.392	0.012	0.269	0.270
2.10	26.742	1.269	33.936	0.021	0.251	0.241
2.06	41.804	1.237	51.712	0.032	0.244	0.220
2.02	69.162	1.215	84.032	0.052	0.240	0.200
1.98	87.722	1.179	103.424	0.064	0.231	0.178
1.95	70.017	1.154	80.800	0.050	0.200	0.155
1.92	51.529	1.129	58.176	0.036	0.152	0.126
1.88	71.660	1.105	79.184	0.049	0.147	0.110
1.85	67.458	1.078	72.720	0.045	0.134	0.098
1.82	63.646	1.041	66.256	0.041	0.132	0.091
1.78	50.146	0.999	50.096	0.031	0.115	0.087
1.75	18.326	0.970	17.776	0.011	0.085	0.075
1.72	8.614	0.938	8.080	0.005	0.069	0.066
1.68	8.988	0.899	8.080	0.005	0.055	0.061
1.65	9.319	0.867	8.080	0.005	0.048	0.049
1.58	10.386	0.778	8.080	0.005	0.034	0.033
1.50	11.761	0.687	8.080	0.005	0.029	0.024

TABLE III

MONOCHROMATIC RADIATION PROPERTIES
OF A METHANOL FLAME (26)

Wave Length microns λ	Emitted Intensity $\frac{\text{watts}}{\text{cm}^2\text{-cm-steradian}}$ I_ν	Absorptivity α_ν	Absorption Coefficient cm^{-1} β_ν	Volume Emission Coefficient $\frac{\text{watts}}{\text{cm}^3\text{-cm-steradian}}$ J_ν
5.220000	58.077999	.043480	.555669D-01	.742230D+02
5.070000	57.020000	.029850	.378807D-01	.723604D+02
4.990000	67.577999	.021740	.274747D-01	.854042D+02
4.910000	78.068999	.014079	.177250D-01	.982797D+02
4.830000	104.922000	.040820	.520956D-01	.133904D+03
4.750000	125.690000	0.000000	.000000D+00	.000000D+00
4.730000	125.190000	0.000000	.000000D+00	.000000D+00
4.710000	162.772000	0.000000	.000000D+00	.000000D+00
4.691000	211.101000	.025809	.326861D-01	.267341D+03
4.670000	237.788000	0.000000	.000000D+00	.000000D+00
4.650000	302.638999	.037970	.483870D-01	.385667D+03
4.640000	376.808999	.050629	.649458D-01	.483353D+03
4.620000	434.992999	.031250	.396858D-01	.552418D+03
4.600000	525.461999	.018749	.236600D-01	.663063D+03
4.580000	641.910999	.031250	.396858D-01	.815193D+03
4.570000	747.725000	.006210	.778670D-02	.937570D+03
4.550000	957.617000	.068320	.884573D-01	.123987D+04
4.540000	1072.987999	0.000000	.000000D+00	.000000D+00
4.520000	1269.899000	0.000000	.000000D+00	.000000D+00
4.500000	1536.183000	.018520	.233670D-01	.193823D+04
4.480000	1787.944999	.043210	.552141D-01	.228465D+04
4.460000	2037.223999	.092590	.121451D-00	.267224D+04

TABLE III--Continued

λ	I_ν	α_ν	β_ν	J_ν
4.440000	2144.495000	.037269	.474778D-01	.273184D+04
4.430000	2369.192999	.223600	.316359D-00	.335204D+04
4.410000	2475.000000	.279500	.409762D-00	.362848D+04
4.390000	2580.484000	.392409	.622818D-00	.409564D+04
4.370000	2491.550000	.339869	.519148D-00	.380581D+04
4.350000	2192.347000	.700000	.150496D+01	.471343D+04
4.330000	1548.980000	.791670	.196078D+01	.383647D+04
4.320000	927.285000	.944440	.361286D+01	.354723D+04
4.299999	461.901000	.983050	.509685D+01	.239483D+04
4.280000	178.956000	.972970	.451350D+01	.830158D+03
4.260000	81.685999	.968750	.433216D+01	.365293D+03
4.240000	81.564000	.968750	.433216D+01	.364747D+03
4.220000	81.261000	.916670	.310618D+01	.275357D+03
4.200000	121.440000	.803570	.203431D+01	.307436D+03
4.180000	302.927000	.724770	.161268D+01	.674042D+03
4.160000	423.472000	.368749	.575066D-00	.660405D+03
4.140000	301.811000	.100000	.131700D-00	.397487D+03
4.130000	100.456000	0.000000	.000000D+00	.000000D+00
4.110000	20.047000	0.000000	.000000D+00	.000000D+00
4.020000	19.800000	0.000000	.000000D+00	.000000D+00
3.820000	19.228999	.005049	.632849D-02	.240971D+02
3.630000	18.727999	.014780	.186128D-01	.235847D+02
3.540000	32.505999	.034649	.440806D-01	.413531D+02
3.430000	15.203999	0.000000	.000000D+00	.000000D+00
3.390000	20.538000	0.000000	.000000D+00	.000000D+00
3.350000	21.547000	0.000000	.000000D+00	.000000D+00
3.310000	22.549000	0.000000	.000000D+00	.000000D+00
3.270000	25.736000	.021189	.267721D-01	.325157D+02
3.220000	32.063000	.021590	.272830D-01	.405177D+02
3.170000	43.675999	.029850	.378807D-01	.554264D+02
3.120000	61.582000	.026029	.329684D-01	.779970D+02

TABLE III--Continued

λ	I_ν	α_ν	β_ν	J_ν
3.080000	81.594000	.038029	.484650D-01	.103982D+03
3.040000	111.120000	.034730	.441842D-01	.141369D+03
2.990000	168.047000	.035400	.450522D-01	.213866D+03
2.970000	201.868000	.040300	.514181D-01	.257560D+03
2.950000	232.518000	.028829	.365671D-01	.294919D+03
2.920000	275.154000	.032260	.409897D-01	.349612D+03
2.899999	328.067999	.059469	.766396D-01	.422784D+03
2.880000	376.183999	.048000	.614878D-01	.481890D+03
2.860000	422.808999	.075409	.980061D-01	.549500D+03
2.840000	425.765999	.072879	.945903D-01	.552598D+03
2.820000	414.086999	.090910	.119138D-00	.542667D+03
2.799999	382.234000	.123809	.165215D-00	.510063D+03
2.780000	338.083999	.131250	.175874D-00	.453032D+03
2.760000	287.620000	.290700	.429345D-00	.424796D+03
2.740000	270.575999	.300000	.445843D-00	.402115D+03
2.720000	302.933000	.272730	.398071D-00	.442155D+03
2.690000	323.841000	.308570	.461241D-00	.484068D+03
2.670000	299.655999	.393940	.625970D-00	.476153D+03
2.650000	228.710000	.380650	.598855D-00	.359816D+03
2.630000	152.981000	.246909	.354463D-00	.219619D+03
2.610000	108.094000	.176470	.242694D-00	.148658D+03
2.590000	96.525999	.193849	.269356D-00	.134123D+03
2.570000	104.469000	.229770	.326332D-00	.148372D+03
2.540000	143.231000	.062690	.809265D-01	.184896D+03
2.520000	197.878000	.037500	.477765D-01	.252104D+03
2.500000	253.532999	.044440	.568221D-01	.324173D+03
2.490000	269.885999	.048119	.616453D-01	.345744D+03
2.470000	244.680000	.075000	.974519D-01	.317927D+03
2.450000	173.223000	.075629	.983035D-01	.225154D+03
2.430000	112.534999	.075270	.978168D-01	.146244D+03
2.410000	56.662000	.054949	.706468D-01	.728478D+02

TABLE III--Continued

λ	I_ν	α_ν	β_ν	J_ν
2.380000	33.073000	.040540	.517308D-01	.422025D+02
2.370000	20.674000	.032629	.414677D-01	.262735D+02
2.320000	10.448000	.032100	.407831D-01	.132742D+02
2.280000	8.227000	.029409	.373139D-01	.104380D+02
2.240000	8.347999	.040230	.513270D-01	.106507D+02
2.210000	8.467000	.043610	.557368D-01	.108214D+02
2.180000	11.051999	.034250	.435628D-01	.140571D+02
2.140000	14.962999	.048149	.616847D-01	.191690D+02
2.100000	26.742000	.045639	.583929D-01	.342143D+02
2.060000	41.804000	.036360	.462968D-01	.532286D+02
2.020000	69.162000	.060000	.773442D-01	.891547D+02
1.980000	87.721999	.061800	.797401D-01	.113187D+03
1.950000	70.016999	.032260	.409897D-01	.889640D+02
1.920000	51.529000	.079369	.103371D-00	.671112D+02
1.880000	71.660000	.109090	.144389D-00	.948480D+02
1.850000	67.458000	.091839	.120418D-00	.884492D+02
1.820000	63.646000	0.000000	.000000D+00	.000000D+00
1.780000	50.146000	.034480	.438605D-01	.637886D+02
1.750000	18.325999	.013330	.167745D-01	.230615D+02
1.720000	8.613999	.030300	.384606D-01	.109339D+02
1.680000	8.987999	.180329	.248566D-00	.123890D+02
1.650000	9.318999	.122450	.163276D-00	.124260D+02
1.579999	10.386000	.121209	.161511D-00	.138392D+02
1.500000	11.761000	0.000000	.000000D+00	.000000D+00

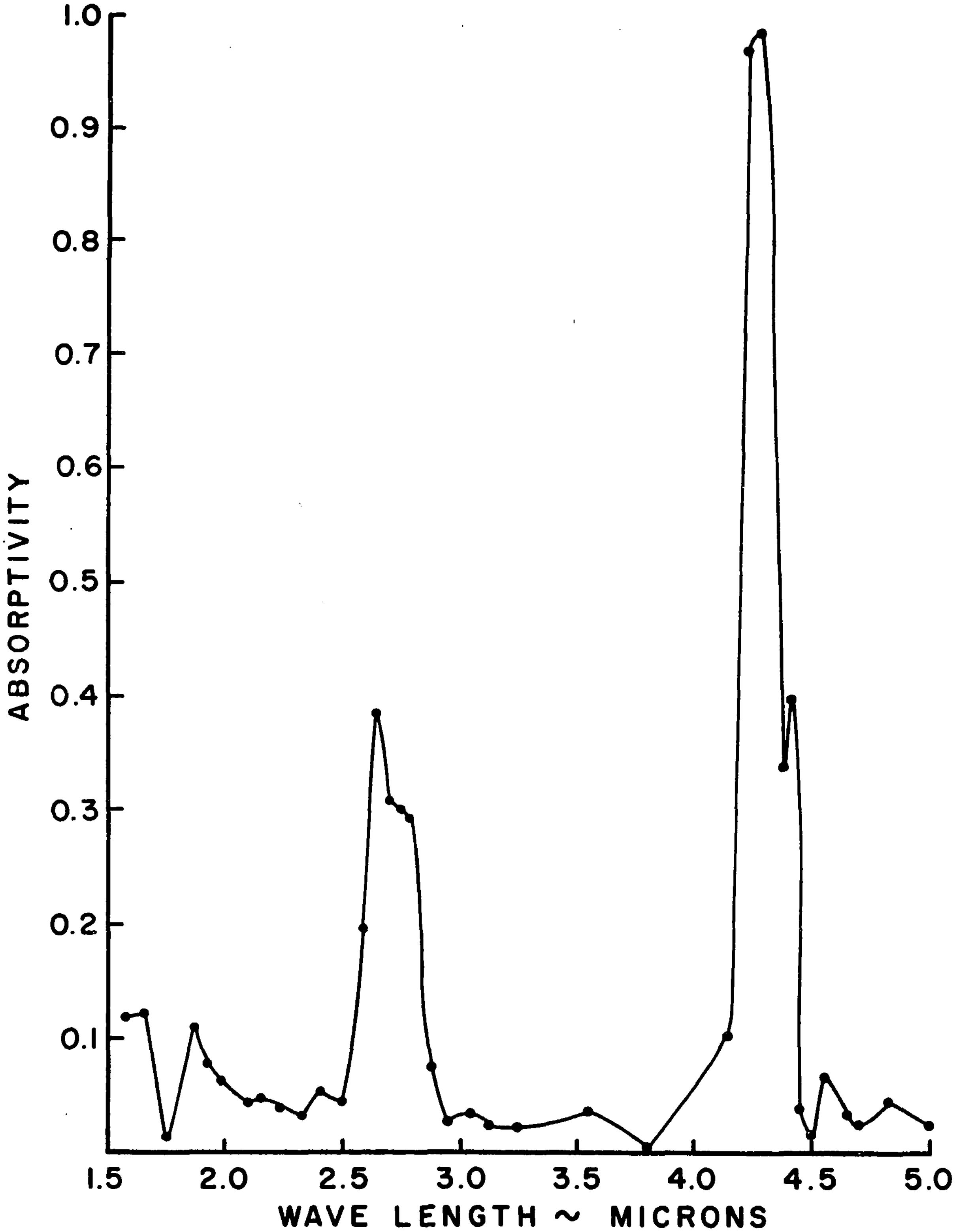

Figure 12. Spectral Absorptivity of Methanol Flame

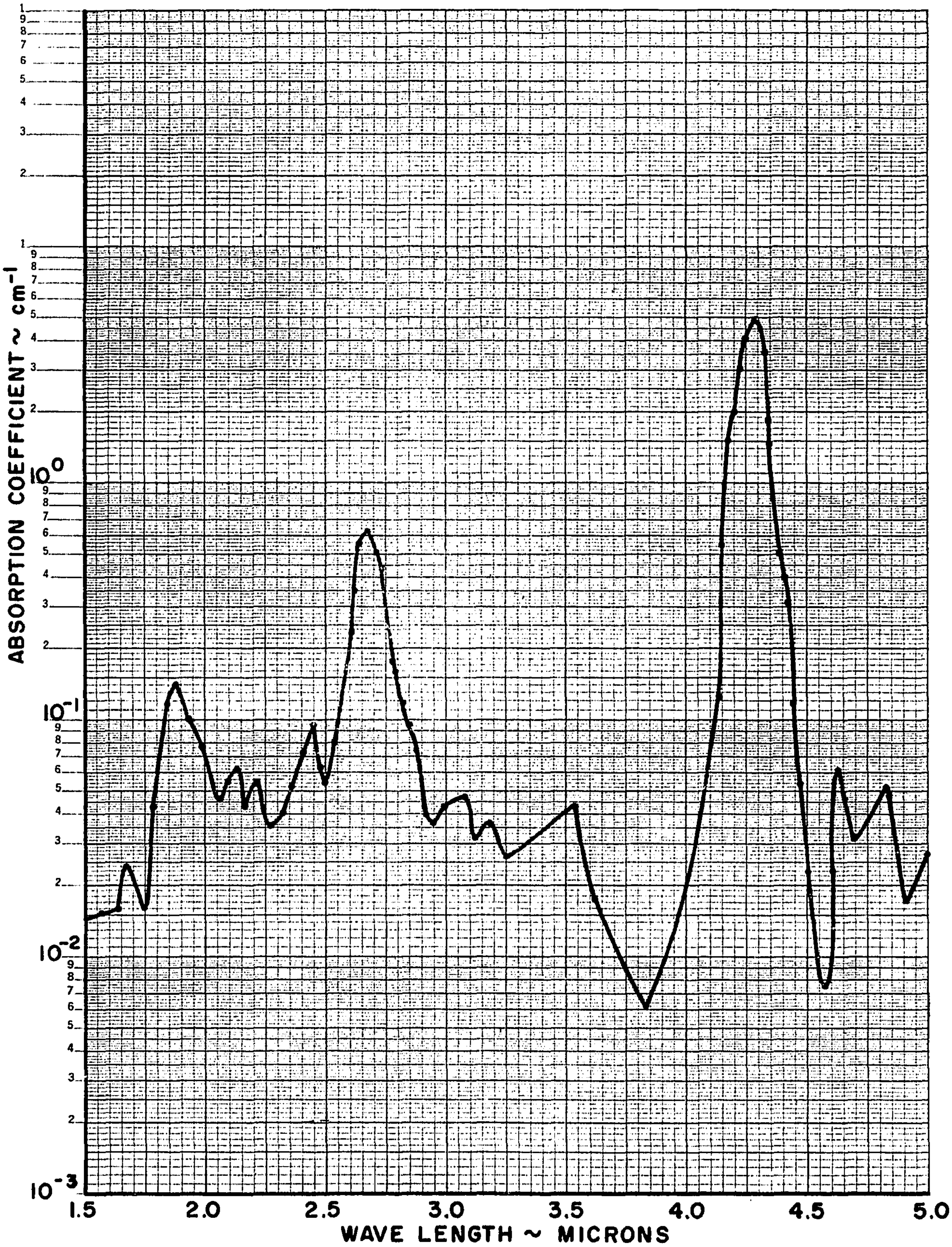

Figure 13. Monochromatic Absorption Coefficient of Methanol Flame

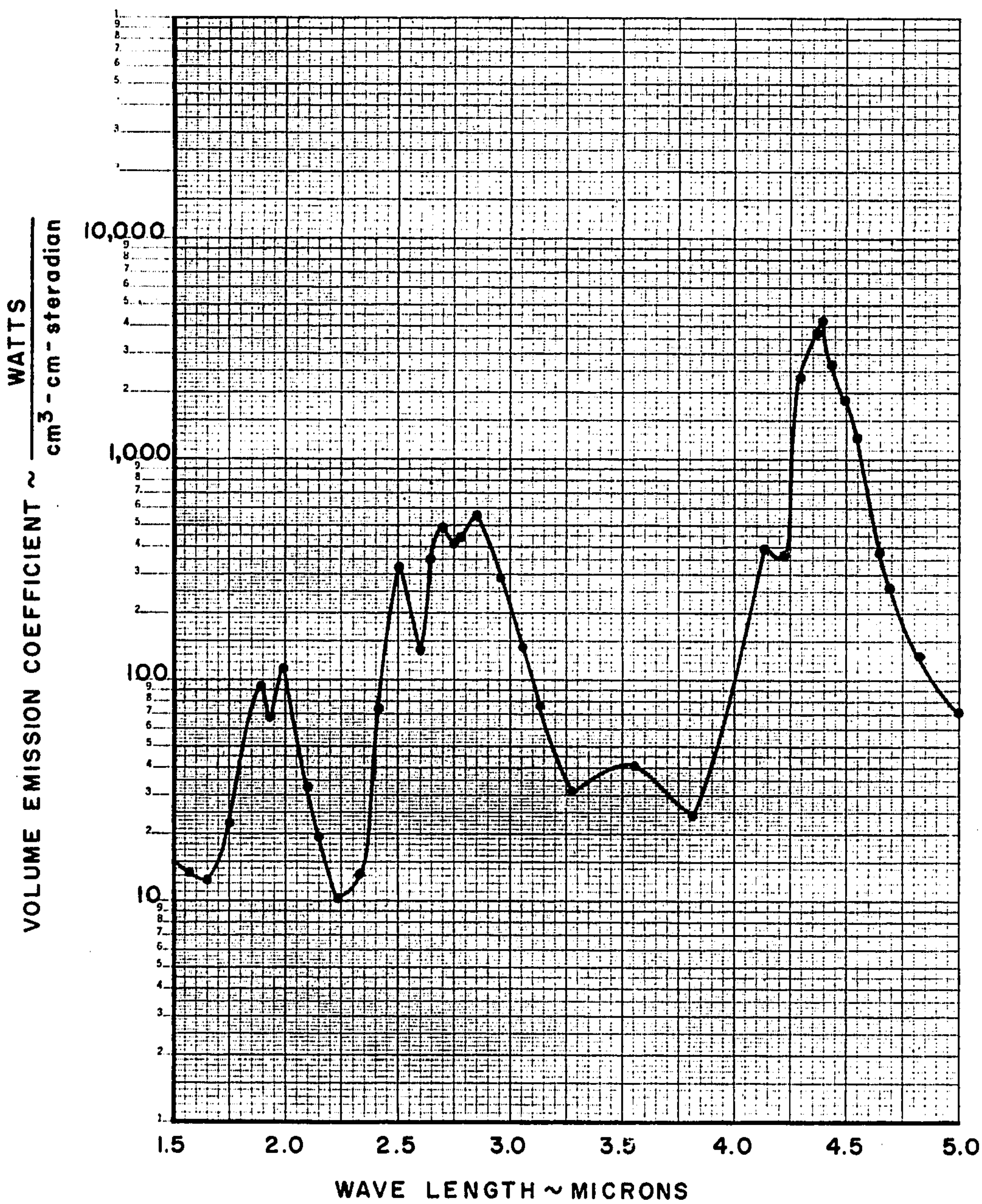

Figure 14. Monochromatic Volume Emission Coefficients of Methanol Flame

TABLE IV

SPECTROSCOPIC RADIATION PROPERTIES OF AN ACETONE FLAME (26)

Wave Length λ	Emitted Intensity $\frac{\text{watts}}{\text{cm}^2\text{-cm-steradian}}$ I_ν	cm^2-cm-steradian $(a\Omega\Delta\lambda) \times 10^{-9}$	Emitted Energy watts $E_\nu \times 10^{-9}$	Flame Pen Deflection DF	Globar + Flame Pen Deflection DGF	Globar Pen Deflection DG
5.22	52.278	1.176	61.479	0.009	0.121	0.118
5.07	62.722	1.198	75.141	0.011	0.149	0.140
4.99	84.472	1.213	102.465	0.015	0.158	0.145
4.91	117.103	1.225	143.451	0.021	0.169	0.151
4.83	160.145	1.237	198.099	0.029	0.179	0.156
4.75	207.662	1.250	259.578	0.038	0.193	0.161
4.73	223.164	1.255	280.071	0.041	0.193	0.162
4.71	233.307	1.259	293.733	0.043	0.200	0.162
4.69	259.816	1.262	327.888	0.048	0.205	0.164
4.67	318.852	1.264	403.029	0.059	0.210	0.164
4.65	372.895	1.264	471.339	0.069	0.222	0.166
4.64	457.553	1.269	580.635	0.085	0.240	0.167
4.62	590.731	1.272	751.410	0.110	0.258	0.168
4.60	793.554	1.274	1010.988	0.148	0.274	0.169
4.58	855.881	1.277	1092.960	0.160	0.297	0.169
4.57	982.724	1.279	1256.904	0.184	0.336	0.170
4.55	1133.180	1.284	1455.003	0.213	0.376	0.171
4.54	1381.073	1.286	1776.060	0.260	0.400	0.172

TABLE IV--Continued

λ	I_ν	$(a\Omega\Delta\lambda) \times 10^{-9}$	$E_\nu \times 10^{-9}$	DF	DGF	DG
4.52	1587.374	1.291	2049.300	0.300	0.439	0.172
4.50	1921.905	1.244	2390.850	0.350	0.464	0.172
4.48	2166.568	1.299	2814.372	0.412	0.530	0.172
4.46	2362.759	1.301	3073.950	0.450	0.576	0.172
4.44	2510.628	1.306	3278.880	0.480	0.595	0.172
4.43	2661.428	1.309	3483.810	0.510	0.605	0.172
4.41	2855.368	1.311	3743.388	0.548	0.620	0.172
4.39	3033.109	1.313	3982.473	0.583	0.630	0.172
4.37	2958.716	1.316	3893.670	0.570	0.620	0.169
4.35	2539.598	1.318	3347.190	0.490	0.535	0.160
4.33	1750.347	1.323	2315.709	0.339	0.340	0.140
4.32	922.133	1.326	1222.749	0.179	0.180	0.110
4.30	379.785	1.331	505.494	0.074	0.075	0.080
4.28	97.147	1.336	129.789	0.019	0.020	0.055
4.26	45.948	1.338	61.479	0.009	0.010	0.042
4.24	45.879	1.340	61.479	0.009	0.010	0.042
4.22	50.788	1.345	68.310	0.010	0.012	0.042
4.20	101.200	1.350	136.620	0.020	0.032	0.060
4.18	252.439	1.353	341.550	0.050	0.100	0.100
4.16	443.637	1.355	601.128	0.088	0.190	0.155
4.14	352.113	1.358	478.170	0.070	0.231	0.185
4.13	100.456	1.360	136.620	0.020	0.212	0.193
4.11	10.023	1.363	13.662	0.002	0.199	0.195
4.02	9.900	1.380	13.662	0.002	0.203	0.199
3.82	14.421	1.421	20.493	0.003	0.209	0.207
3.63	38.092	1.459	40.986	0.006	0.216	0.211
3.54	37.150	1.471	54.648	0.008	0.217	0.211
3.43	38.011	1.488	56.560	0.035	0.844	0.815
3.39	54.047	0.495	80.800	0.050	0.848	0.798
3.35	87.264	1.500	130.896	0.081	0.859	0.783
3.31	82.679	1.505	124.432	0.077	0.862	0.786

TABLE IV--Continued

λ	I_ν	$(a\Omega\Delta\lambda) \times 10^{-9}$	$E_\nu \times 10^{-9}$	DF	DGF	DG
3.22	74.814	1.512	113.120	0.070	0.837	0.770
3.17	106.526	1.157	161.600	0.100	0.841	0.759
3.12	116.793	1.522	177.760	0.110	0.851	0.754
3.08	121.862	1.575	185.840	0.115	0.840	0.735
3.04	128.052	1.527	195.536	0.121	0.835	0.715
2.99	170.161	1.529	260.176	0.161	0.850	0.701
2.97	181.787	1.529	277.952	0.172	0.862	0.690
2.95	215.608	1.529	329.664	0.204	0.880	0.680
2.92	243.405	1.527	371.680	0.230	0.891	0.670
2.90	298.436	1.527	455.712	0.282	0.900	0.658
2.88	326.379	1.525	497.728	0.308	0.946	0.645
2.86	347.572	1.525	530.048	0.328	0.959	0.631
2.84	363.122	1.522	552.672	0.342	0.960	0.611
2.82	371.616	1.522	565.600	0.350	0.930	0.583
2.80	352.504	1.522	536.512	0.332	0.850	0.546
2.78	329.579	1.520	500.960	0.310	0.760	0.508
2.76	276.968	1.517	420.160	0.260	0.604	0.436
2.74	273.772	1.517	415.312	0.257	0.534	0.395
2.72	296.533	1.515	449.248	0.278	0.535	0.379
2.69	325.979	1.512	492.880	0.305	0.560	0.372
2.67	294.305	1.510	444.400	0.275	0.500	0.355
2.65	225.488	1.505	339.360	0.210	0.420	0.330
2.63	161.600	1.500	242.400	0.150	0.405	0.345
2.61	97.284	1.495	145.440	0.090	0.404	0.360
2.59	79.173	1.490	117.968	0.073	0.370	0.340
2.57	84.881	1.485	126.048	0.078	0.368	0.328
2.54	109.337	1.478	161.600	0.100	0.410	0.355
2.52	147.309	1.470	216.544	0.134	0.505	0.413
2.50	195.110	1.466	286.032	0.177	0.610	0.466
2.49	223.430	1.461	326.432	0.202	0.681	0.499
2.47	189.071	1.453	274.720	0.170	0.676	0.505

TABLE IV--Continued

λ	I_ν	$(a\Omega\Delta\lambda) \times 10^{-9}$	$E_\nu \times 10^{-9}$	DF	DGF	DG
2.45	145.283	1.446	210.080	0.130	0.637	0.499
2.43	90.027	1.436	129.280	0.080	0.574	0.488
2.41	56.662	1.426	80.800	0.050	0.530	0.478
2.39	34.213	1.417	48.480	0.030	0.499	0.463
2.38	26.416	1.407	37.168	0.023	0.478	0.450
2.32	23.218	1.392	32.320	0.020	0.445	0.421
2.28	17.629	1.375	24.240	0.015	0.410	0.391
2.24	11.926	1.355	16.160	0.010	0.375	0.362
2.21	12.096	1.336	16.160	0.010	0.349	0.333
2.18	12.280	1.316	16.160	0.010	0.323	0.306
2.14	13.716	1.296	17.776	0.011	0.296	0.280
2.10	25.469	1.269	32.320	0.020	0.277	0.253
2.06	39.191	1.237	48.480	0.030	0.267	0.231
2.02	57.192	1.215	69.488	0.043	0.258	0.207
1.98	69.903	1.179	82.416	0.051	0.243	0.185
1.95	56.014	1.154	64.640	0.040	0.205	0.159
1.92	40.078	1.129	45.248	0.028	0.161	0.131
1.88	49.723	1.105	54.944	0.034	0.152	0.111
1.85	56.965	1.078	61.408	0.038	0.140	0.100
1.78	46.910	0.999	46.864	0.029	0.120	0.089
1.75	33.320	0.970	32.320	0.020	0.098	0.078
1.72	17.228	0.938	16.160	0.010	0.078	0.069
1.68	10.785	0.899	9.696	0.006	0.068	0.060
1.65	11.183	0.867	9.696	0.006	0.060	0.051
1.58	12.463	0.778	9.696	0.006	0.042	0.035
1.50	16.466	0.687	11.312	0.007	0.042	0.025

TABLE V

MONOCHROMATIC RADIATION PROPERTIES
OF AN ACETONE FLAME (26)

Wave Length microns λ	Emitted Intensity $\frac{\text{watts}}{\text{cm}^2\text{-cm-steradian}}$ I_ν	Absorptivity α_ν	Absorption Coefficient cm^{-1} β_ν	Volume Emission Coefficient $\frac{\text{watts}}{\text{cm}^3\text{-cm-steradian}}$ J_ν
5.220000	52.278000	.050849	.652355D-01	.670675D+02
5.070000	62.721999	.014279	.179786D-01	.789676D+02
4.990000	84.471999	.013790	.173574D-01	.106324D+03
4.910000	117.103000	.019869	.250875D-01	.147852D+03
4.830000	160.145000	.038460	.490238D-01	.204132D+03
4.750000	207.662000	.037269	.474778D-01	.264538D+03
4.730000	223.164000	.061729	.796469D-01	.287936D+03
4.710000	233.307000	.030859	.391827D-01	.296228D+03
4.690000	259.816000	.042859	.547570D-01	.331935D+03
4.670000	318.851999	.079270	.103235D-00	.415249D+03
4.650000	372.895000	.078310	.103932D-00	.485382D+03
4.640000	457.552999	.071860	.932158D-01	.593531D+03
4.620000	590.731000	.119050	.158443D-00	.786200D+03
4.600000	793.554000	.254440	.367024D-00	.114468D+04
4.580000	855.881000	.189349	.262398D-00	.118606D+04
4.570000	982.723999	.105879	.139894D-00	.129842D+04
4.550000	1133.180000	.046779	.598869D-01	.145067D+04
4.540000	1381.072999	.186050	.257320D-00	.191012D+04
4.520000	1587.373999	.191859	.266274D-00	.220305D+04
4.500000	1921.904999	.337209	.514121D-00	.293019D+04
4.480000	2166.567999	.313949	.471005D-00	.325041D+04

TABLE V--Continued

λ	I_ν	α_ν	β_ν	J_ν
4.460000	2362.759000	.267440	.389012D-00	.343681D+04
4.440000	2540.628000	.331400	.503211D-00	.381224D+04
4.430000	2661.427999	.447670	.742011D-00	.441131D+04
4.410000	2855.367999	.581400	.108854D+01	.534607D+04
4.390000	3033.109000	.726740	.162166D+01	.676814D+04
4.370000	2958.716000	.704140	.152233D+01	.639668D+04
4.350000	2539.598000	.716750	.157678D+01	.558687D+04
4.330000	1750.347000	.992860	.617755D+01	.108906D+05
4.320000	922.132999	.990910	.587572D+01	.546790D+04
4.299999	379.785000	.980500	.547753D+01	.210661D+04
4.280000	97.147000	.981819	.500929D+01	.495648D+03
4.260000	45.948000	.976190	.467206D+01	.219907D+03
4.240000	45.879000	.976190	.467206D+01	.219577D+03
4.220000	50.788000	.956380	.380562D+01	.202944D+03
4.200000	101.200000	.800000	.201179D+01	.254492D+03
4.180000	252.439000	.500000	.866433D-00	.437443D+03
4.160000	443.637000	.341940	.523073D-00	.678642D+03
4.140000	352.112999	.129730	.173689D-00	.471428D+03
4.130000	100.456000	.005180	.649182D-02	.125896D+03
4.110000	10.022999	0.000000	.000000D+00	.000000D+00
4.020000	9.899999	0.000000	.000000D+00	.000000D+00
3.820000	14.421000	.014500	.182576D-01	.181582D+02
3.630000	28.092000	.004739	.593908D-02	.351984D+02
3.540000	37.150000	.009480	.119065D-01	.466590D+02
3.430000	38.011000	.007359	.923402D-02	.476894D+02
3.390000	54.047000	0.000000	.000000D+00	.000000D+00
3.350000	87.263999	.006380	.800054D-02	.109429D+03
3.310000	82.679000	.026719	.338543D-01	.104754D+03
3.270000	75.063000	.016750	.211148D-01	.946234D+02
3.220000	74.814000	.003900	.488453D-02	.937003D+02
3.170000	106.525999	.023719	.300073D-01	.134762D+03
3.120000	116.792999	.017229	.217252D-01	.147263D+03

TABLE V--Continued

λ	I_ν	α_ν	β_ν	J_ν
3.080000	121.862000	.013600	.171166D-01	.153372D+03
3.040000	128.052000	.001400	.175122D-02	.160177D+03
2.990000	170.161000	.017139	.216107D-01	.214545D+03
2.970000	181.787000	0.000000	.000000D+00	.000000D+00
2.950000	215.608000	.005879	.737169D-02	.270305D+03
2.920000	243.405000	.013420	.168885D-01	.306316D+03
2.899999	298.436000	.060789	.783952D-01	.384865D+03
2.880000	326.379000	.010949	.136366D-01	.410203D+03
2.860000	347.570000	0.000000	.000000D+00	.000000D+00
2.840000	363.121999	0.000000	.000000D+00	.000000D+00
2.820000	371.615999	.005150	.645413D-02	.465720D+03
2.799999	352.504000	.051279	.658019D-01	.452329D+03
2.780000	329.578999	.114170	.151537D-00	.437450D+03
2.760000	276.967999	.210999	.296236D-00	.388852D+03
2.740000	273.771999	.298729	.443577D-00	.406518D+03
2.720000	296.532999	.321900	.485575D-00	.447310D+03
2.690000	325.978999	.314520	.472044D-00	.489243D+03
2.670000	294.305000	.366200	.570027D-00	.458115D+03
2.650000	225.487999	.363640	.564988D-00	.350341D+03
2.630000	161.600000	.260870	.377851D-00	.234066D+03
2.610000	97.283999	.127780	.170891D-00	.130106D+03
2.590000	79.173000	.126469	.169016D-00	.105807D+03
2.570000	84.880999	.115850	.153910D-00	.112767D+03
2.545000	109.336999	.126759	.169431D-00	.146142D+03
2.520000	147.308999	.101689	.134050D-00	.194186D+03
2.500000	195.110000	.078200	.101783D-00	.253951D+03
2.490000	223.430000	.040080	.511316D-01	.285038D+03
2.470000	189.071000	0.000000	.000000D+00	.000000D+00
2.450000	145.282999	0.000000	.000000D+00	.000000D+00
2.430000	90.027000	0.000000	.000000D+00	.000000D+00
2.410000	56.662000	0.000000	.000000D+00	.000000D+00
2.390000	34.212999	0.000000	.000000D+00	.000000D+00

TABLE V--Continued

λ	I_ν	α_ν	β_ν	J_ν
2.380000	26.415999	0.000000	.000000D+00	.000000D+00
2.320000	23.218000	0.000000	.000000D+00	.000000D+00
2.280000	17.629000	0.000000	.000000D+00	.000000D+00
2.240000	11.925999	0.000000	.000000D+00	.000000D+00
2.210000	12.095999	0.000000	.000000D+00	.000000D+00
2.180000	12.280000	0.000000	.000000D+00	.000000D+00
2.140000	13.716000	0.000000	.000000D+00	.000000D+00
2.100000	25.468999	0.000000	.000000D+00	.000000D+00
2.060000	39.191000	0.000000	.000000D+00	.000000D+00
2.020000	57.192000	0.000000	.000000D+00	.000000D+00
1.980000	69.903000	0.000000	.000000D+00	.000000D+00
1.950000	56.013999	0.000000	.000000D+00	.000000D+00
1.920000	40.077999	0.000000	.000000D+00	.000000D+00
1.880000	49.723000	0.000000	.000000D+00	.000000D+00
1.850000	56.965000	0.000000	.000000D+00	.000000D+00
1.850000	52.780000	0.000000	.000000D+00	.000000D+00
1.780000	46.910000	0.000000	.000000D+00	.000000D+00
1.750000	33.320000	0.000000	.000000D+00	.000000D+00
1.720000	17.227999	.014490	.182450D-01	.216925D+02
1.680000	10.784999	0.000000	.000000D+00	.000000D+00
1.650000	11.183000	0.000000	.000000D+00	.000000D+00
1.579999	12.462999	0.000000	.000000D+00	.000000D+00
1.500000	16.466000	0.000000	.000000D+00	.000000D+00

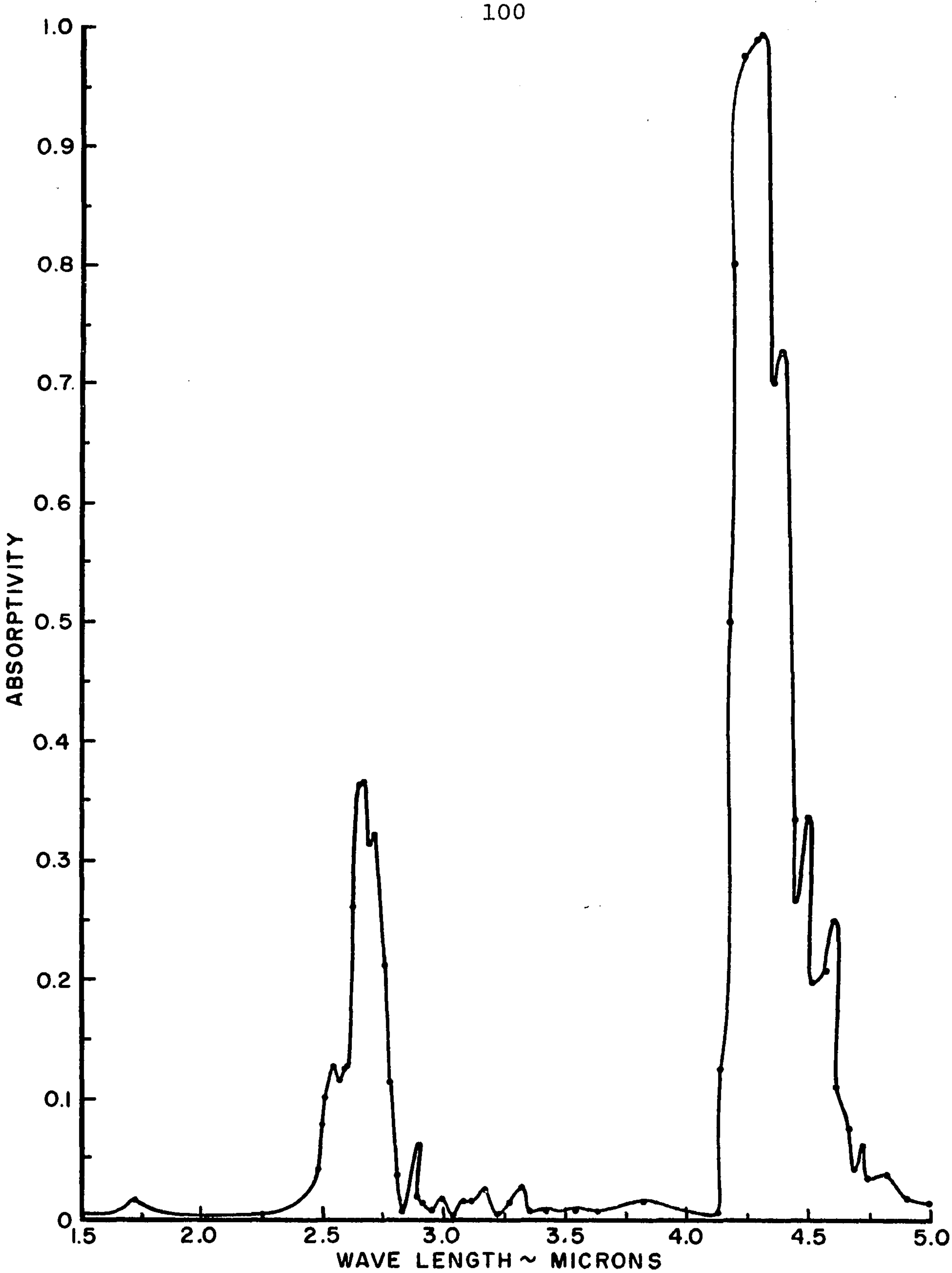

Figure 15. Spectral Absorptivity of Acetone Flame
Optical Path Length--0.8 cm

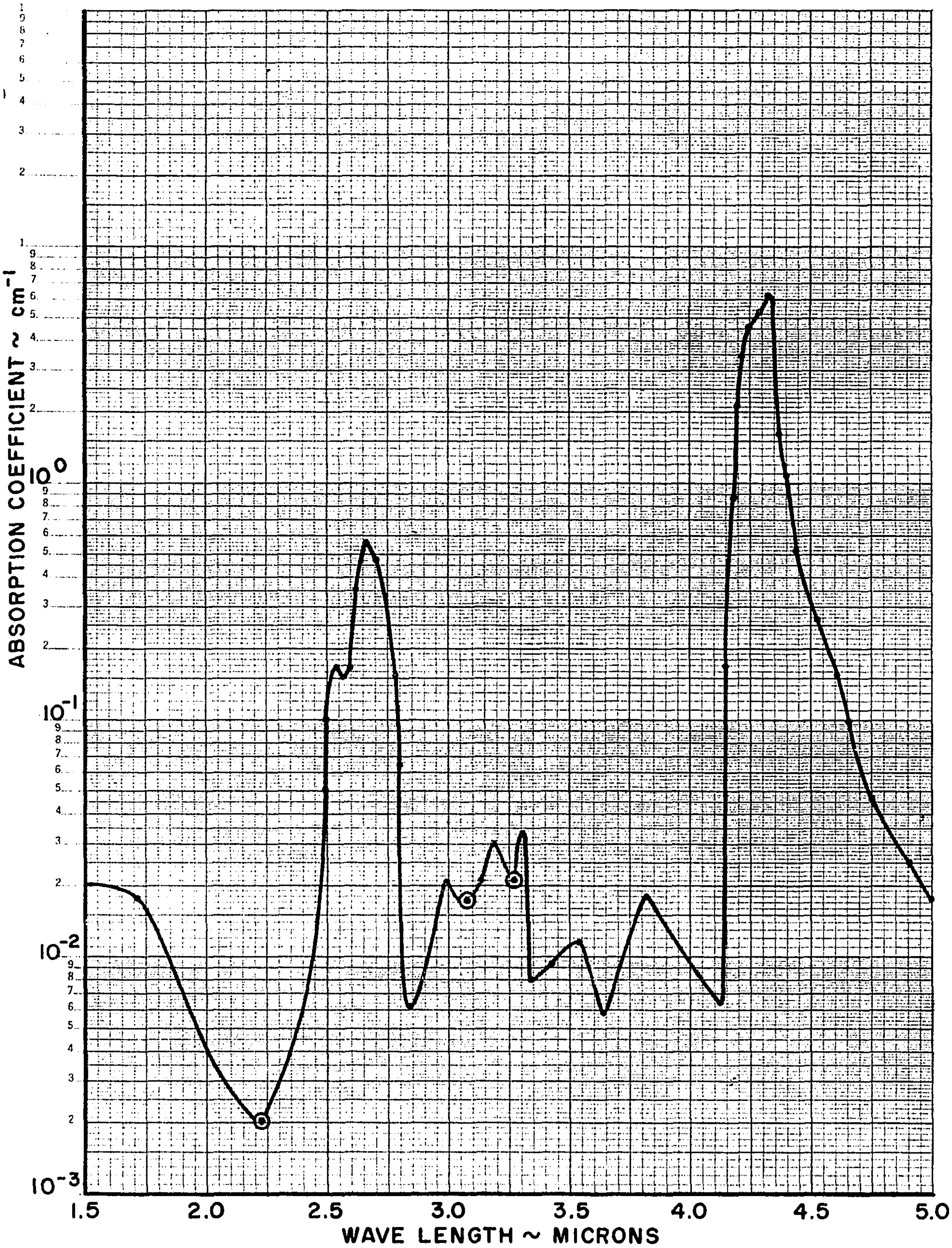

Figure 16. Monochromatic Absorption Coefficient of Acetone Flame

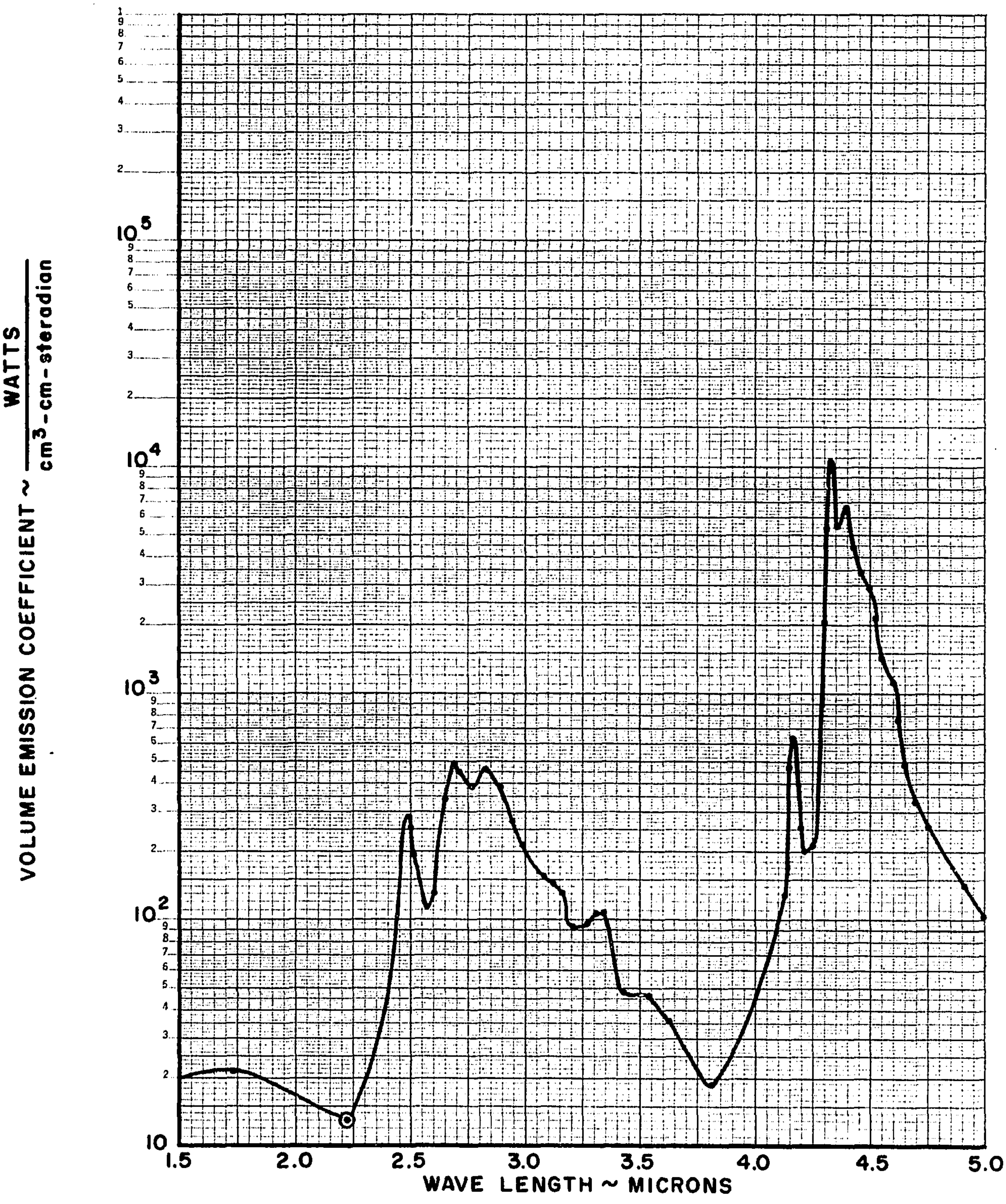

Figure 17. Monochromatic Volume Emission Coefficients of Acetone Flame

APPENDIX B

SOME THEORETICAL MONOCHROMATIC RADIATION FLUX CALCULATIONS (METHODS I AND II) OF AN ACETONE AND A METHANOL FLAME WITH A GIVEN SIZE AND POSITION TO A TARGET.

COMPUTER INPUT CODE

AB(m)	β_ν, monochromatic volume extinction coefficient, L^{-1}
AX(m)	ϵ_ν, monochromatic emissivity
DS	Optical depth, L
AY(m)	I_ν, monochromatic emitted intensity of radiation, $\frac{\text{watts}}{\text{cm}^2\text{-cm-steradian}}$
HH	Height, L
BB	Width, L
C	Depth, L
RR	Radius, L
BT	α, flame angle of tilt
AT	β, flame angle of tilt
W	Target angle of tilt

.829610D-02 = 0.00829610

.670675D+02 = 67.0675

```
Program 201;
Begin Comment Monochromatic flux calculation from a sheet of
      flame based on thermodynamic equilibrium;
Integer j,m,N;
Real PI,PI2,PI3,PI4,PI6,BB,HH,B,C,DS,AT,BT,H,D,W,X,T,P,
      FH,FC,FD,FAJV,FAB,E2,FW,FJ,FT,FSI,PW1,PW2,PW3;
Format FO(J7,S4,'WAVE',S5,'ABSORPTIVITY',S2,'ABSORPTION',S3,
      'BLACK BODY',J1,S3,'LENGTH',S21,'COEF',S7,'INTENSITY'),
      F1(J1,2(F10.6,S1),2(R6,S1)),
      F2(J7,'N=',I3,S3,'AT=',F10.9,S3,'BT=',F10.9,S3,'D=',
      F10.8,2(J1), ' WAVE LENGTH',S7,'P,W=0',S10,
      'P,W=PI/4',S9,'P,W=PI/2'),
      F3(J1,F10.6,3(S1,R10));
READPT(DECIMAL,N);
Begin Real Array AZ,AY,AX,AB,AJ,AJV,EE,FI,FX[1:N];
PI←3.1415926536; PI2←PI/2; PI3←PI/3; PI4←PI/4.0; PI6←PI/6.0;
BB←12.7/2.0; HH←10.16/6.0; B←BB/3.0; C←2.54; DS←0.8;
PRINT(FO);
For m←1 Step 1 Until N Do
Begin READPT(DECIMAL,AZ[m],AX[m]);
      AB[m]←-LN(1.-AX[m])/12.7;
      AJV[m]←1.177D8/AZ[m]5/(EXP(14320./AZ[m]/1400.)-1.);
      PRINT(F1,AZ[m],AX[m],AB[m],AJV[m]) End;
For AT←PI2,PI3,PI6 Do
For BT←PI2,PI3,PI6 Do
```

```
For D←10.0,D-1.0 While 0.0<D Do
        Begin PRINT(F2,N,AT,BT,D);
        H←HH/SIN(AT)/ SIN(BT); FH←(H+H)*B*SIN(AT);
        FC←C*SIN(BT); FD←D+C/2.0;
        For j←1,2,3,4,5,6 Do Begin      X←(j-.5)*H;
        E2←EE[j]←FD*FD+X*X-2.0*X*FD*COS(BT);
        X←X*SIN(BT);
        X←FI[j]←ARCTAN(X/SQRT(E2-X*X));
        FX[j]←SIN(BT+X) End;
For m←1,m+1 While m≤N Do Begin
        If AX[m]=0.0 Then Begin PW1←PW2←PW3←0.0; Goto L1 End;
        FAJV←AJV[m]*FH; FAB←-AB[m]*FC;
For W←0.0,PI4,PI2 Do Begin P←0.0;
For j←1,2,3,4,5,6 Do Begin E2←EE[j];
        FW←COS(PI2-W-FI[j])*FAJV*FX[j]; FJ←FAB/FX[j];
For T←BB-.5*B,T-B,T-B Do
        Begin FT←T*T+E2;
        FSI←SQRT(E2/FT);
        P←P+FW*(1.0-EXP(FJ/FSI))*FSI/FT;
        End T loop End j loop;
        PW1←PW2; PW2←PW3; PW3←P End W loop;
L1:     PRINT(F3,AZ[m],PW1,PW2,PW3) End m loop;
        End D loop End block End Program;
```

```
Program 202;
Begin Comment Monocromatic flux calculation from a sheet of
      flame;
Integer j,m,N;
Real PI,PI2,PI3,PI4,PI6,BB,HH,B,C,DS,AT,BT,H,D,W,X,T,P,
      FH,FC,FD,FAJV,FAB,E2,FW,FJ,FT,FSI,PW1,PW2,PW3;
Format FO(J7,S4, 'WAVE',S8, 'EMITTED',S3, 'ABSORPTIVITY', S2,
      'ABSORPTION', S2, 'VOL EMISSION',J1,S3, 'LENGTH',S6,
      'INTENSITY',S19,'COEF',S9,'COEF'),
      F1(J1,3(F10.6,S1), 2(R6,S1)),
      F2(J7,'N=',I3,S3,'AT=',F10.9,S3,'BT=',F10.9,S3,'D=',
      F10.8,2(J1),' WAVE LENGTH',S7,'P,W=0',S10,
      'P,W=PI/4',S9,'P,W=PI/2'),
      F3(J1,F10.6,3(S1,R10));
READPT(DECIMAL,N);
Begin Real Array AZ,AY,AX,AB,AJ,AJV,EE,FI,FX[1:N];
PI←3.1415926536; PI2←PI/2; PI3←PI/3; PI4←PI/4.0; PI6←PI/6.0;
BB←12.7/2.0; HH←10.16/6.0; B←BB/3.0; C←2.54; DS←0.8;
PRINT(FO);
For m←1 Step 1 Until N Do
Begin READPT(DECIMAL,AZ[m],AY[m],AX[m]);
      AB[m]←-LN(1-AX[m])/DS;
      AJ[m]←AY[m]*AB[m]/AX[m];
      AJV[m]←AJ[m]/AB[m];
      PRINT(F1,AZ[m], AY[m], AX[m], AB[m], AJ[m]) End;
```

```
For AT←PI2,PI3,PI6 Do
For BT←PI2,PI3,PI6 Do
For D←10.0,D-1.0 While 0.0<D Do
      Begin PRINT(F2,N,AT,BT,D);
      H←HH/SIN(AT)/ SIN(BT); FH←(H+H)*B*SIN(AT);
      FC←C*SIN(BT); FD←D+C/2.0;
      For j←1,2,3,4,5,6 Do Begin     X←(j-.5)*H;
      E2←EE[j]←FD*FD+X*X-2.0*X*FD*COS(BT);
      X←X*SIN(BT);
      X←FI[j]←ARCTAN(X/SQRT(E2-X*X));
      FX[j]←SIN(BT+X) End;
For m←1,m+1 While m≤N Do Begin
      If AX[m]=0.0 Then Begin PW1←PW2←PW3←0.0; Goto L1 End;
      FAJV←AJV[m]*FH; FAB←-AB[m]*FC;
For W←0.0,PI4,PI2 Do Begin P←0.0;
For j←1,2,3,4,5,6 Do Begin E2←EE[j];
      FW←COS(PI2-W-FI[j])*FAJV*FX[j]; FJ←FAB/FX[j];
ForT←BB-.5*B,T-B,T-B Do
      Begin FT←T*T+E2;
      FSI←SQRT(E2/FT);
      P←P+FW*(1.0-EXP(FJ/FSI))*FSI/FT;
      End T loop End j loop;
      PW1←PW2; PW2←PW3; PW3←P End W loop;
L1:   PRINT(F3,AZ[m],PW1,PW2,PW3) End m loop;
      End D loop End block End Program;
```

```
Program 203;
Begin Comment Monochromatic flux calculation from a cylindrical
      flame based on thermodynamic equilibrium;
Integer j,k,m,N;
Real PI,PI2,R,RR,H,D,W,P,PW1,PW2,FD,FJ,E2,FI,SINFI,FK,SI,SINSI,
      OM,BT,GA,T;
Format FO(J7,S4,'WAVE',S5,'ABSORPTIVITY',S2,'ABSORPTION',S3,
      'BLACK BODY',J1,S3,'LENGTH',S21,'COEF',S7,'INTENSITY'),
      F1(J1,2(F10.6,S1),2(R6,S1)),
      F2(J7,'N=',I3,S3,'D=',F10.8,2(J1),
      ' WAVE LENGTH',S7,'P,W=0',S10,'P,W=PI/2',J1),
      F3(J1,F10.6,2(S1,R10));
READPT(DECIMAL,N);
Begin Real Array AZ,AX,AB,AJ,AJV[1:N];
PI←3.1415926536; PI2←PI/2; R←1.27; RR←R/3; H←10.16/6;
PRINT(FO);
For m←1 Step 1 Until N Do
Begin READPT(DECIMAL,AZ[m],AX[m]);
      AB[m]←-LN(1.0-AX[m])/12.7;
      AJV[m]←1.177D8/AZ[m]5/(EXP(14320./AZ[m]/1400.0)-1.);
      PRINT(F1,AZ[m],AX[m],AB[m],AJV[m])
End;
For D←0.0 Step 1.0 Until 10.0 Do Begin FD←D+R; PRINT(F2,N,D);
For m←1 Step 1 Until N Do Begin
      If AX[m]=0.0 Then Begin PW1←PW2←0.0; Goto L1 End;
```

```
For W←0.0, PI2 Do Begin P←0.0;
For j←1,2,3,4,5,6 Do Begin FJ←(j-.5)*H;
        E2←FD*FD+FJ*FJ;
        FI←ARCTAN(FJ/FD); SINFI←SIN(FI);
For k←1,2,3 Do Begin FK←R-(k-.5)*RR;
        SI←ARCTAN(FK/SQRT(E2)); SINSI←SIN(SI);
        OM←RR*H*SIN(PI2-SI)*SINFI/(E2+FK*FK);
        BT←ARCTAN(D*SINSI/SQRT(R*R-D*D*SINSI*SINSI));
        GA←ARCTAN(FD*SINSI/SQRT(R*R-FD*FD*SINSI*SINSI));
        T←(R*SIN(PI-SI-GA)-SIN(PI-SI-BT))/(SINSI*SINFI);
        P←P+(OM+OM)*AJV[m]*(1.0-EXP(-AB[m]*T))*COS(PI2-FI-W);
        End k loop End j loop;
        PW1←PW2; PW2←P End W loop;
L1:     PRINT(F3,AZ[m],PW1,PW2) End m loop; End D loop; End
End Program;
```

```
Program 204;
Begin Comment Monochromatic flux calculation from a
      cylindrical flame;
Integer j,k,m,N;
Real PI,PI2,R,RR,H,D,W,P,PW1,PW2,FD,FJ,E2,FI,SINFI,FK,SI,SINSI,
      OM,BT,GA,T;
Format FO(J7,S4,'WAVE',S8,'EMITTED',S3,'ABSORPTIVITY',S2,
      'ABSORPTION',S2,'VOL EMISSION',J1,S3,'LENGTH',S6,
      'INTENSITY',S19,'COEF',S9,'COEF'),
      F1(J1,3(F10.6,S1),2(R6,S1)),
      F2(J7,'N=',I3,S3,'D=',F10.8,2(J1),
      ' WAVE LENGTH',S7,'P,W=0',S10,'P,W=PI/2',J1),
      F3(J1,F10.6,2(S1,R10));
READPT(DECIMAL,N);
Begin Real Array AZ,AY,AX,AB,AJ,AJV[1:N];
PI←3.1415926536; PI2←PI/2; R←1.27; RR←R/3; H←10.16/6;
PRINT(FO);
For m←1 Step 1 Until N Do
Begin READPT(DECIMAL,AZ[m],AY[m],AX[m]);
      AB[m]←-LN(1.0-AX[m])/0.8;
      AJ[m]←AY[m]*AB[m]/AX[m];
      AJV[m]←AJ[m]/AB[m];
      PRINT(F1,AZ[m],AY[m],AX[m],AB[m],AJ[m])
End;
For D←0.0 Step 1.0 Until 10.0 Do Begin FD←D+R; PRINT(F2,N,D);
```

```
For m←1 Step 1 Until N Do Begin
        If AX[m]=0.0 Then Begin PW1←PW2←0.0; Goto L1 End;
For W←0.0, PI2 Do Begin P←0.0;
For j←1,2,3,4,5,6 Do Begin FJ←(j-.5)*H;
        E2←FD*FD+FJ*FJ;
        FI←ARCTAN(FJ/FD); SINFI←SIN(FI);
For k←1,2,3 Do Begin FK←R-(k-.5)*RR;
        SI←ARCTAN(FK/SQRT(E2)); SINSI←SIN(SI);
        OM←RR*H*SIN(PI2-SI)*SINFI/(E2+FK*FK);
        BT←ARCTAN(D*SINSI/SQRT(R*R-D*D*SINSI*SINSI));
        GA←ARCTAN(FD*SINSI/SQRT(R*R-FD*FD*SINSI*SINSI));
        T←(R*SIN(PI-SI-GA)-SIN(PI-SI-BT))/(SINSI*SINFI);
        P←P+(OM*OM)*AJV[m]*(1.0-EXP(-AB[m]*T))*COS(PI2-FI-W);
        End k loop End j loop;
        PW1←PW2; PW2←P End W loop;
L1:     PRINT(F3,AZ[m],PW1,PW2) End m loop; End D loop; End
End Program;
```

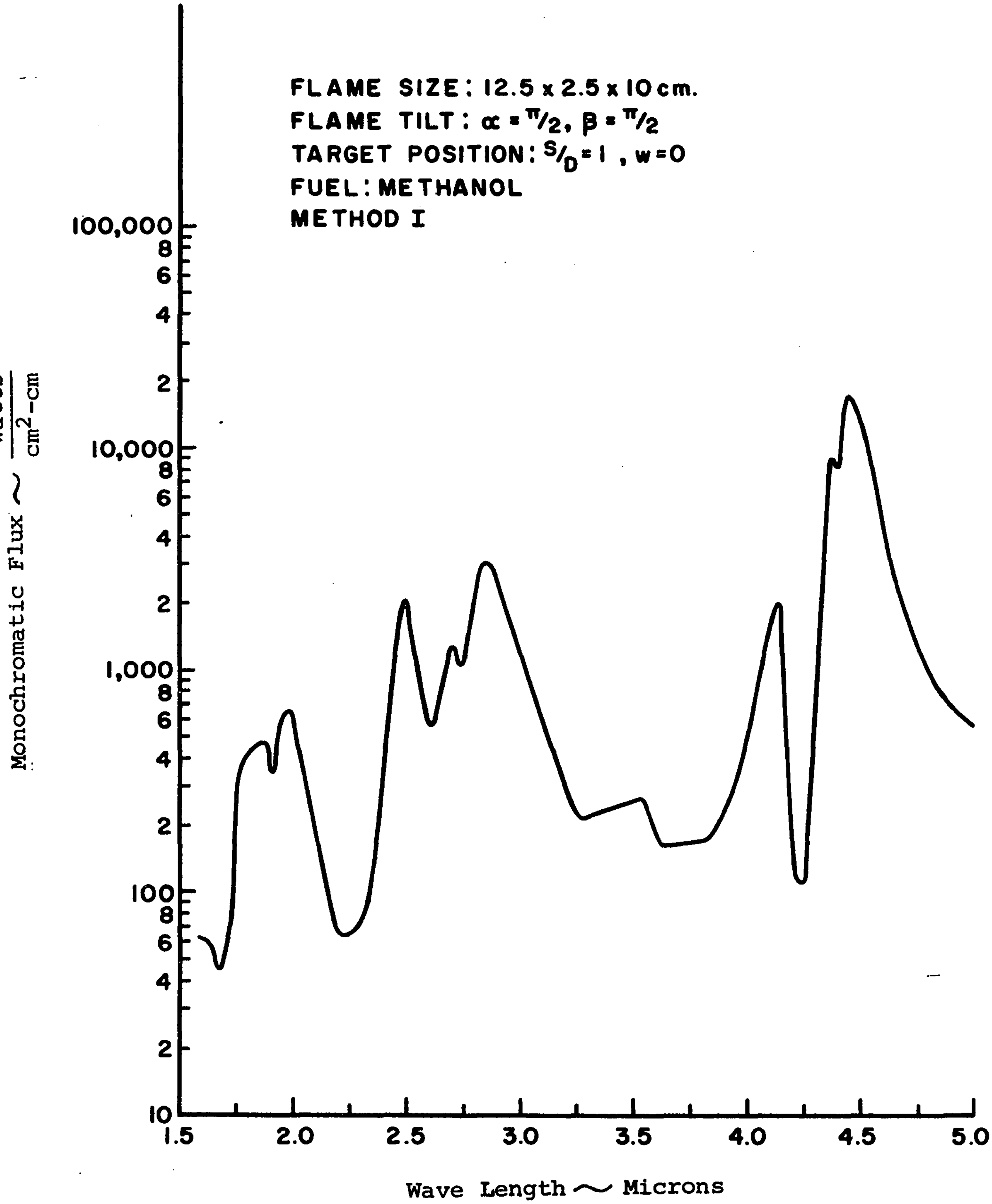

Figure 18. Monochromatic Flux to Target from a Sheet Flame

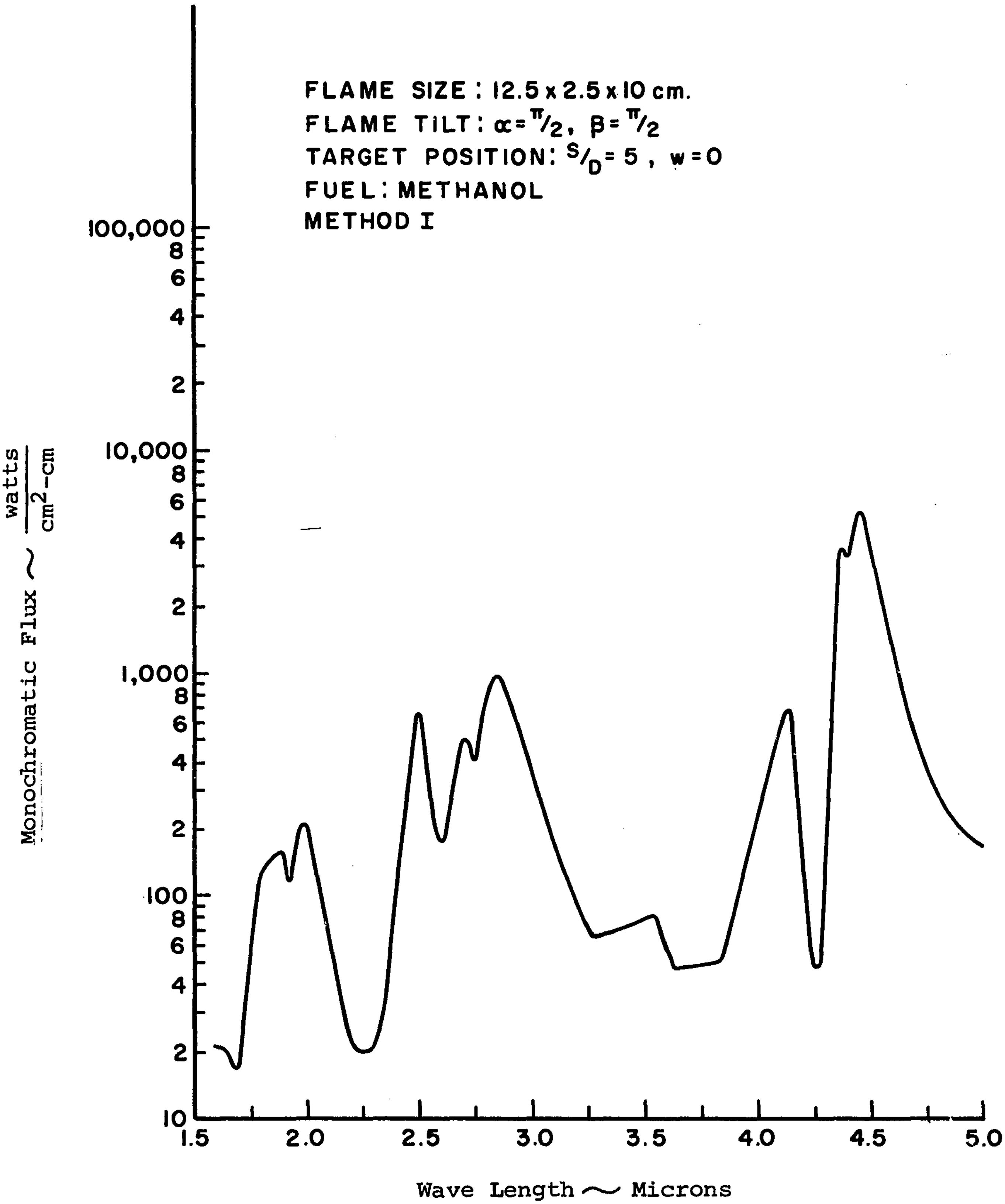

Figure 19. Monochromatic Flux to Target from a Sheet Flame

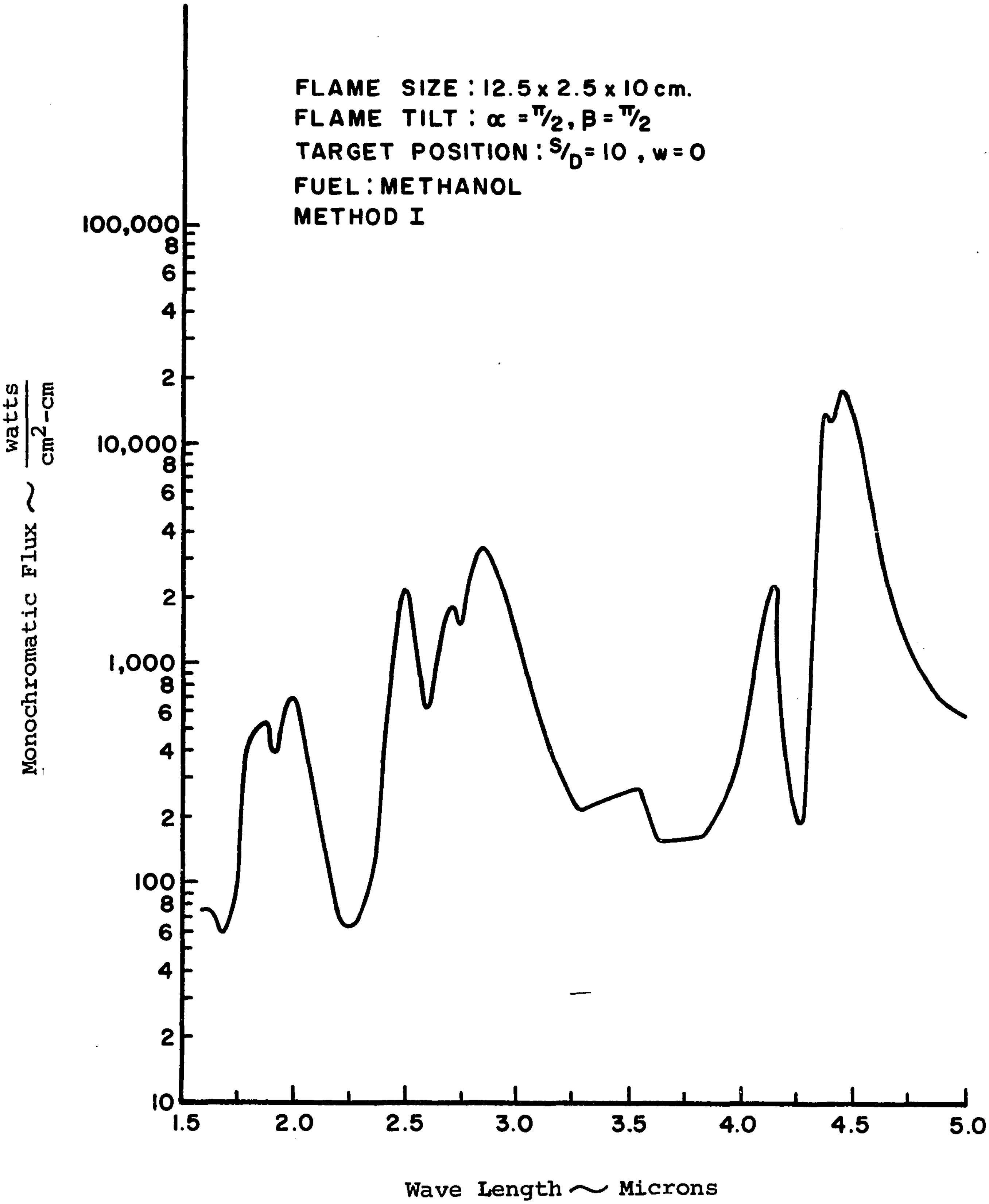

Figure 20. Monochromatic Flux to Target from a Sheet Flame

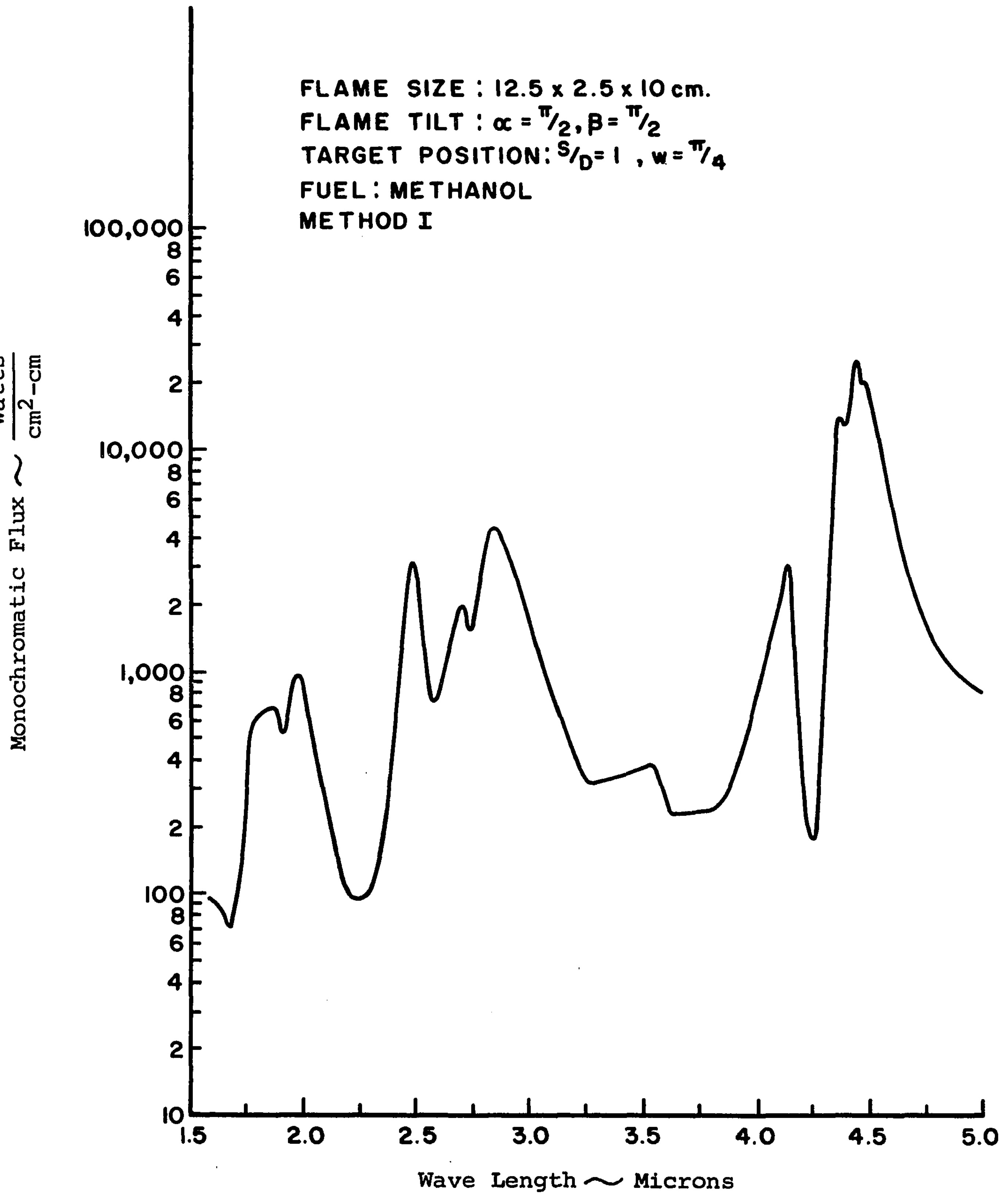

Figure 21. Monochromatic Flux to Target from a Sheet Flame

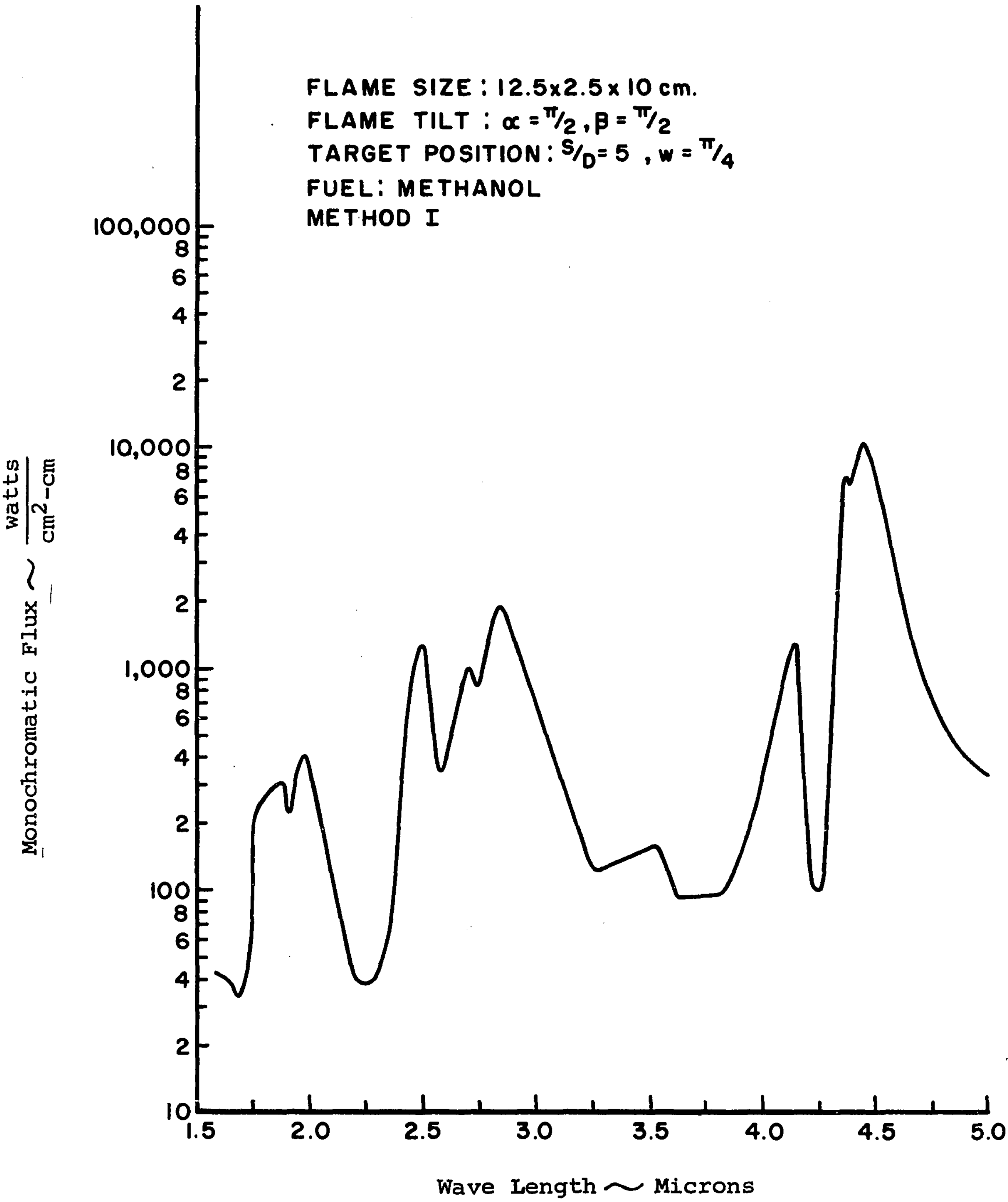

Figure 22. Monochromatic Flux to Target from a Sheet Flame

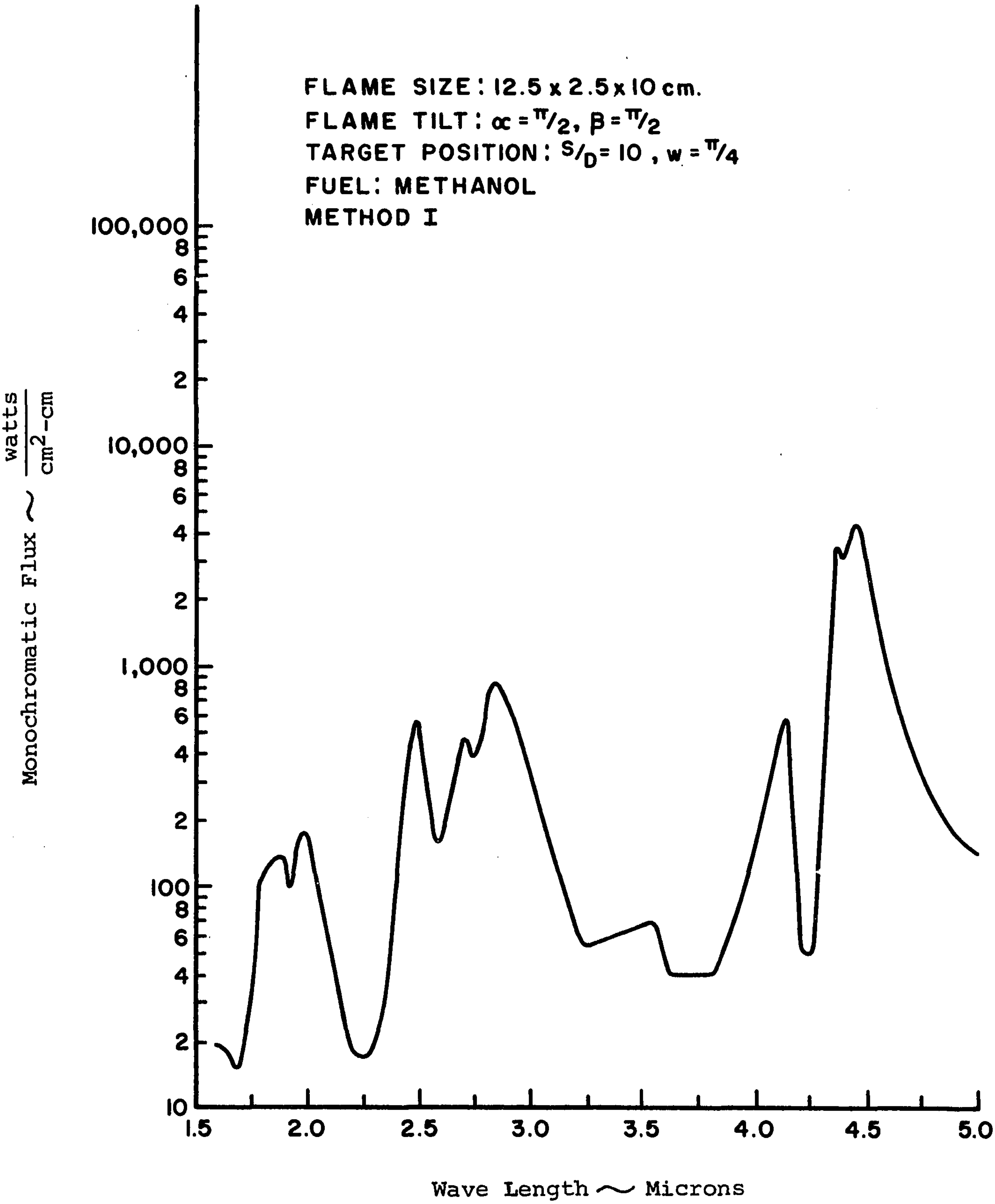

Figure 23. Monochromatic Flux to Target from a Sheet Flame

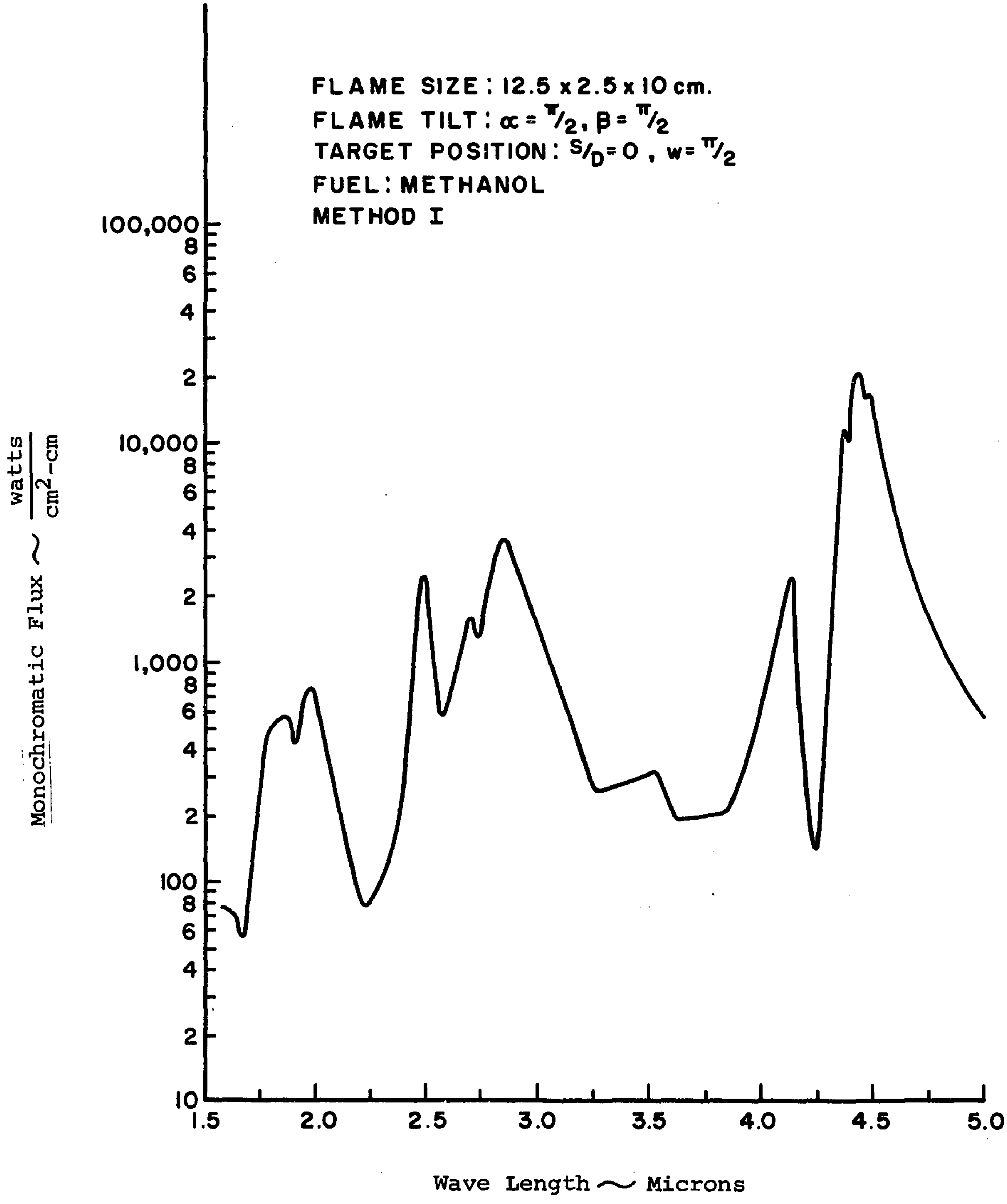

Figure 24. Monochromatic Flux to Target from a Sheet Flame

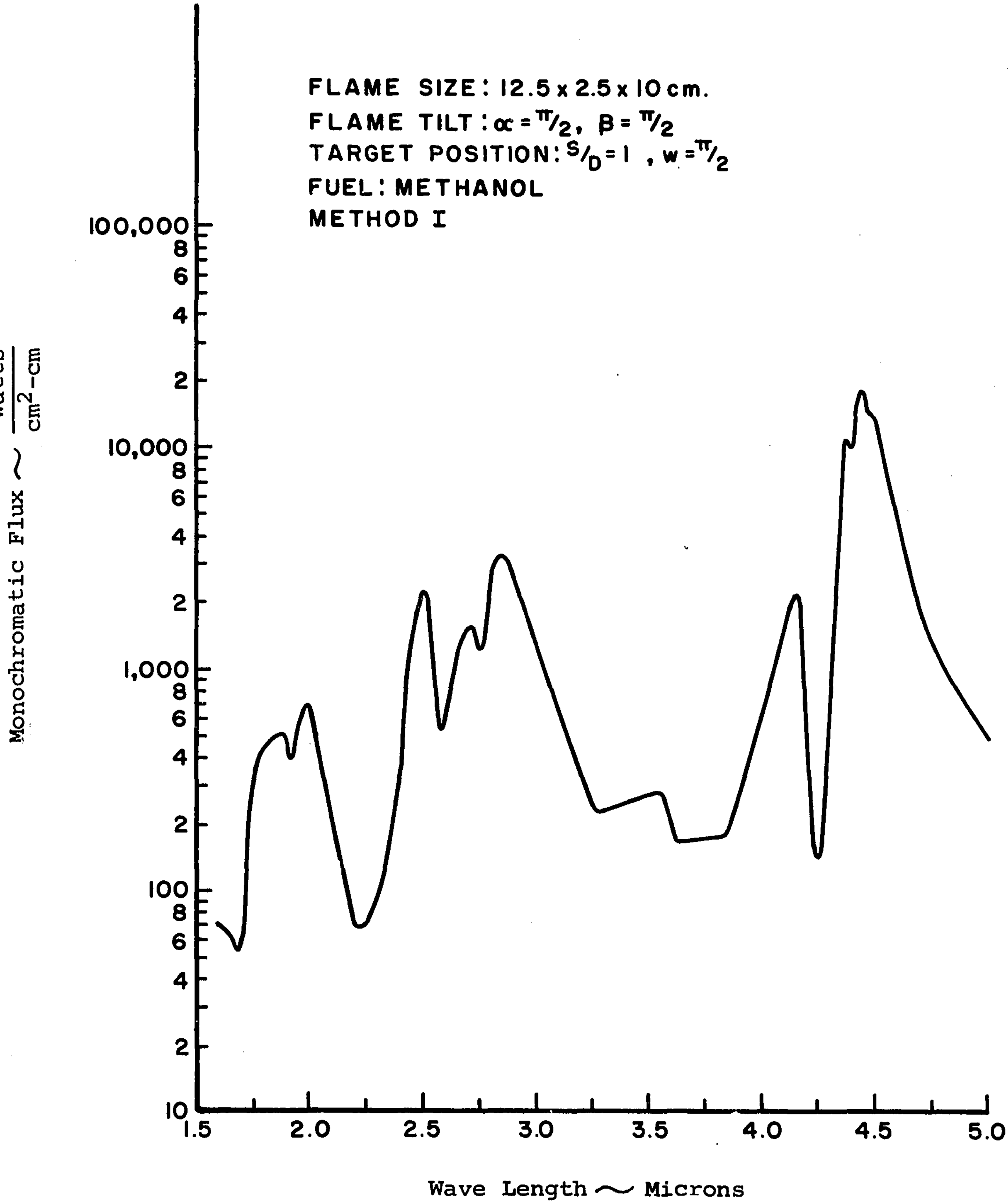

Figure 25. Monochromatic Flux to Target from a Sheet Flame

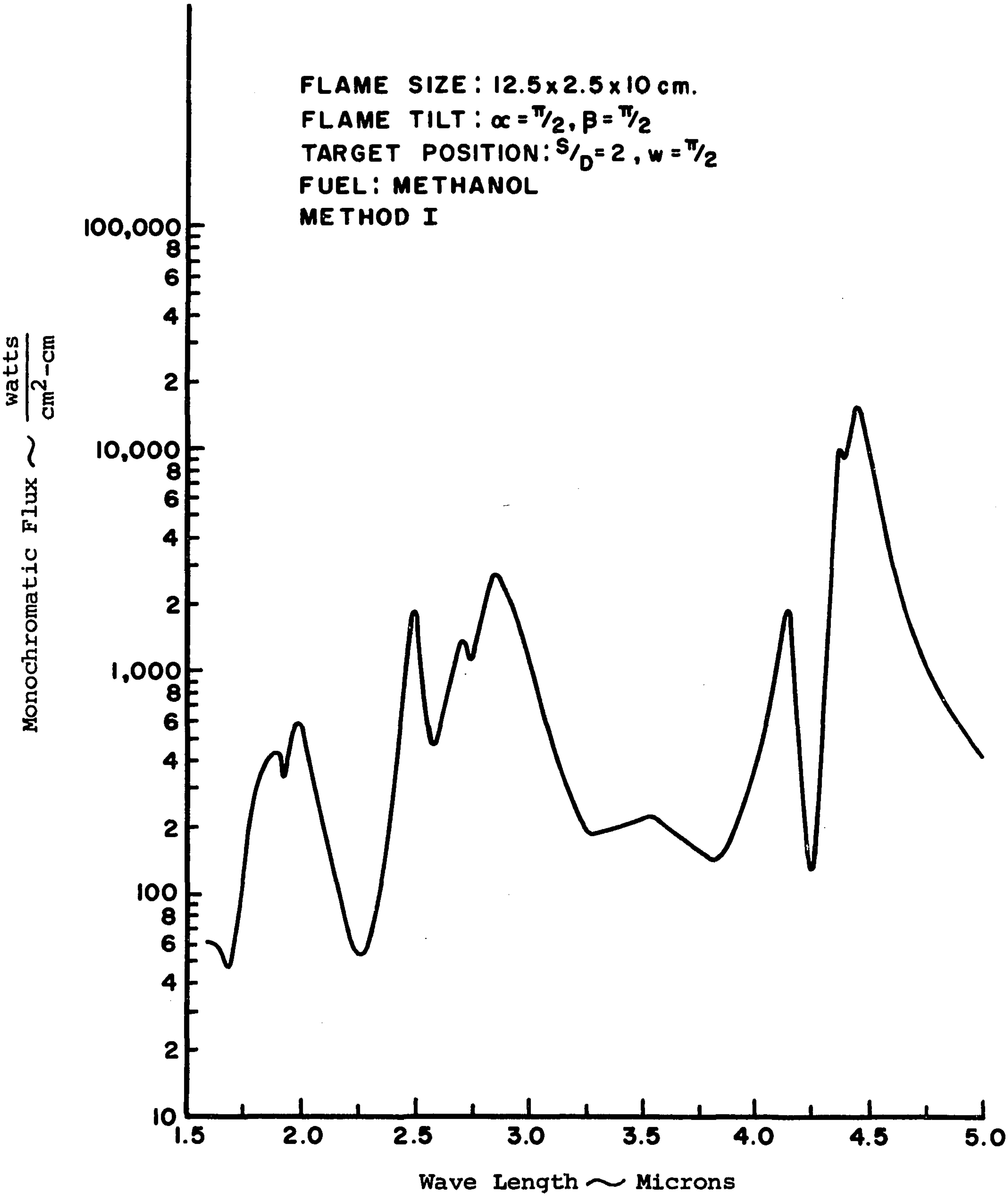

Figure 26. Monochromatic Flux to Target from a Sheet Flame

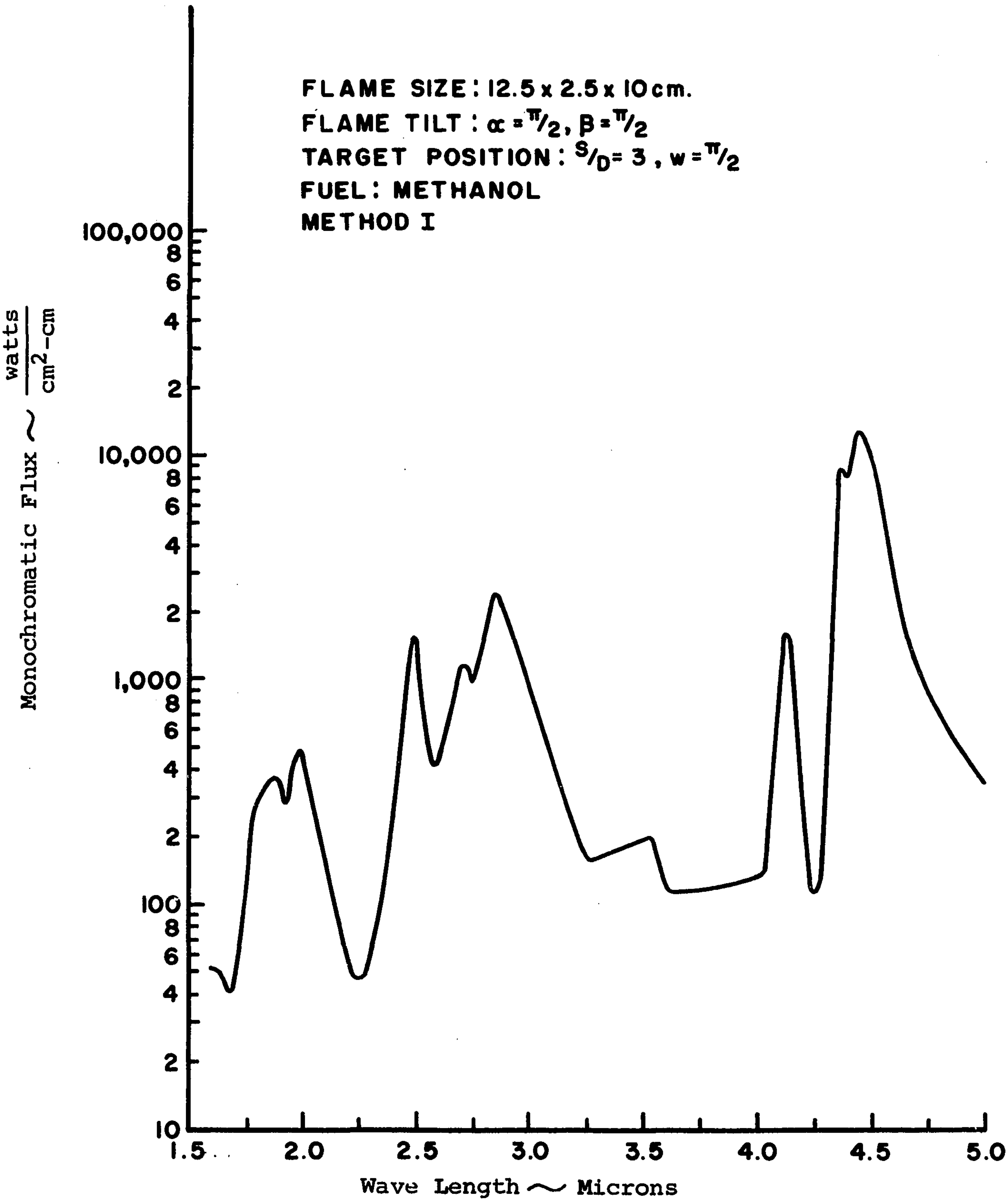

Figure 27. Monochromatic Flux to Target from a Sheet Flame

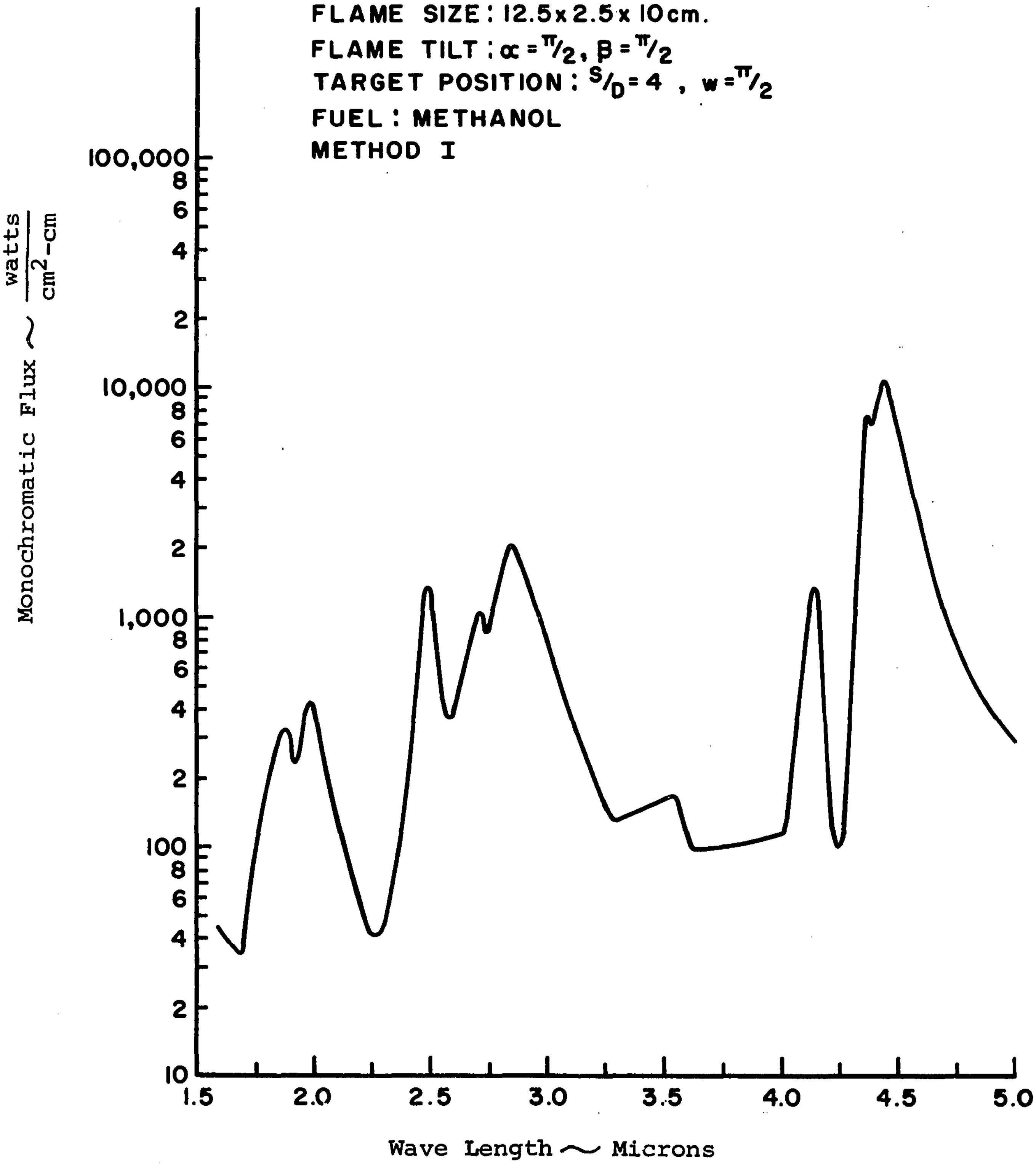

Figure 28. Monochromatic Flux to Target from a Sheet Flame

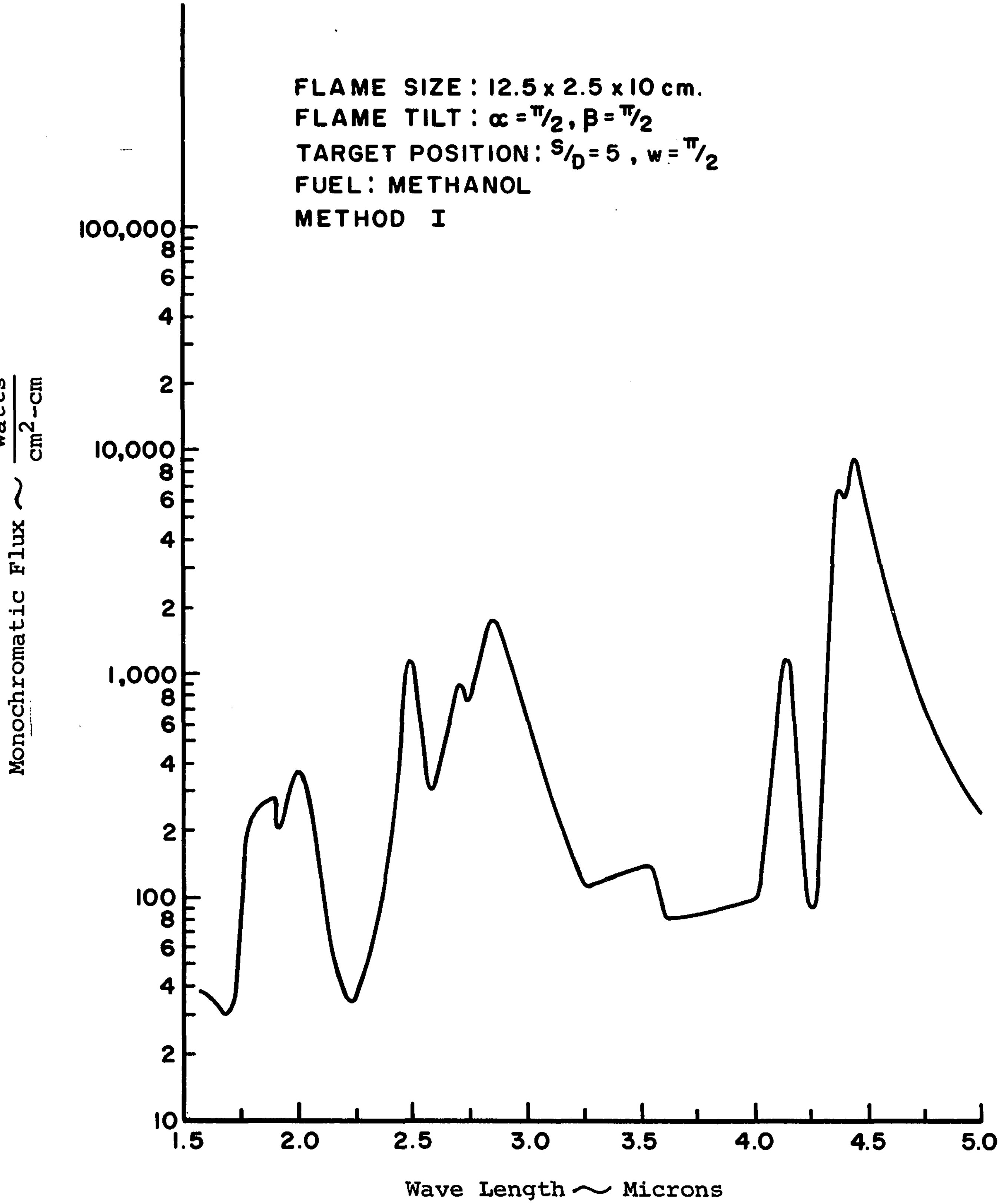

Figure 29. Monochromatic Flux to Target from a Sheet Flame

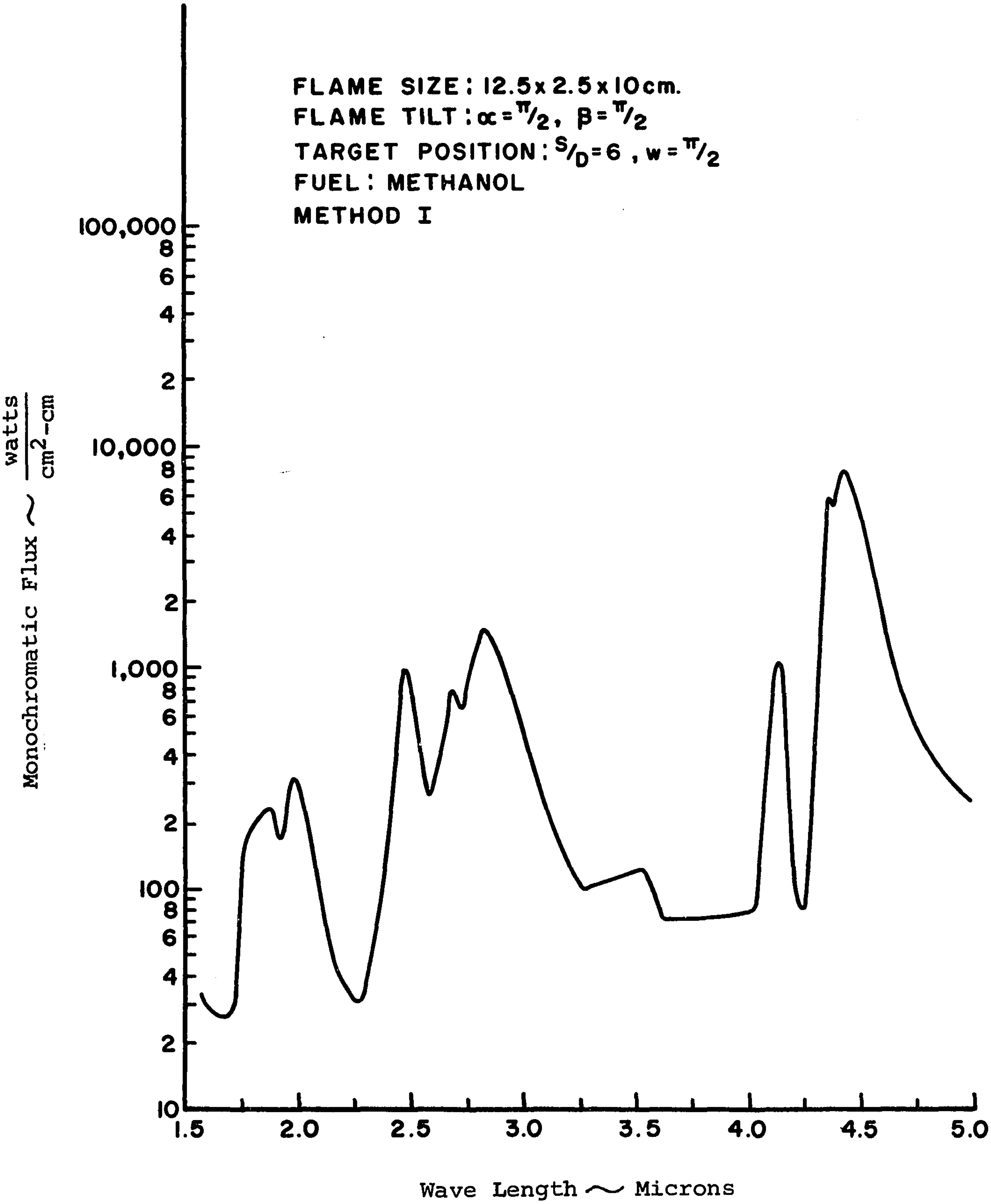

Figure 30. Monochromatic Flux to Target from a Sheet Flame

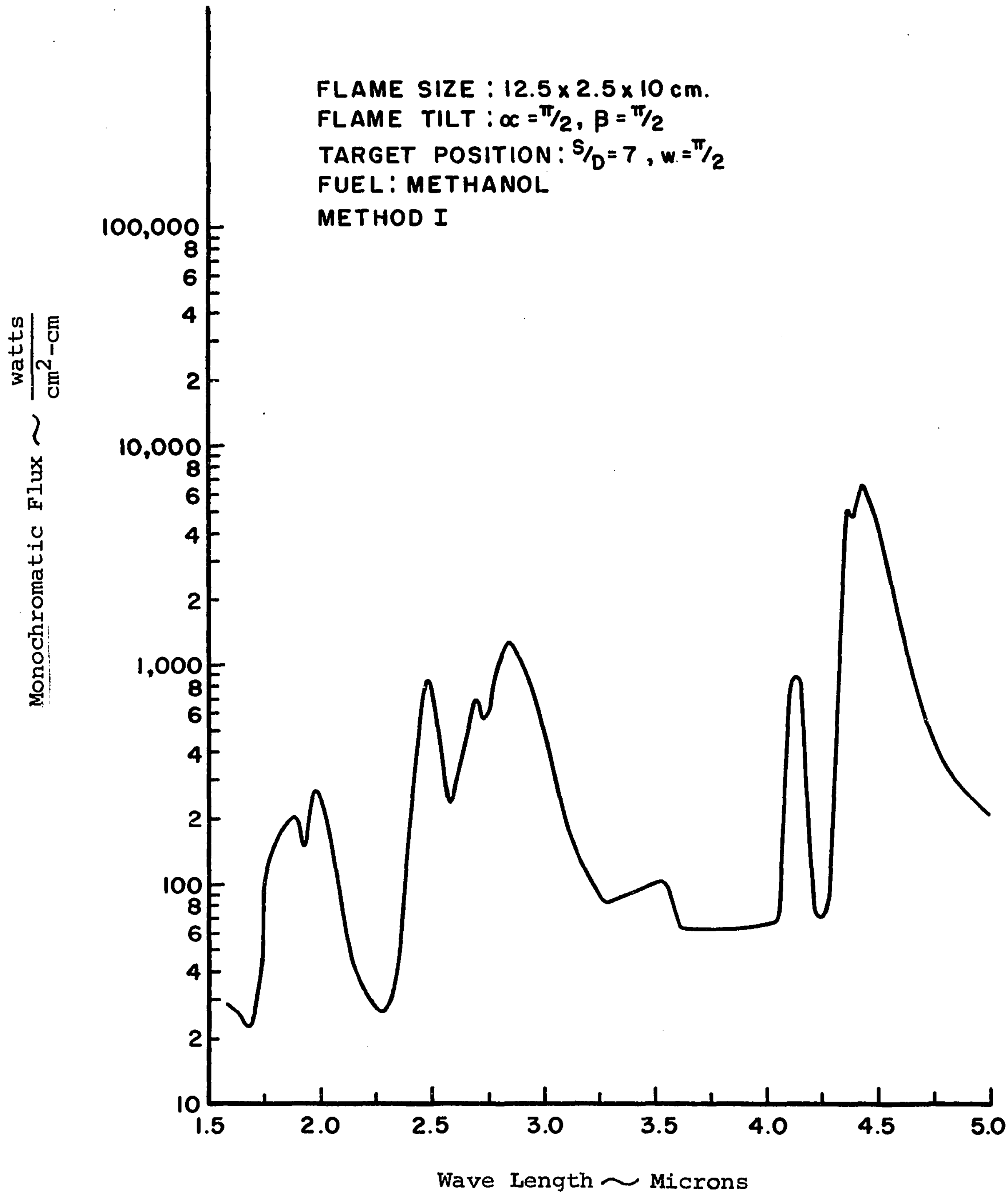

Figure 31. Monochromatic Flux to Target from a Sheet Flame

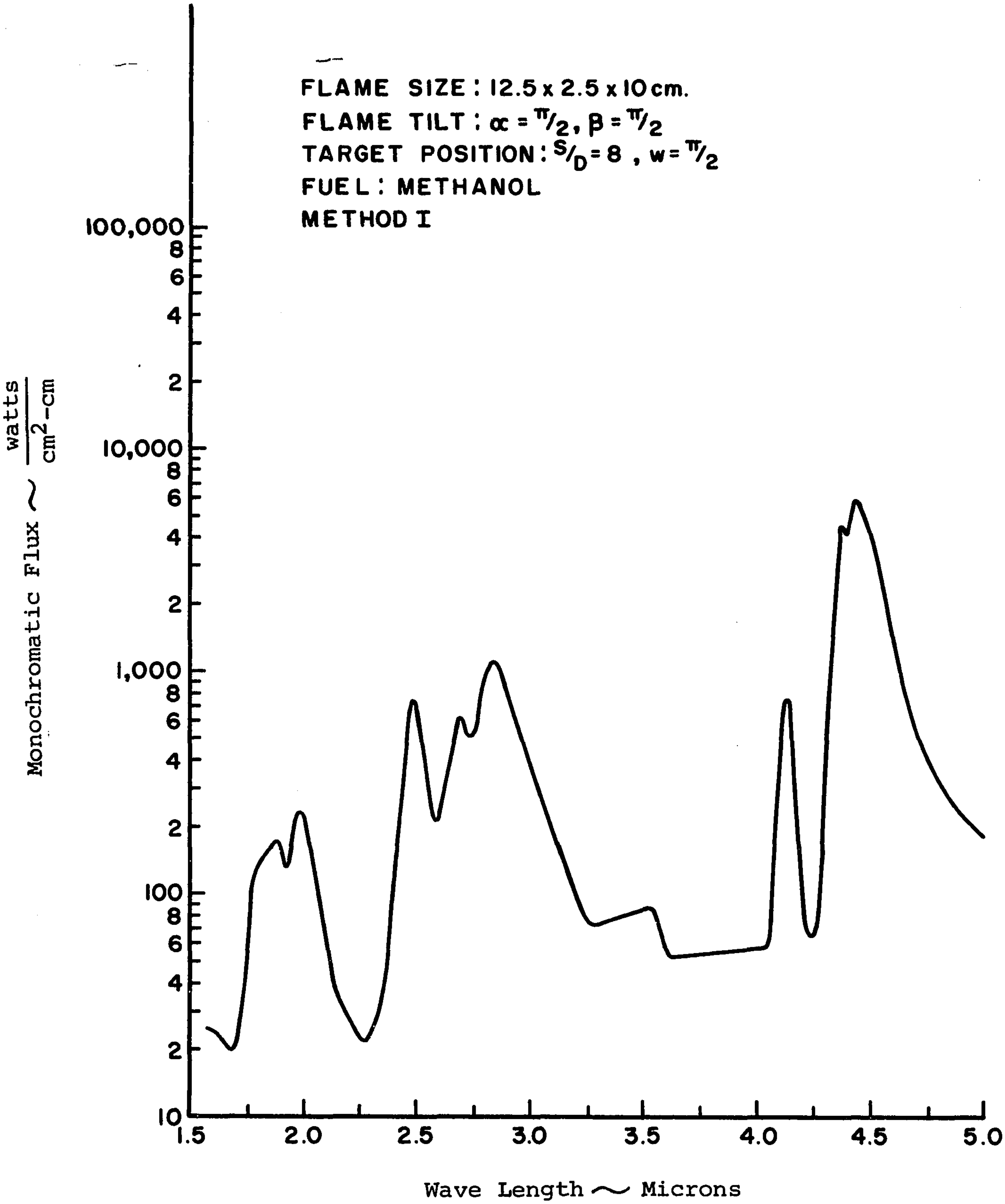

Figure 32. Monochromatic Flux to Target from a Sheet Flame

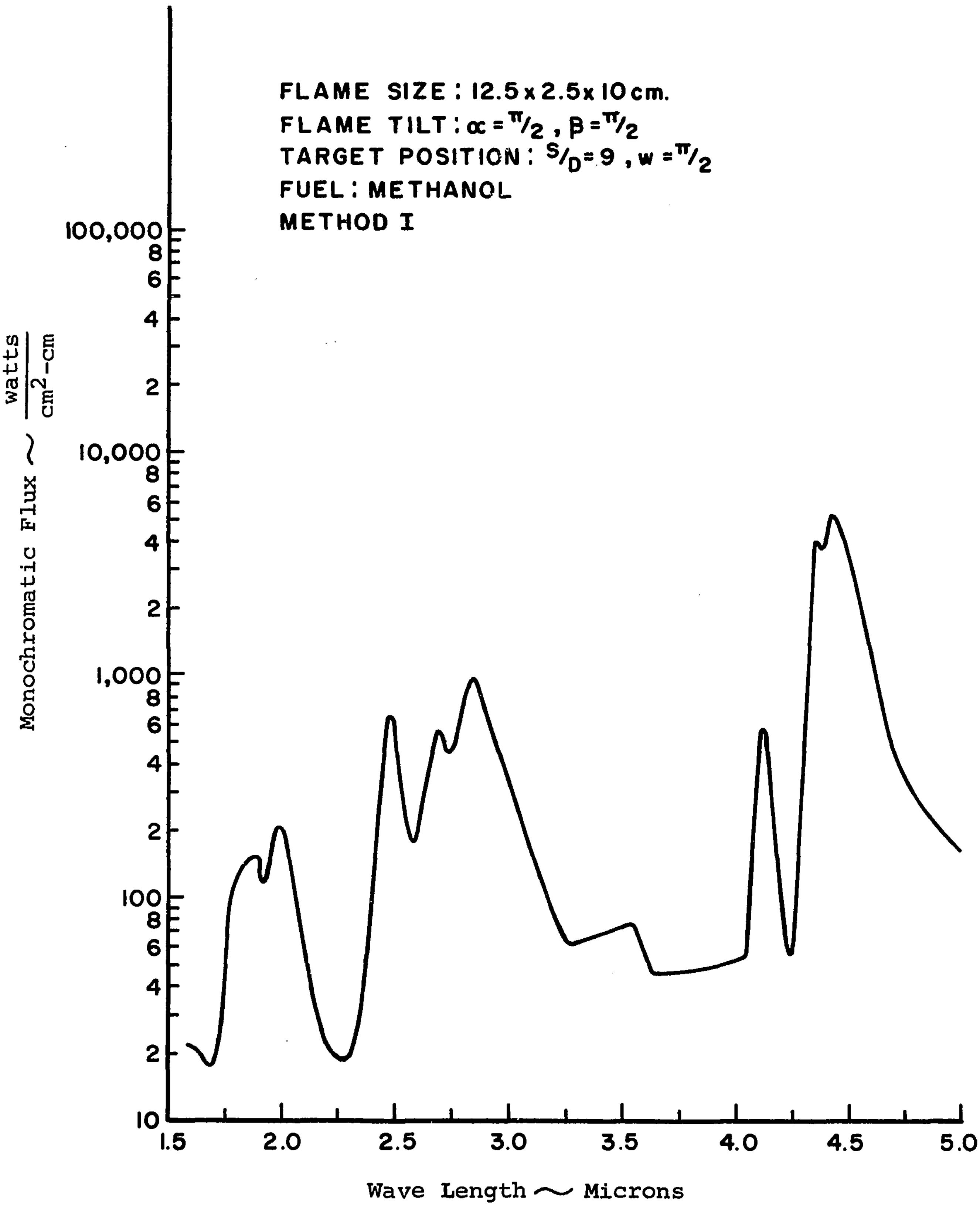

Figure 33. Monochromatic Flux to Target from a Sheet Flame

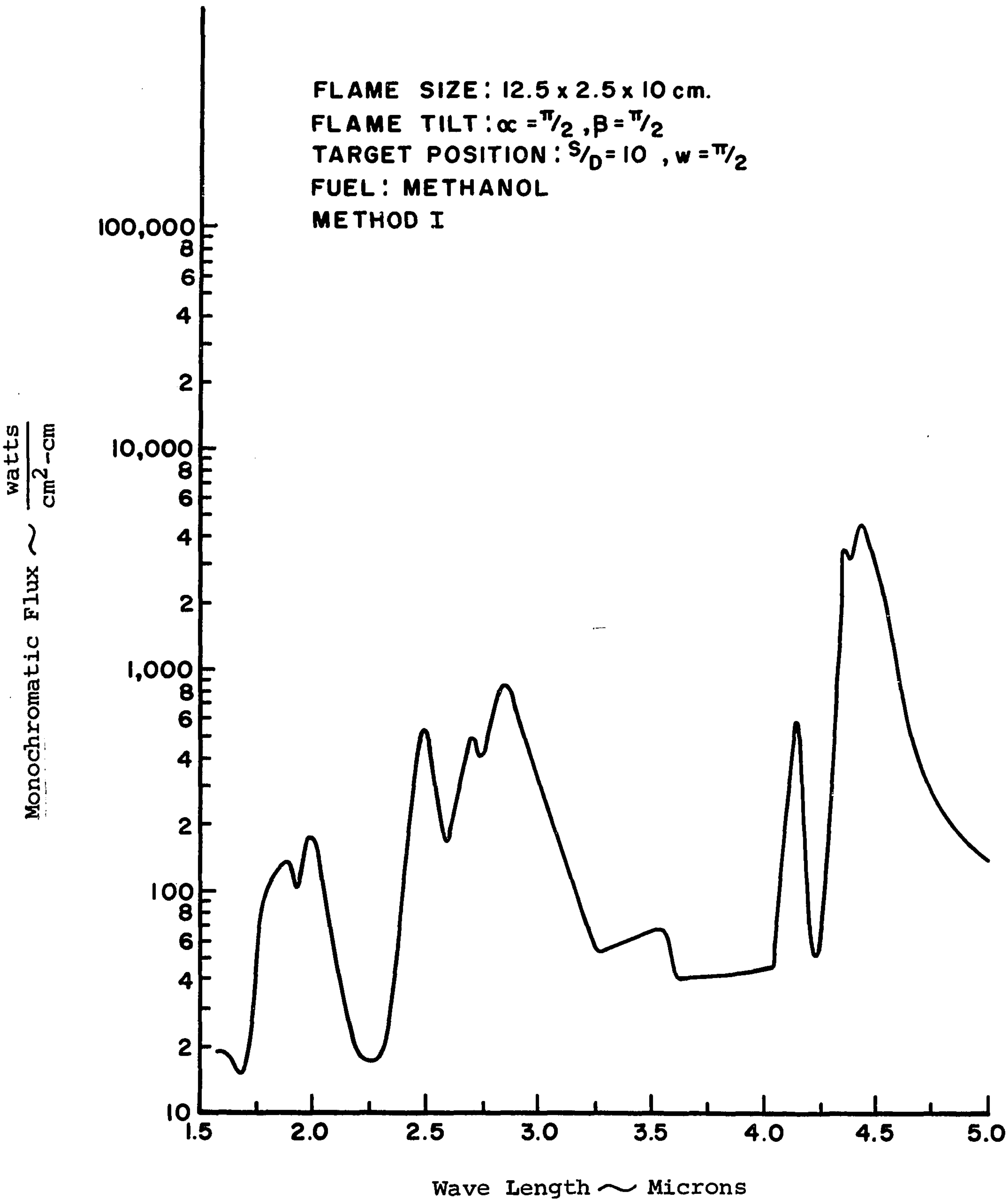

Figure 34. Monochromatic Flux to Target from a Sheet Flame

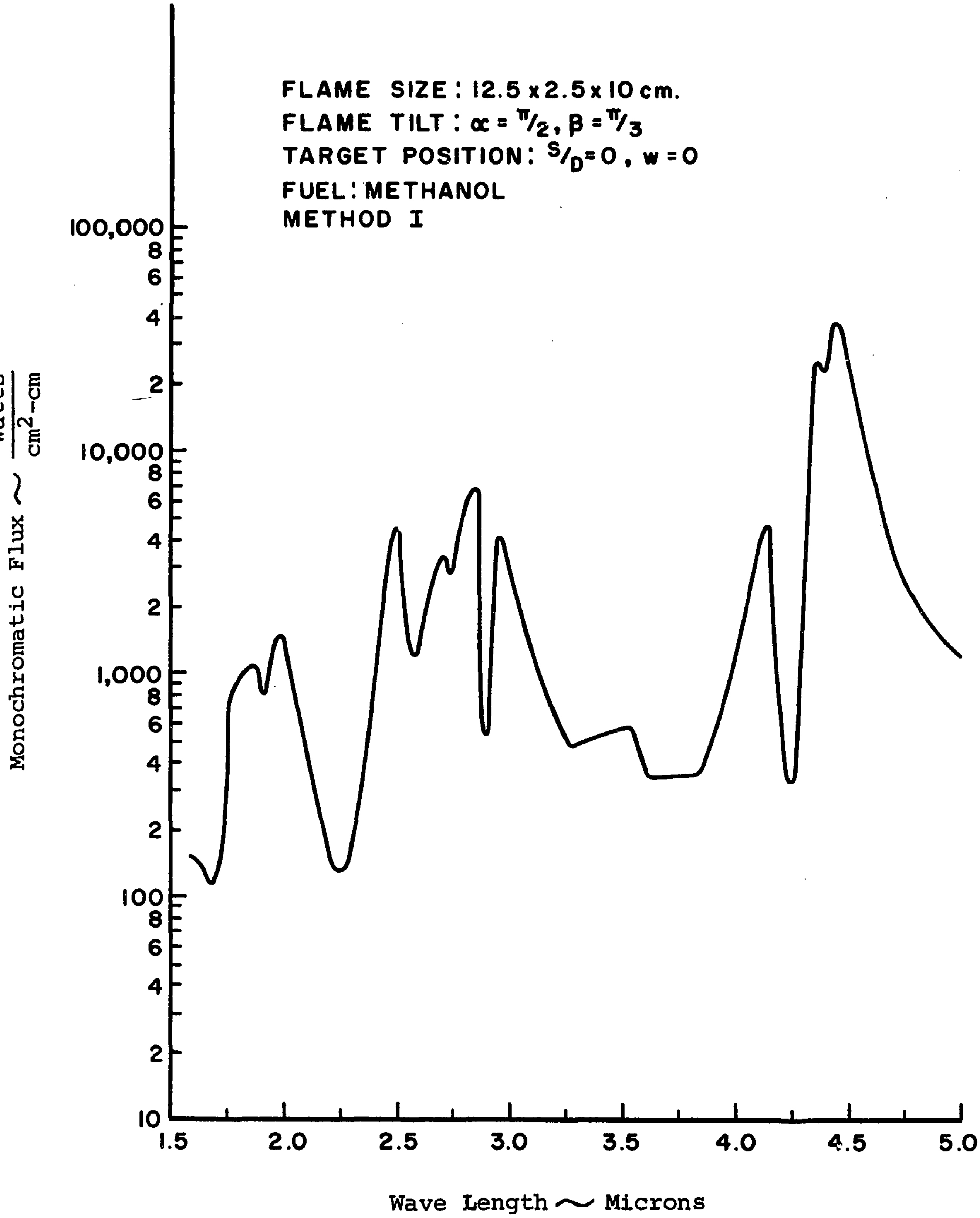

Figure 35. Monochromatic Flux to Target from a Sheet Flame

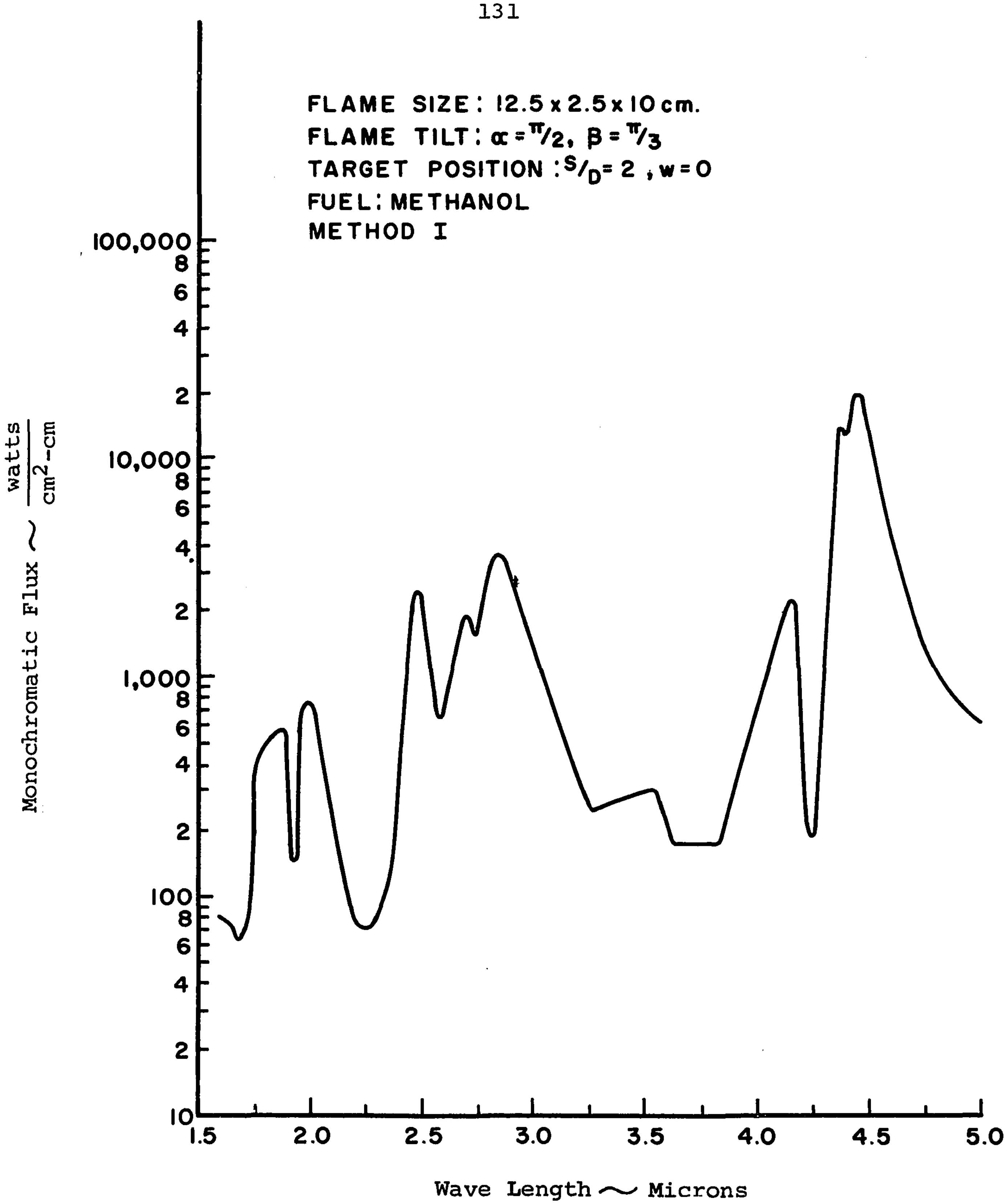

Figure 36. Monochromatic Flux to Target from a Sheet Flame

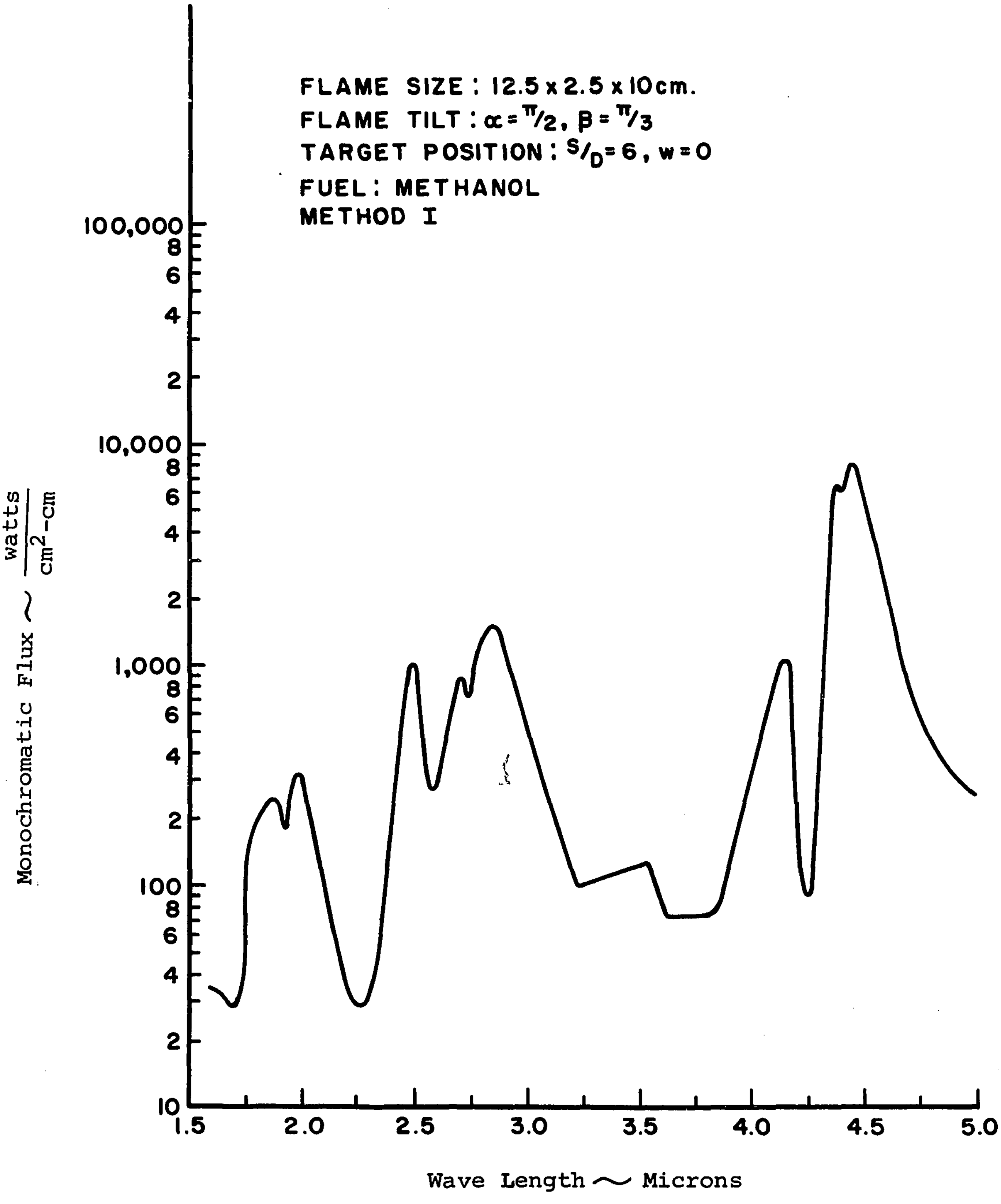

Figure 37. Monochromatic Flux to Target from a Sheet Flame

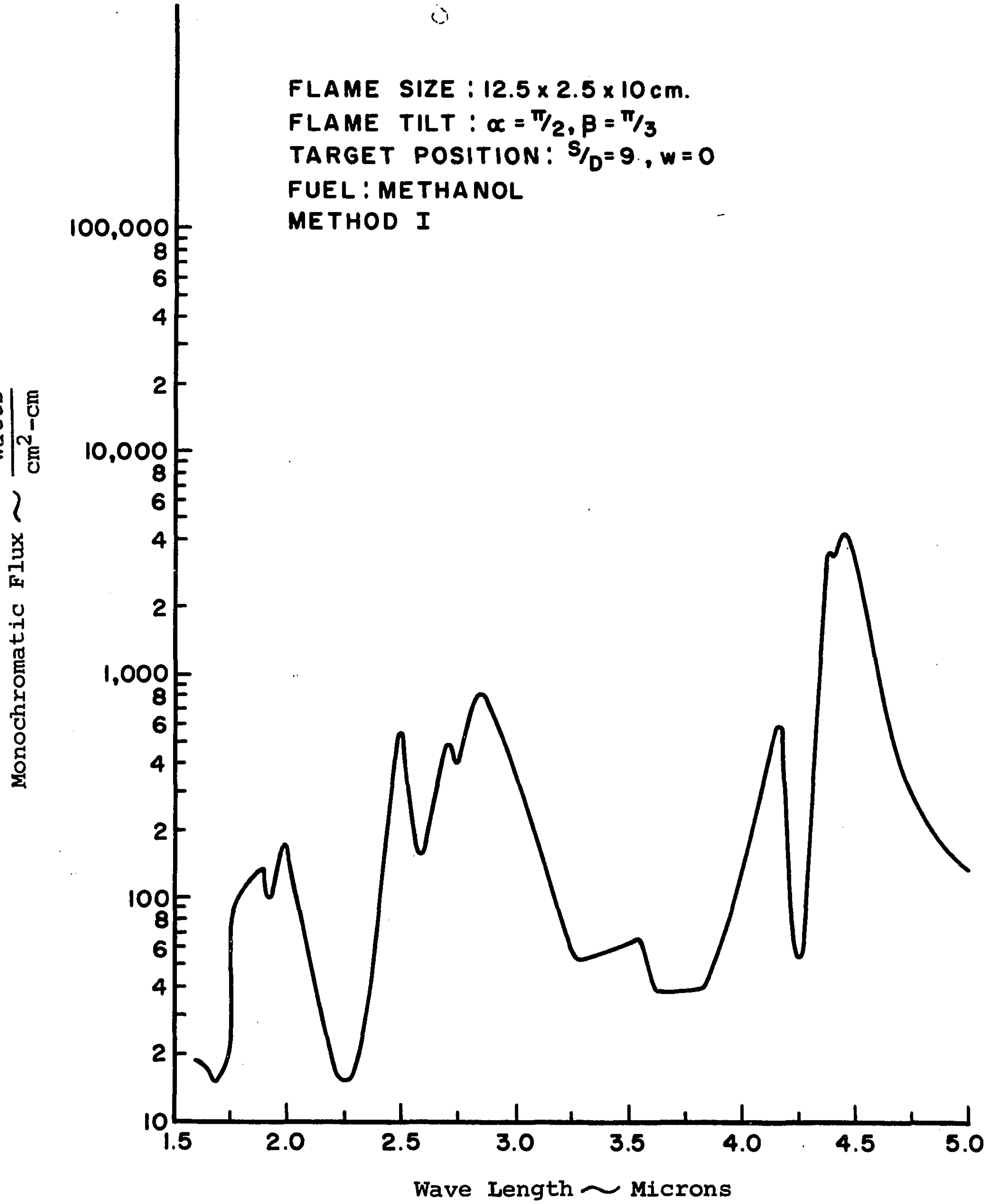

Figure 38. Monochromatic Flux to Target from a Sheet Flame

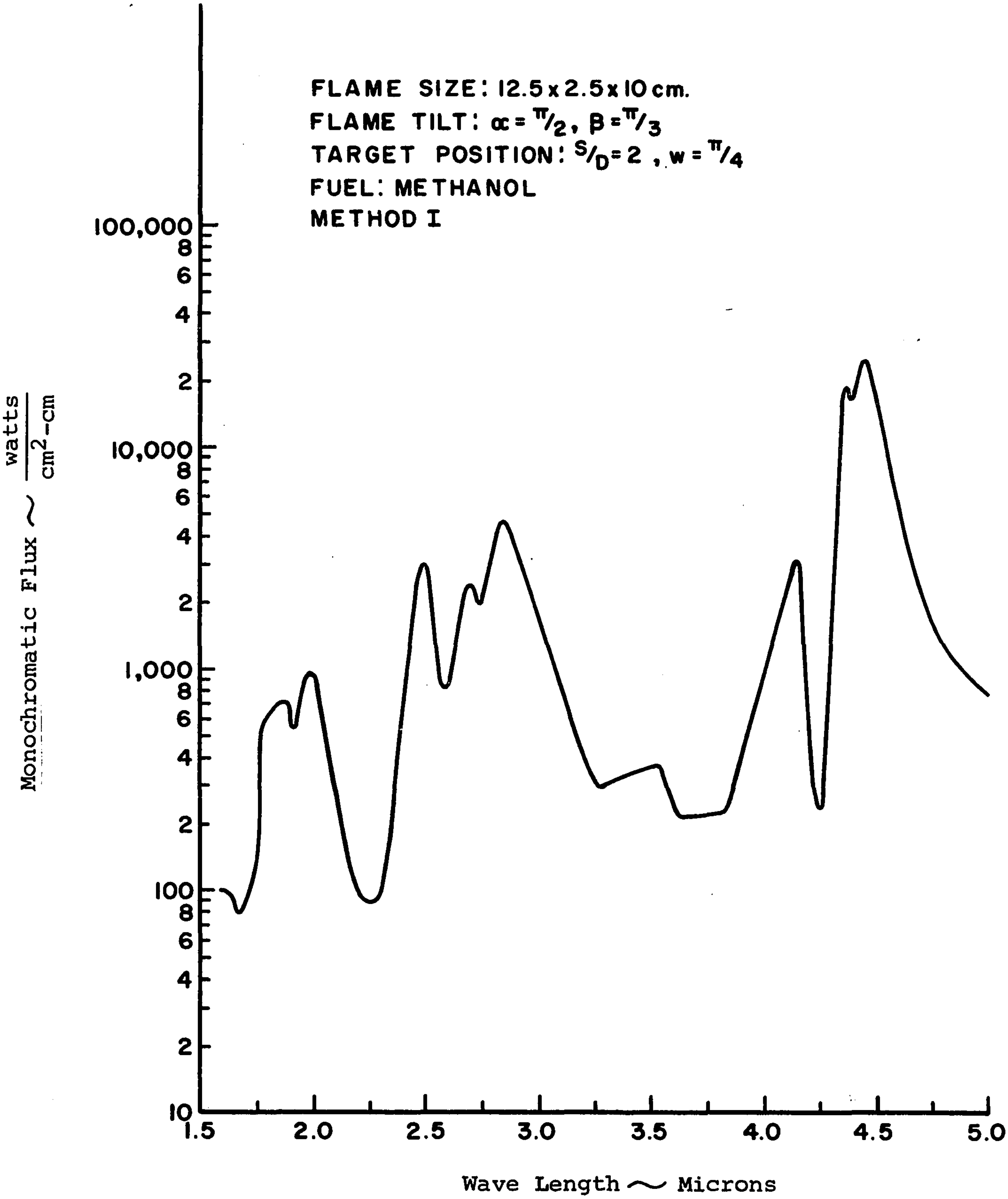

Figure 39. Monochromatic Flux to Target from a Sheet Flame

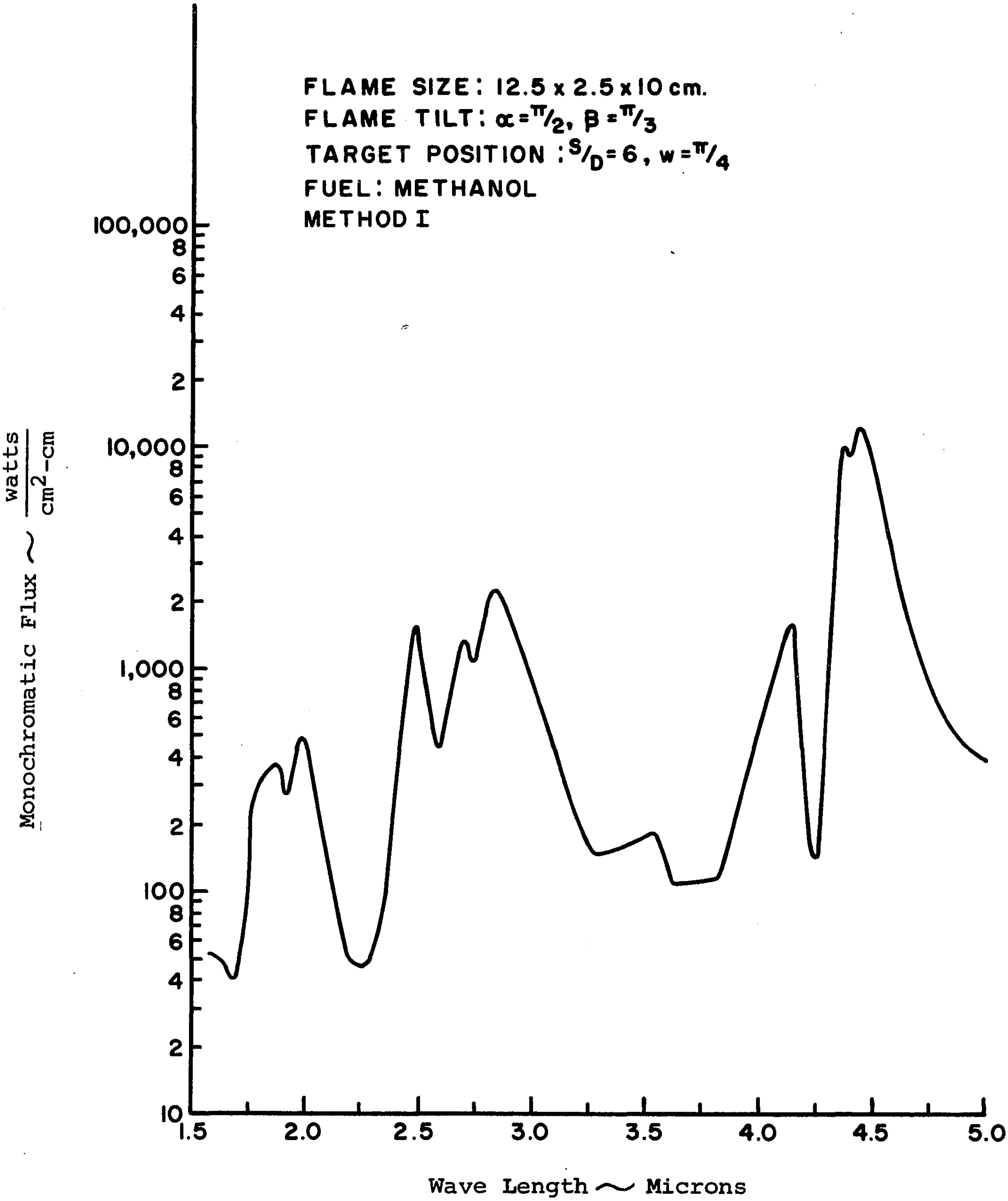

Figure 40. Monochromatic Flux to Target from a Sheet Flame

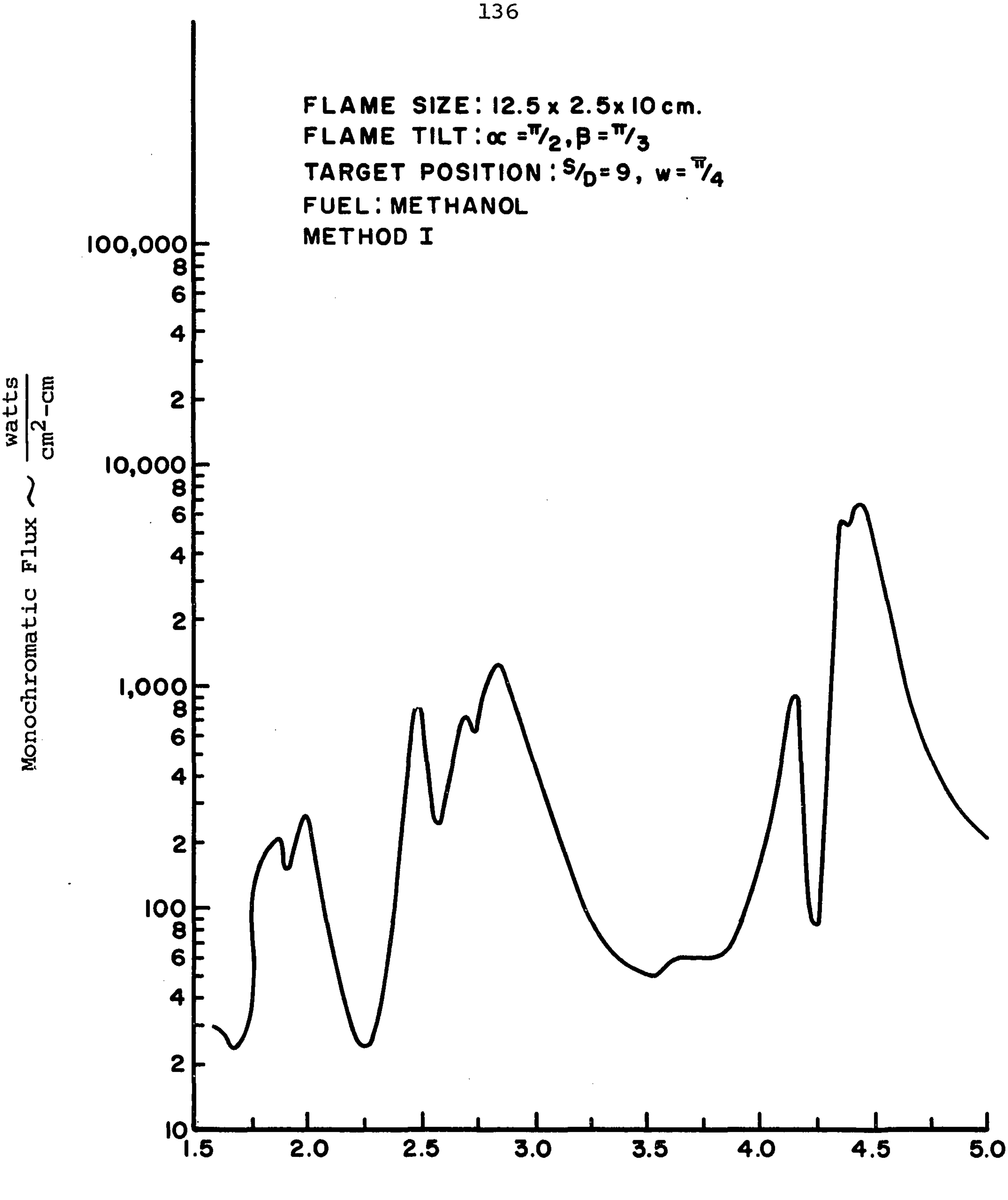

Figure 41. Monochromatic Flux to Target from a Sheet Flame

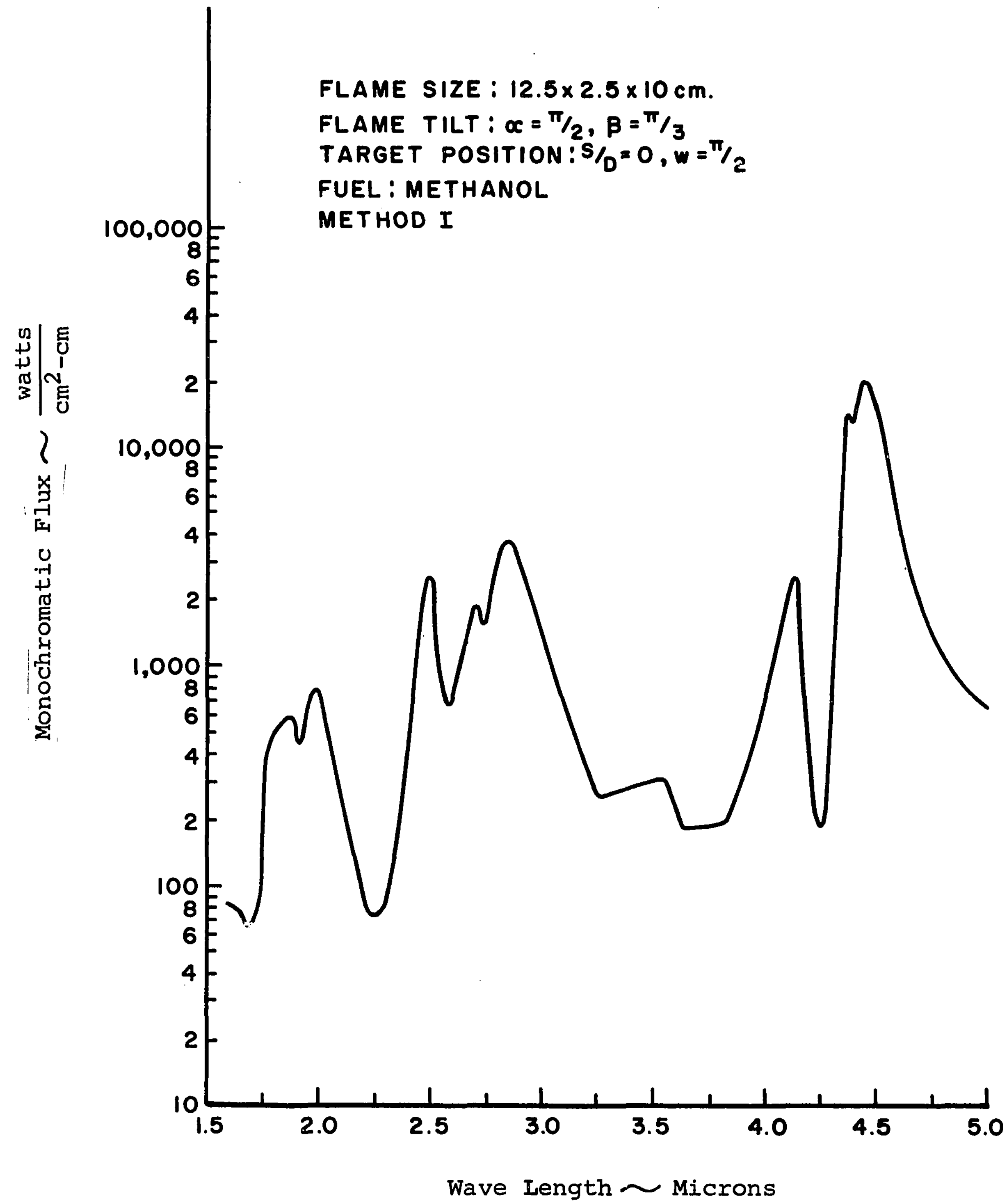

Figure 42. Monochromatic Flux to Target from a Sheet Flame

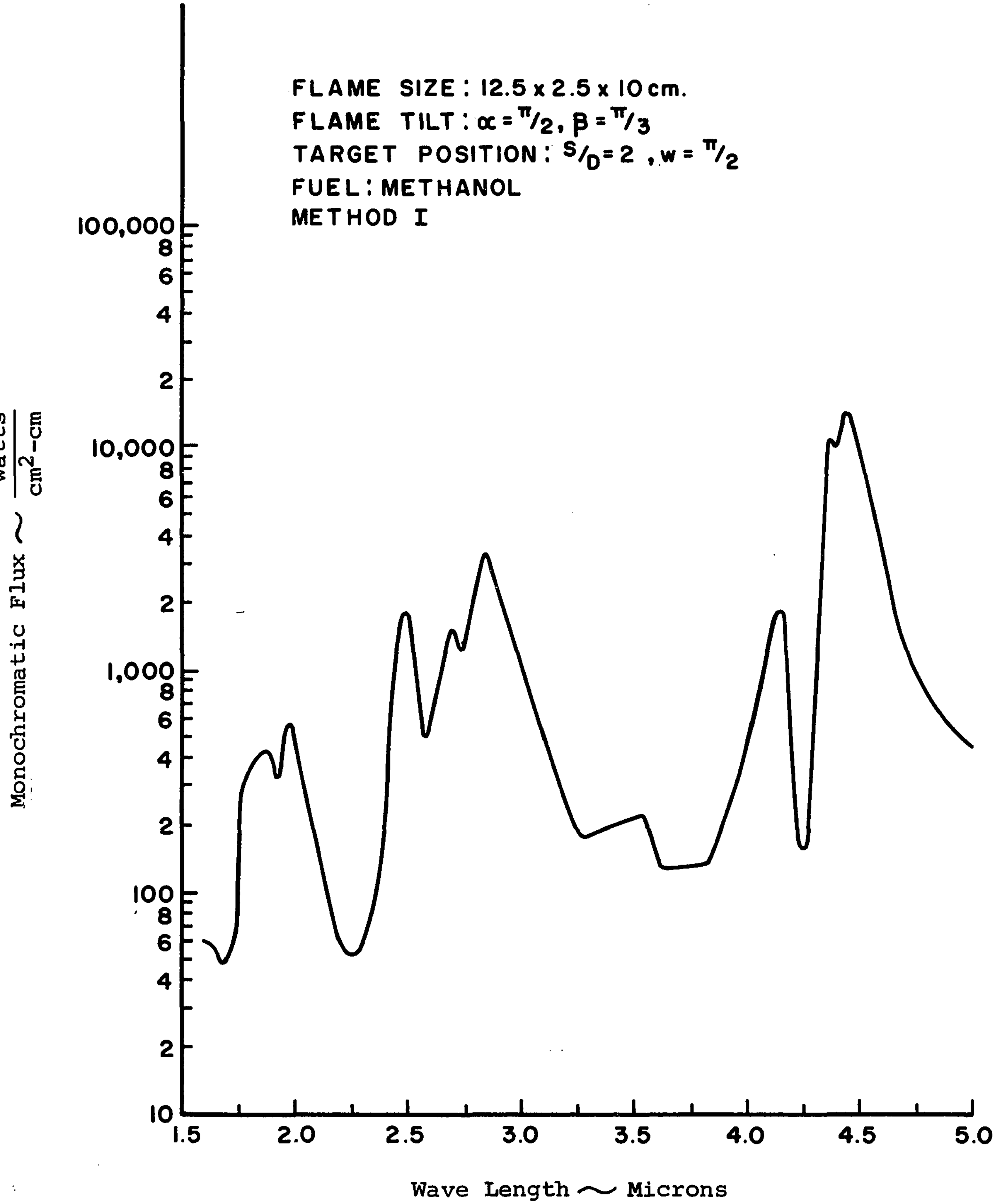

Figure 43. Monochromatic Flux to Target from a Sheet Flame

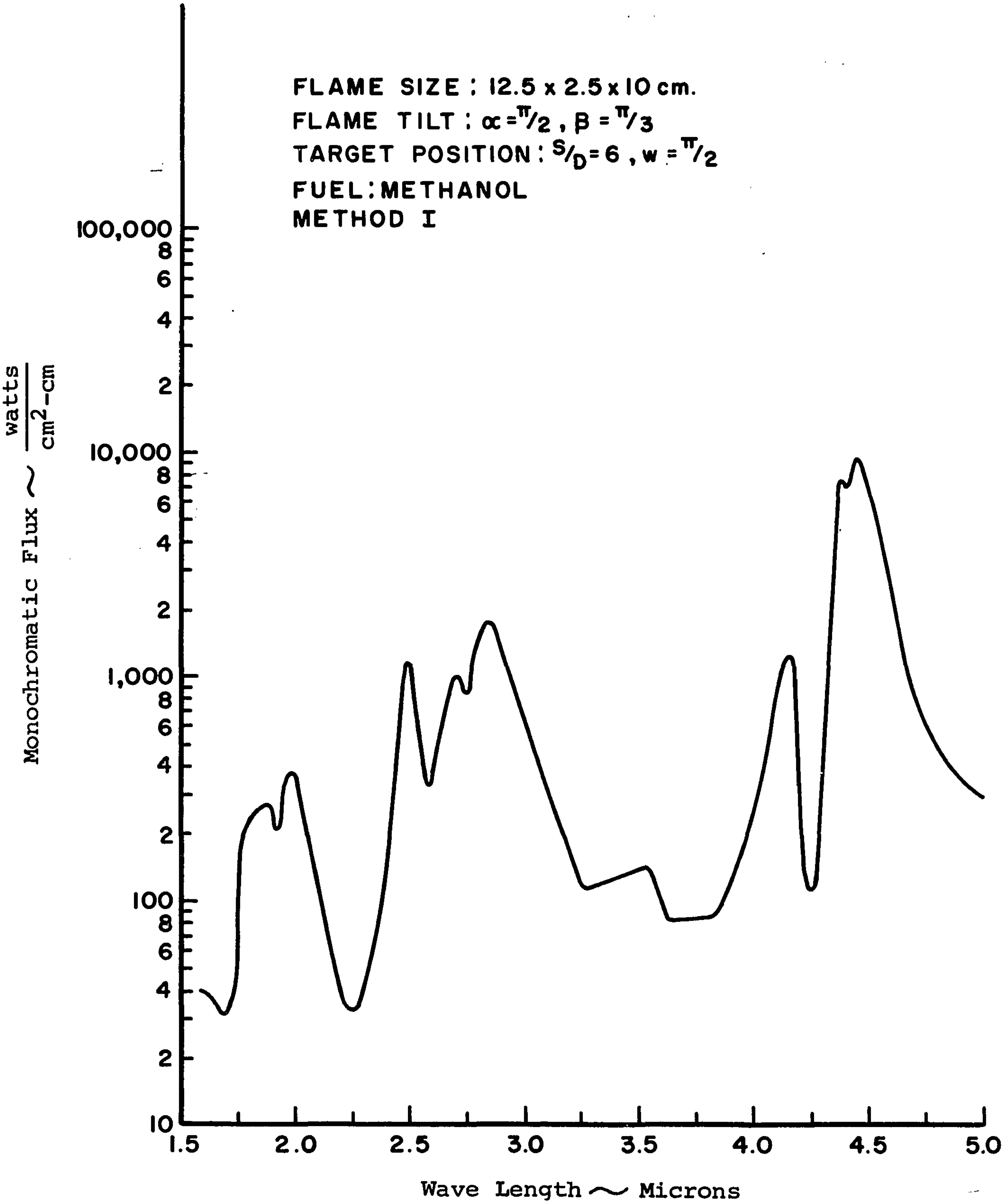

Figure 44. Monochromatic Flux to Target from a Sheet Flame

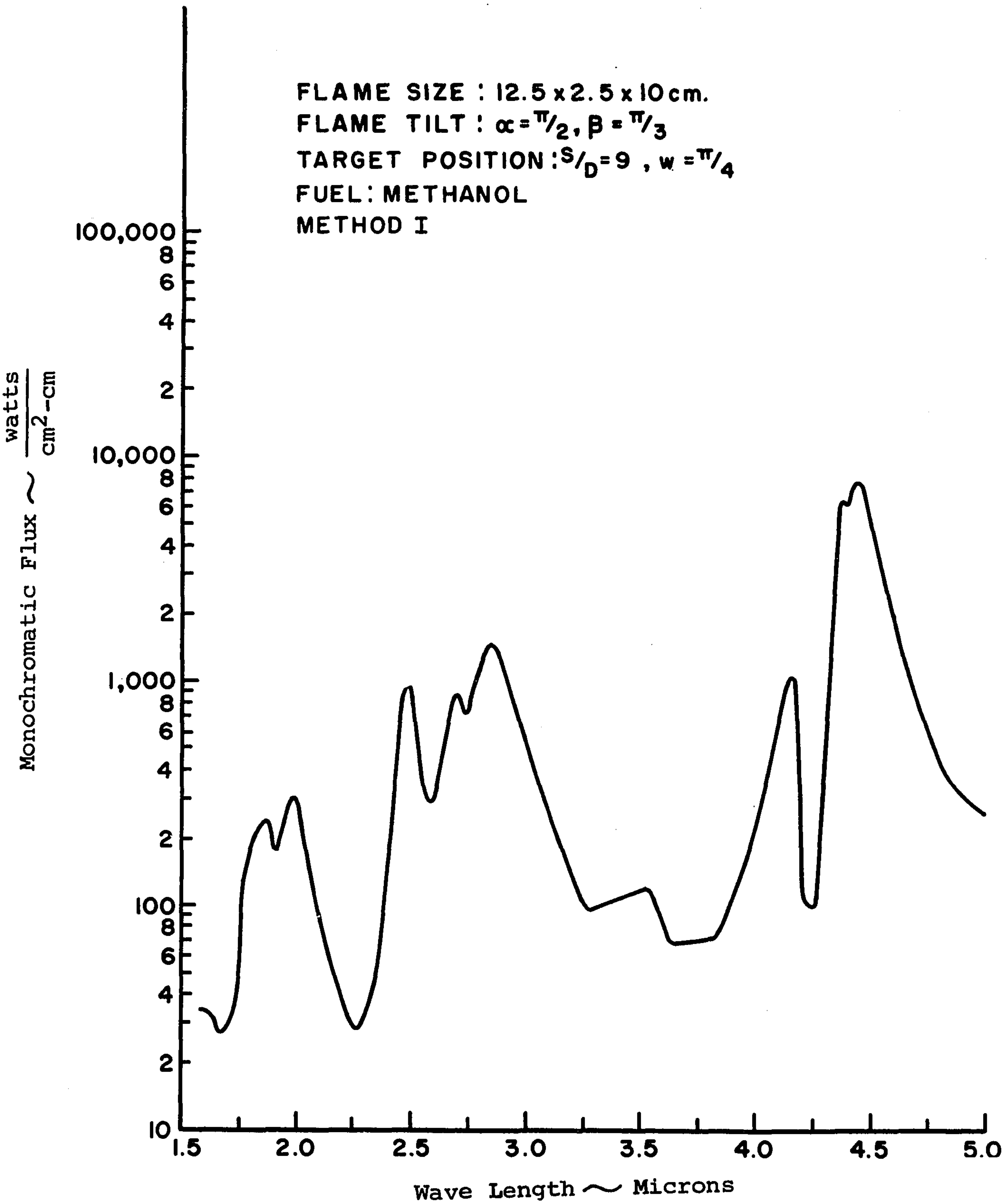

Figure 45. Monochromatic Flux to Target from a Sheet Flame

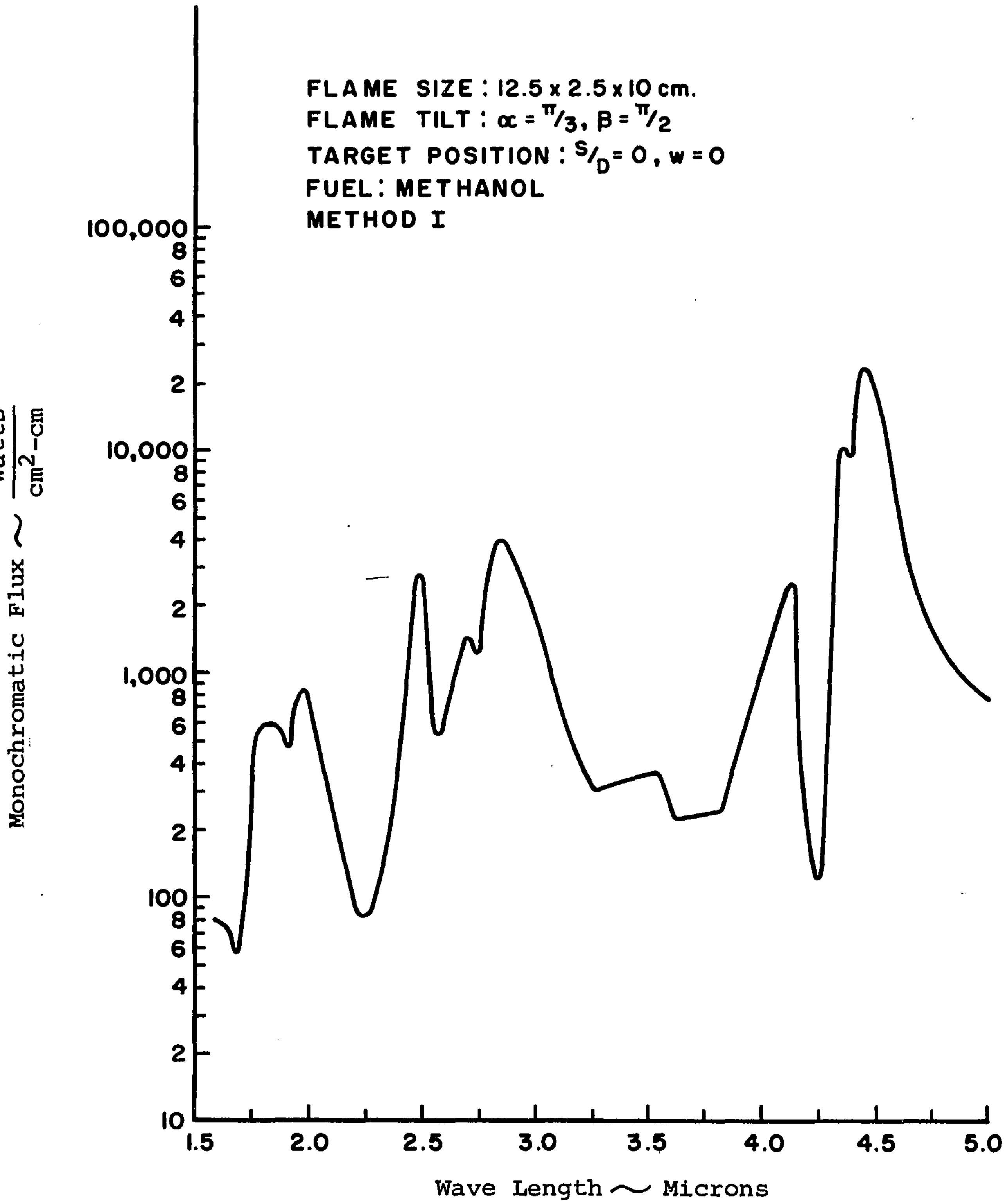

Figure 46. Monochromatic Flux to Target from a Sheet Flame

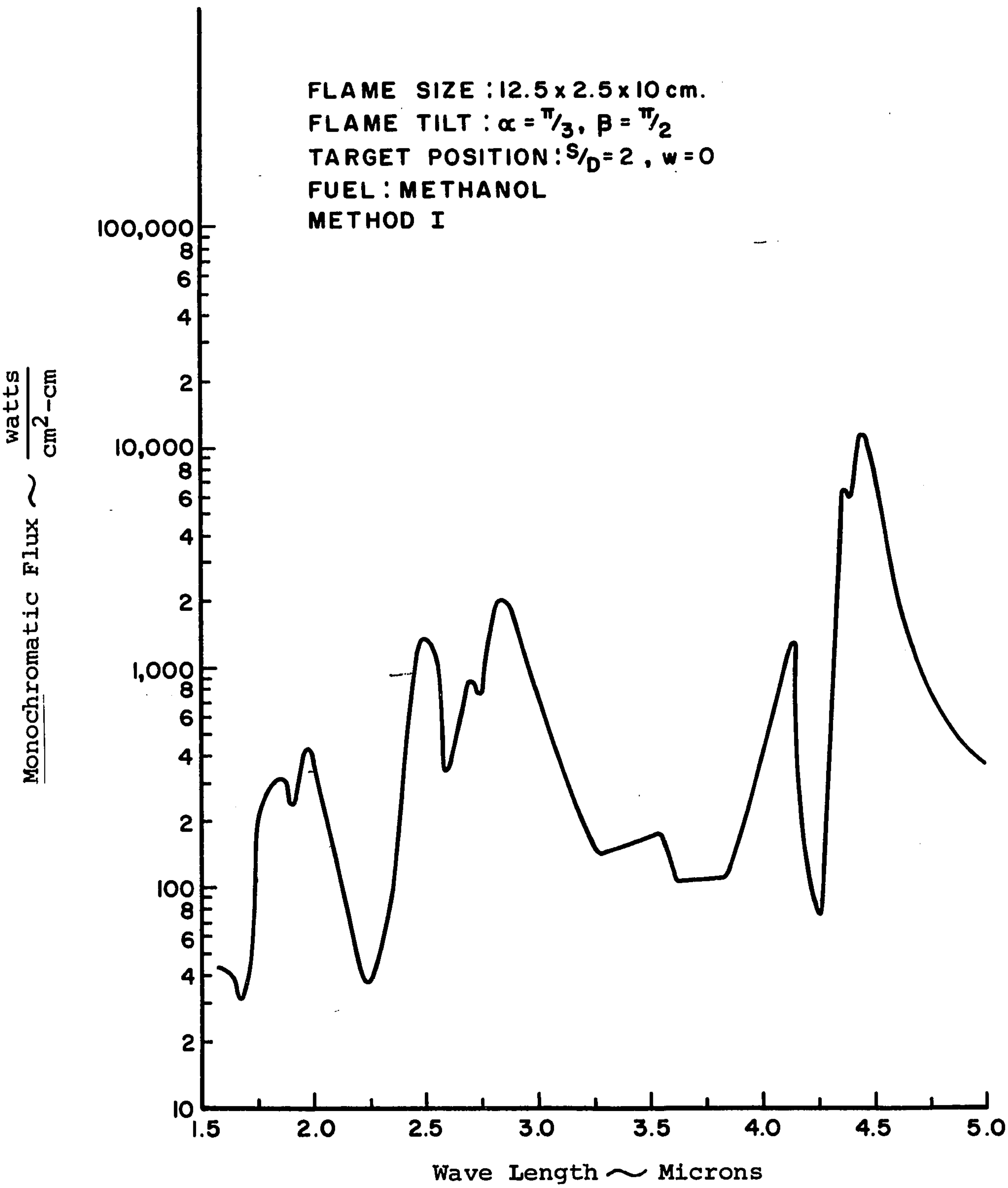

Figure 47. Monochromatic Flux to Target from a Sheet Flame

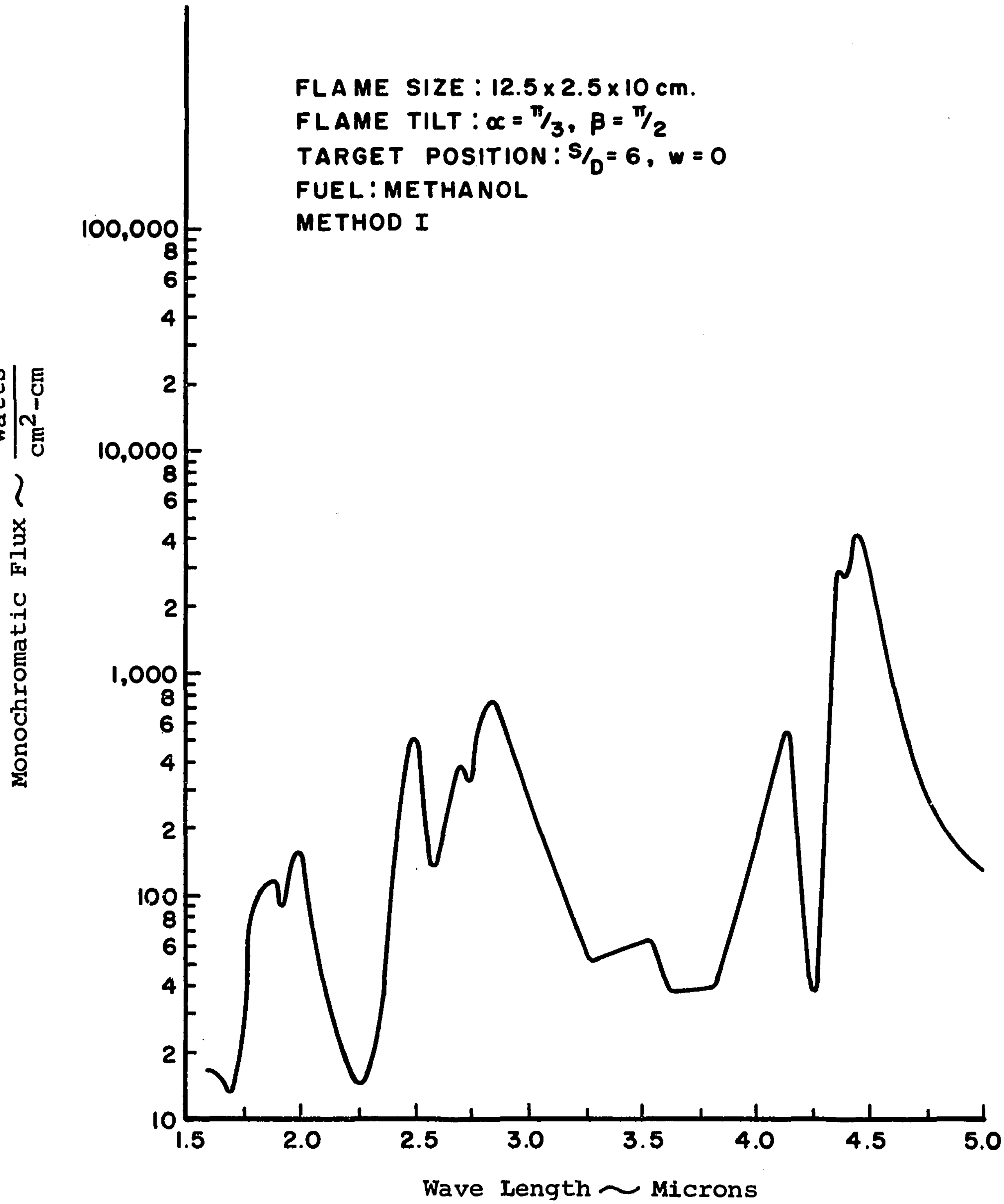

Figure 48. Monochromatic Flux to Target from a Sheet Flame

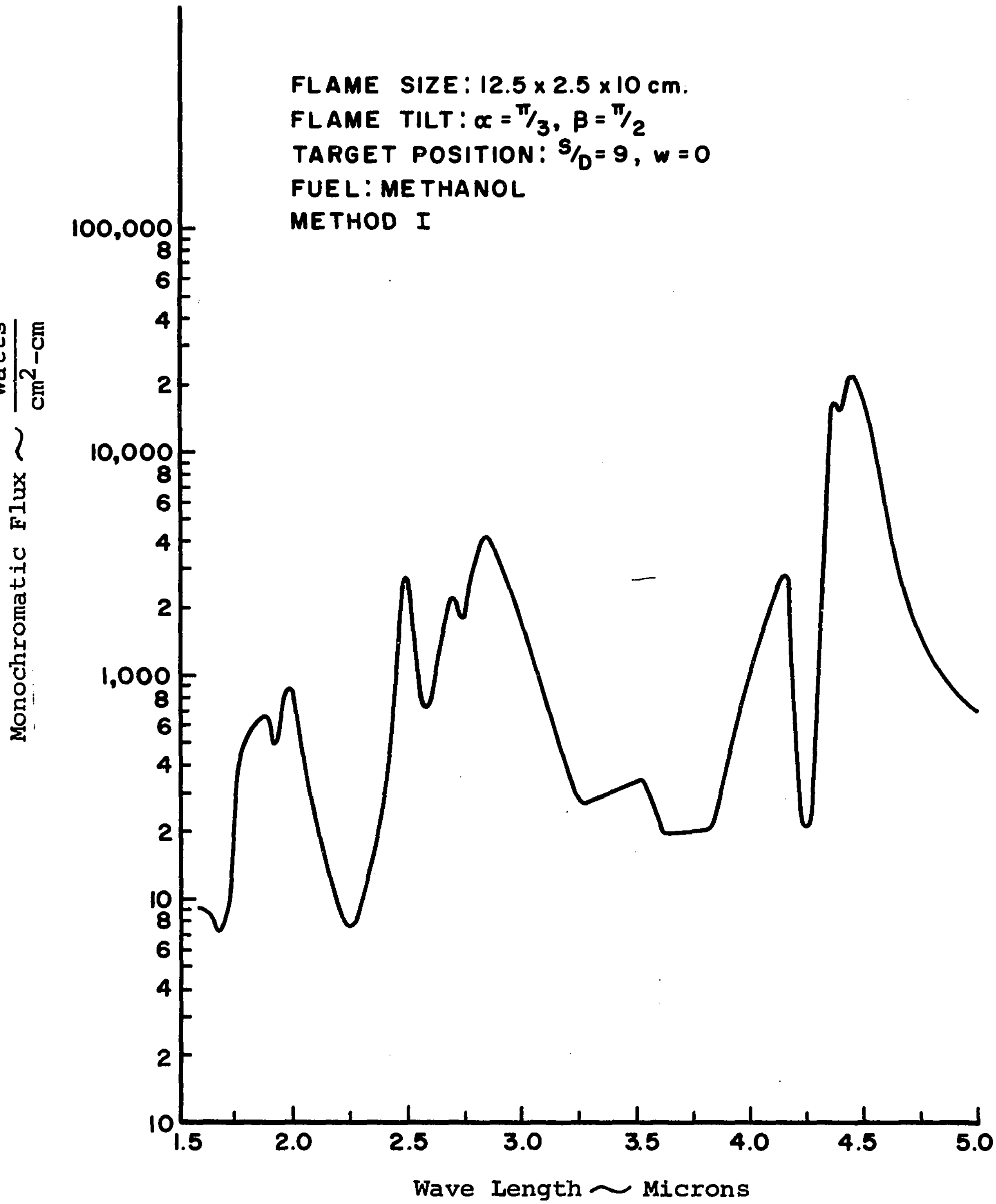

Figure 49. Monochromatic Flux to Target from a Sheet Flame

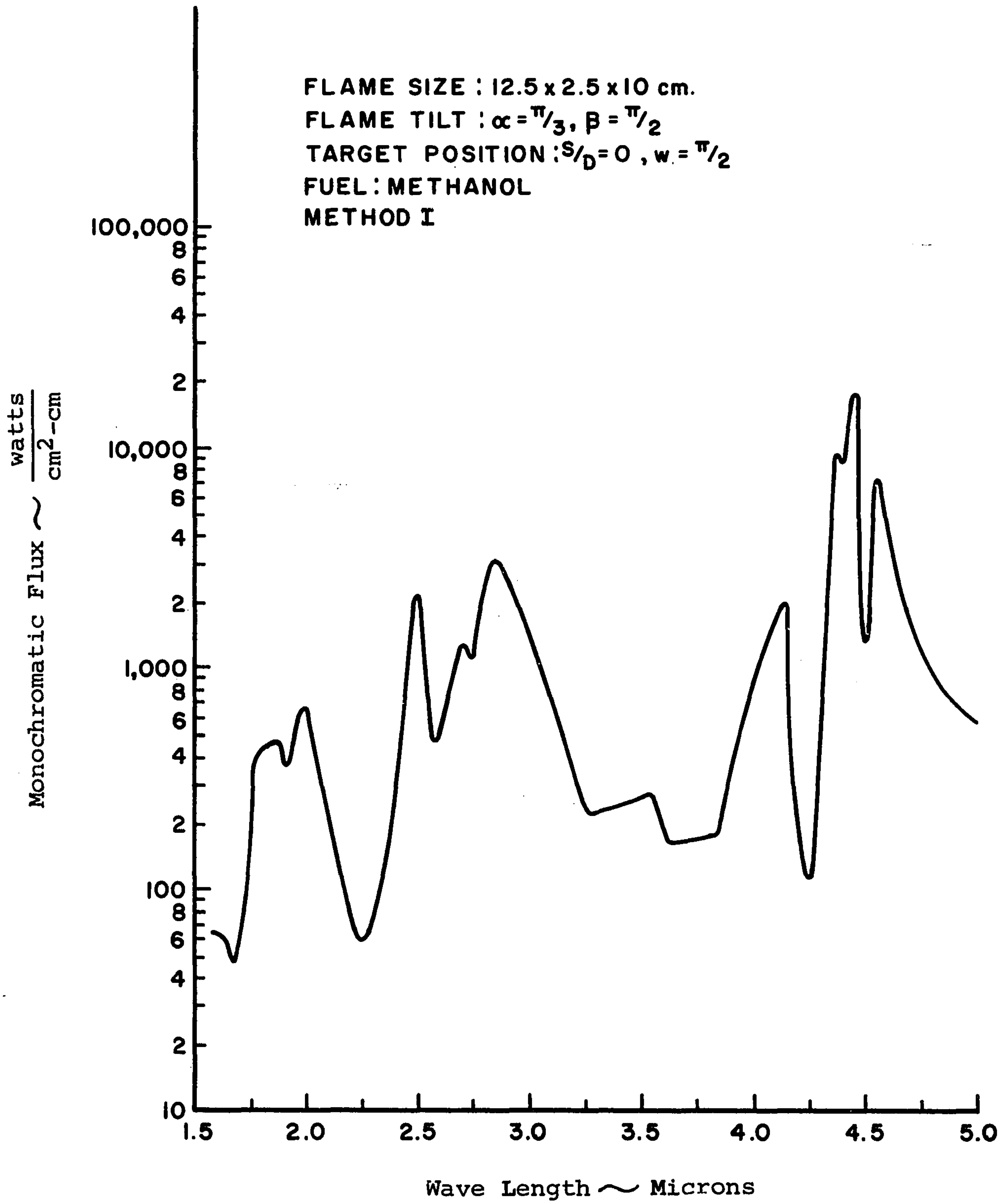

Figure 50. Monochromatic Flux to Target from a Sheet Flame

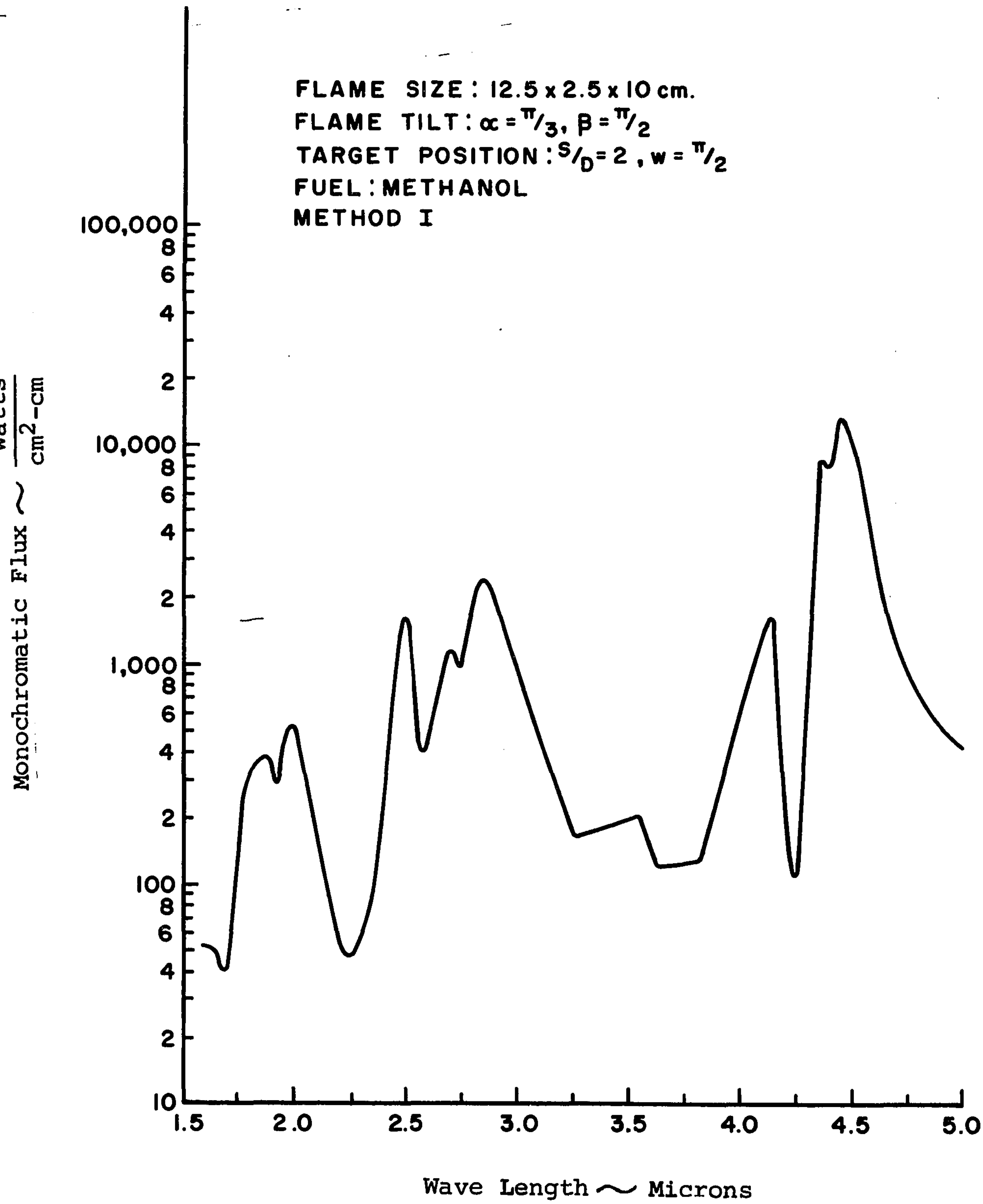

Figure 51. Monochromatic Flux to Target from a Sheet Flame

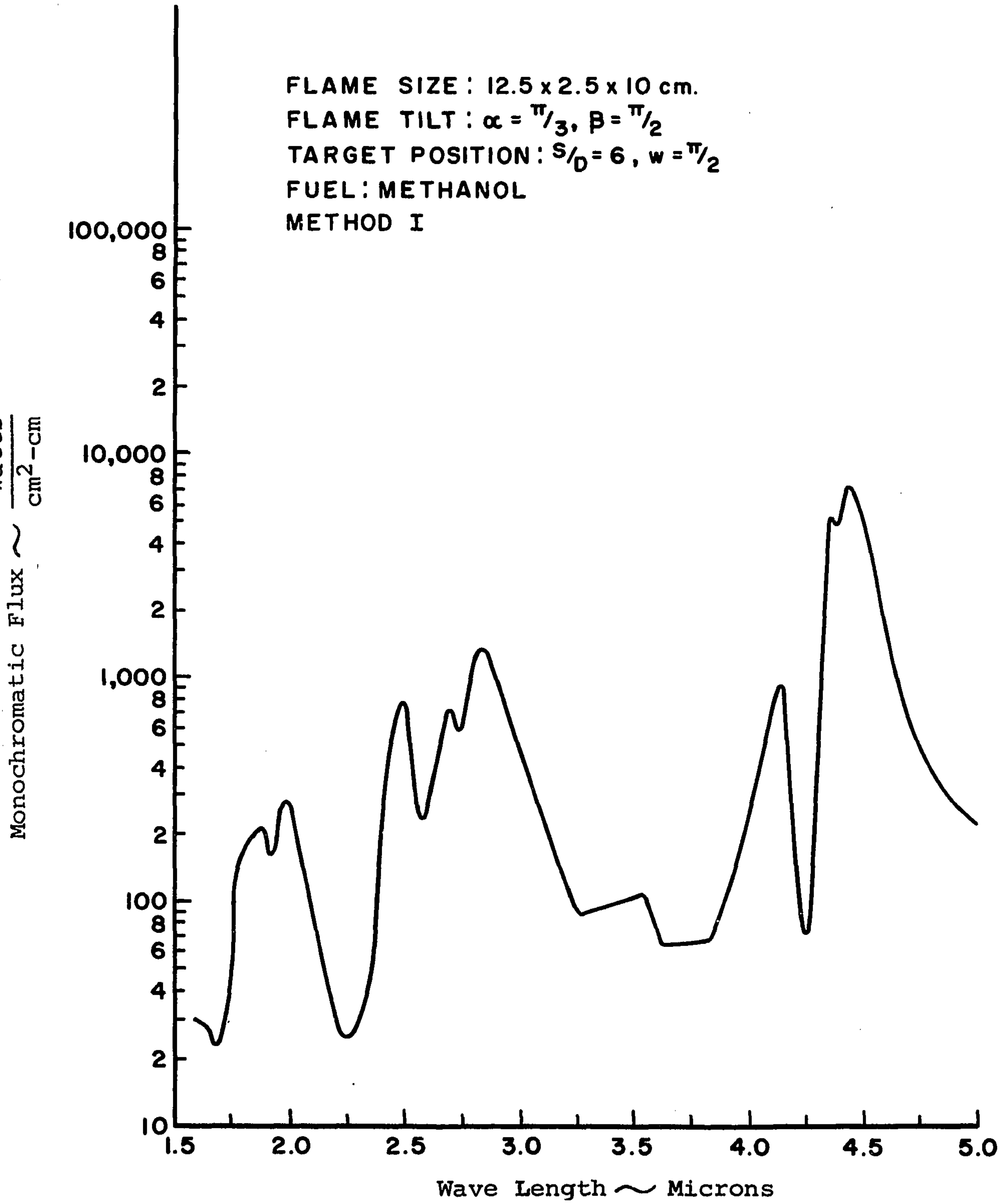

Figure 52. Monochromatic Flux to Target from a Sheet Flame

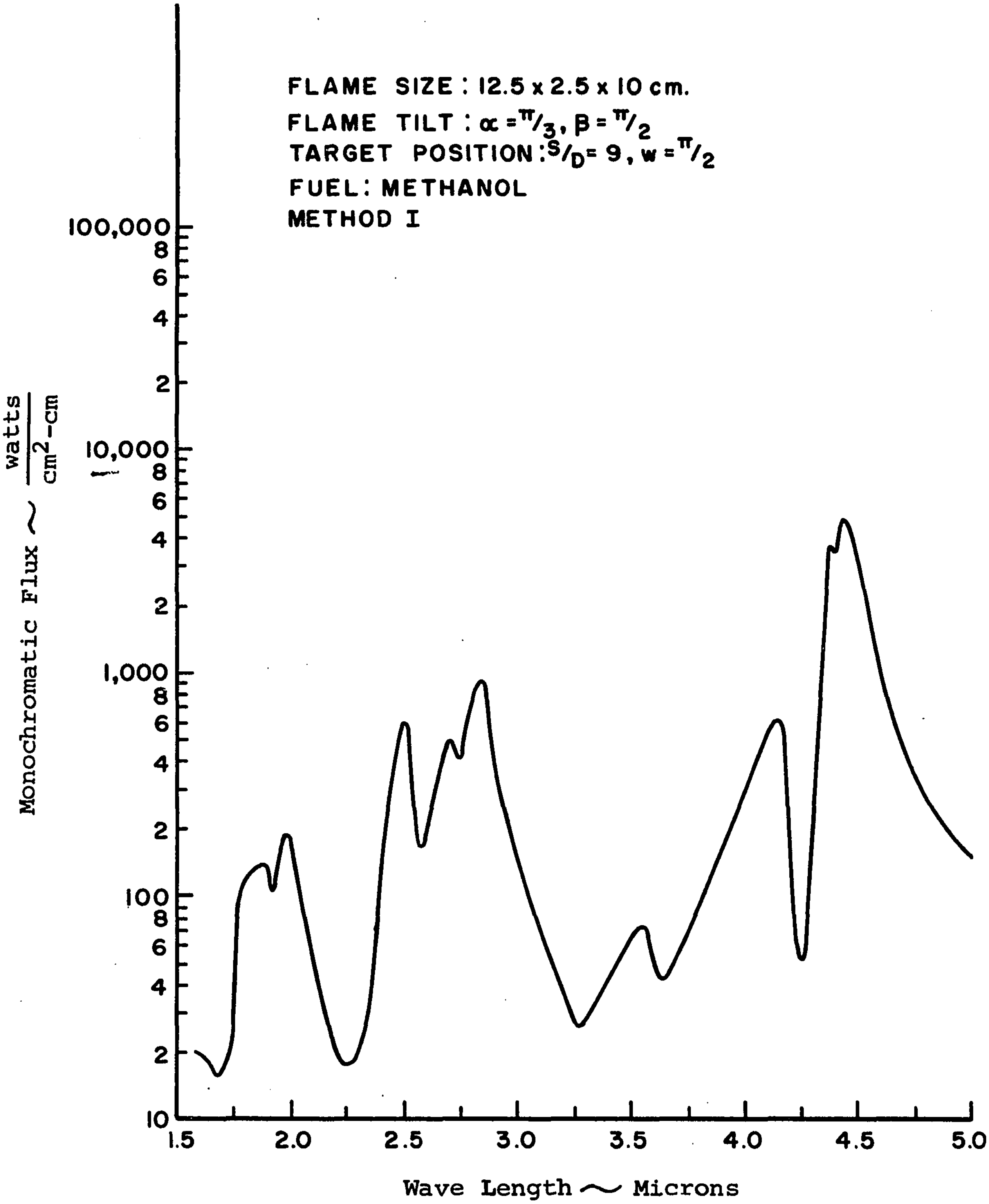

Figure 53. Monochromatic Flux to Target from a Sheet Flame

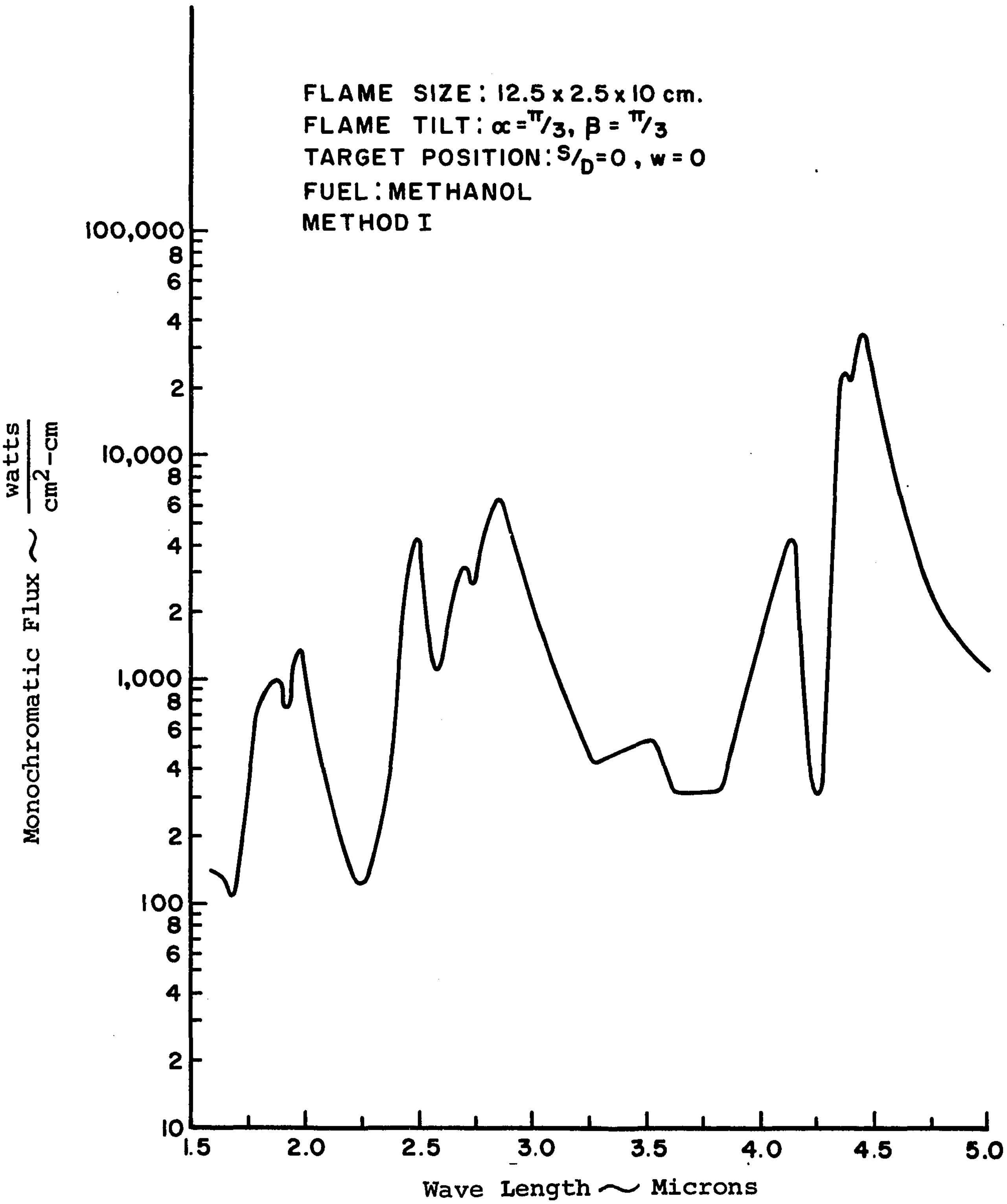

Figure 54. Monochromatic Flux to Target from a Sheet Flame

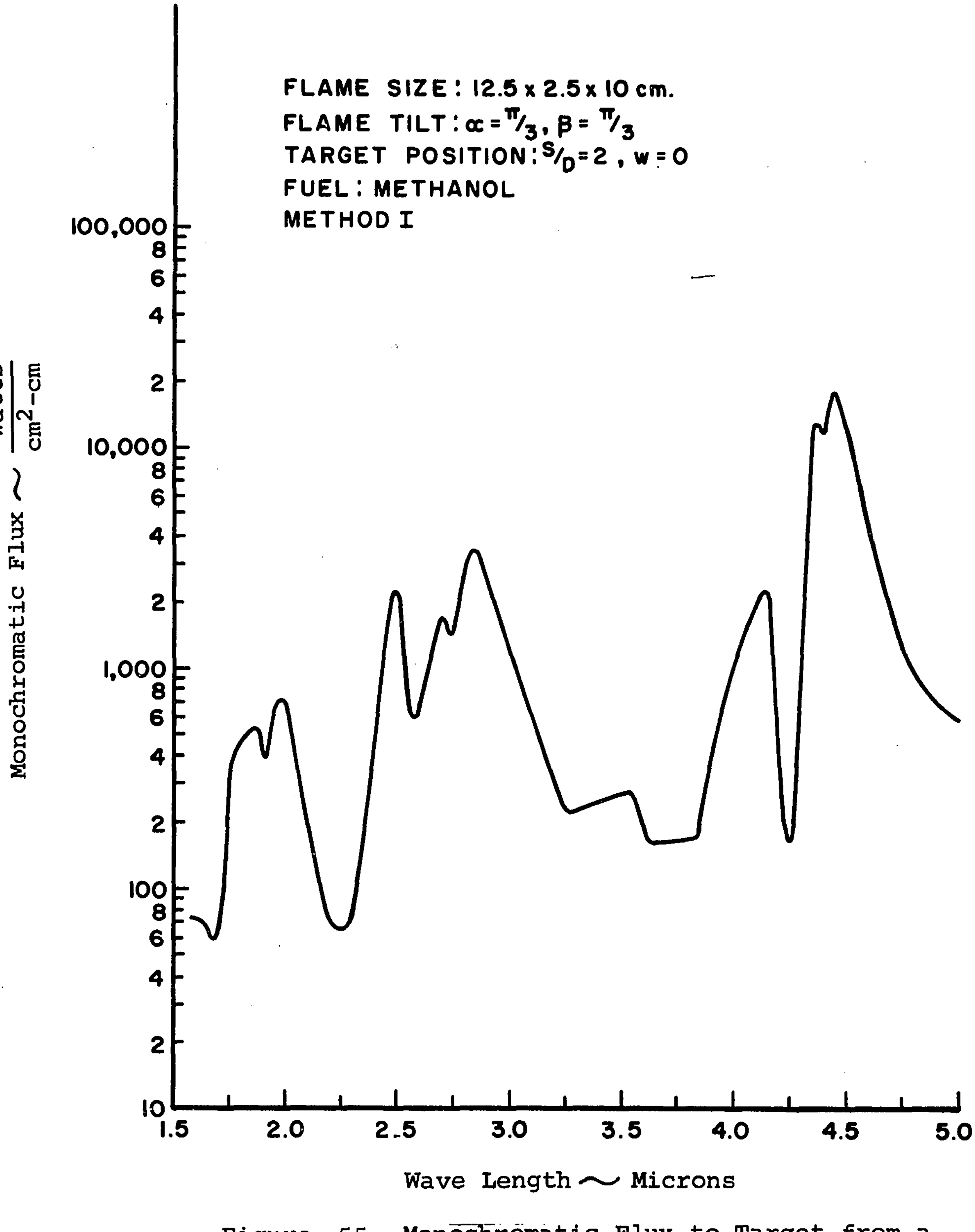

Figure 55. Monochromatic Flux to Target from a Sheet Flame

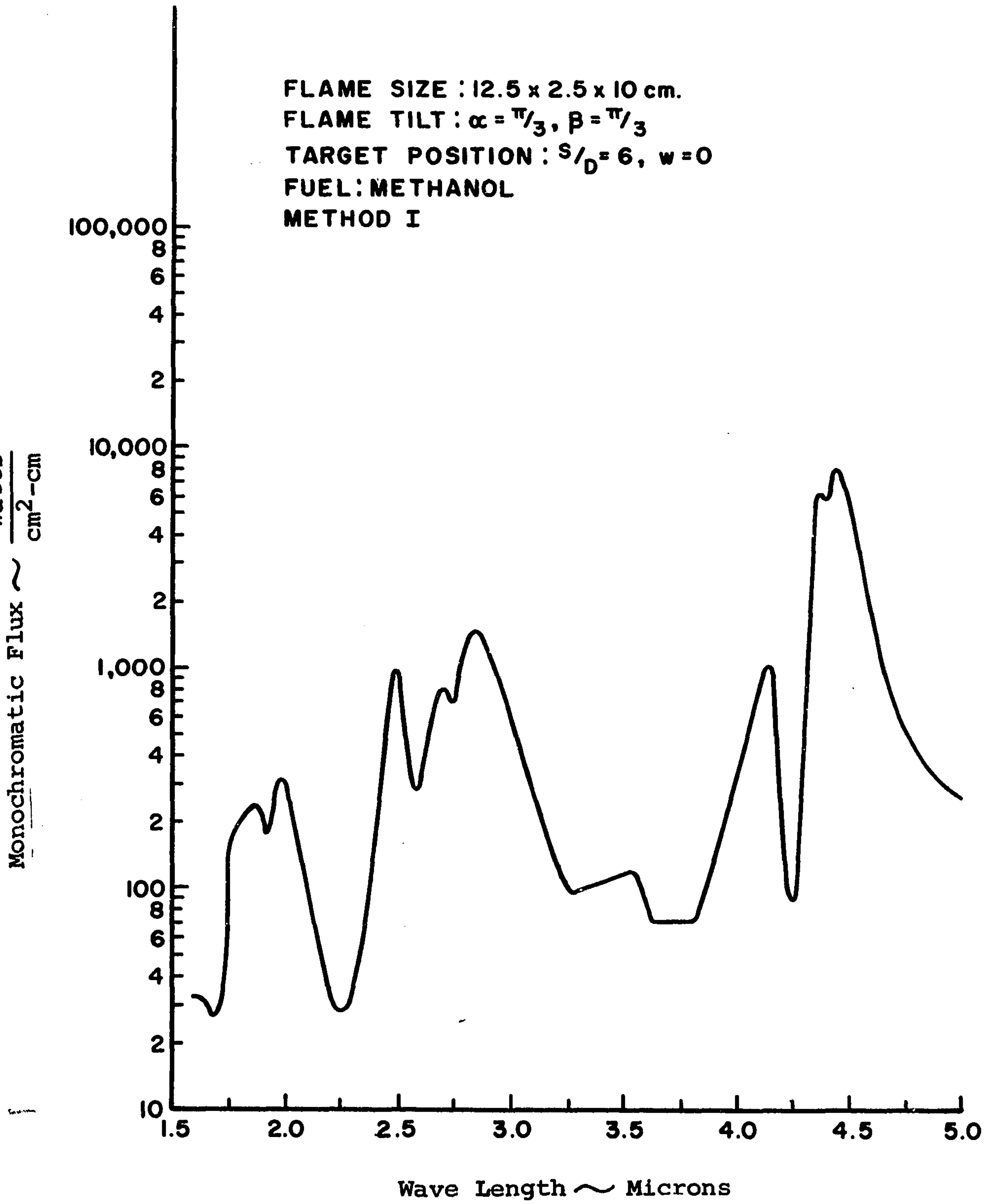

Figure 56. Monochromatic Flux to Target from a Sheet Flame

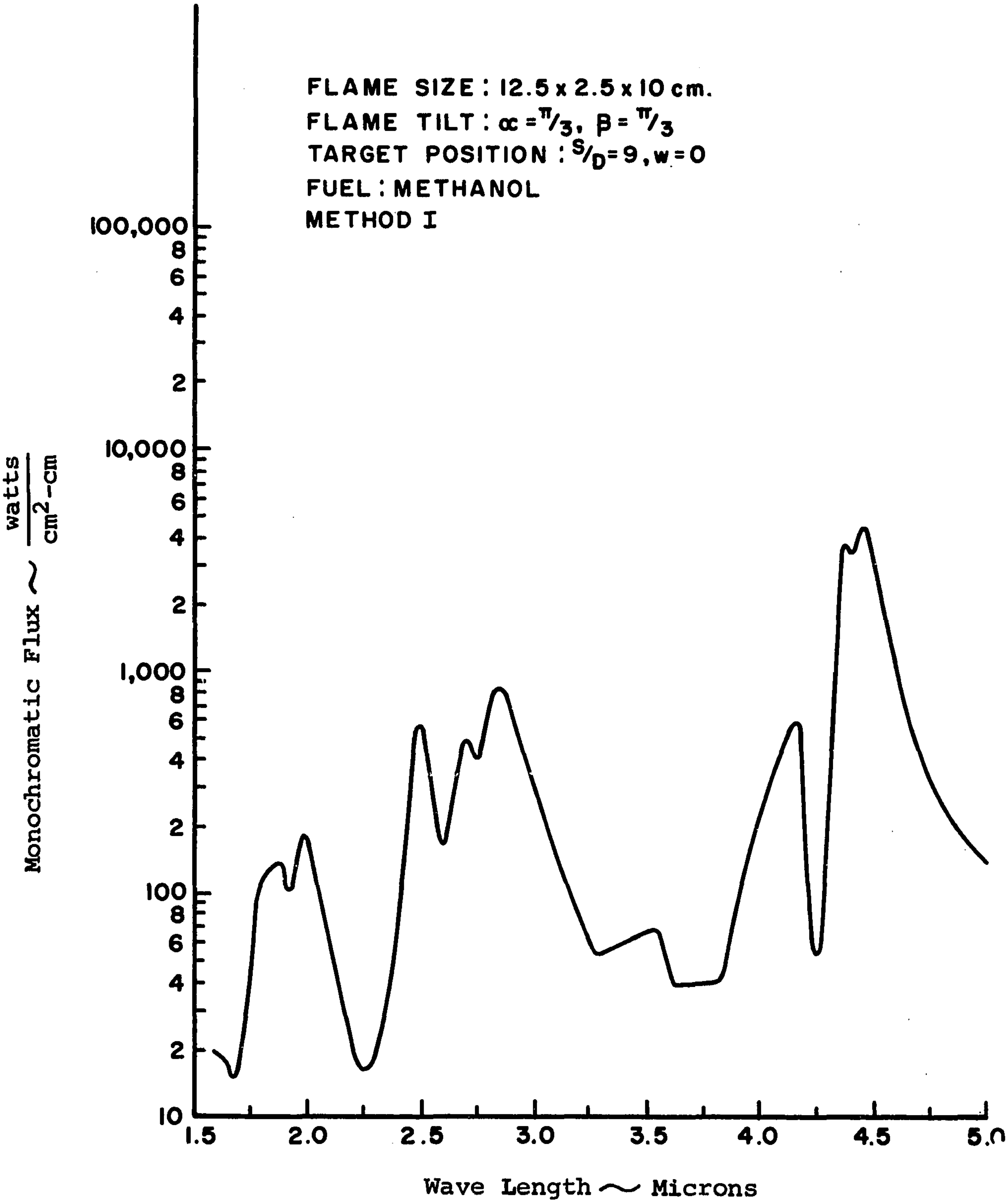

Figure 57. Monochromatic Flux to Target from a Sheet Flame

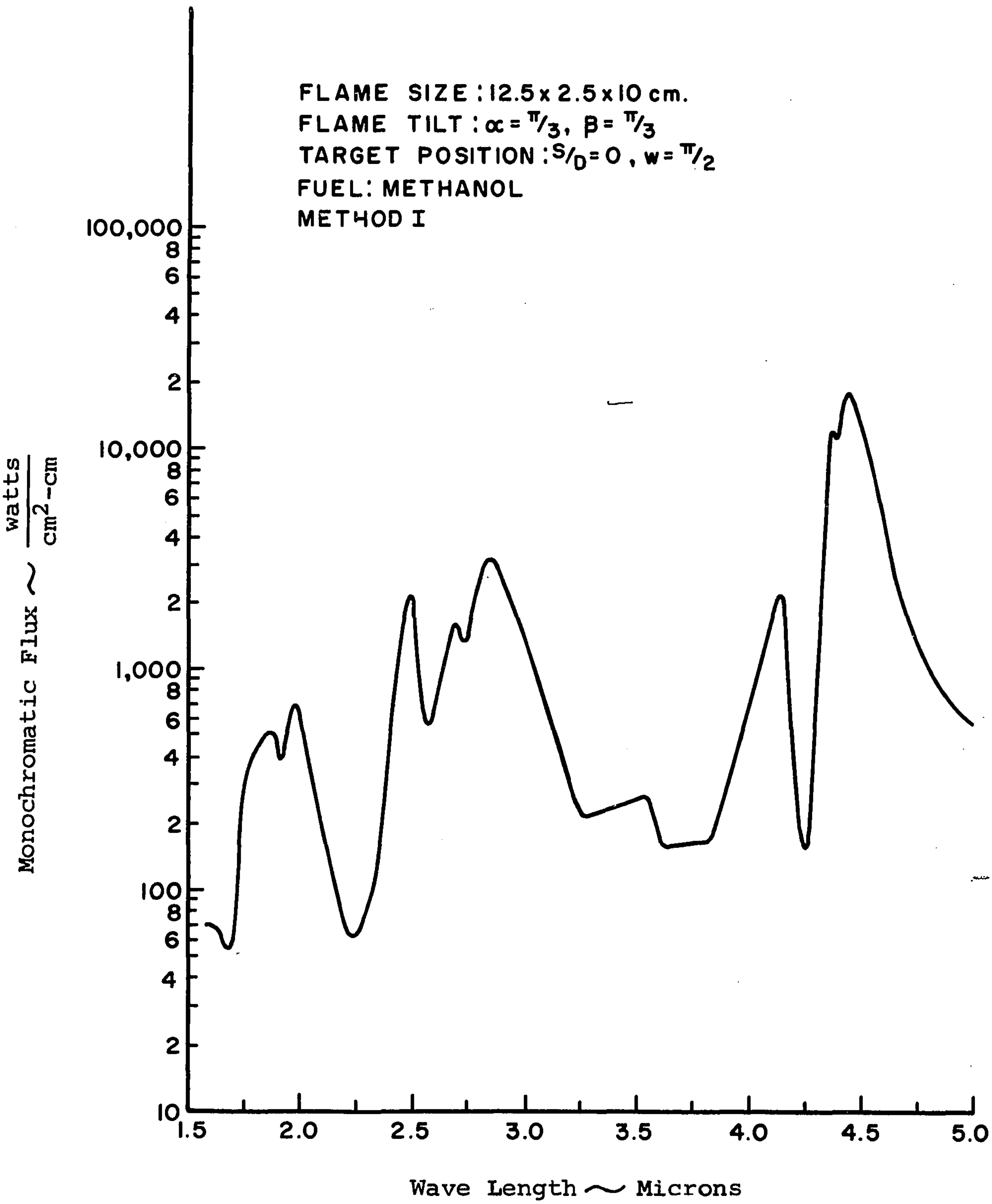

Figure 58. Monochromatic Flux to Target from a Sheet Flame

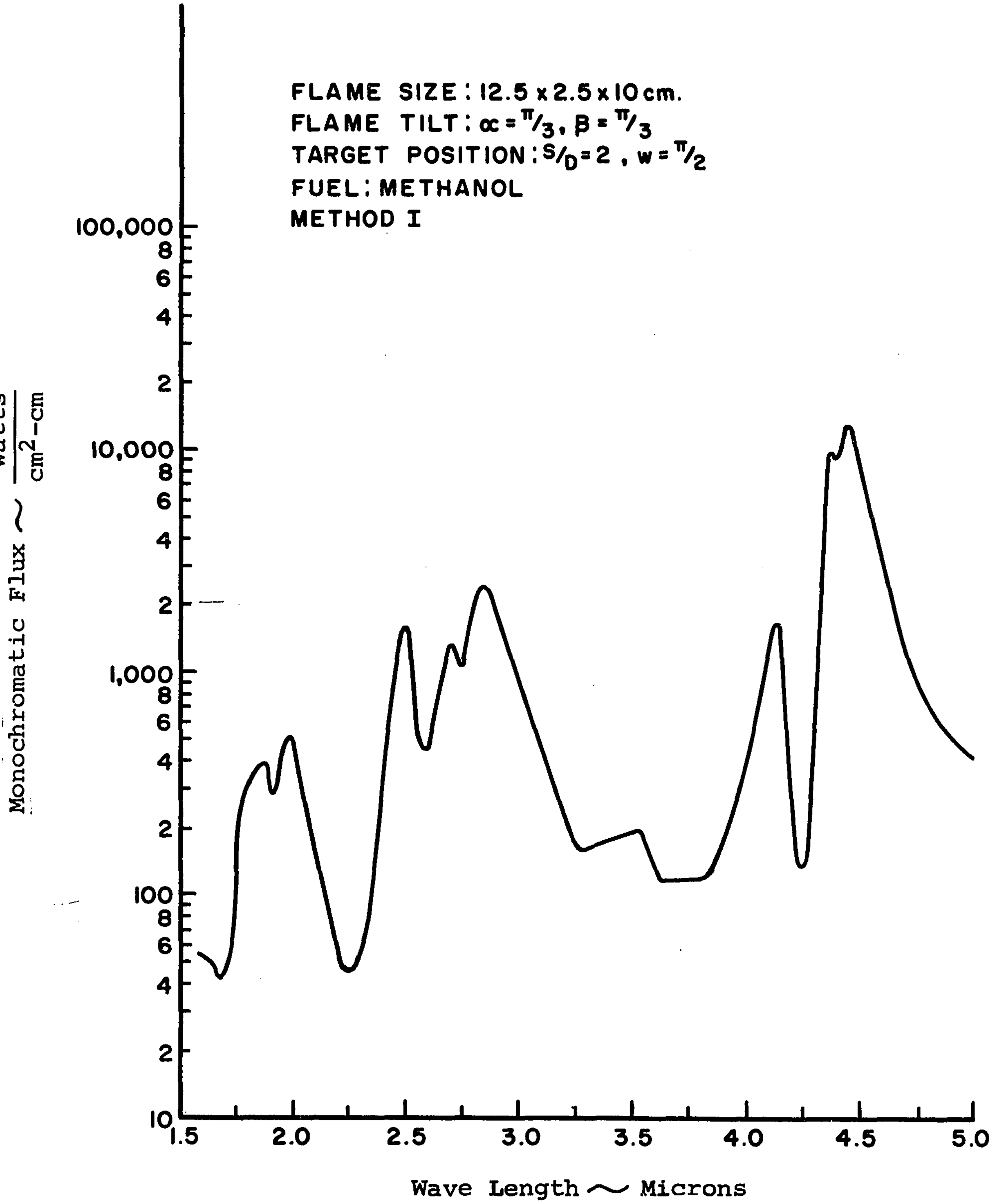

Figure 59. Monochromatic Flux to Target from a Sheet Flame

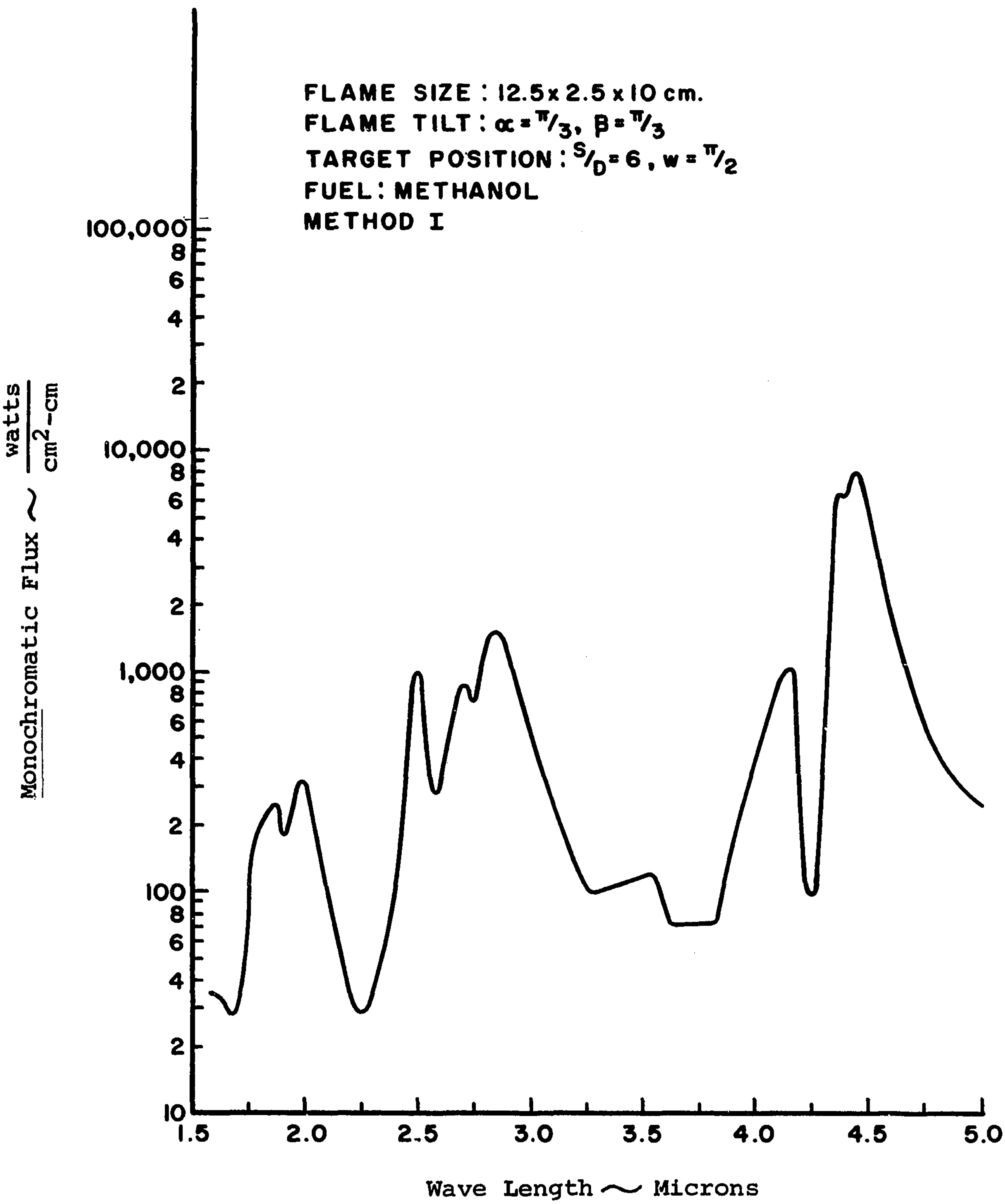

Figure 60. Monochromatic Flux to Target from a Sheet Flame

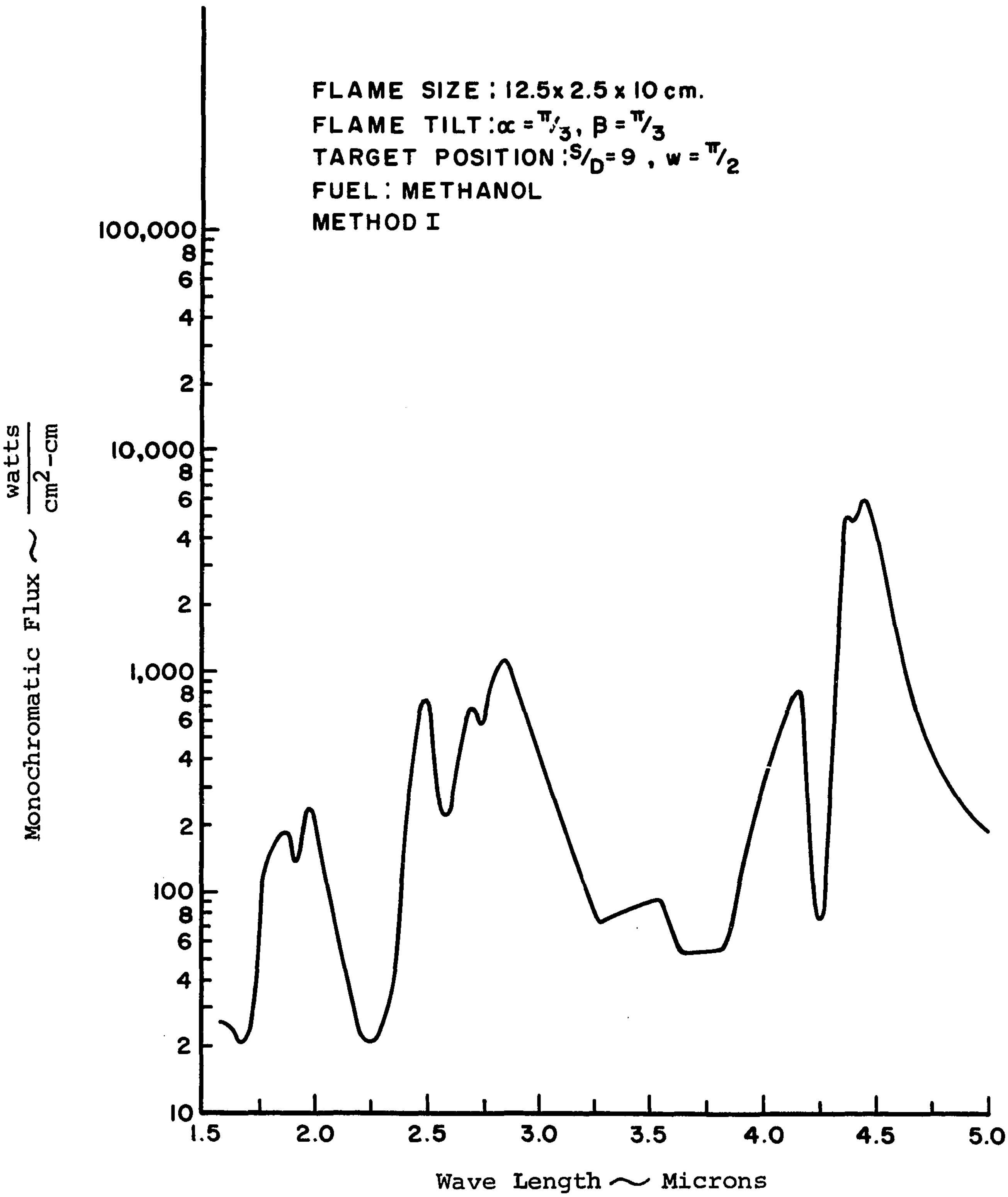

Figure 61. Monochromatic Flux to Target from a Sheet Flame

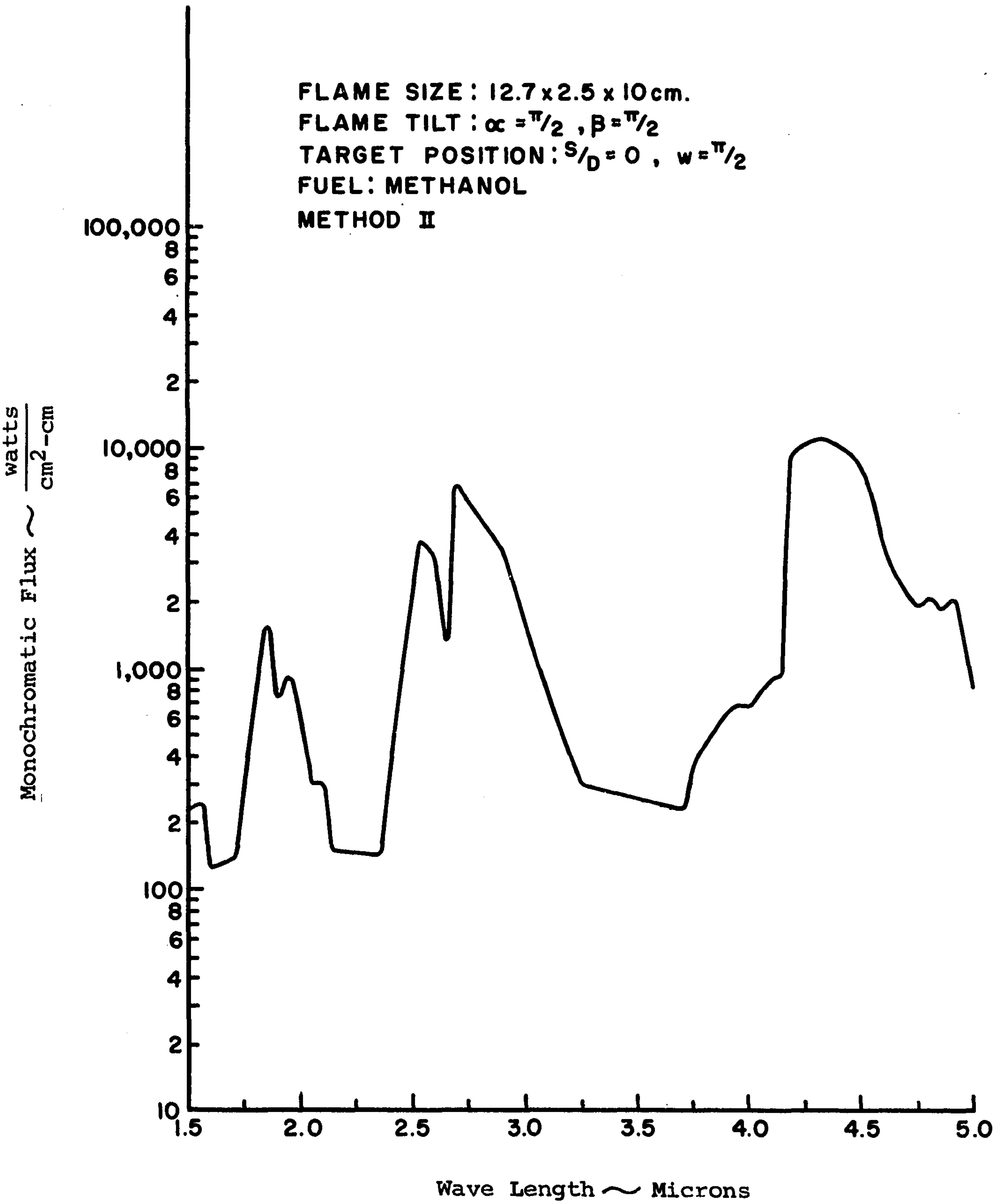

Figure 62. Monochromatic Flux to Target from a Sheet Flame

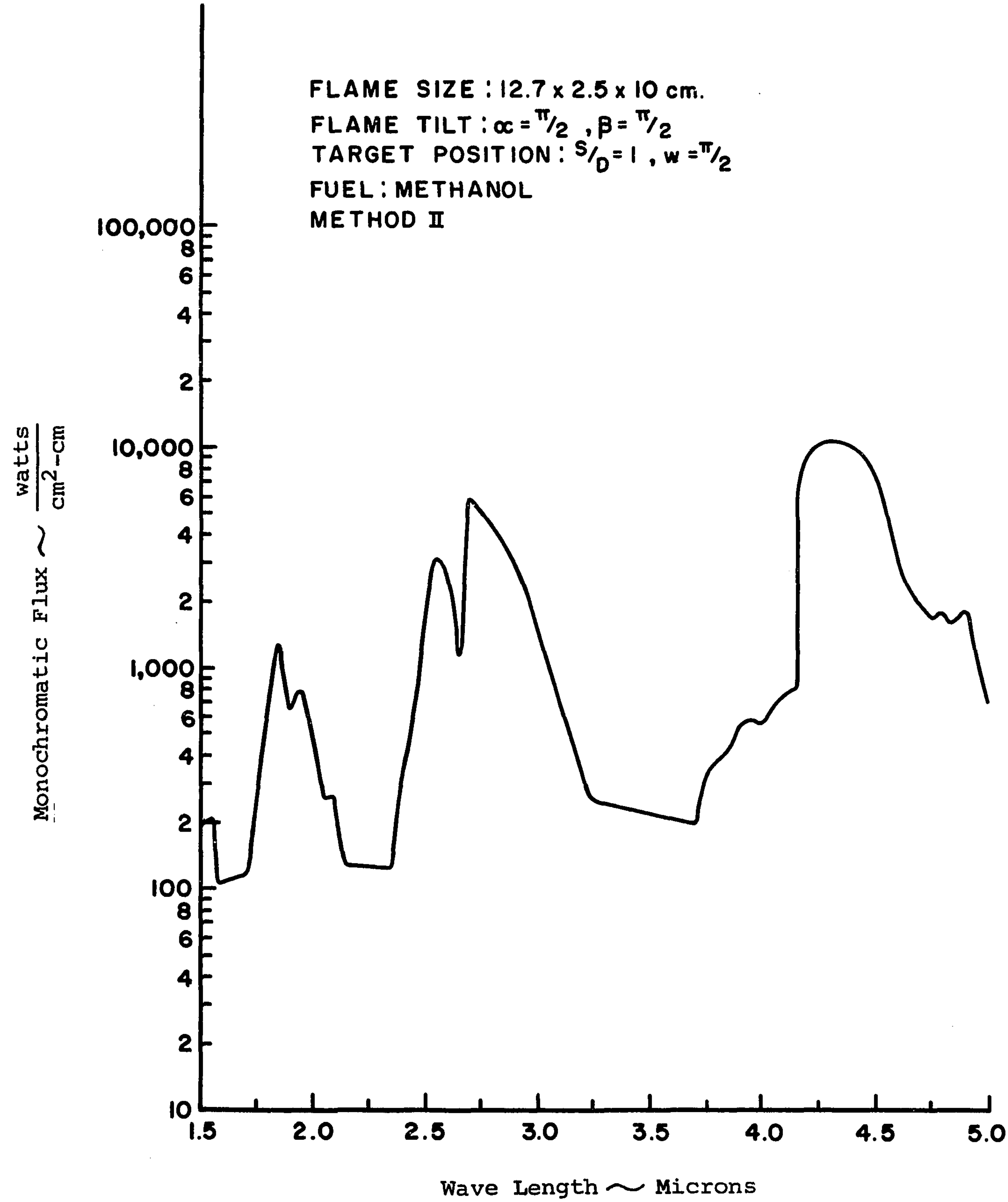

Figure 63. Monochromatic Flux to Target from a Sheet Flame

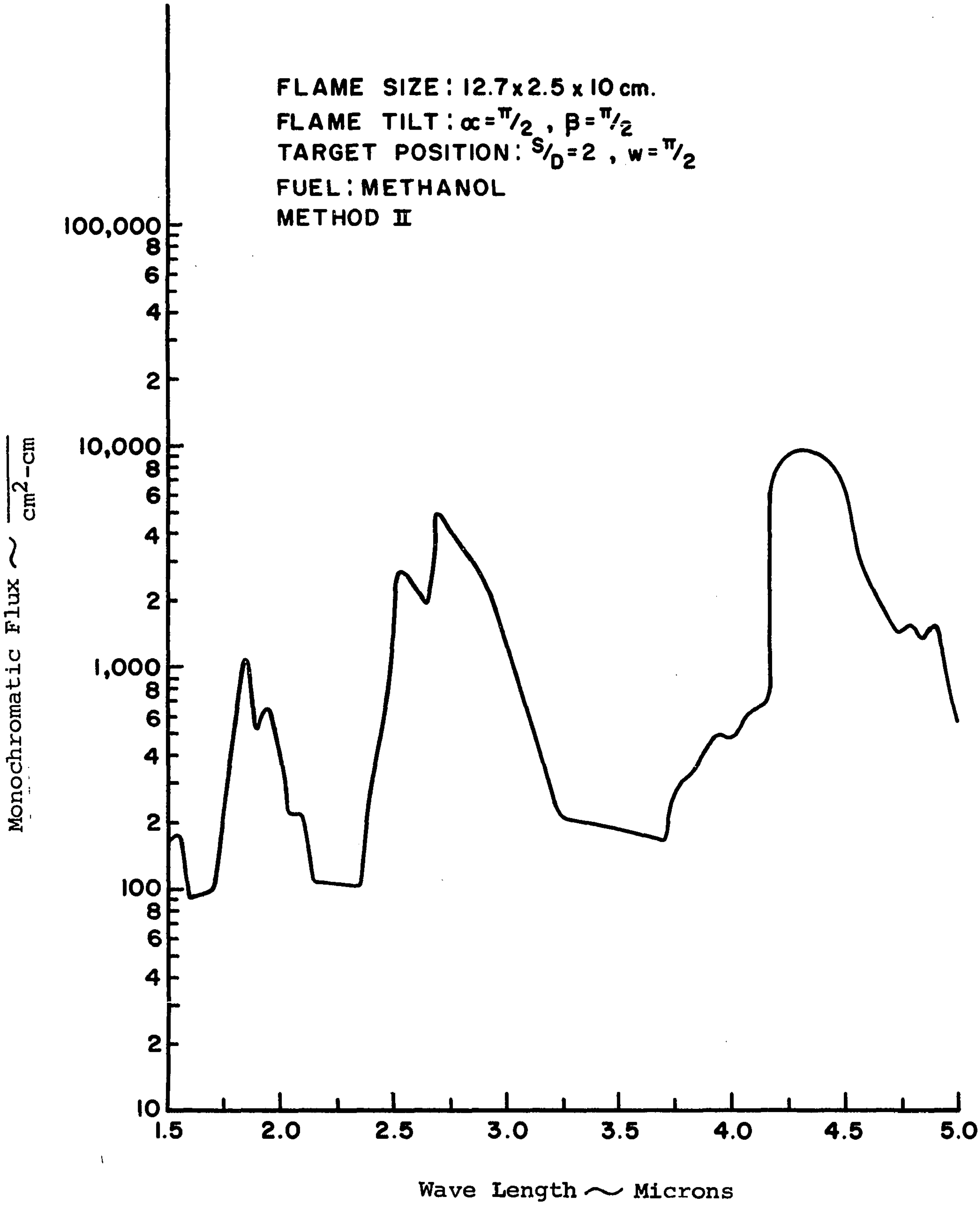

Figure 64. Monochromatic Flux to Target from a Sheet Flame

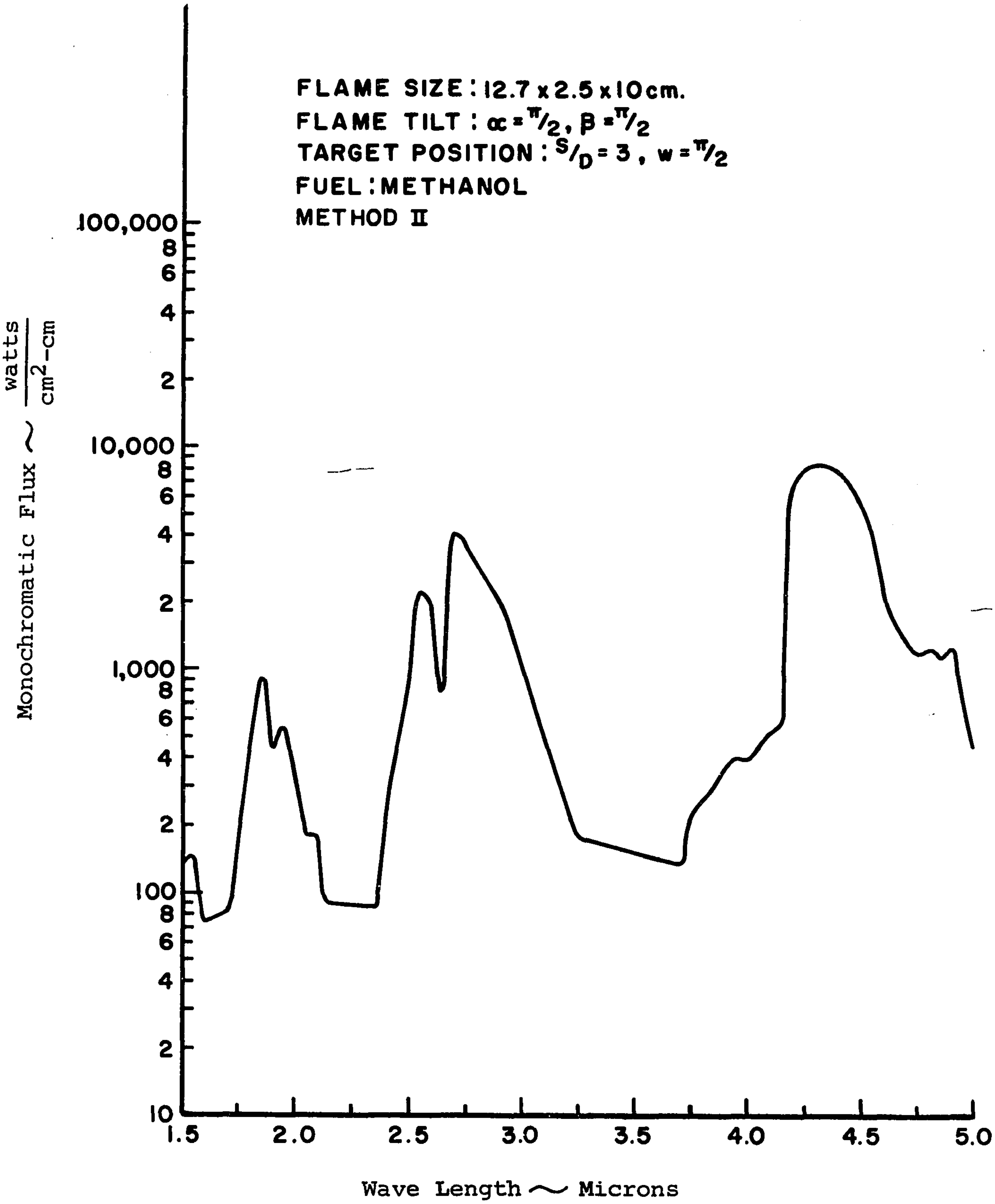

Figure 65. Monochromatic Flux to Target from a Sheet Flame

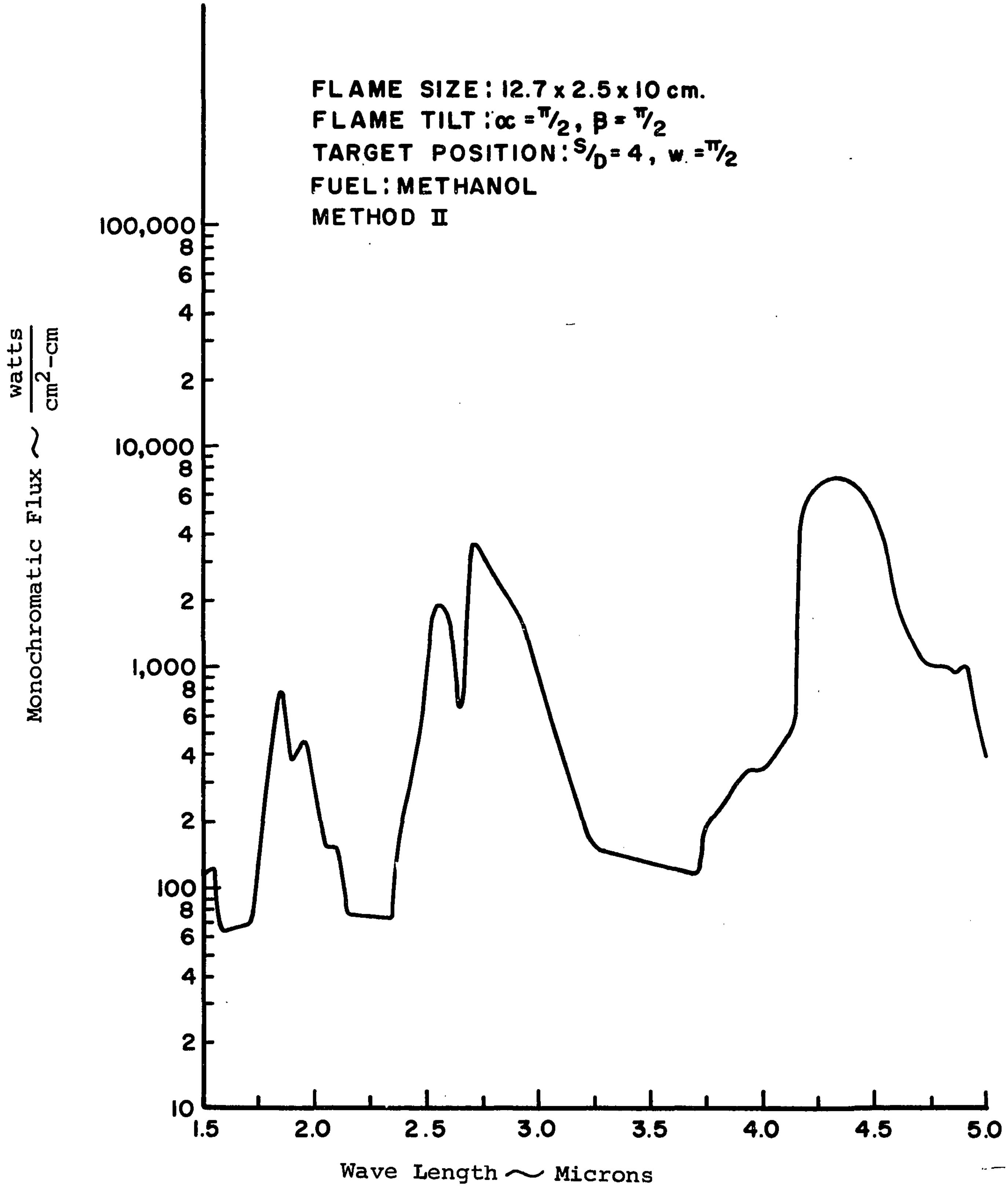

Figure 66. Monochromatic Flux to Target from a Sheet Flame

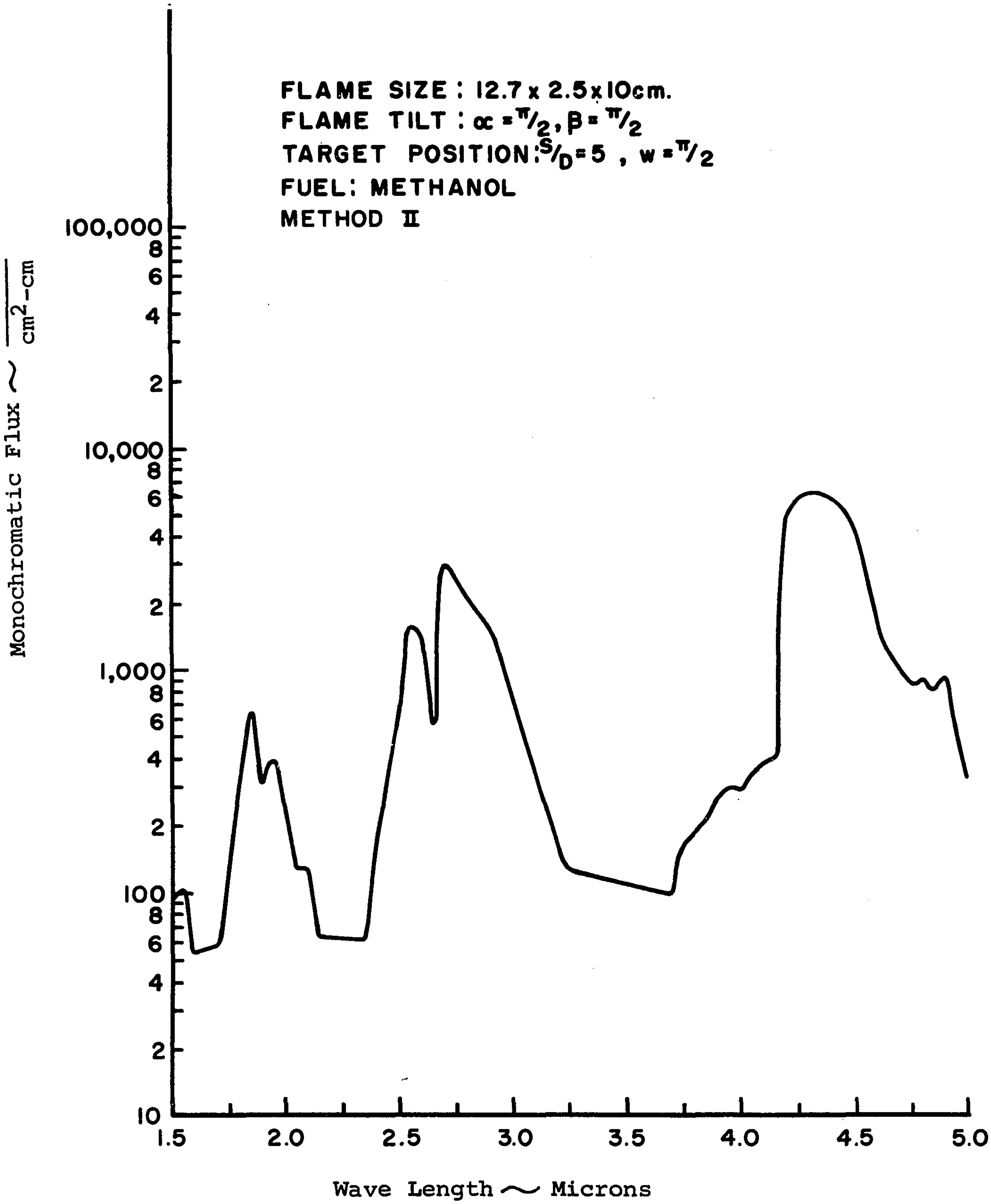

Figure 67. Monochromatic Flux to Target from a Sheet Flame

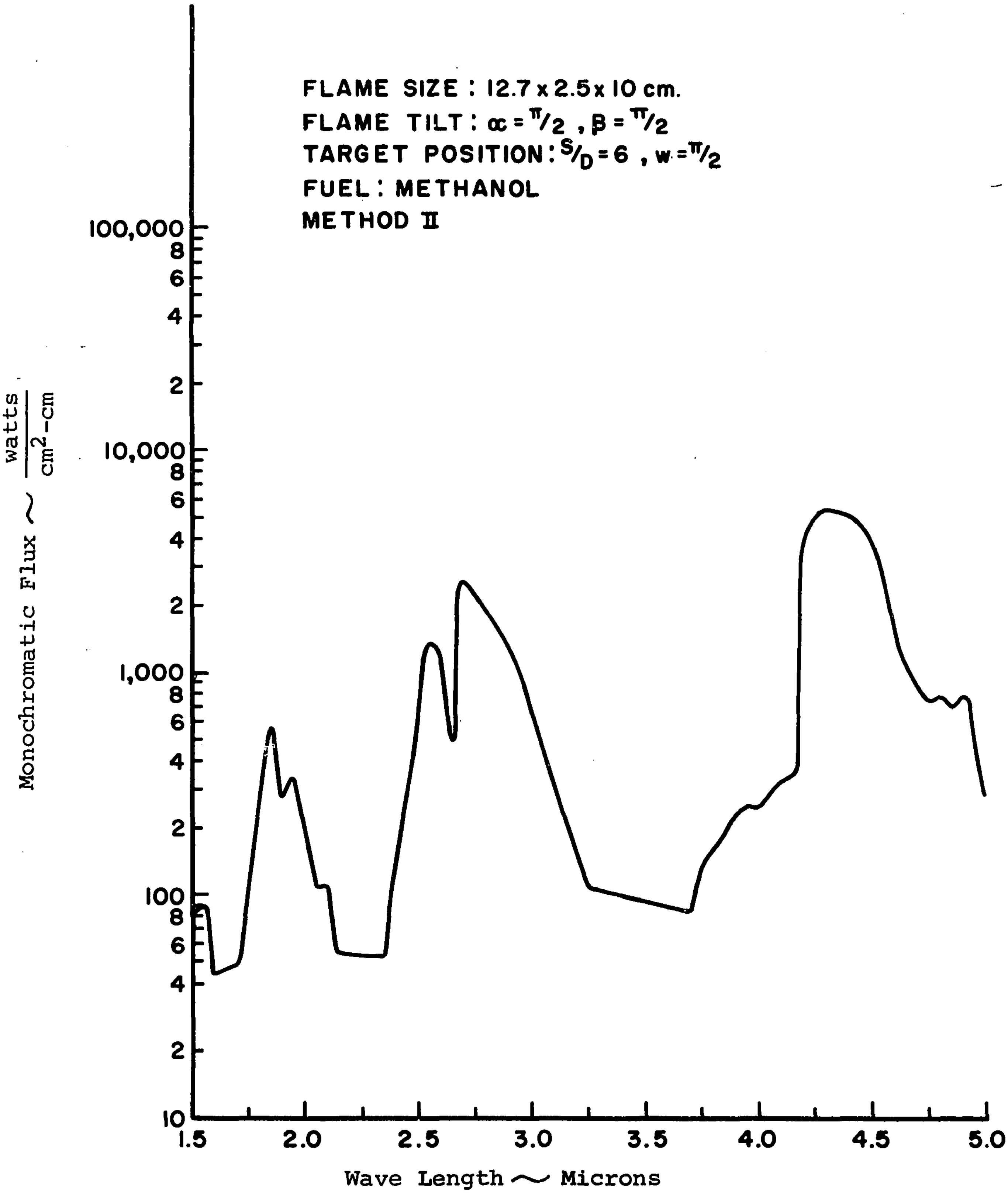

Figure 68. Monochromatic Flux to Target from a Sheet Flame

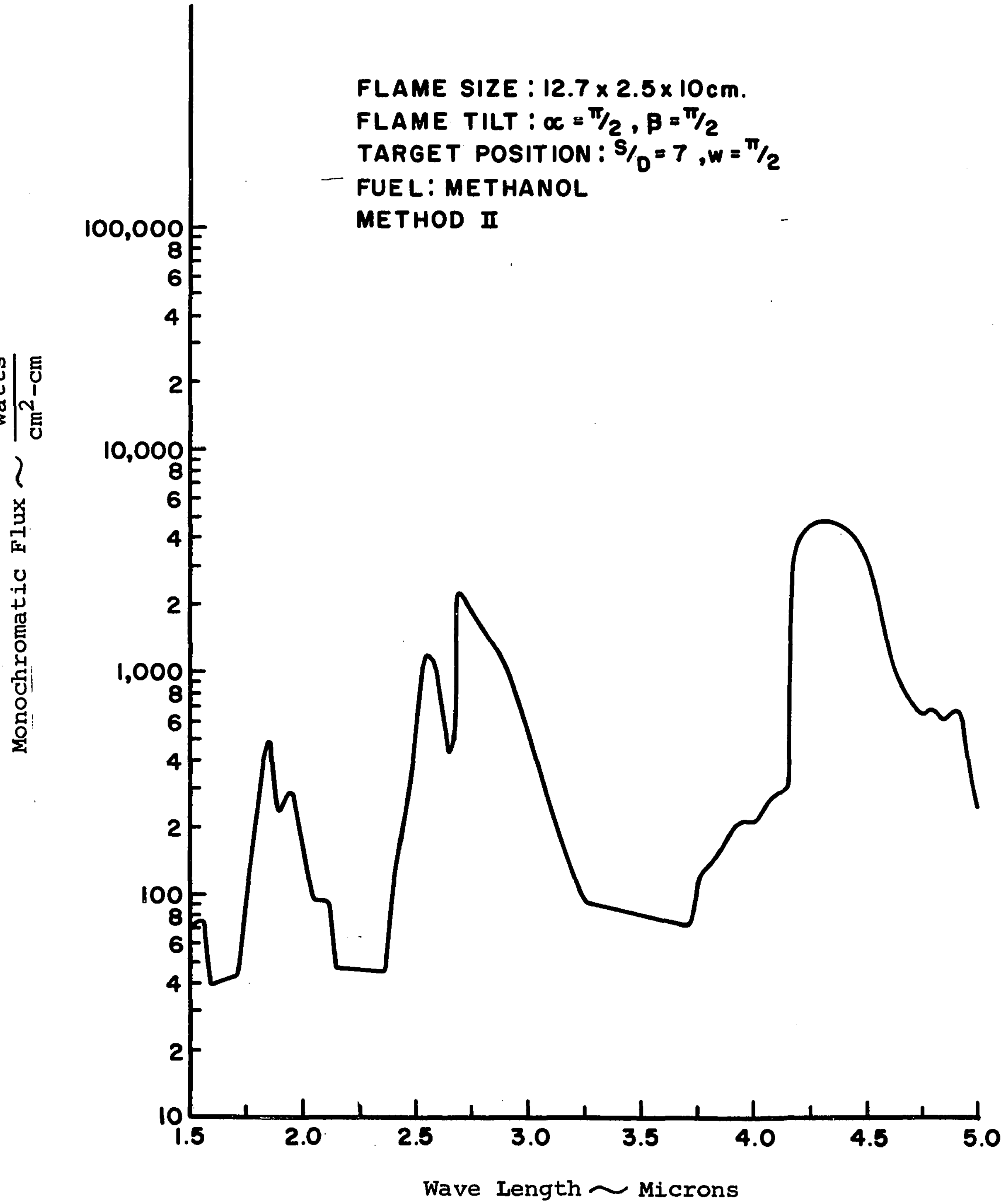

Figure 69. Monochromatic Flux to Target from a Sheet Flame

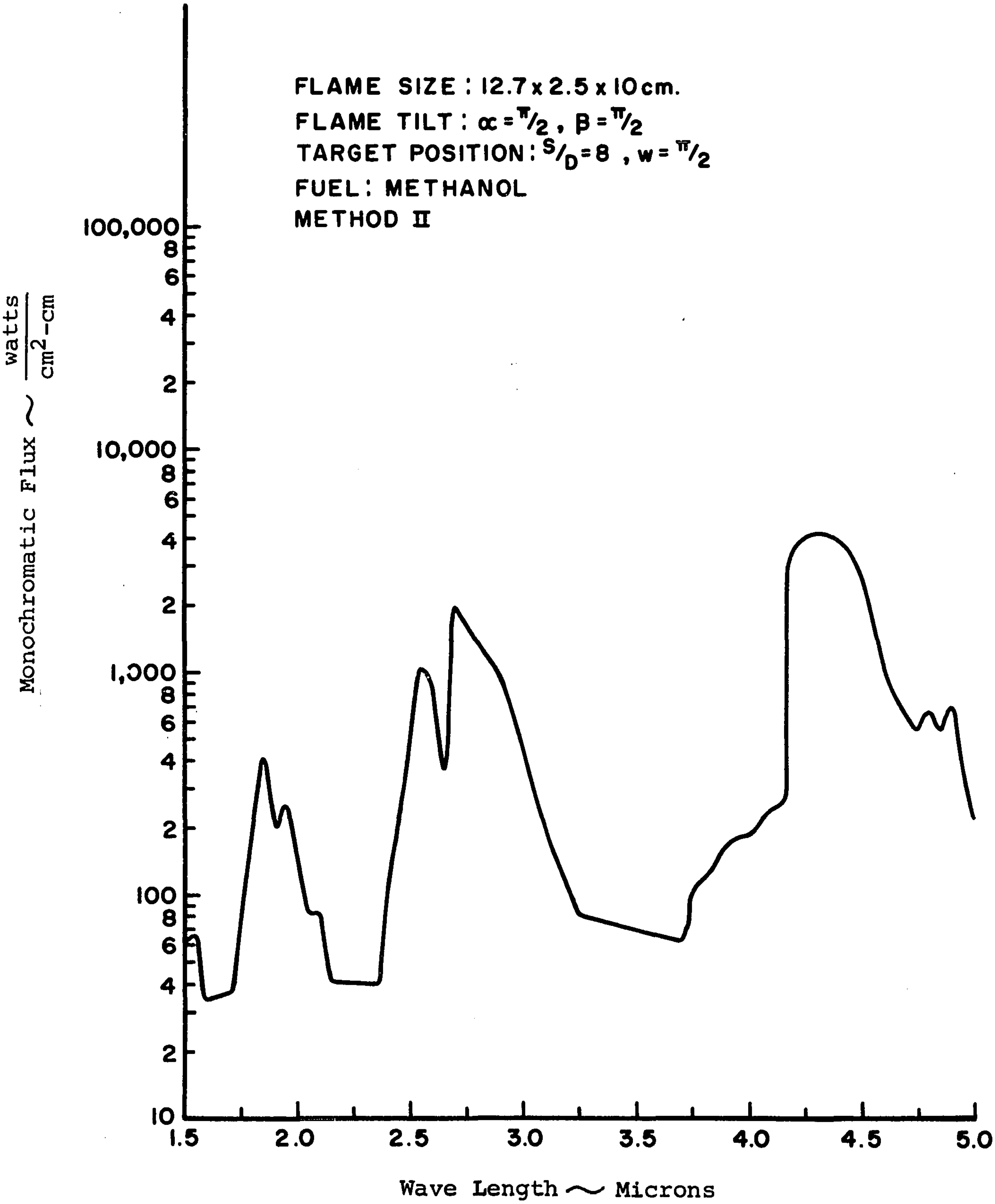

Figure 70. Monochromatic Flux to Target from a Sheet Flame

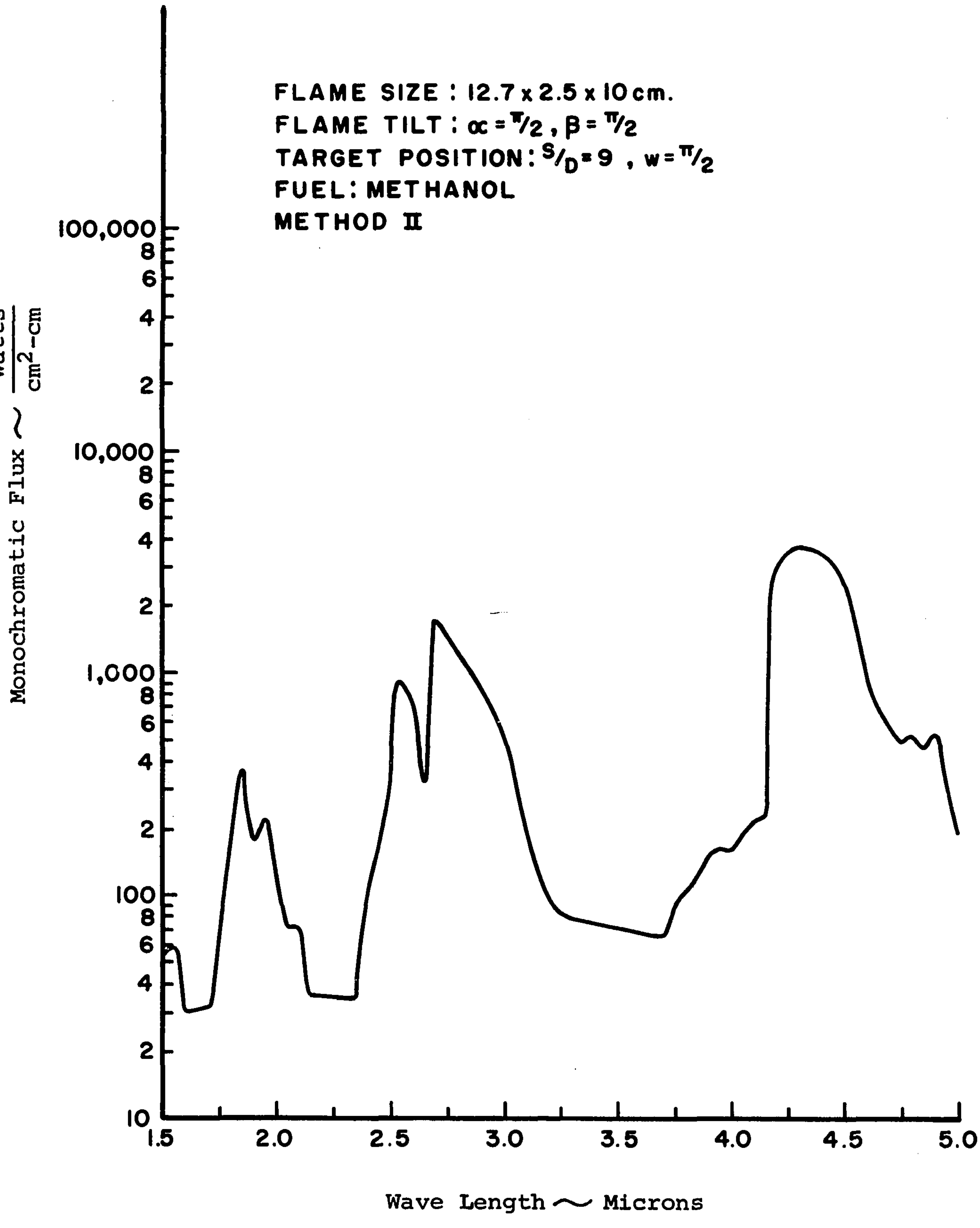

Figure 71. Monochromatic Flux to Target from a Sheet Flame

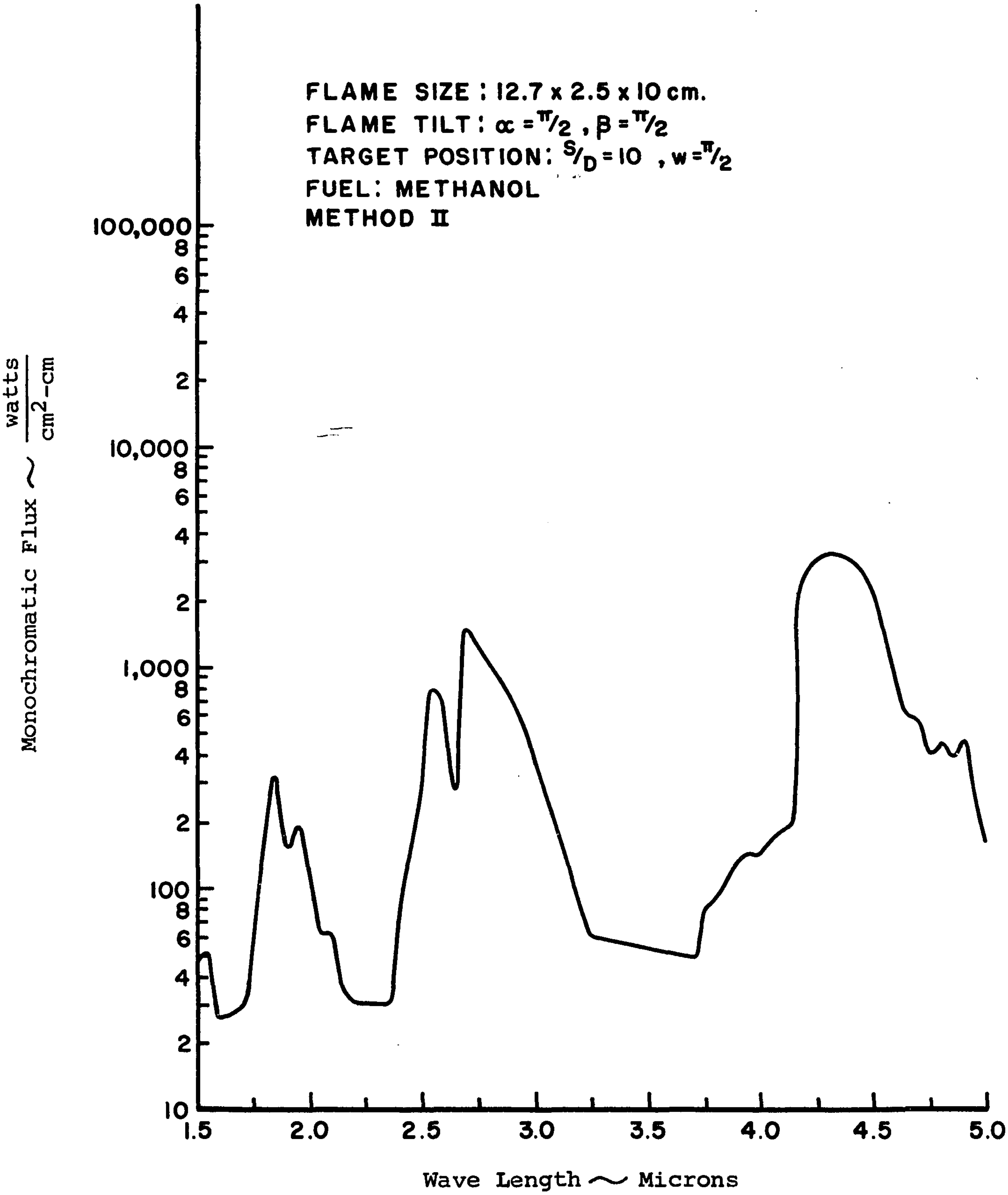

Figure 72. Monochromatic Flux to Target from a Sheet Flame

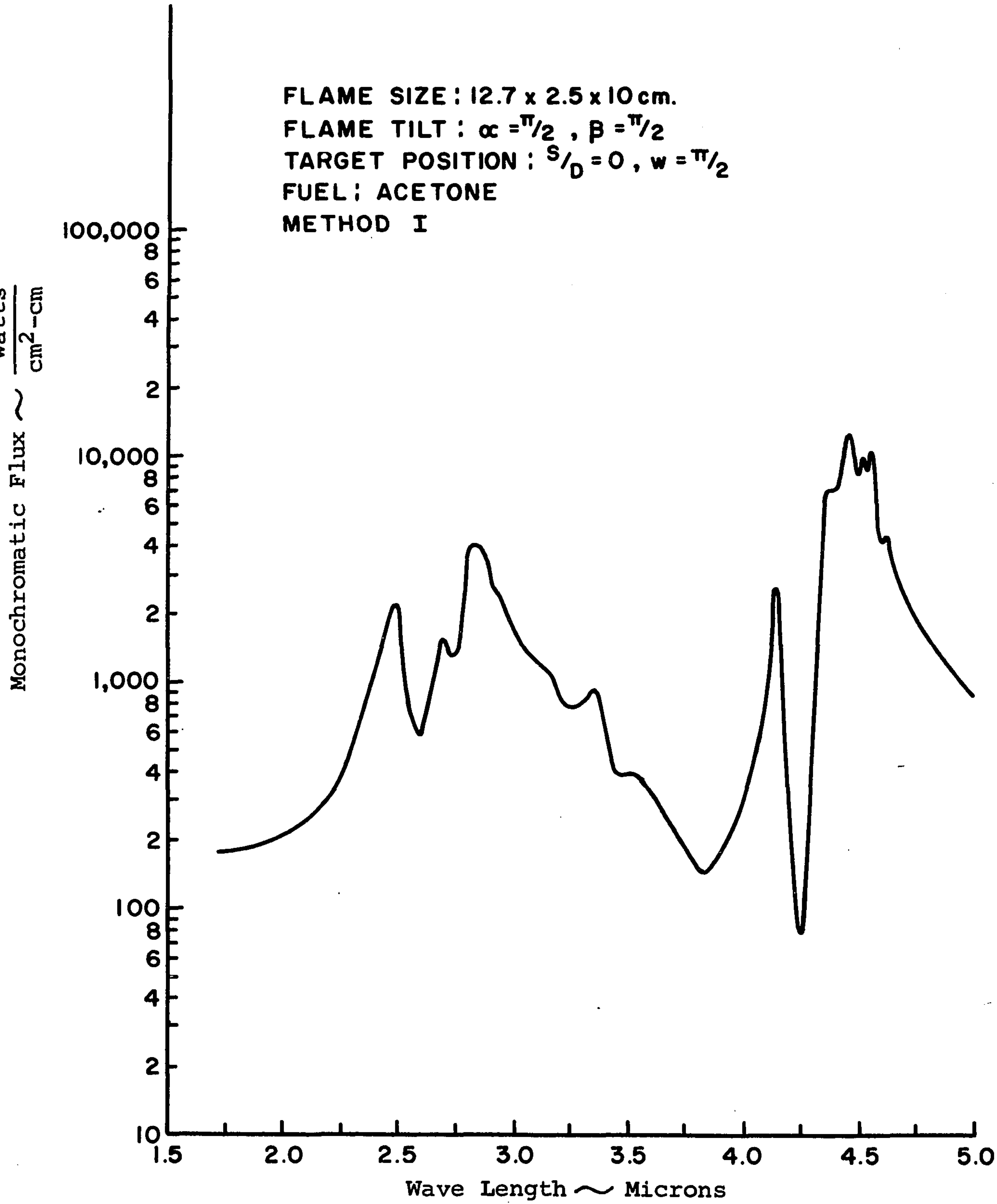

Figure 73. Monochromatic Flux to Target from a Sheet Flame

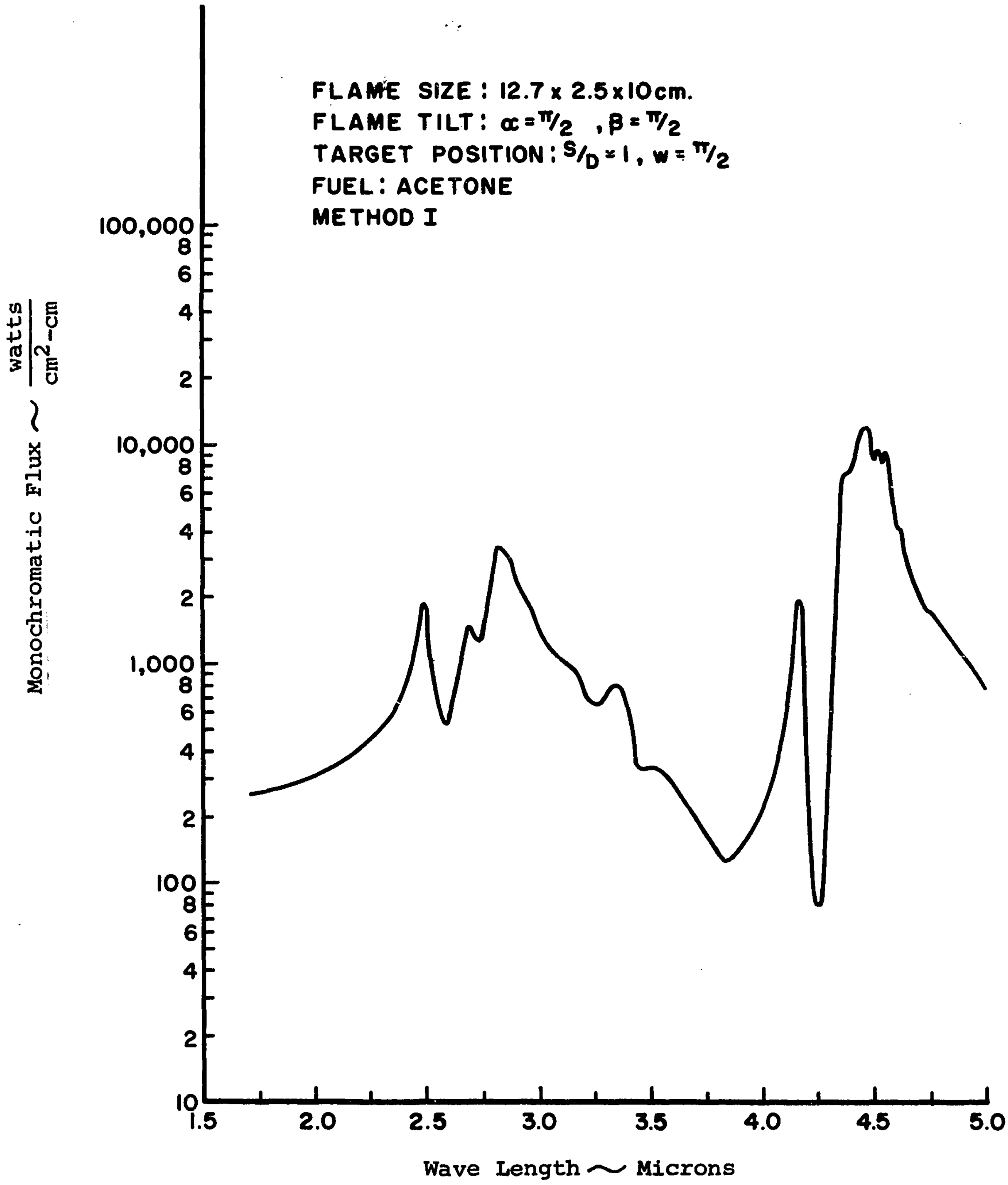

Figure 74. Monochromatic Flux to Target from a Sheet Flame

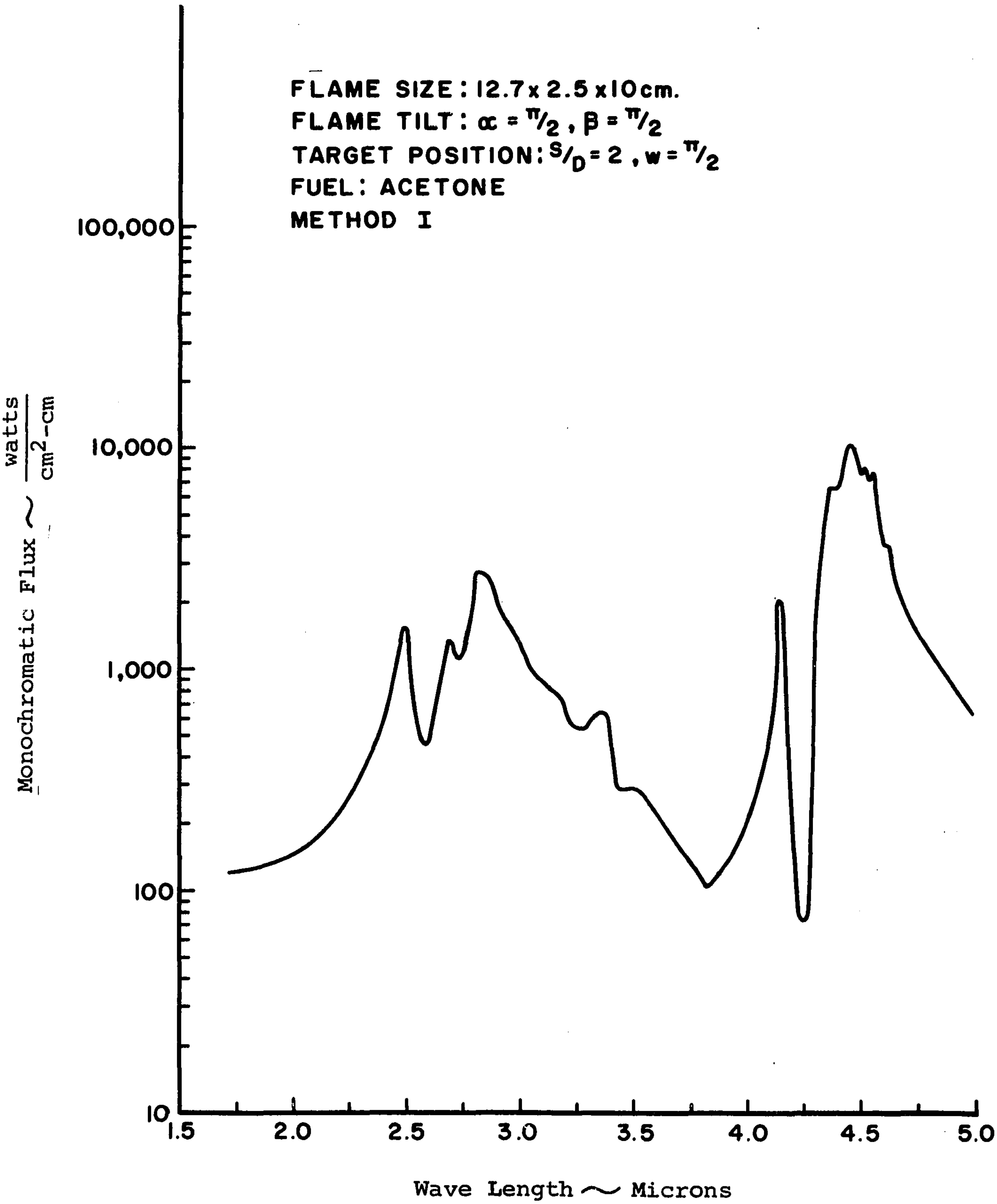

Figure 75. Monochromatic Flux to Target from a Sheet Flame

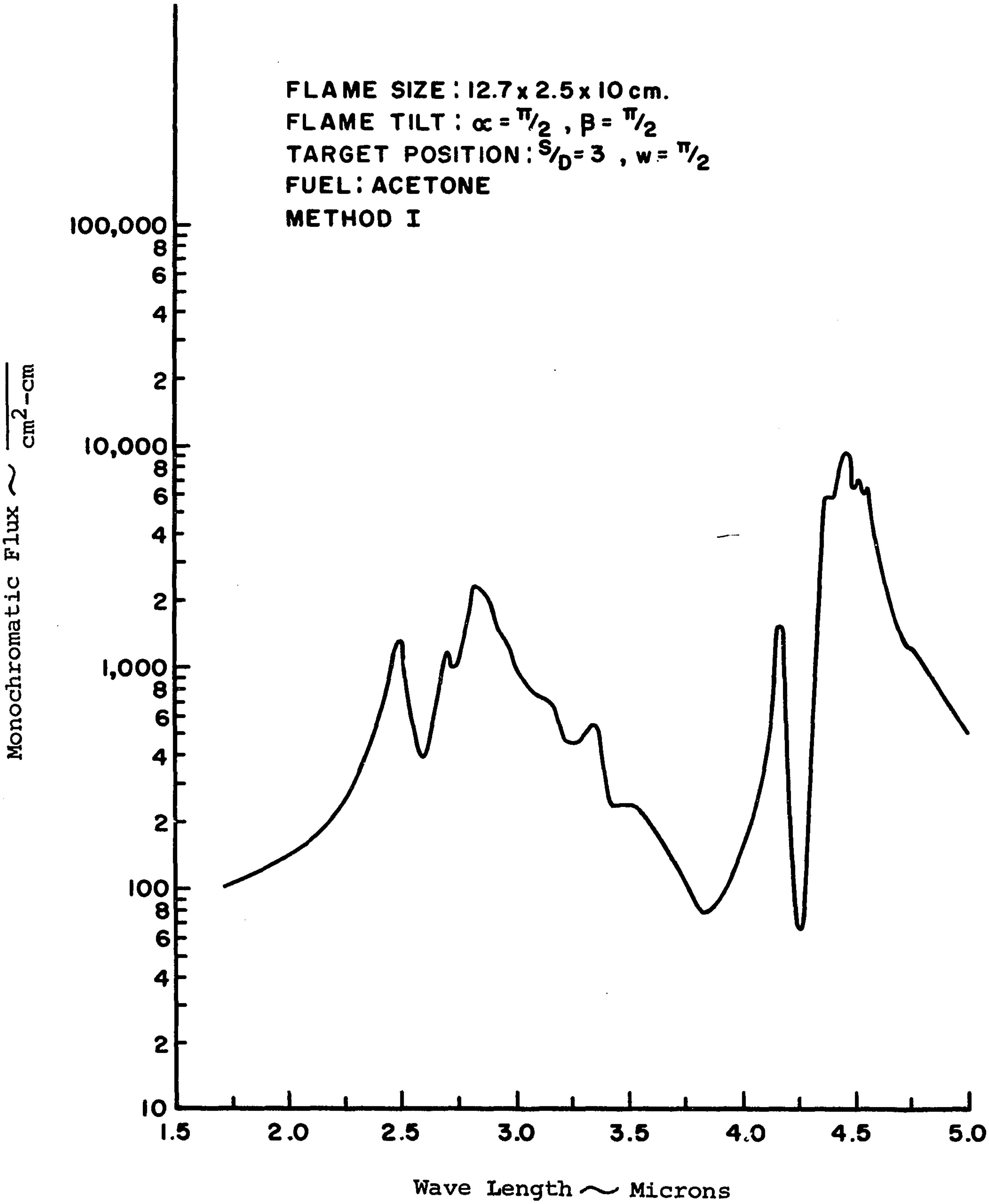

Figure 76. Monochromatic Flux to Target from a Sheet Flame

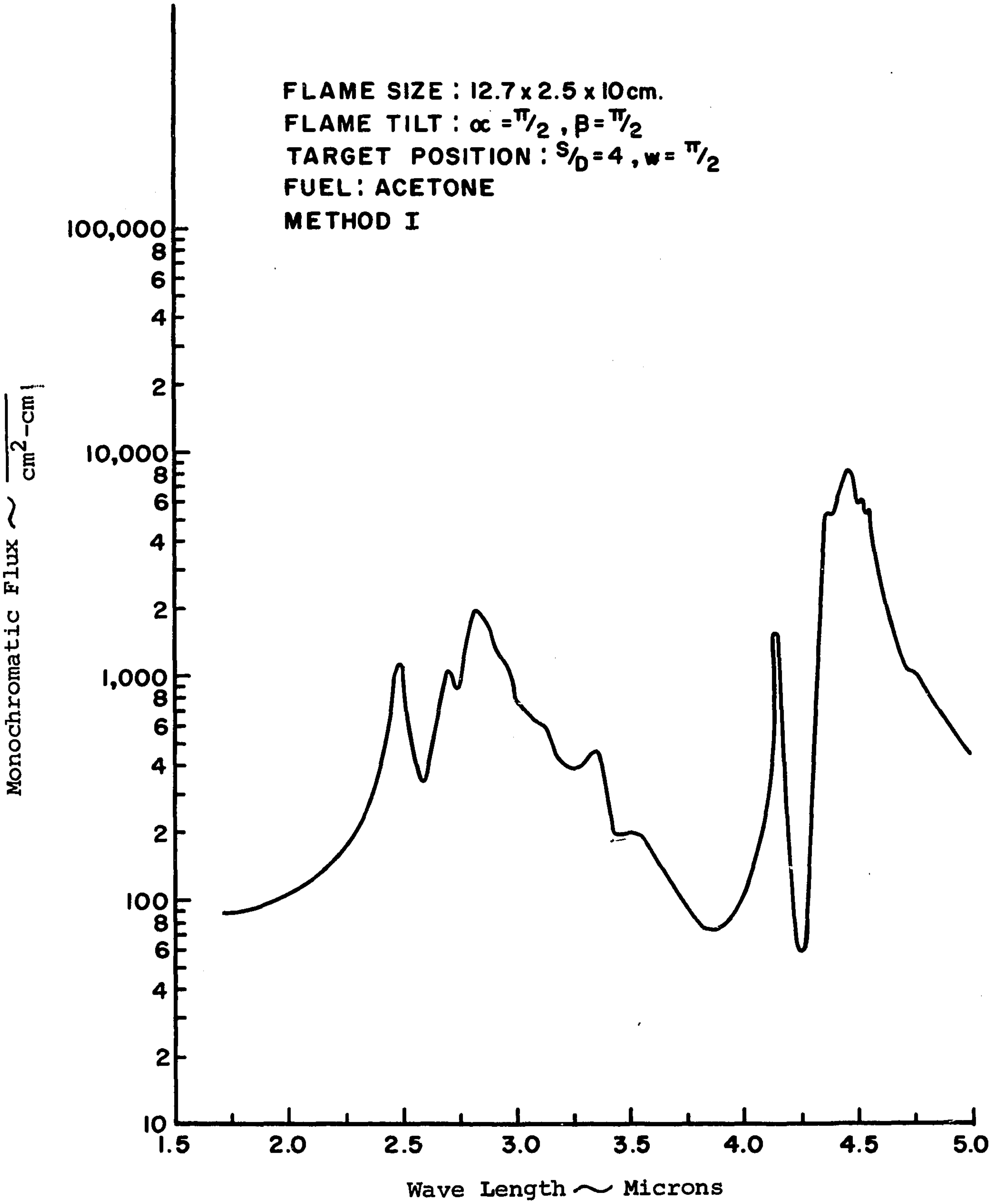

Figure 77. Monochromatic Flux to Target from a Sheet Flame

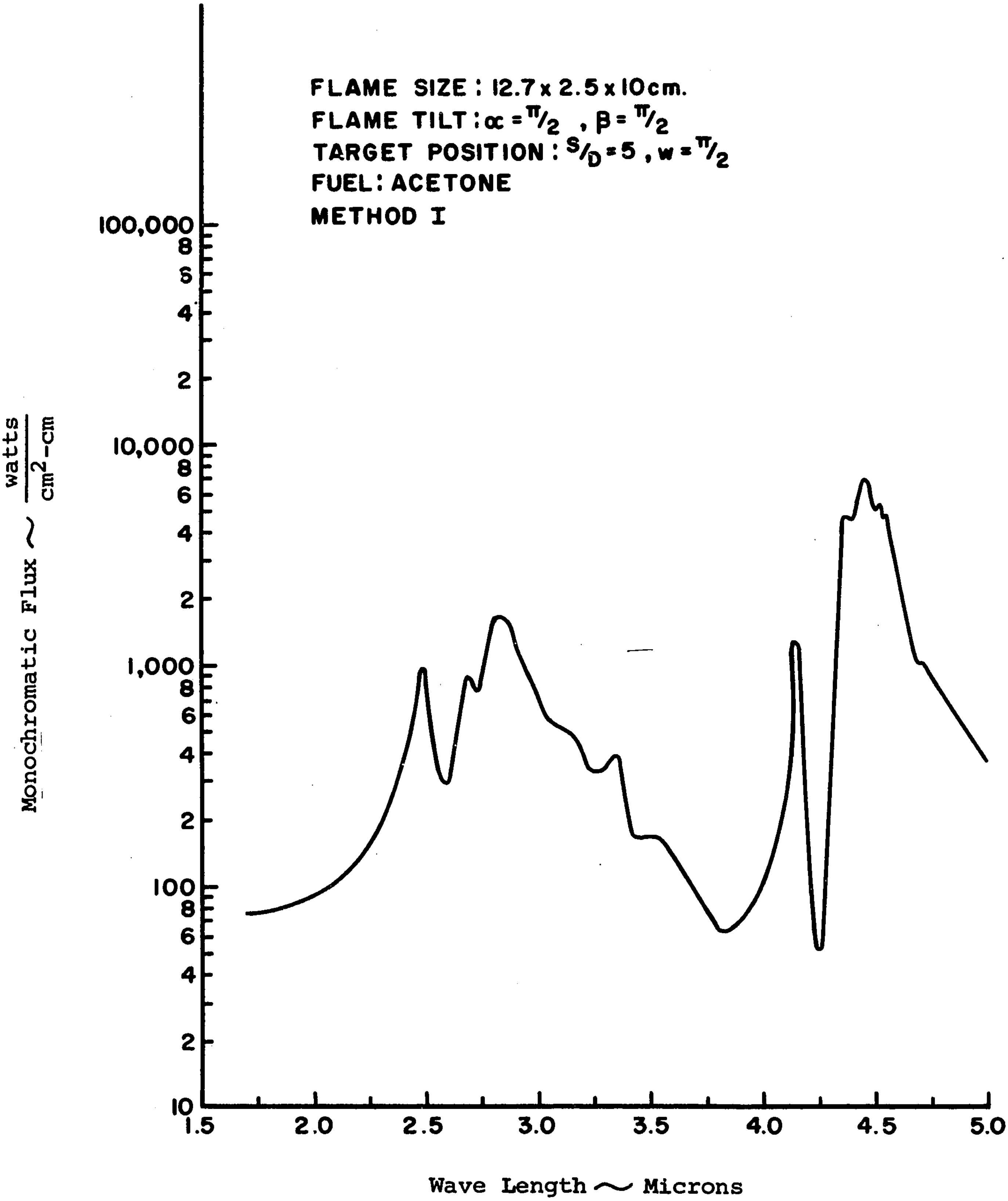

Figure 78. Monochromatic Flux to Target from a Sheet Flame

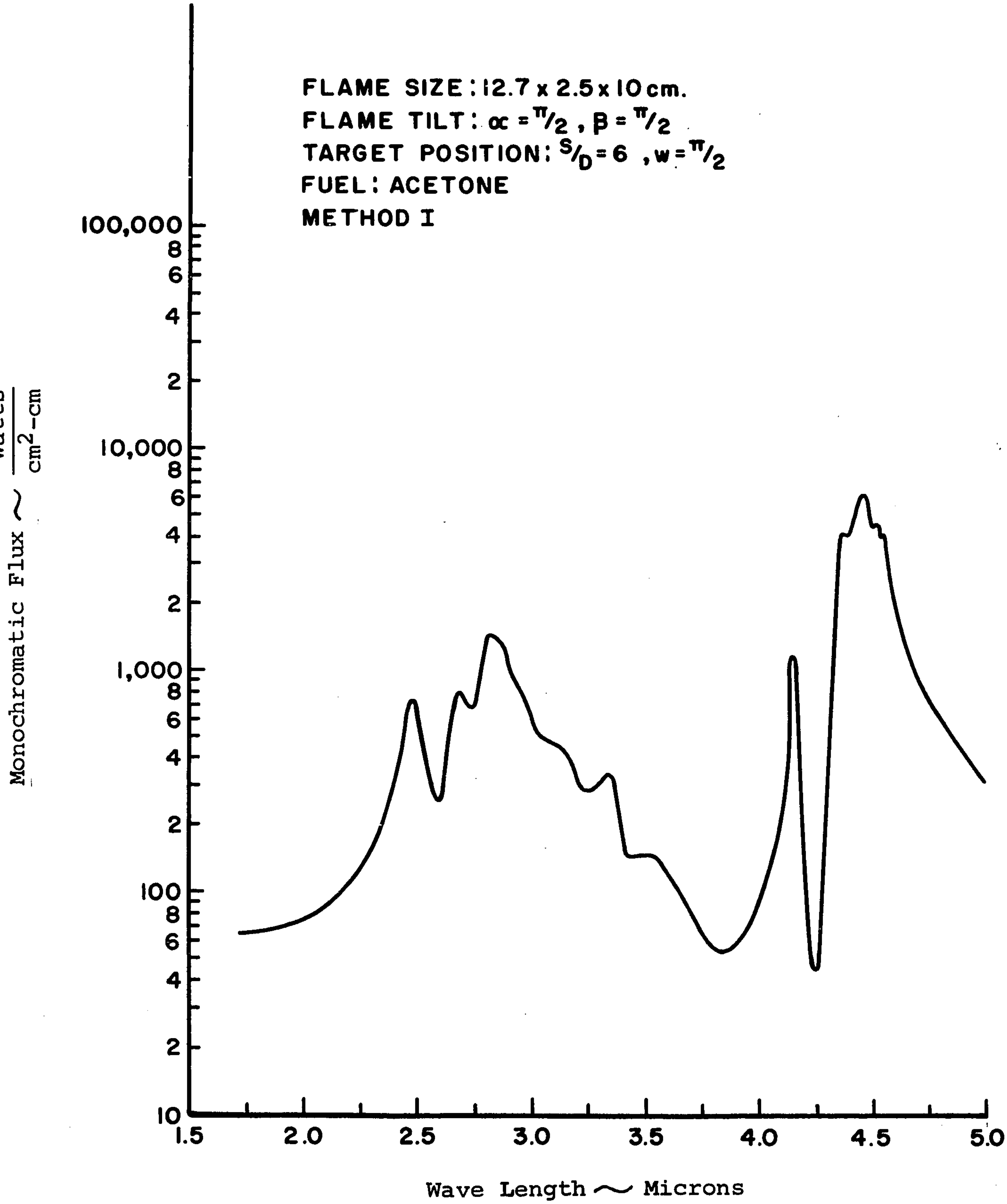

Figure 79. Monochromatic Flux to Target from a Sheet Flame

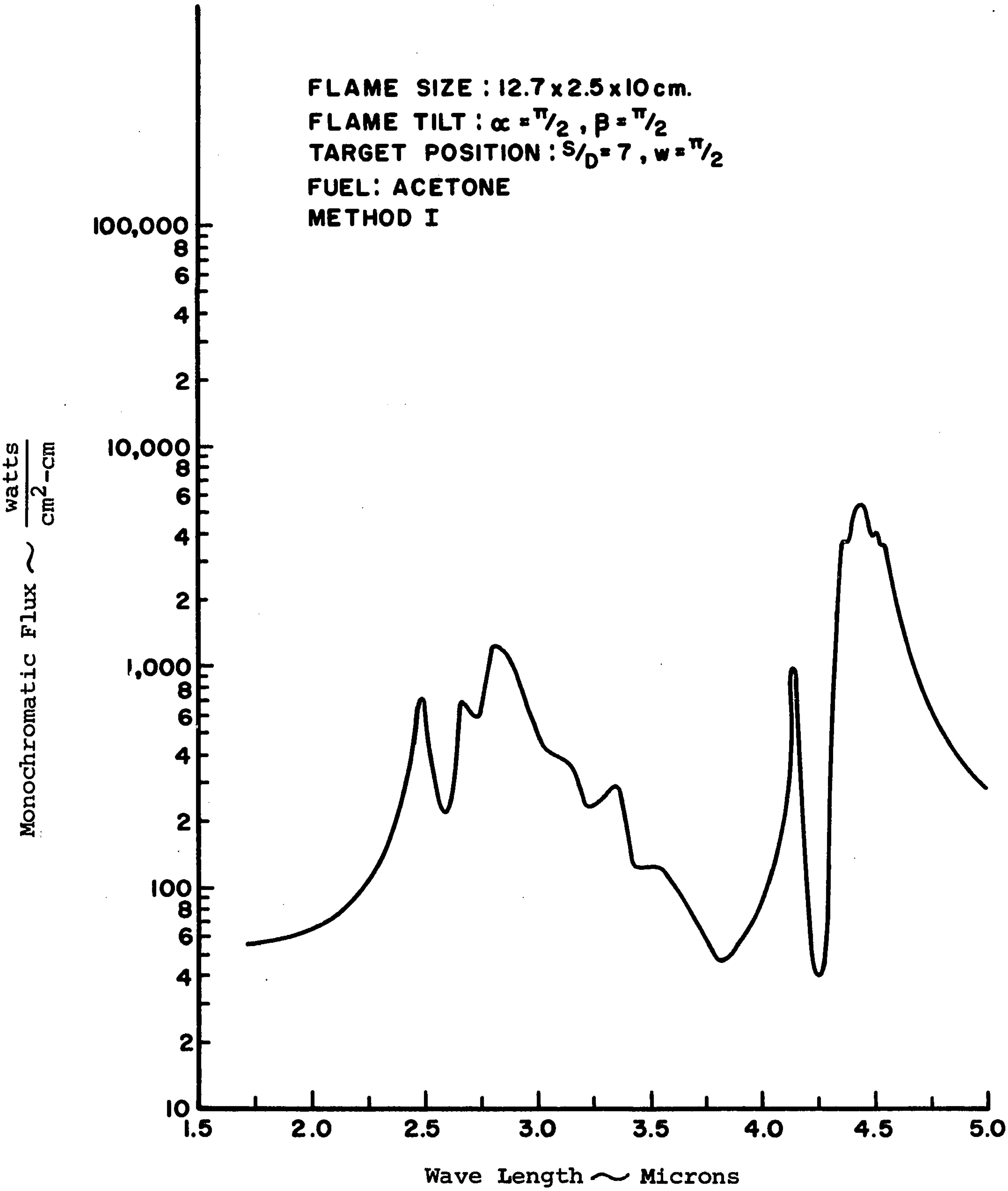

Figure 80. Monochromatic Flux to Target from a Sheet Flame

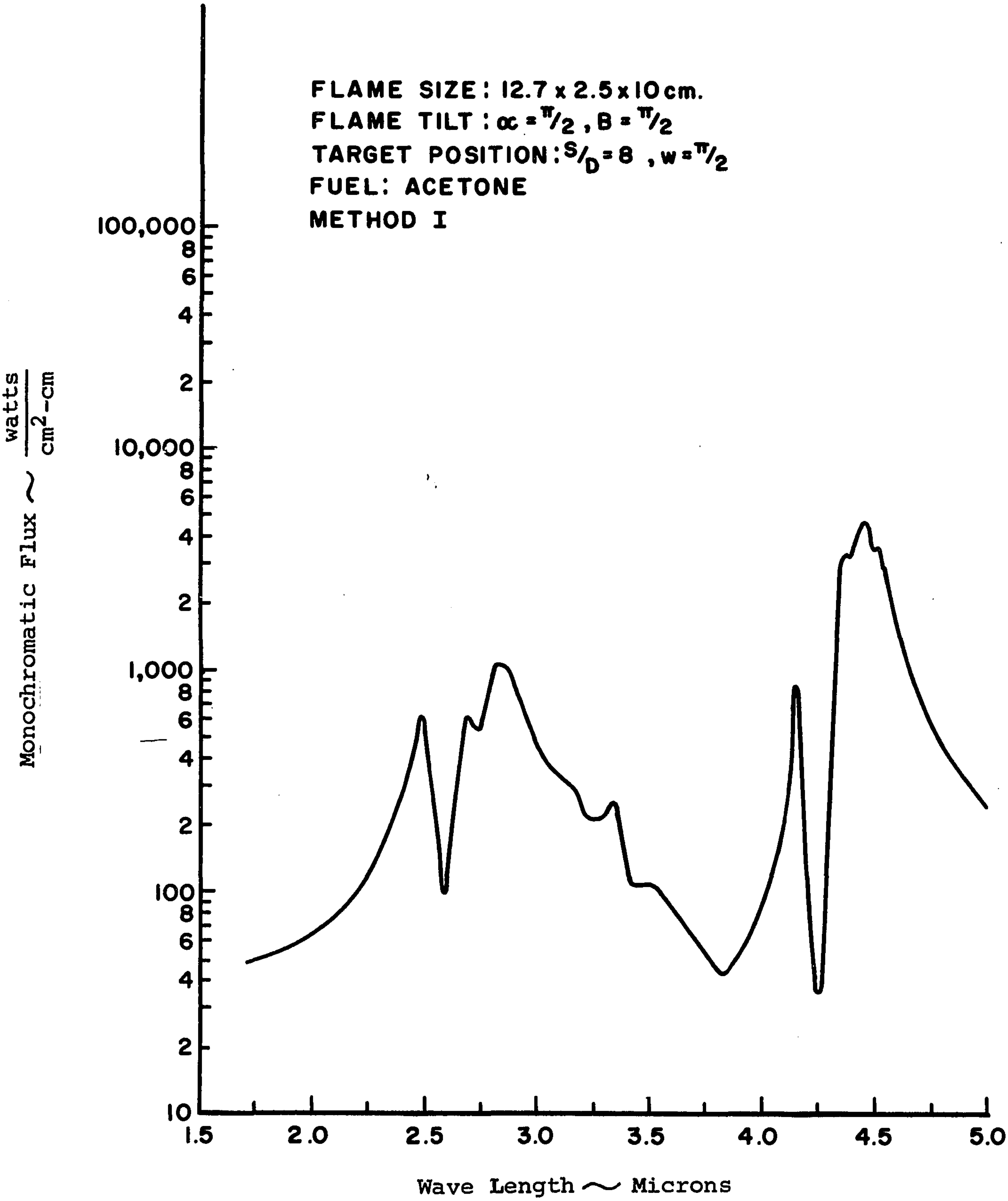

Figure 81. Monochromatic Flux to Target from a Sheet Flame

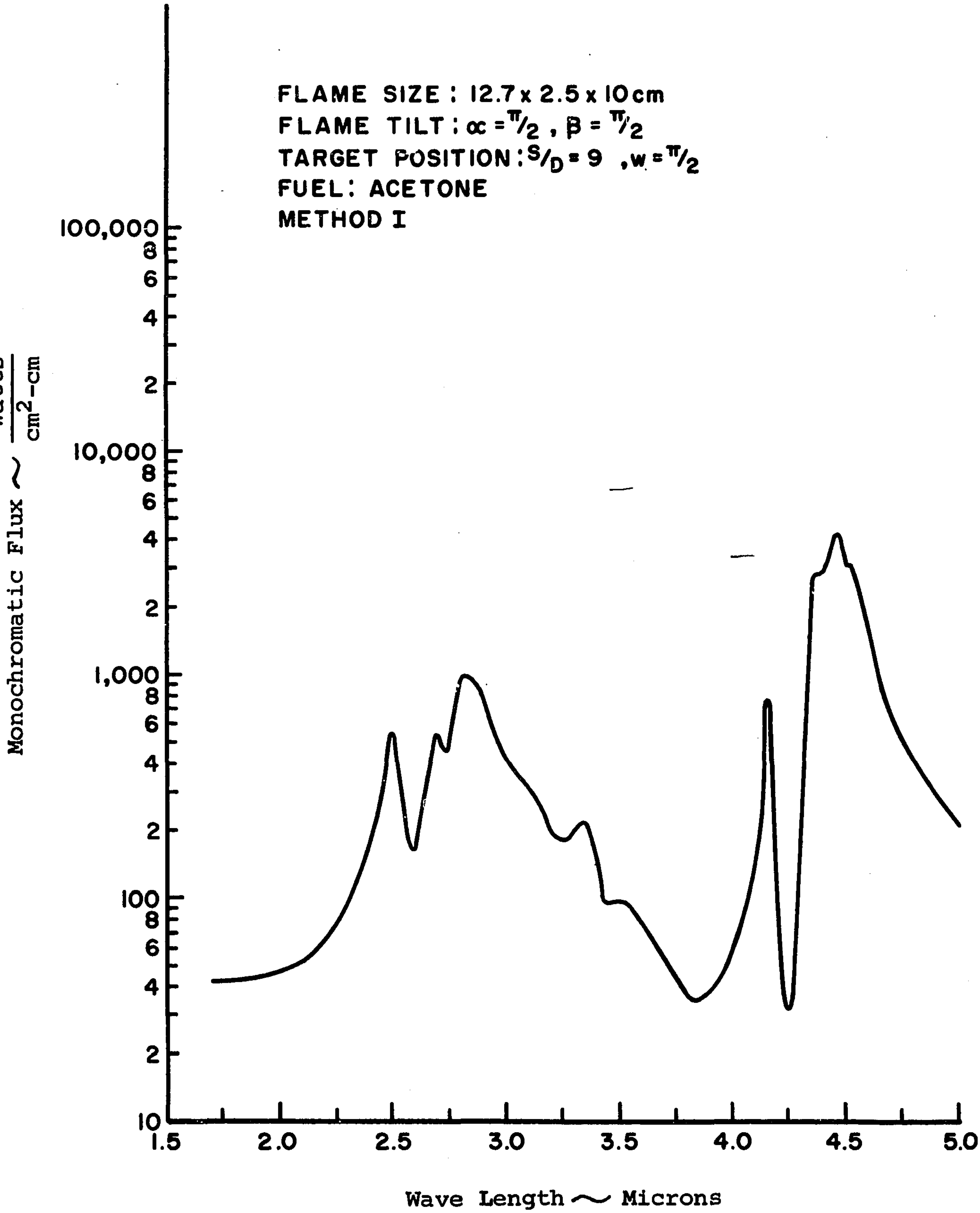

Figure 82. Monochromatic Flux to Target from a Sheet Flame

APPENDIX C

TOTAL RADIATION FLUX CALCULATIONS (METHODS I AND II) AND EXPERIMENTAL RADIATION FLUX MEASUREMENTS OF AN ACETONE AND A METHANOL FLAME WITH A GIVEN SIZE AND POSITION TO A TARGET

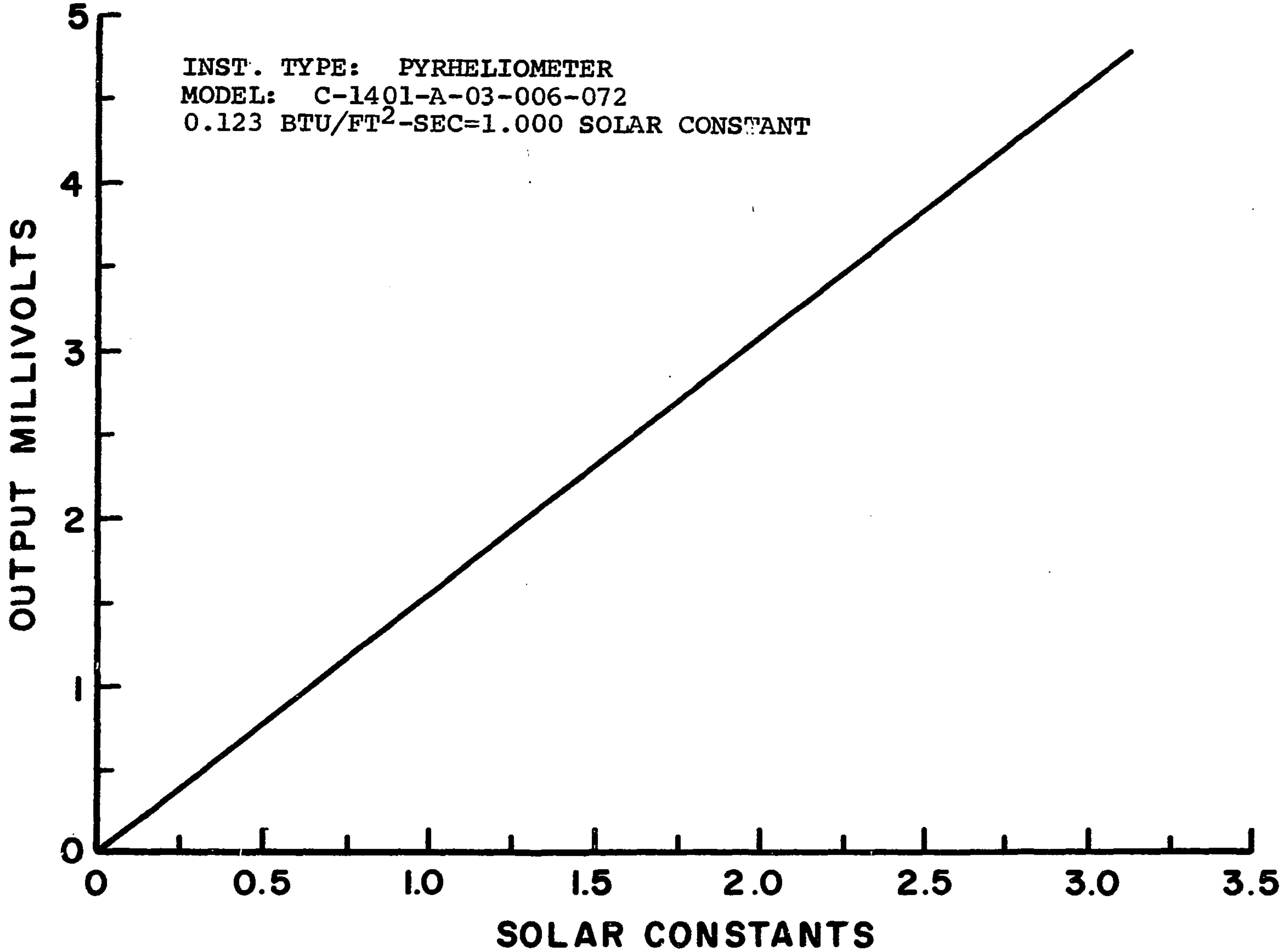

Figure 83. RADIOMETER CALIBRATION

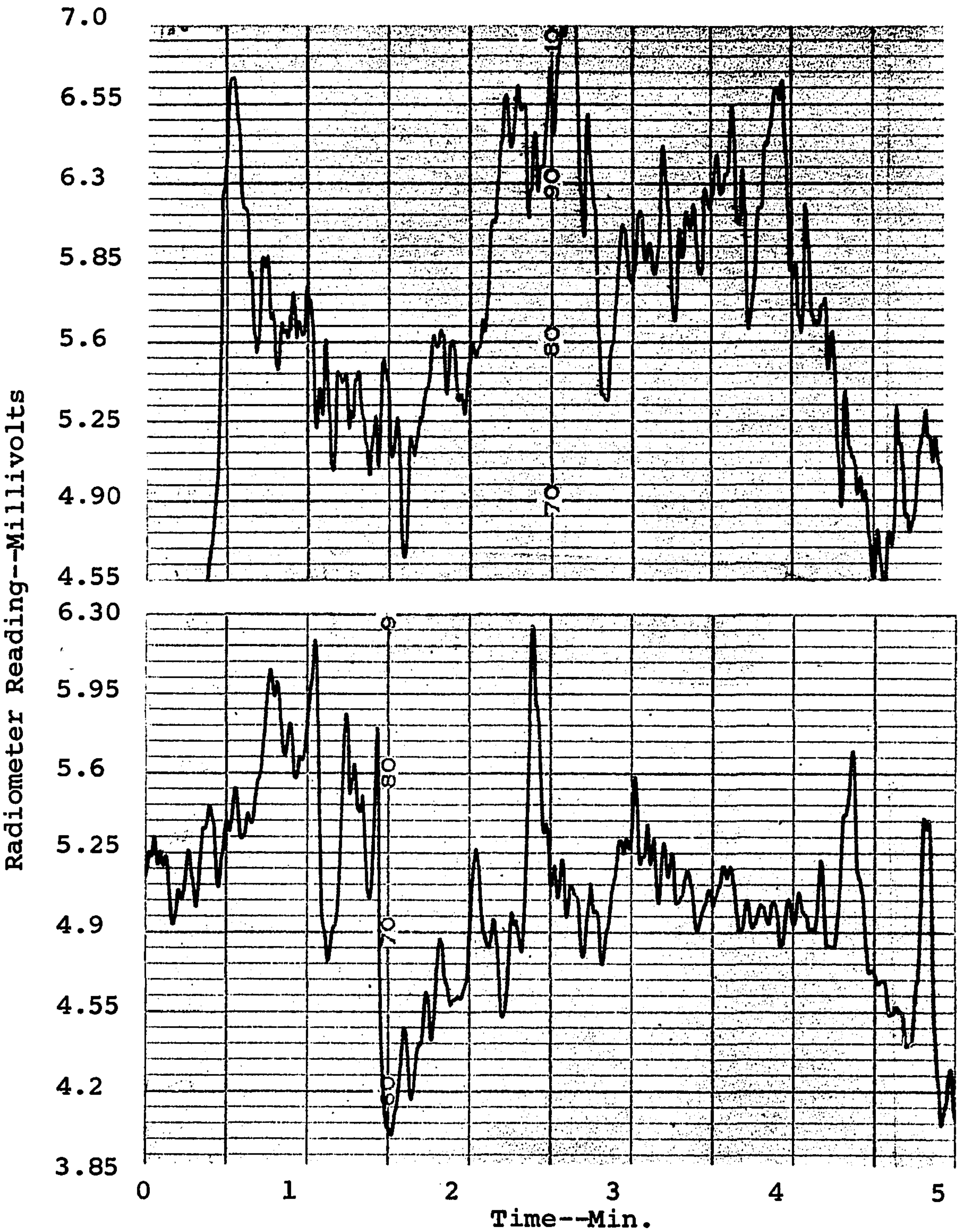

Flame Dimensions:
12.5 x 2.5 x 10 cm

Flame Tilt:
$\alpha = 90°$, $\beta = 90°$

Separation Distance Between Radiometer Face and Burner Periphery:
Upper Trace 1 cm
Lower Trace 2 cm

Figure 84. Fluctuation of Radiation Intensity from Free-Burning Acetone Diffusion Flame. (Vertical Target and Burner at Same Elevation)

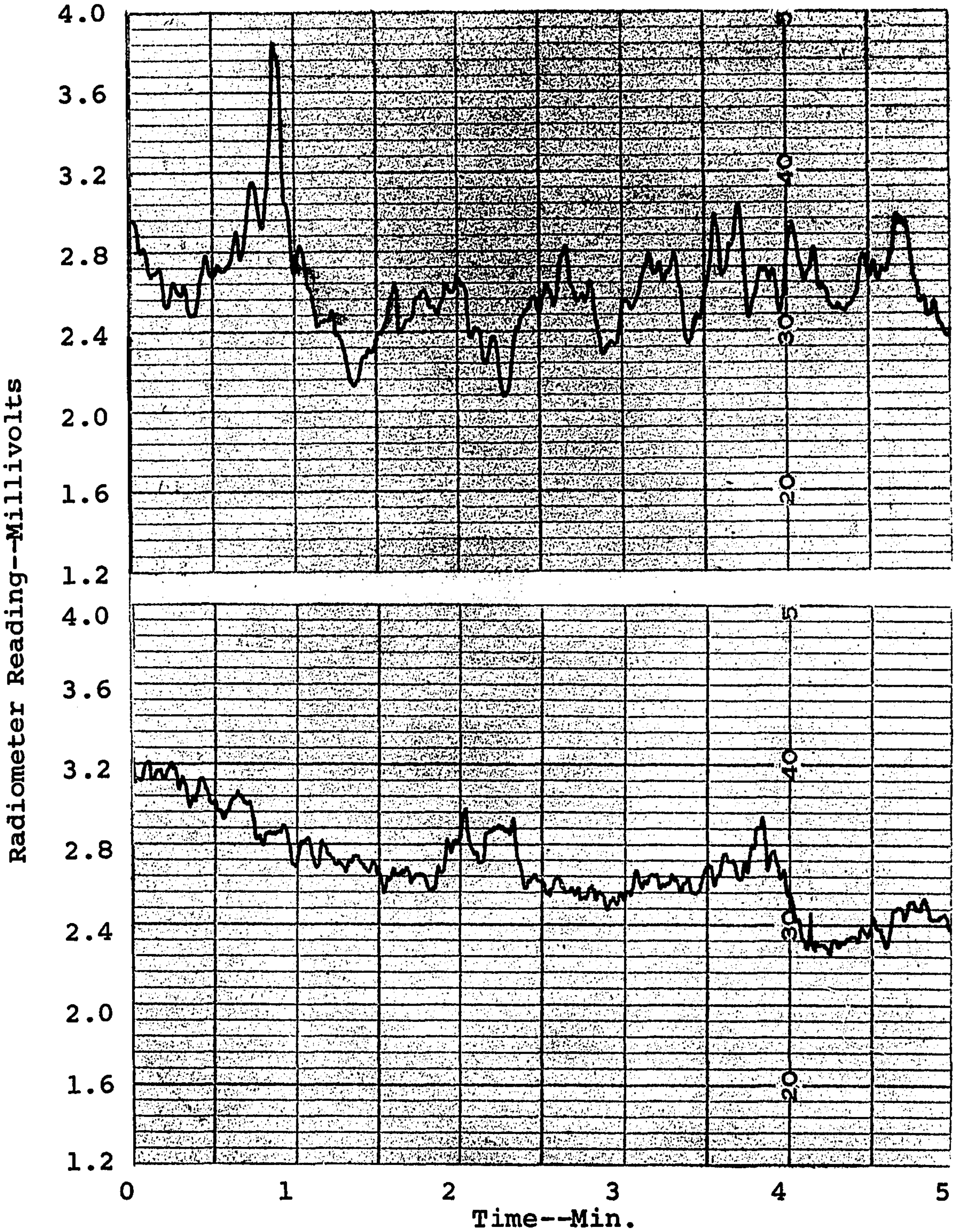

<u>Flame Dimensions</u>:
12.5 x 2.5 x 10 cm
<u>Flame Tilt</u>:
$\alpha = 90°$, $\beta = 90°$

<u>Separation Distance Between Radiometer Face and Burner Periphery</u>:
Upper Trace 3 cm
Lower Trace 4 cm

Figure 85 . Fluctuation of Radiation Intensity from Free-Burning Acetone Diffusion Flame. (Vertical Target and Burner at Same Elevation)

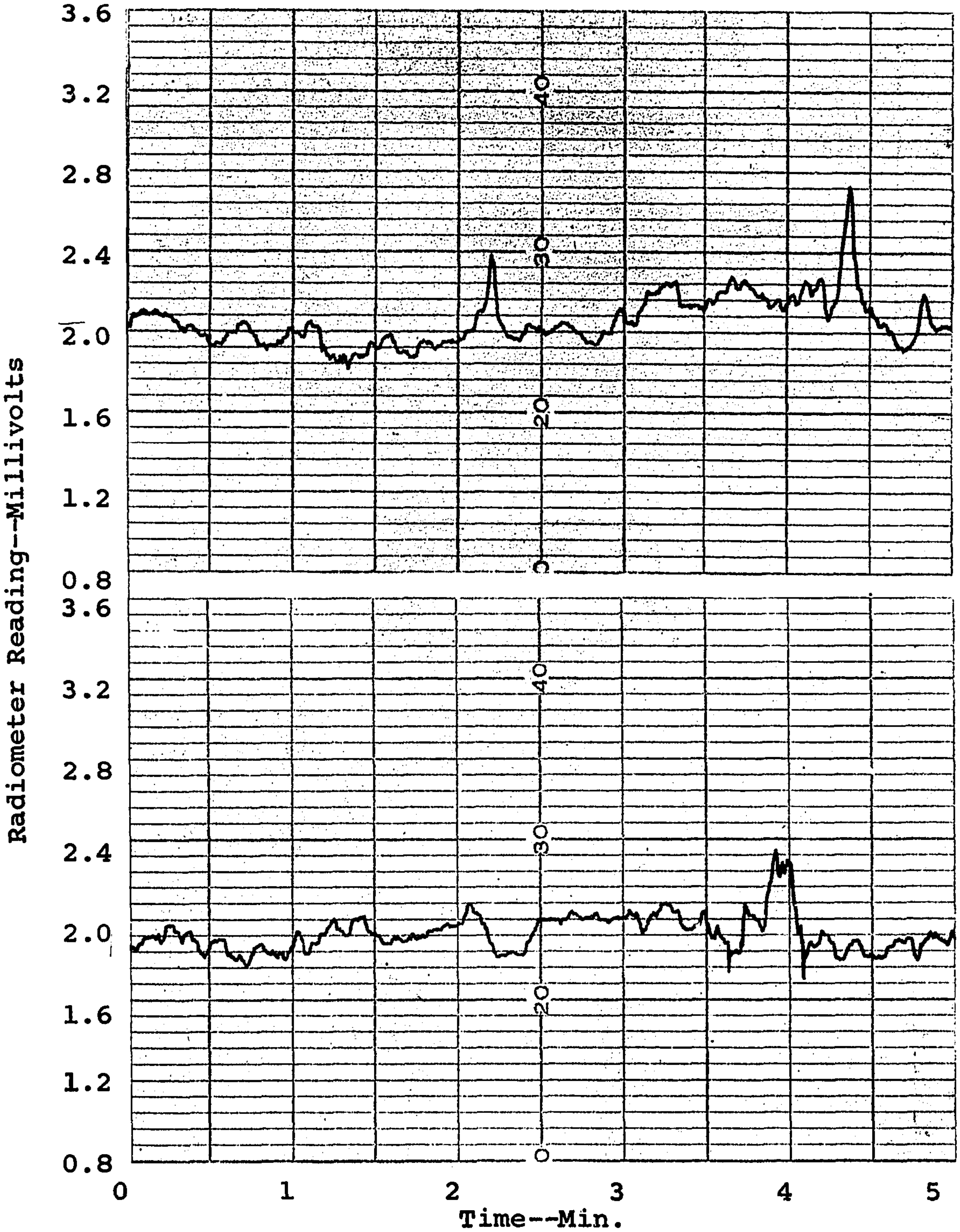

Flame Dimensions:
12.5 x 2.5 x 10 cm

Flame Tilt:
$\alpha = 90°$, $\beta = 90°$

Separation Distance Between Radiometer Face and Burner Periphery:
Upper Trace 5 cm
Lower Trace 6 cm

Figure 86. Fluctuation of Radiation Intensity from Free-Burning Acetone Diffusion Flame. (Vertical Target and Burner at Same Elevation)

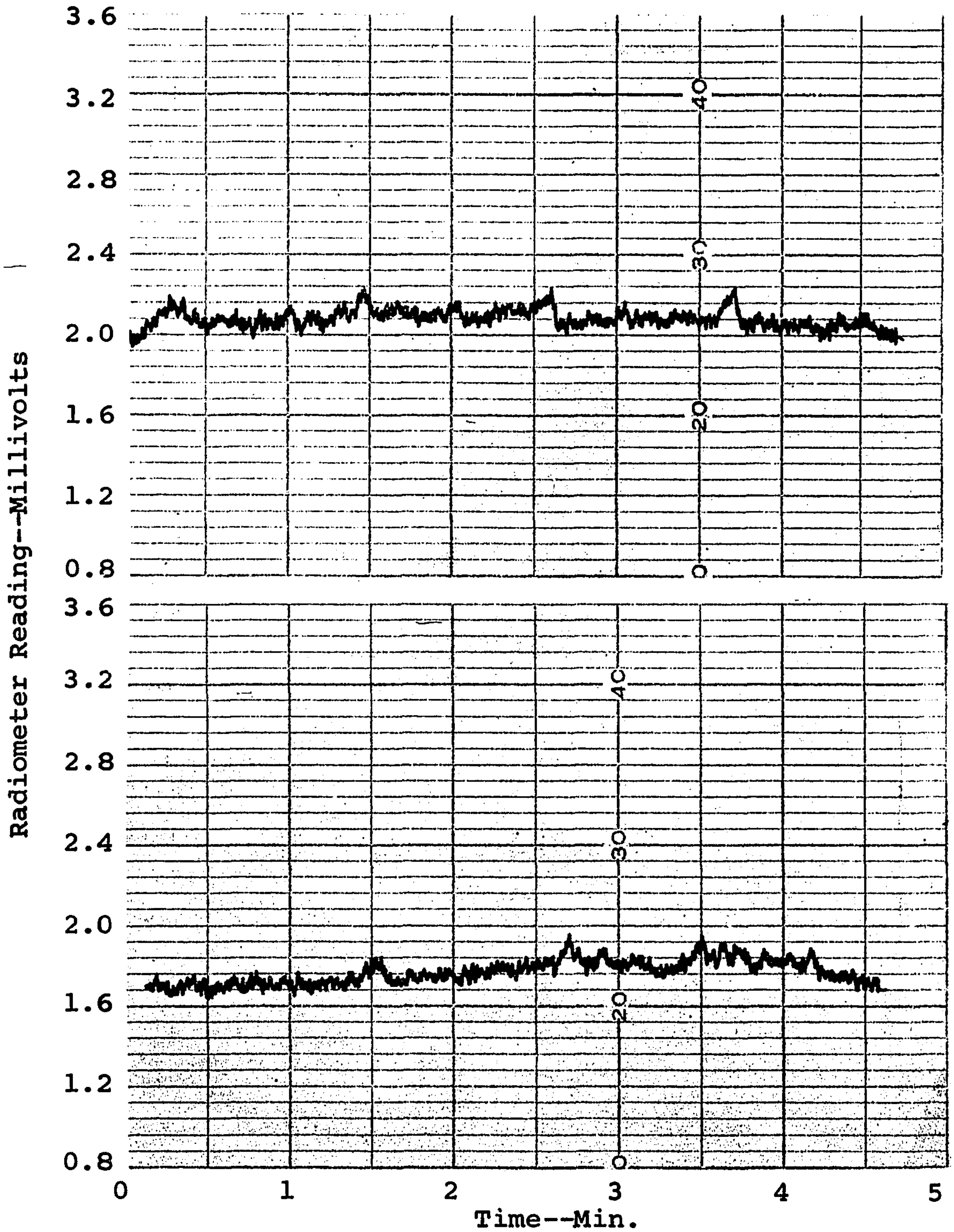

Flame Dimensions:
12.5 x 2.5 x 10 cm
Flame Tilt:
$\alpha = 90°$, $\beta = 90°$

Separation Distance Between Radiometer Face and Burner Periphery:
Upper Trace 7 cm
Lower Trace 8 cm

Figure 87. Fluctuation of Radiation Intensity from Free-Burning Acetone Diffusion Flame. (Vertical Target and Burner at Same Elevation)

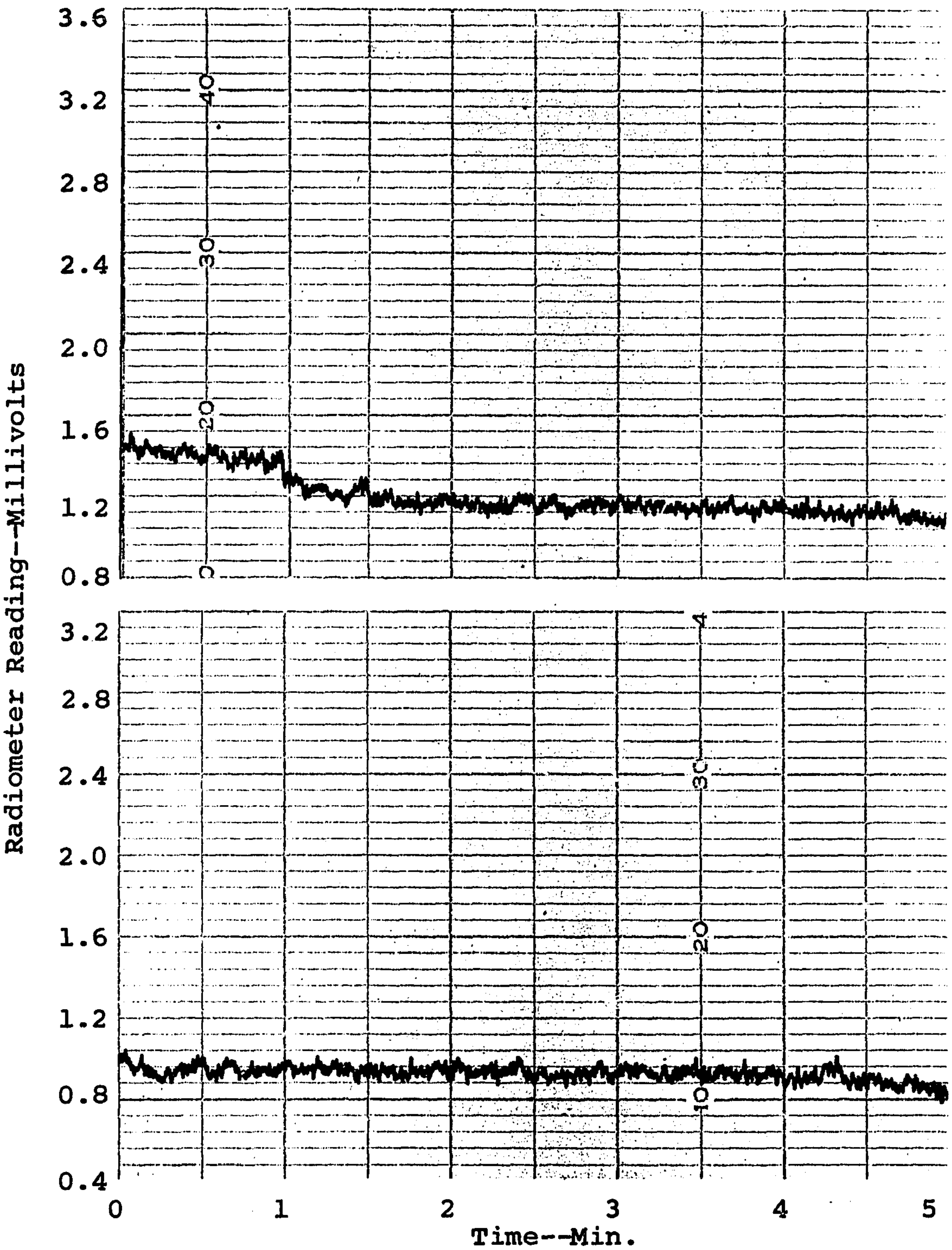

Flame Dimensions:
12.5 x 2.5 x 10 cm

Flame Tilt:
$\alpha = 90°$, $\beta = 90°$

Separation Distance Between Radiometer Face and Burner Periphery:
Upper Trace 9 cm
Lower Trace 10 cm

Figure 88. Fluctuation of Radiation Intensity from Free-Burning Acetone Diffusion Flame. (Vertical Target and Burner at Same Elevation)

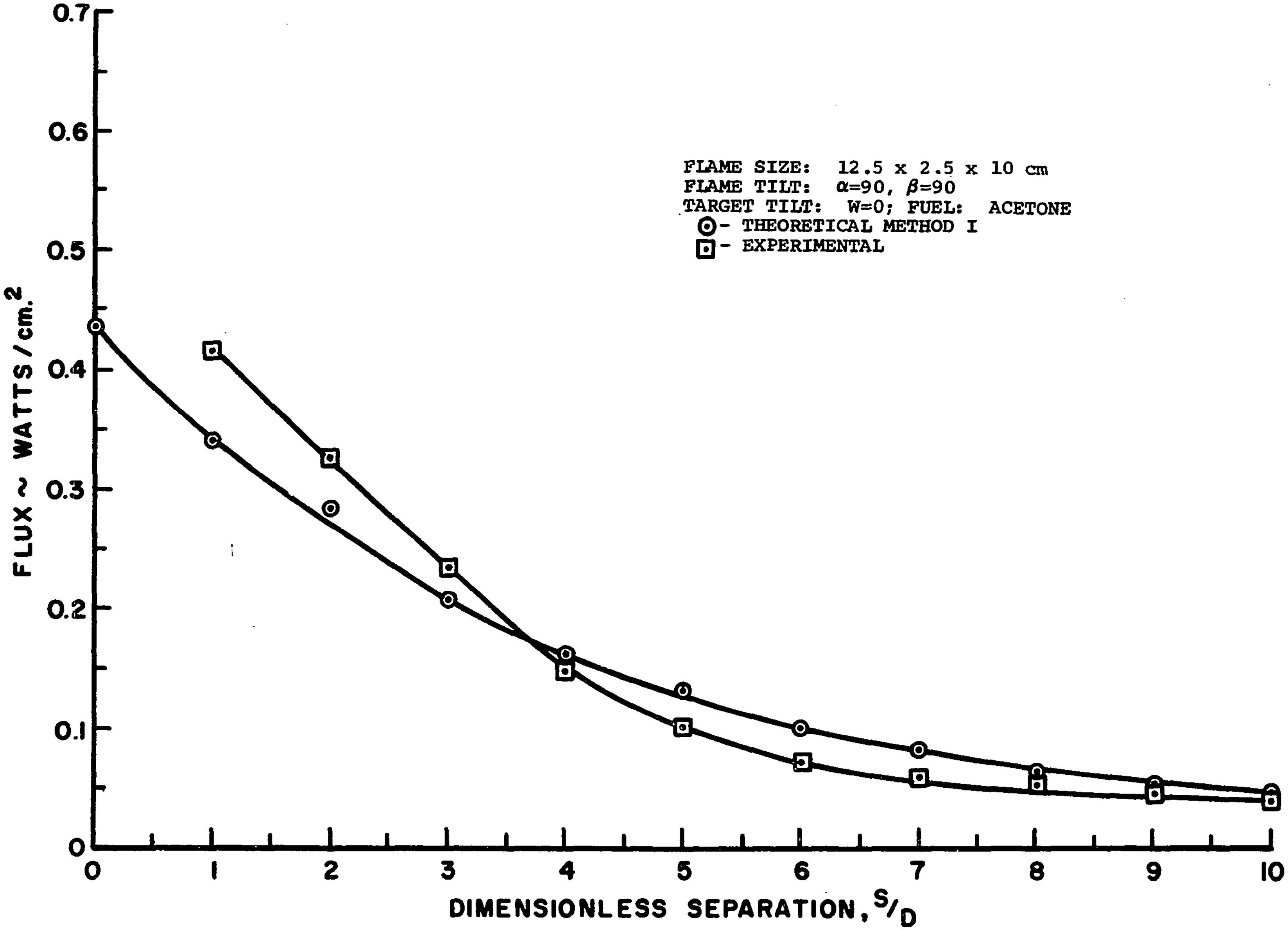

Figure 89. Radiation Flux Variation with Dimensionless Separation

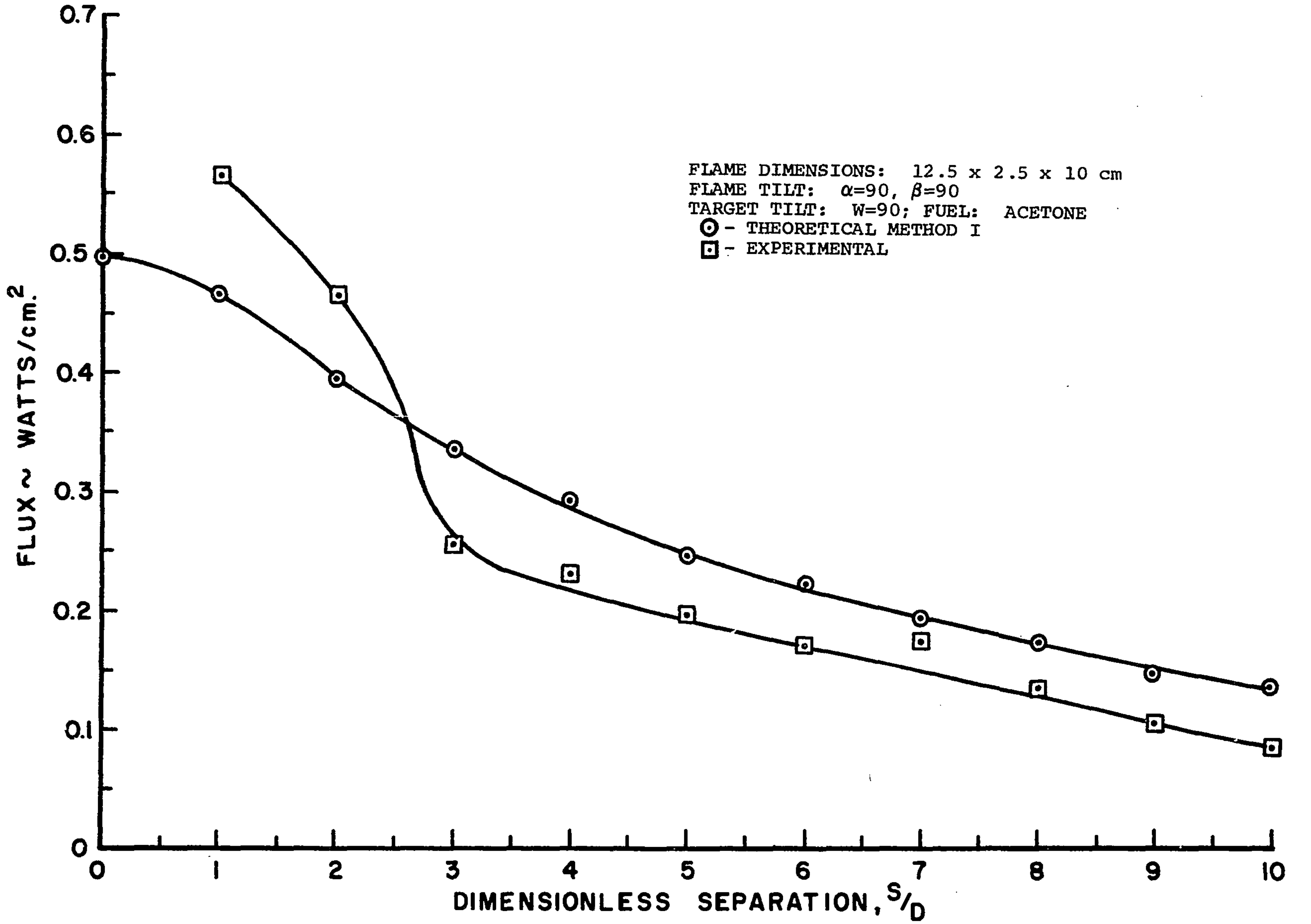

Figure 90. Radiation Flux Variation with Dimensionless Separation

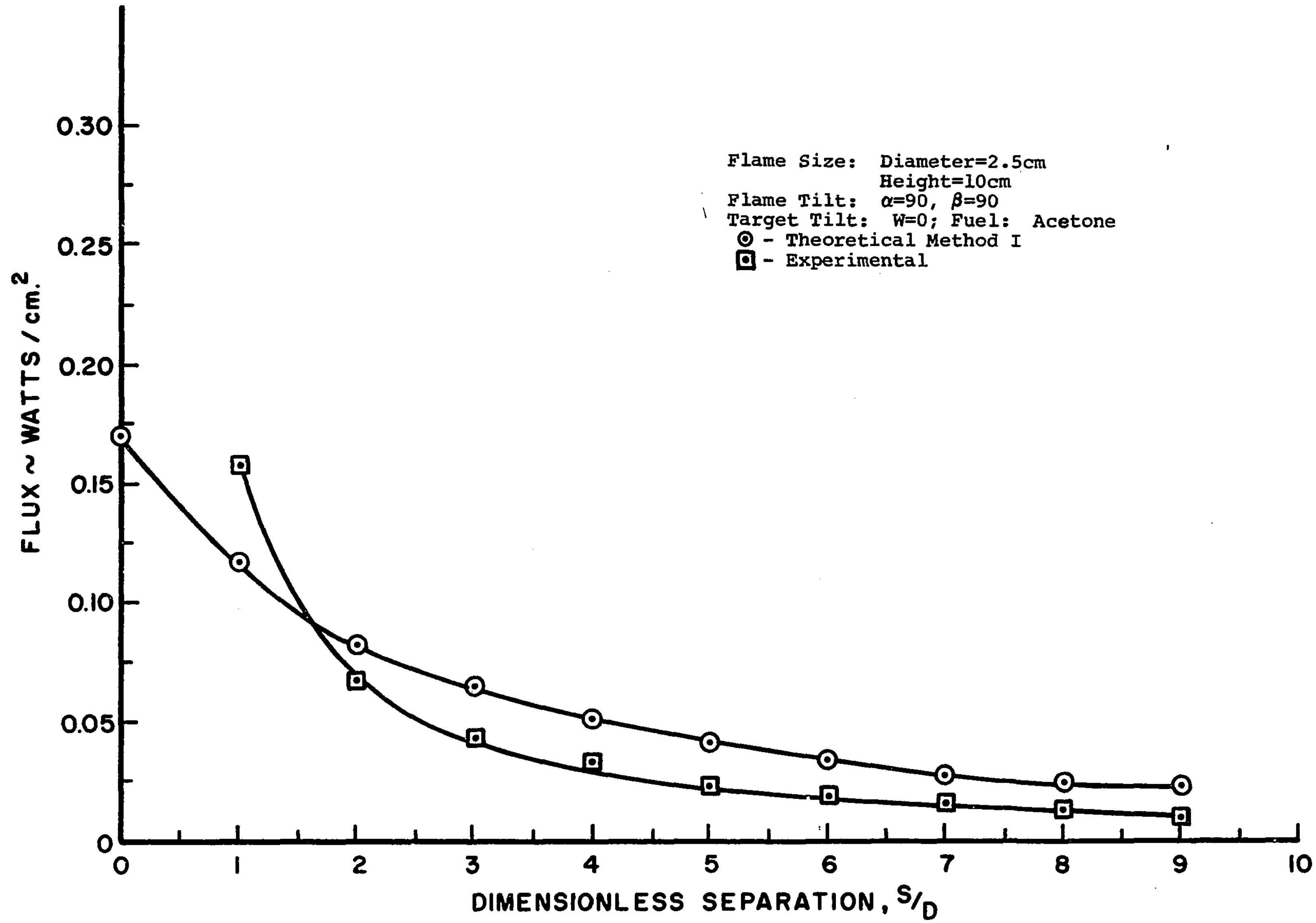

Figure 91. Radiation Flux Variation with Dimensionless Separation

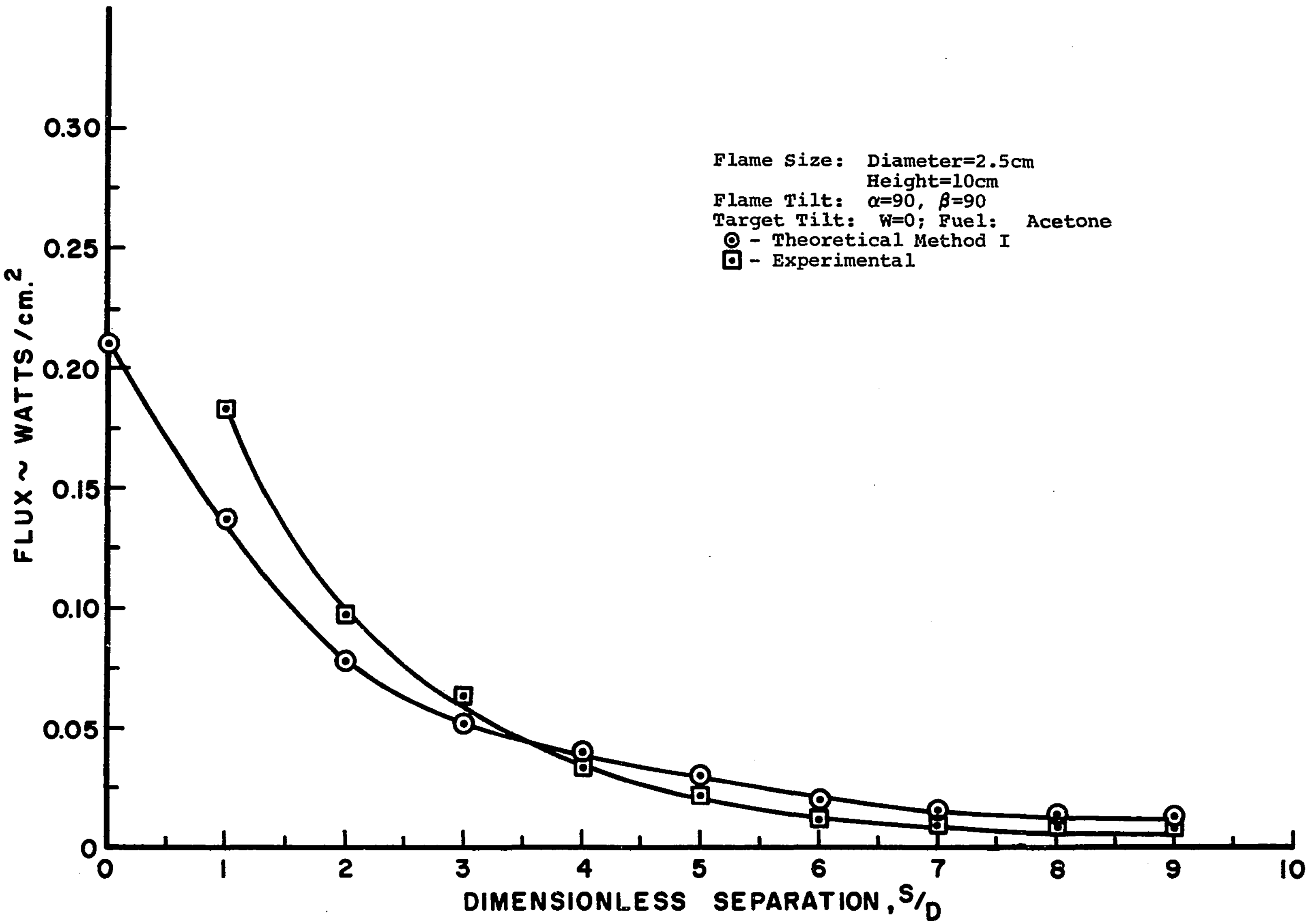

Figure 92. Radiation Flux Variation with Dimensionless Separation

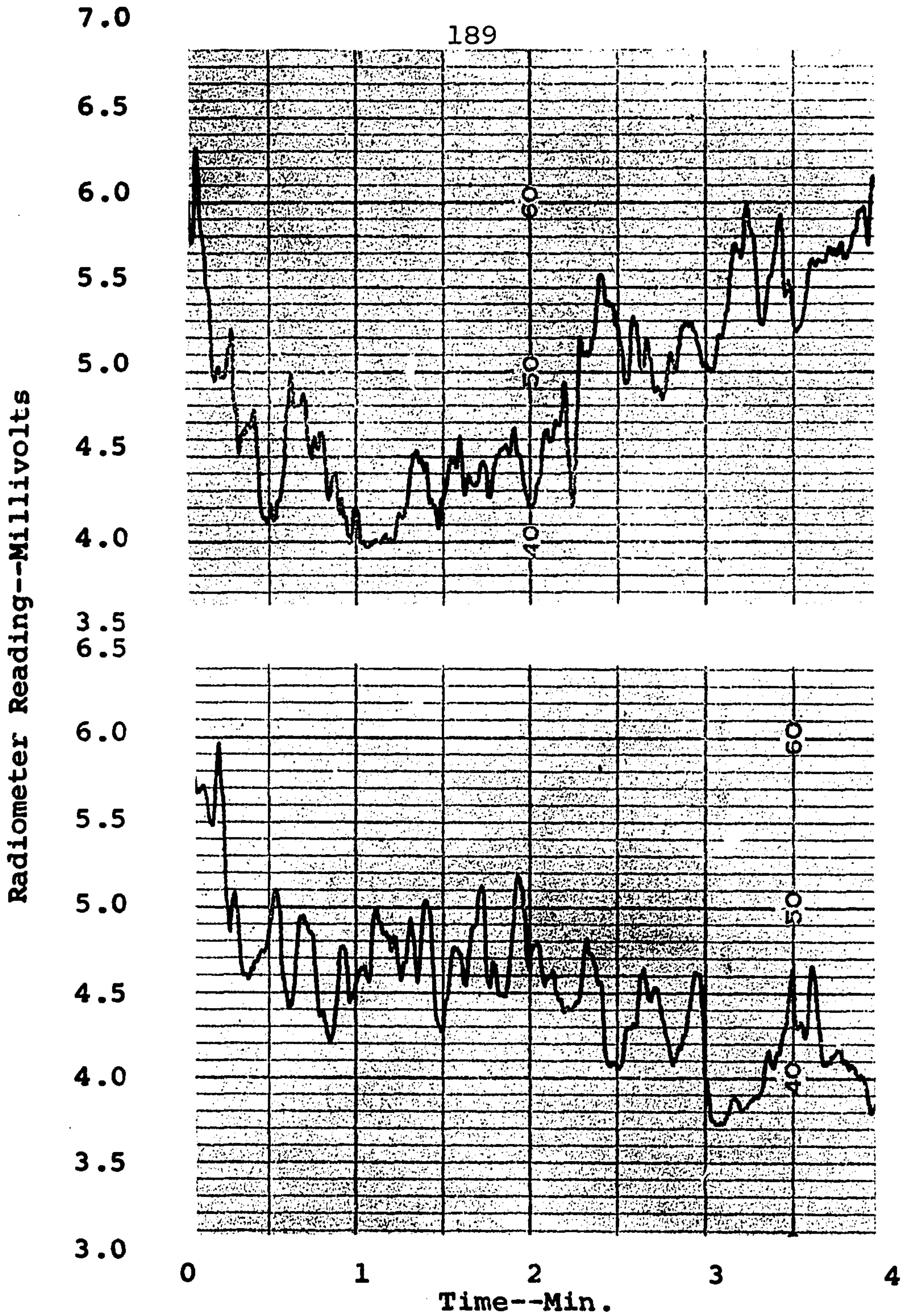

Flame Dimensions:
12.5 x 2.5 x 10 cm

Flame Tilt:
$\alpha = 90°$, $\beta = 90°$

Separation Distance Between Radiometer Face and Burner Periphery:
Upper Trace 1 cm
Lower Trace 2 cm

Figure 93. Fluctuation of Radiation Intensity from Free-Burning Methanol Diffusion Flame. (Vertical Target and Burner at Same Elevation)

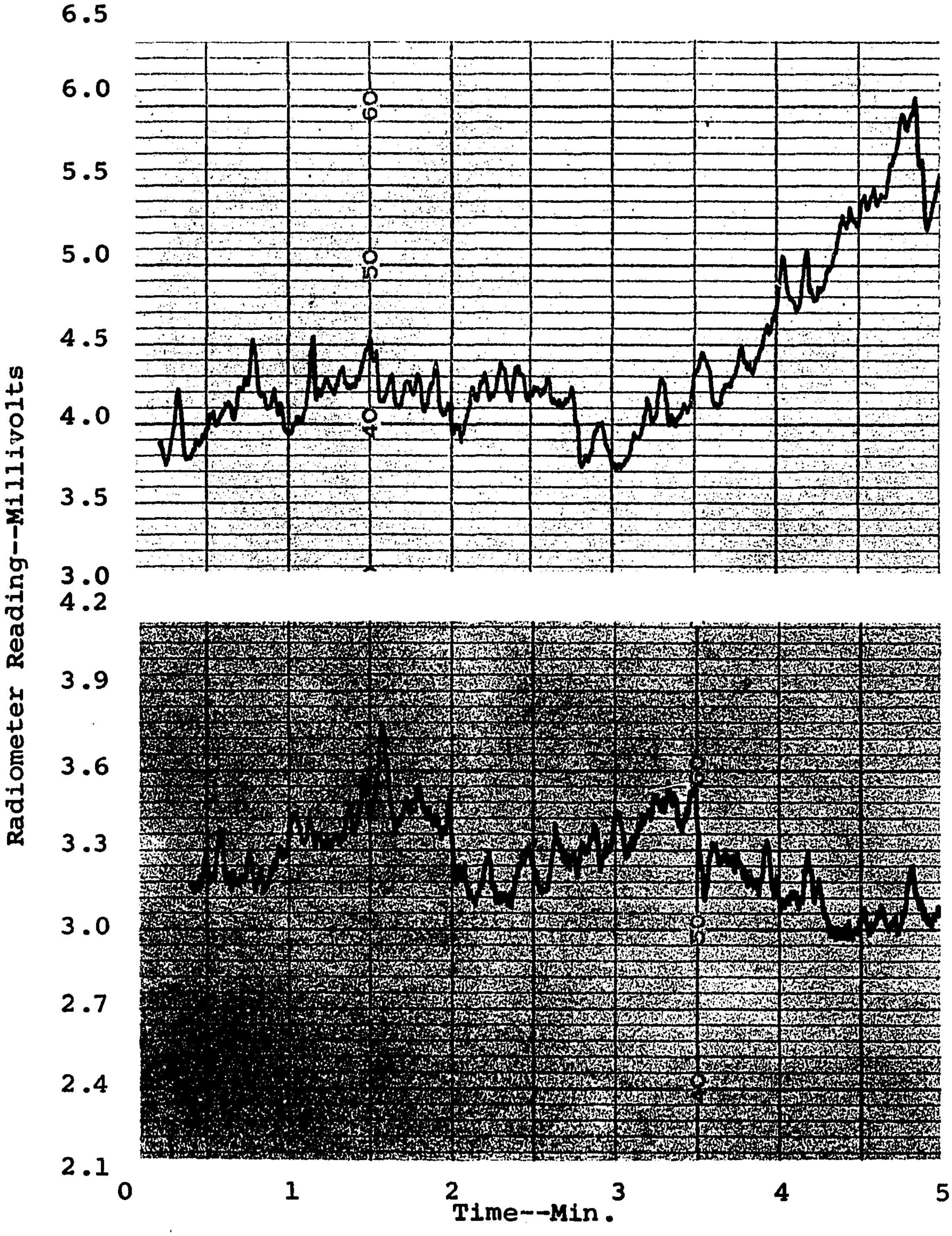

Flame Dimensions:
12.5 x 2.5 x 10 cm
Flame Tilt:
$\alpha = 90°$, $\beta = 90°$

Separation Distance Between Radiometer Face and Burner Periphery:
Upper Trace 3 cm
Lower Trace 4 cm

Figure 94. Fluctuation of Radiation Intensity from Free-Burning Methanol Diffusion Flame. (Vertical Target and Burner at Same Elevation)

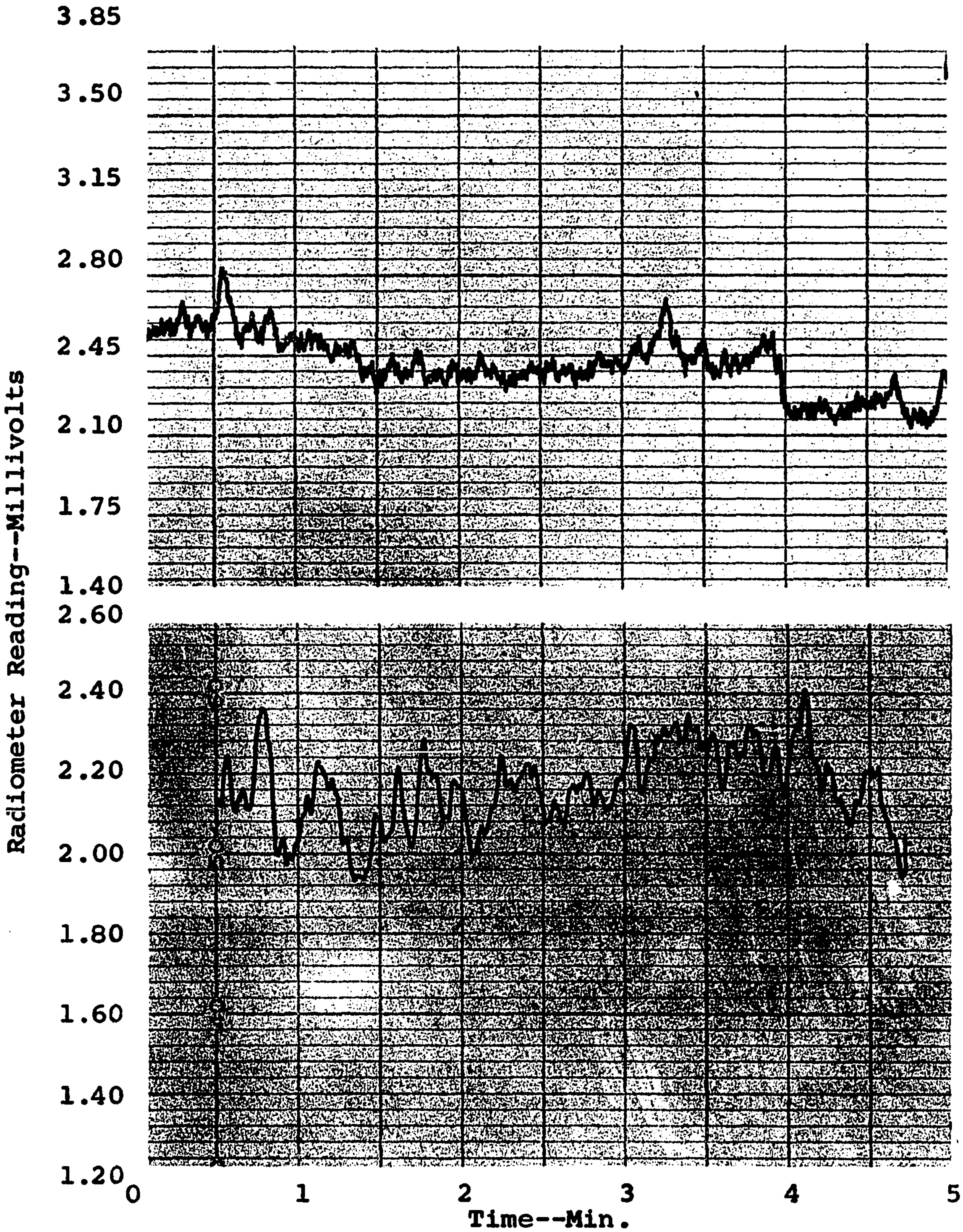

Flame Dimensions:
12.5 x 2.5 x 10 cm
Flame Tilt:
$\alpha = 90°$, $\beta = 90°$

Separation Distance Between Radiometer Face and Burner Periphery:
Upper Trace 5 cm
Lower Trace 6 cm

Figure 95. Fluctuation of Radiation Intensity from Free-Burning Methanol Diffusion Flame. (Vertical Target and Burner at Same Elevation)

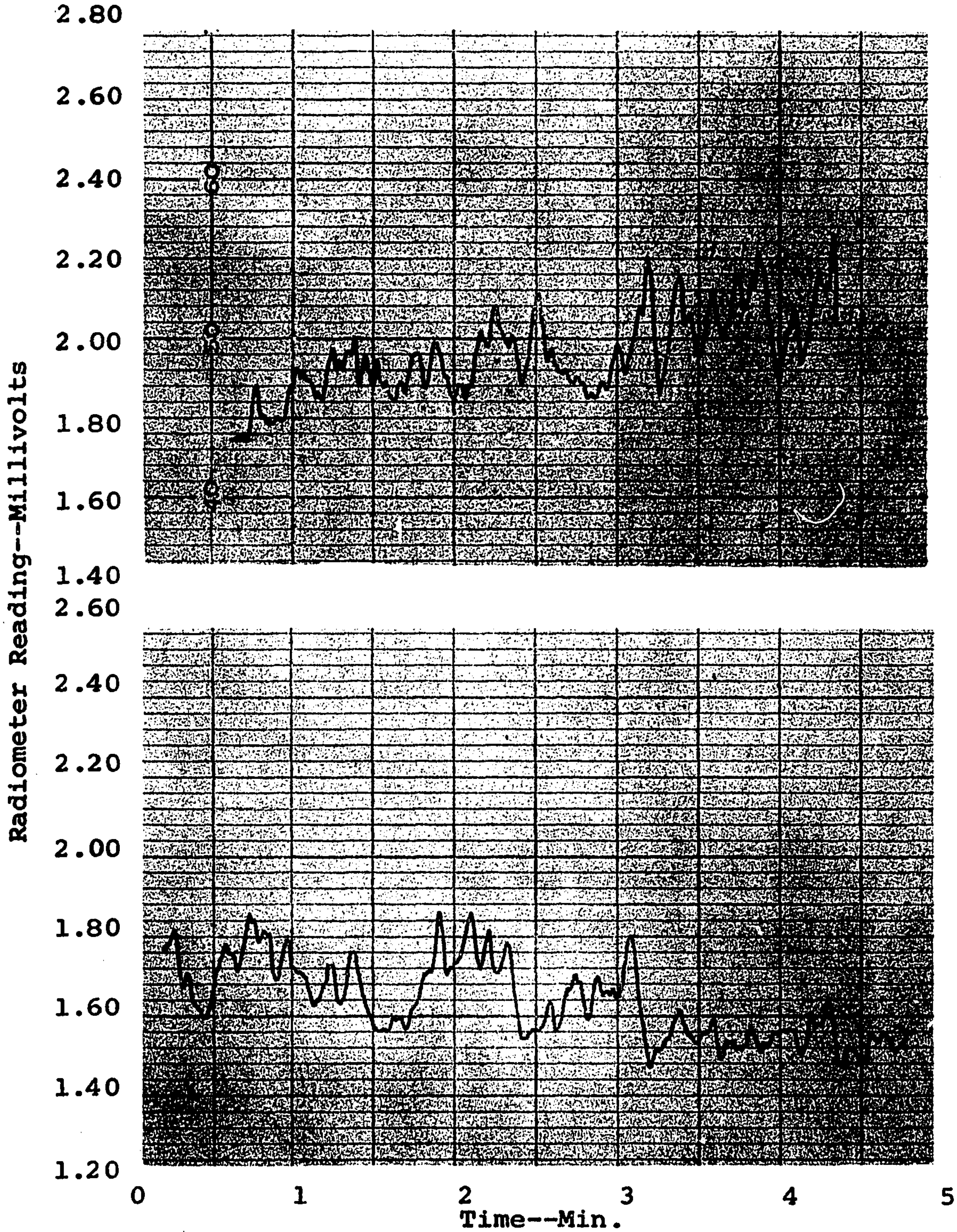

<u>Flame Dimensions:</u>
12.5 x 2.5 x 10 cm
<u>Flame Tilt:</u>
$\alpha = 90°$, $\beta = 90°$

<u>Separation Distance Between Radiometer Face and Burner Periphery:</u>
Upper Trace 7 cm
Lower Trace 8 cm

Figure 96. Fluctuation of Radiation Intensity from Free-Burning Methanol Diffusion Flame. (Vertical Target and Burner at Same Elevation)

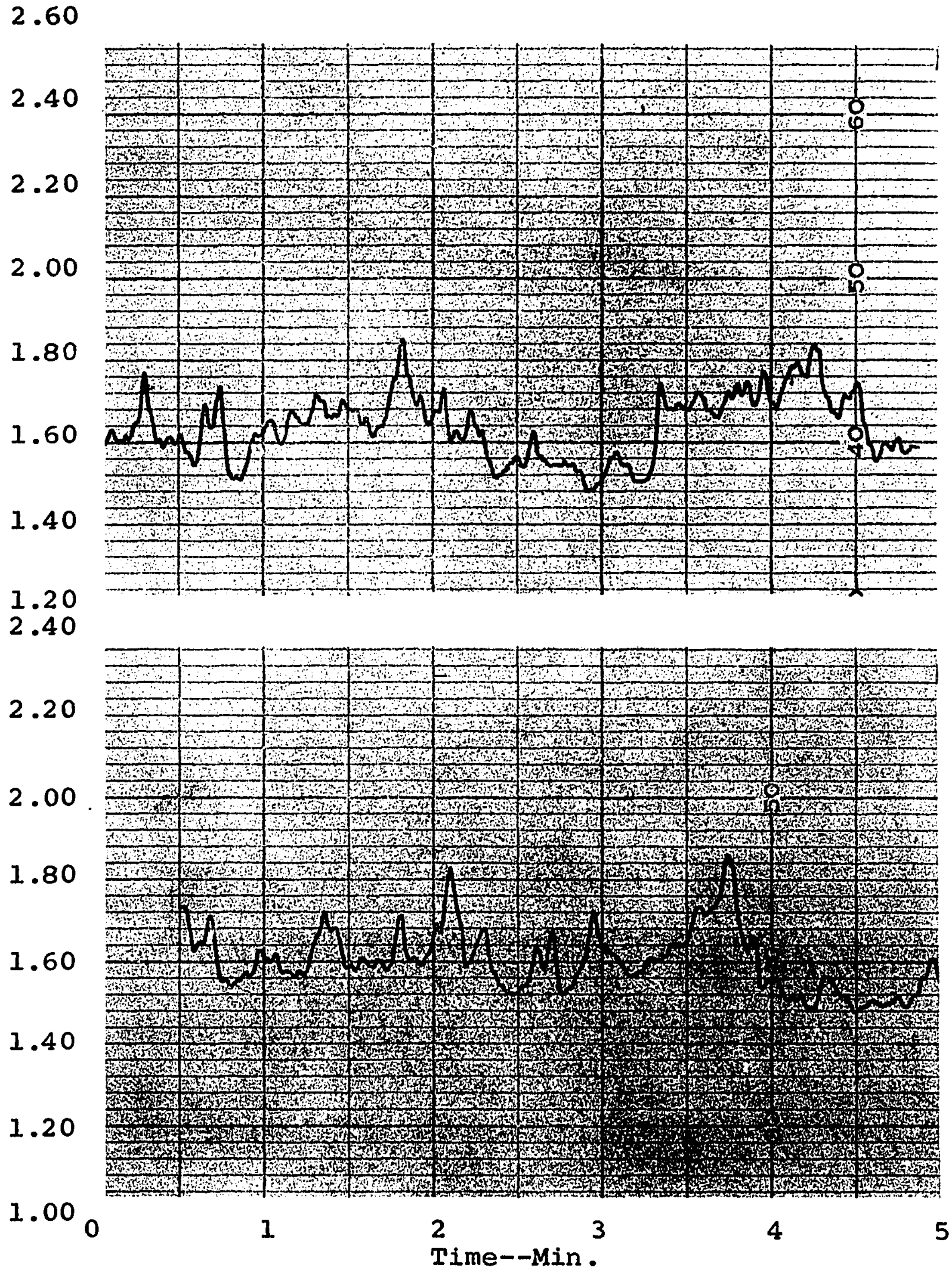

<u>Flame Dimensions</u>:
12.5 x 2.5 x 10 cm
<u>Flame Tilt</u>:
$\alpha = 90°$, $\beta = 90°$

<u>Separation Distance Between Radiometer Face and Burner Periphery</u>:

Upper Trace 9 cm
Lower Trace 10 cm

Figure 97. Fluctuation of Radiation Intensity from Free-Burning Methanol Diffusion Flame. (Vertical Target and Burner at Same Elevation)

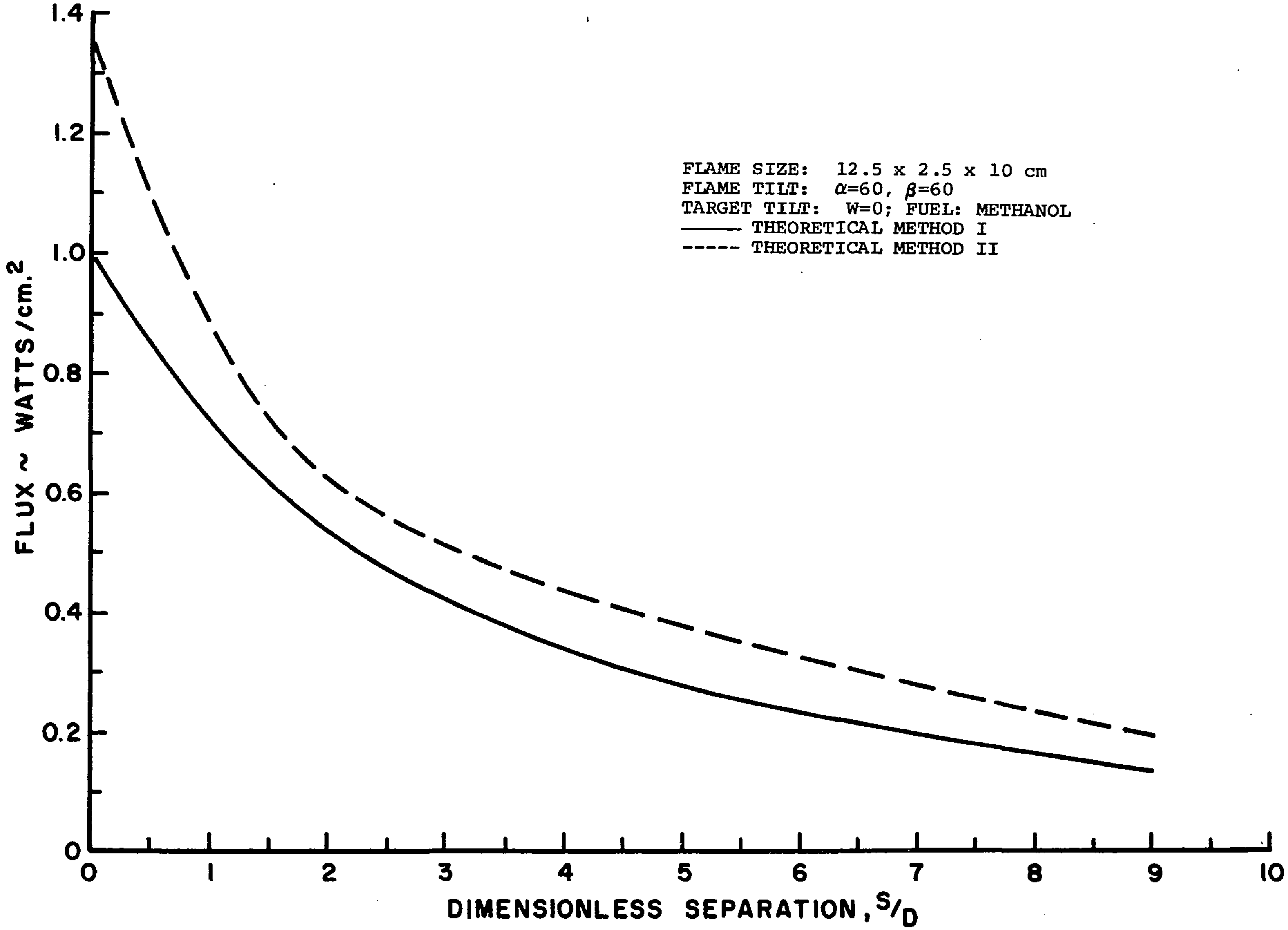

Figure 98. Radiation Flux Variation with Dimensionless Separation

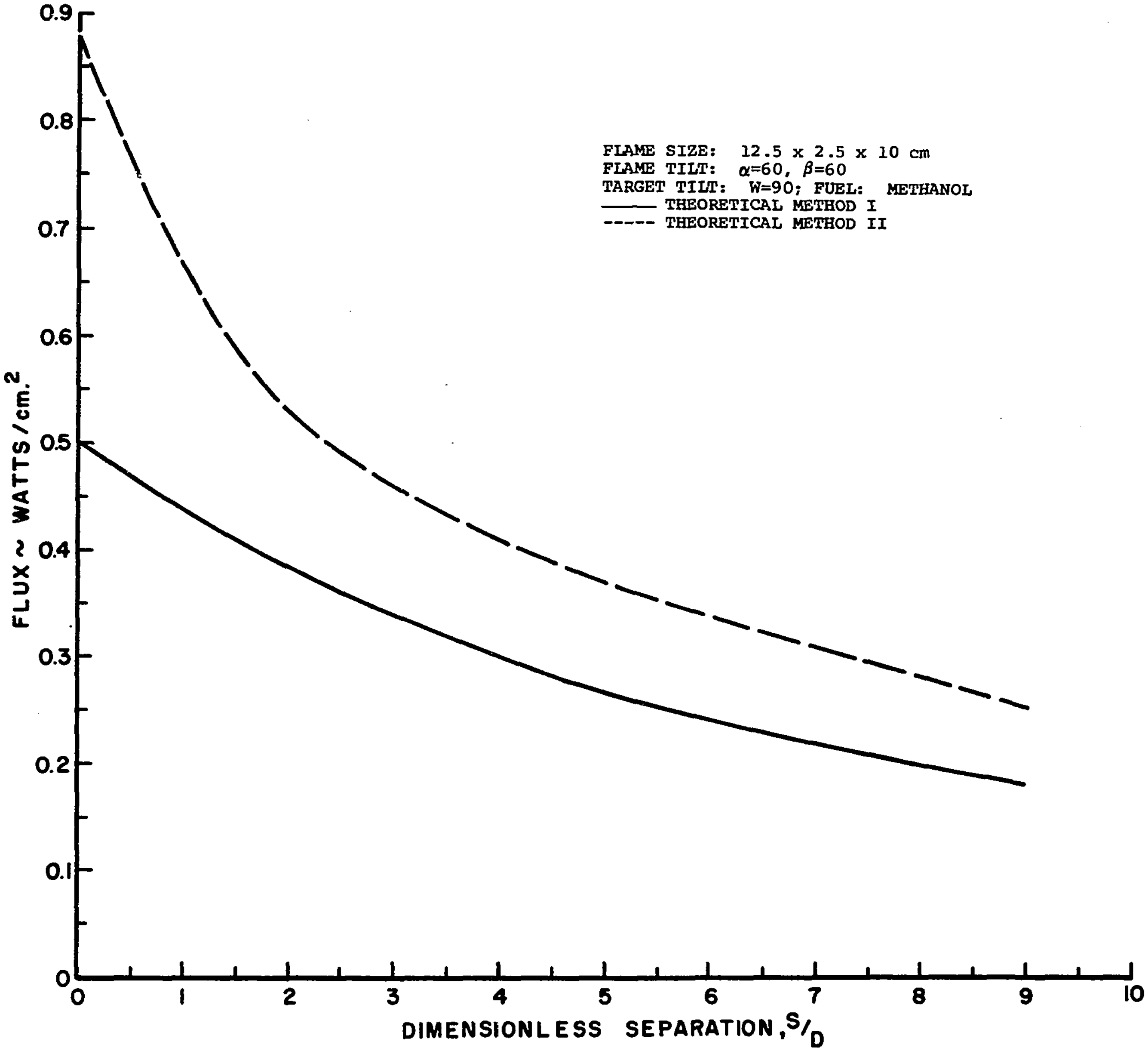

Figure 99. Radiation Flux Variation with Dimensionless Separation

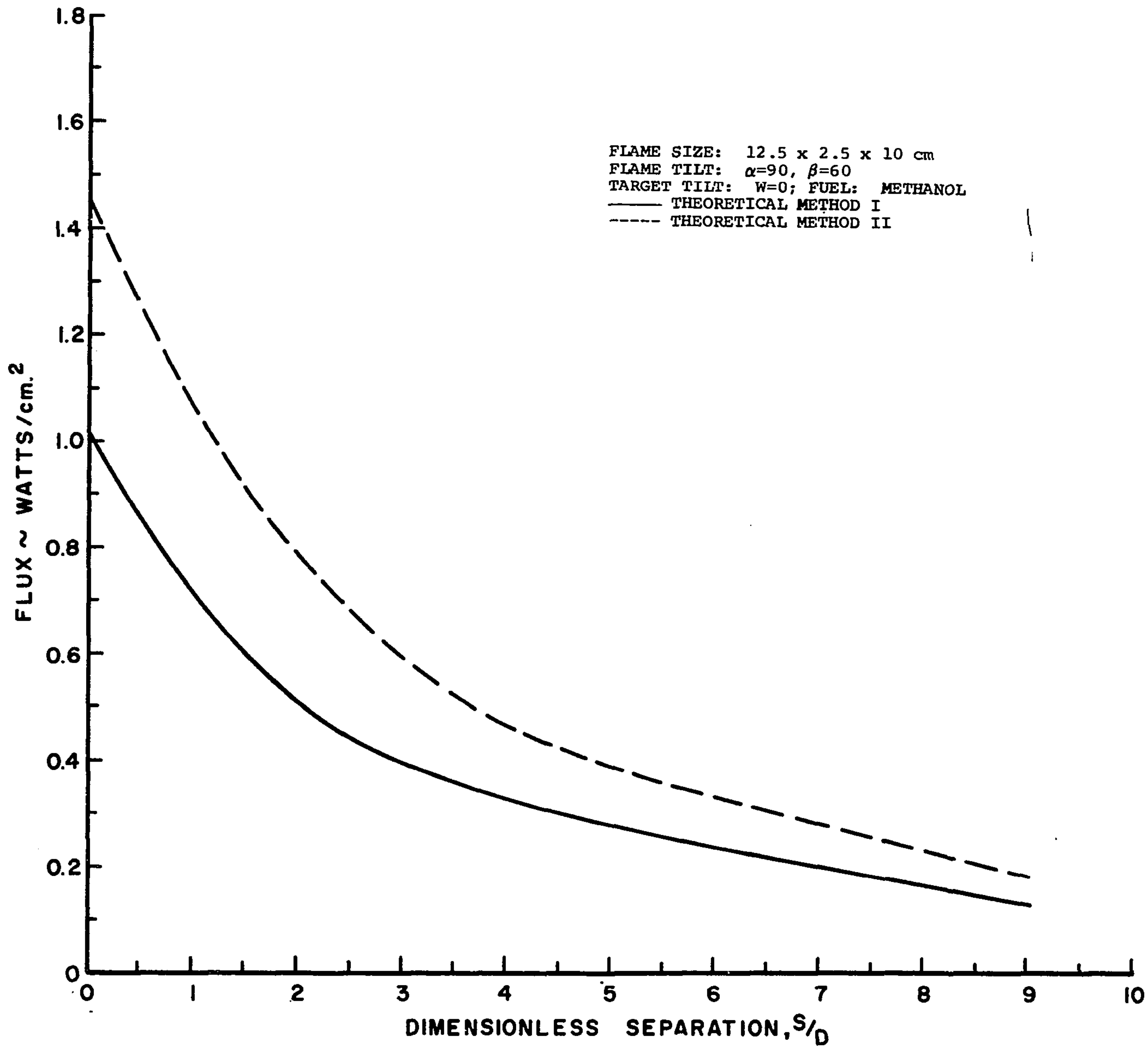

Figure 100. Radiation Flux Variation with Dimensionless Separation

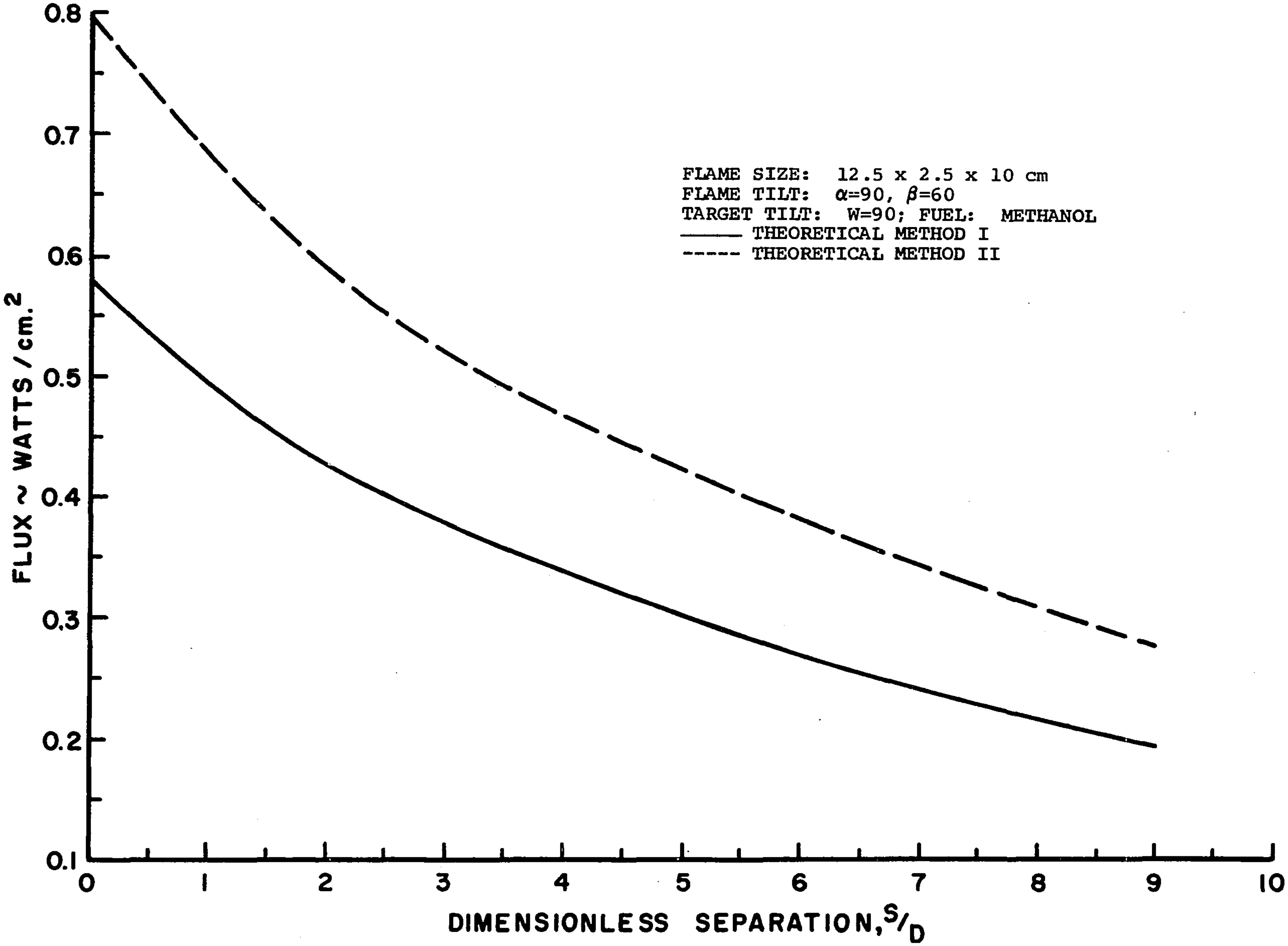

Figure 101. Radiation Flux Variation with Dimensionless Separation

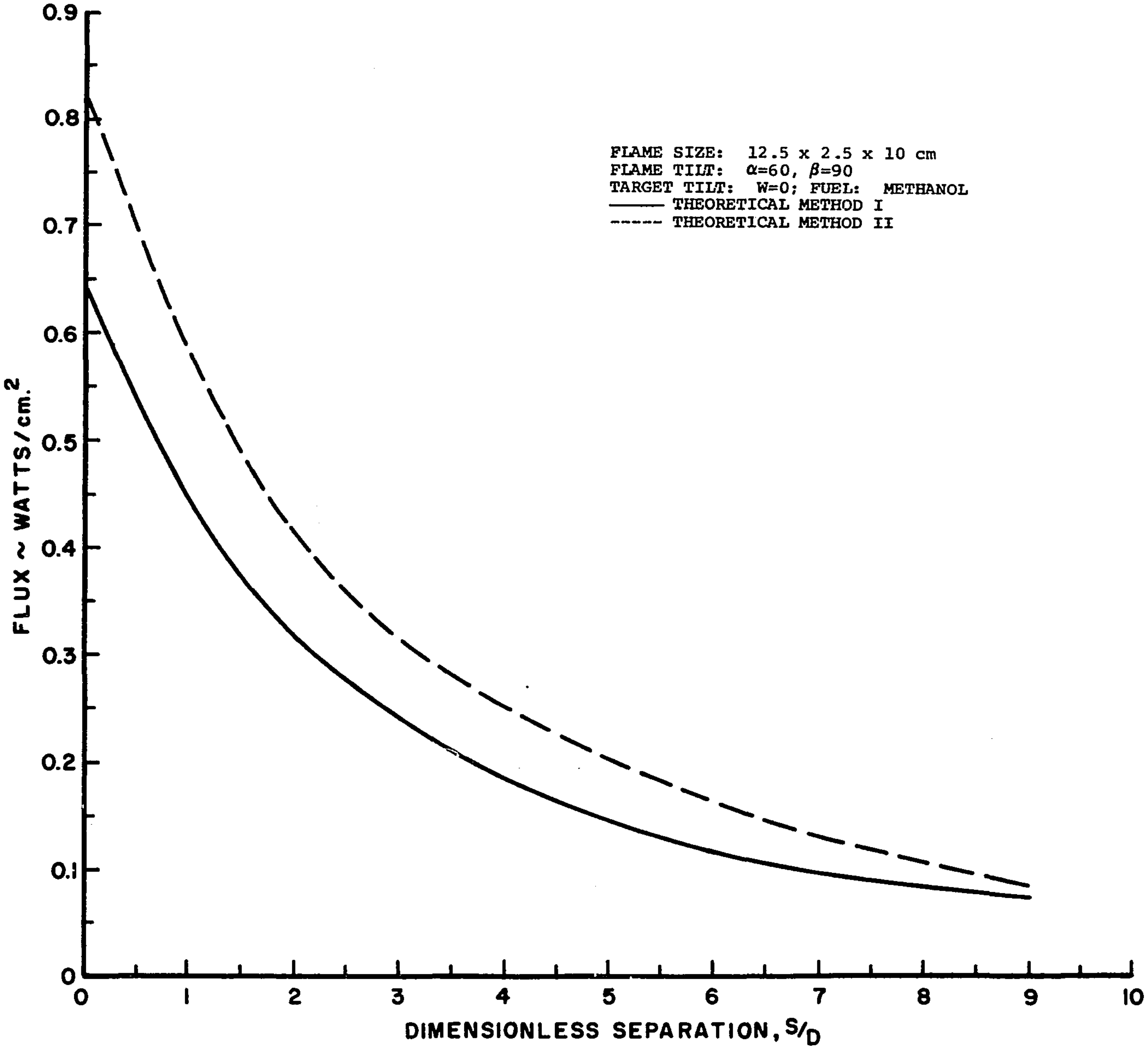

Figure 102. Radiation Flux Variation with Dimensionless Separation

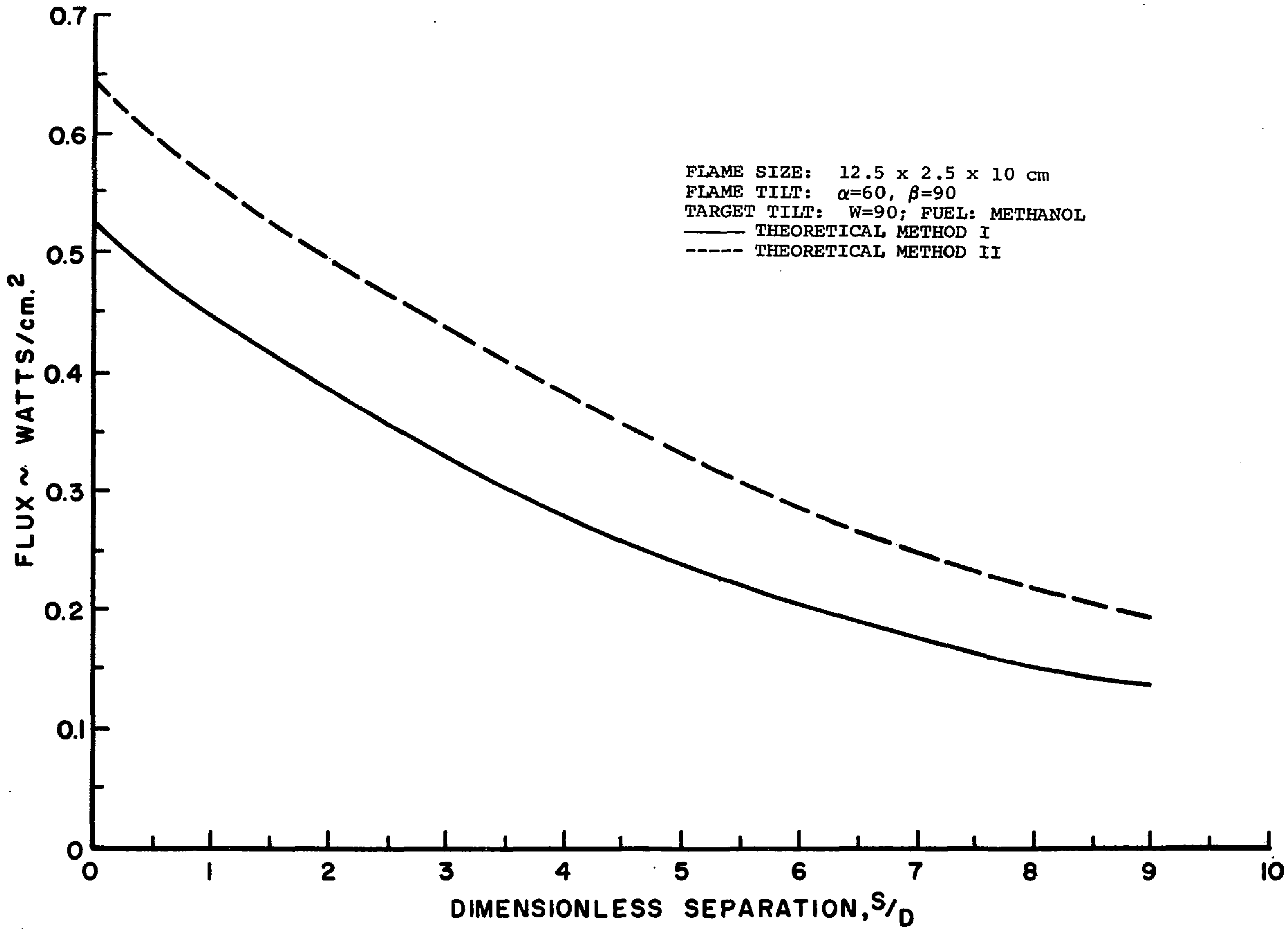

Figure 103. Radiation Flux Variation with
Dimensionless Separation

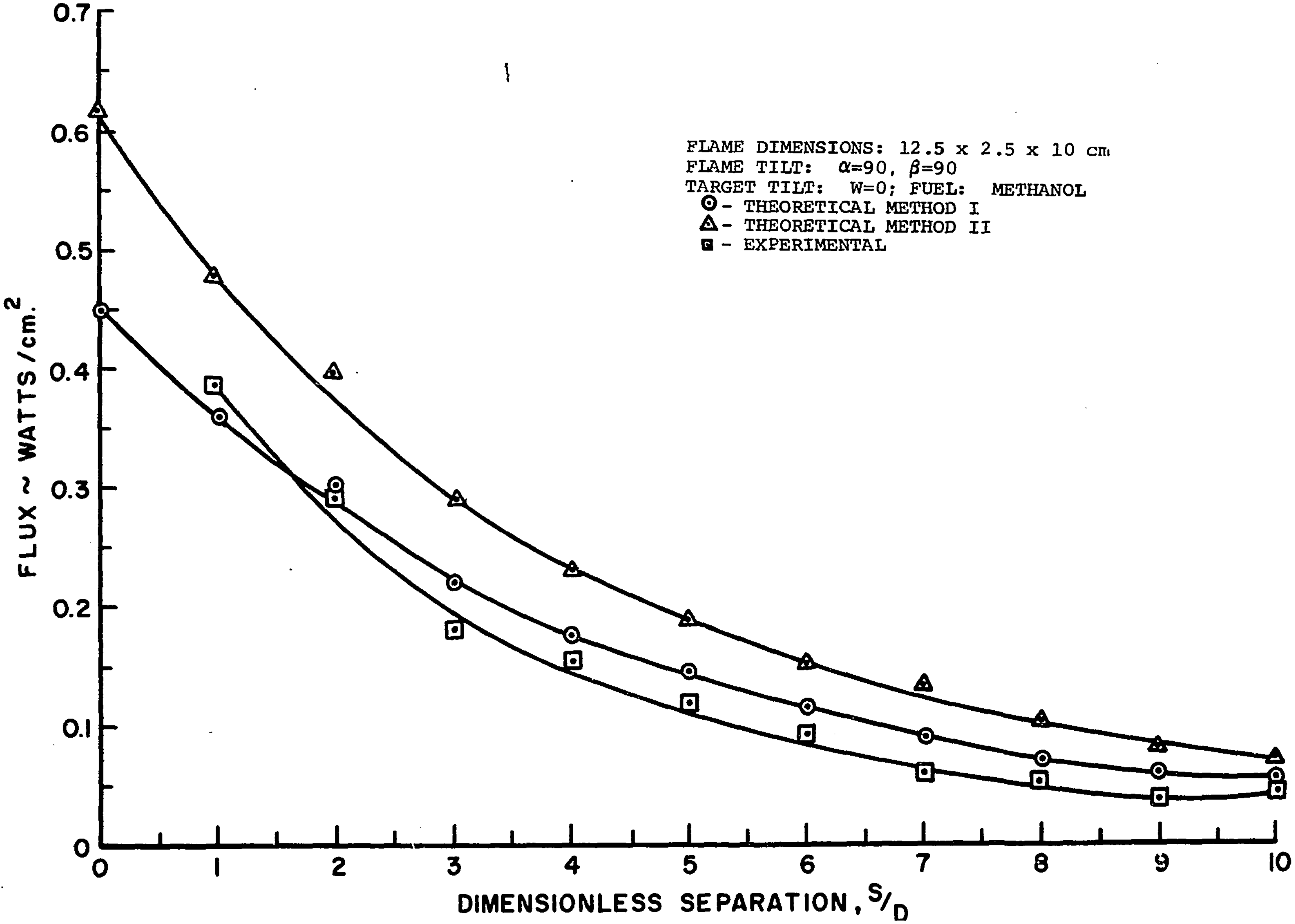

Figure 104. Radiation Flux Variation with Dimensionless Separation

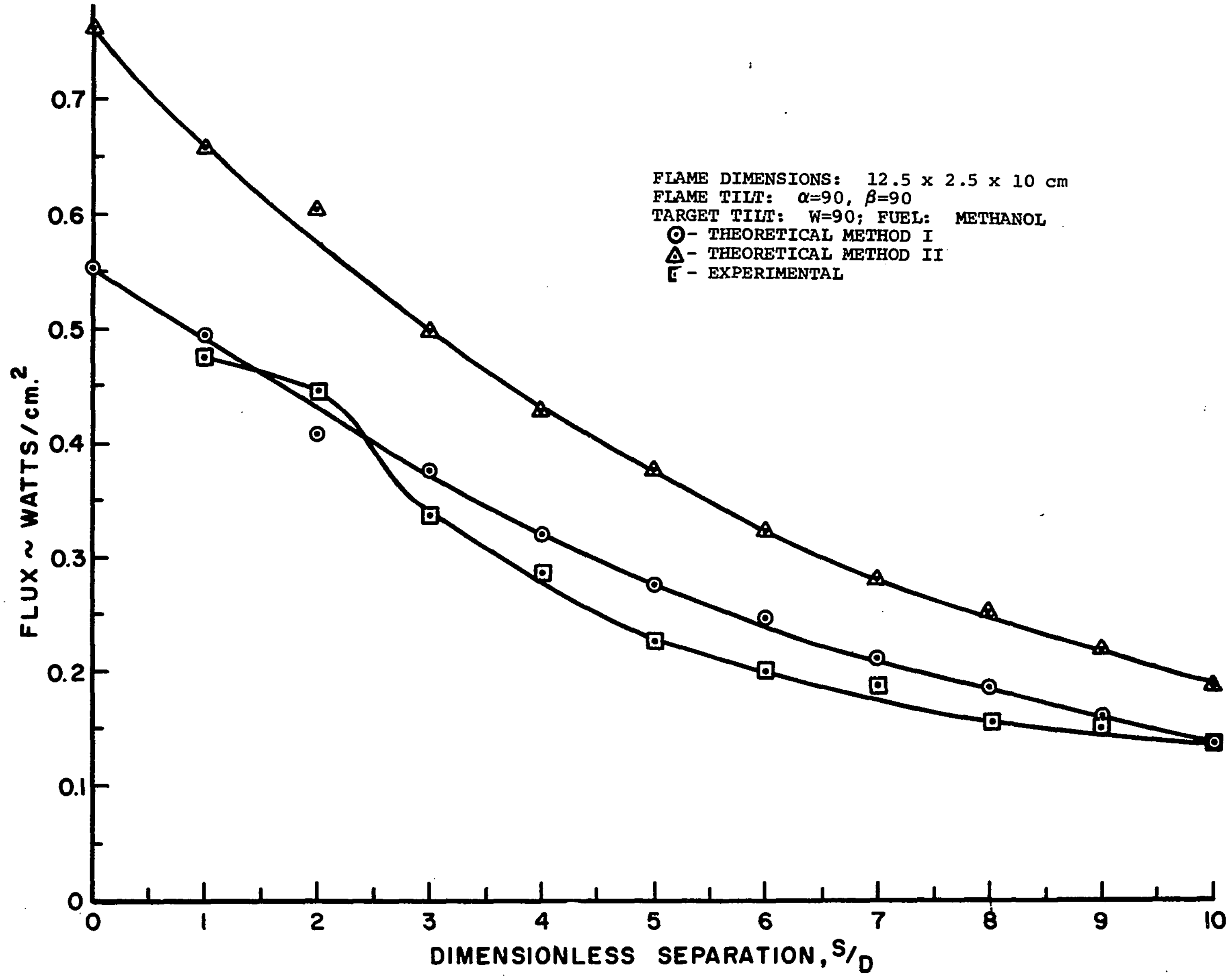

Figure 105. Radiation Flux Variation with Dimensionless Separation

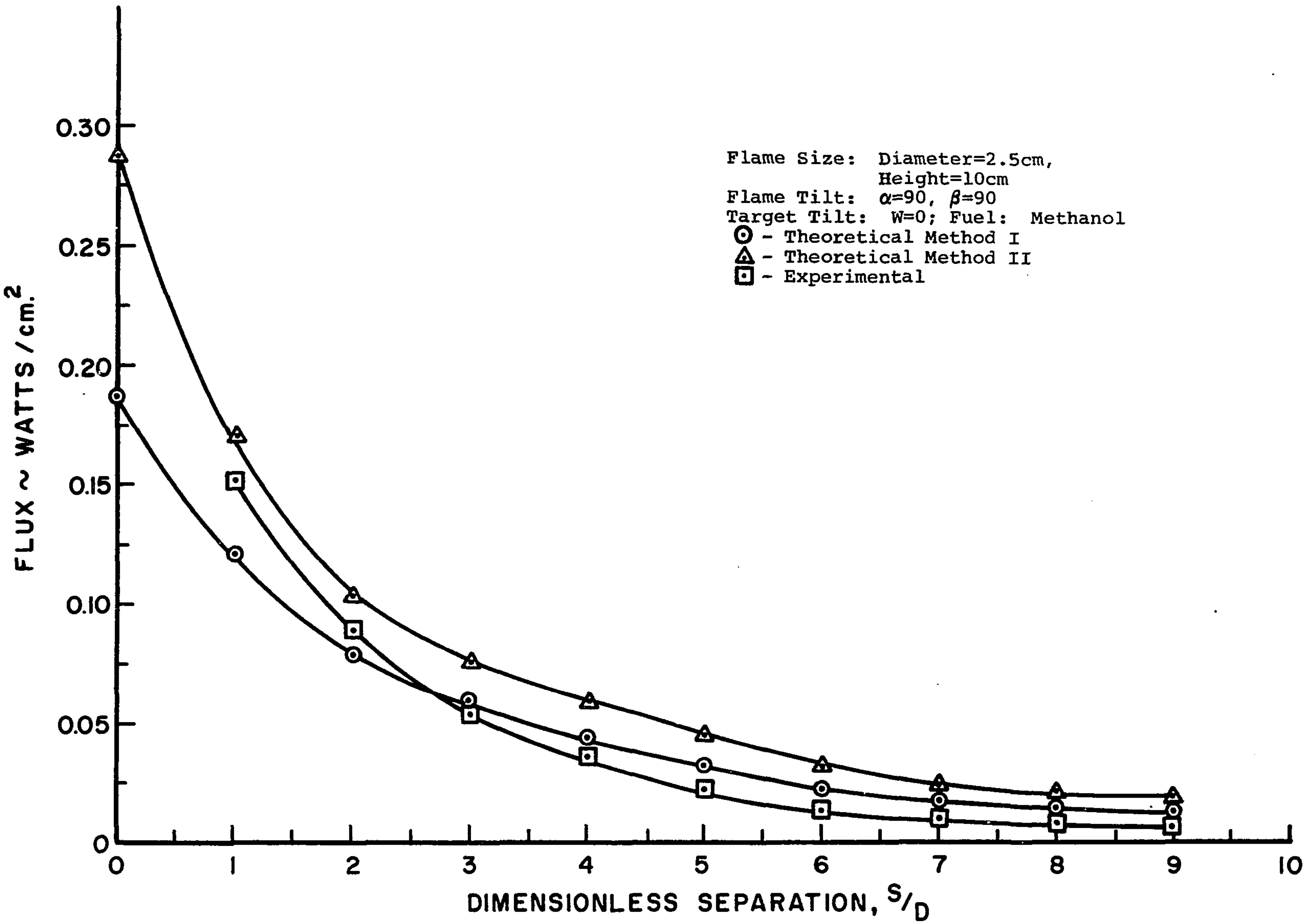

Figure 106. Radiation Flux Variation with Dimensionless Separation

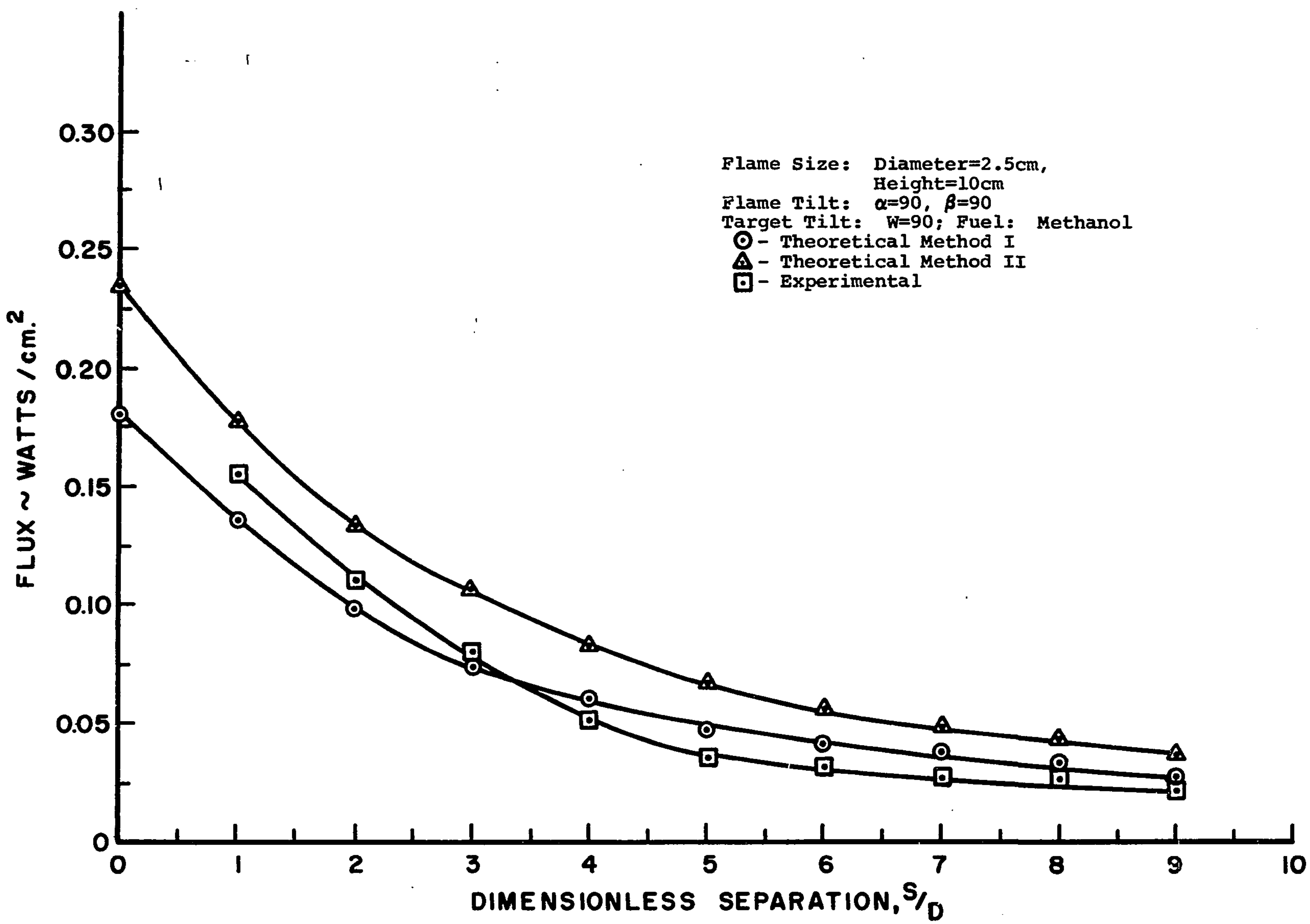

Figure 107. Radiation Flux Variation with Dimensionless Separation

66

1874